Impact of Sulphur Contamination on the Performance of Mixed Ionic-Electronic Conducting Membranes for Oxygen Separation and Hydrogen Production

Yousef Alqaheem

A thesis submitted in part fulfilment of the requirements for the degree of Doctor of Philosophy in Chemical Engineering at Newcastle University.

November 2015

Abstract

Mixed ionic-electronic conducting (MIEC) membranes are a promising technology for oxygen separation but they are not commercialised yet due to sealing issue and sensitivity to impurities in feedstock. In this study, $La_{0.6}Sr_{0.4}Co_{0.2}Fe_{0.8}O_{3-\delta}$ (LSCF6428) was successfully sealed for long-term operation of 963 h using a gold-glass-ceramic sealant. The membrane was then tested for air separation in presence of hydrogen sulphide for 100 h and results showed that the impurity caused a drop in oxygen flux to zero within few hours. The flux could not be fully restored after hydrogen sulphide removal and only 6 to 35% was recovered. It was proposed that hydrogen sulphide was adsorbed on the membrane in the form of sulphur and it occupied oxygen vacancies. With time, strontium segregates toward sulphur to form irreversible layer of strontium sulphate. To restore the damaged surface, the membrane was treated by 1% (mol) of hydrogen for 20 h and the recovery improved from 6 to 12%. It was discovered that the poisoning mechanism is a function of oxygen partial pressure and change of partial pressure from 0.21 to 0.01 bar resulted in 90% recovery and this can be used as a strategy to reduce the damage. The next step was to test the membrane for hydrogen production using 1% (mol) of methane and results showed that methane conversion was steady at 33% for 350 h. Methane oxidation was also carried in presence of hydrogen sulphide but it resulted in drop of conversion to 8%. However, the conversion was slowly regenerating with time and it reached a constant value of 15%. This recovery was interpreted by the reaction of methane with hydrogen sulphide or methane decomposition and the membrane acted as a catalyst for these reactions. After hydrogen sulphide removal from the feed, the conversion kept on decreasing and this was linked to the change of membrane properties and therefore the membrane could not provide the sites for methane-oxygen reaction. For better stability under hydrogen sulphide, the membrane was modified by adding a powder of LSCF6428 material over the dense membrane. This dual layer membrane was stable for air separation under hydrogen for 33 h and the flux was only reduced by 5%.

Acknowledgements

In the name of God, The Most Gracious, Most Merciful

At the beginning, I want to thank Kuwait Institute for Scientific Research for giving me the opportunity to study abroad and get a higher degree. As a return, I will do my best to serve the research centre and my country Kuwait.

This thesis is dedicated for my family who always provided me with support. They created a safe, quite environment and without them I could not achieve this degree.

Special thanks go to my supervisor Prof. Ian Metcalfe. I enjoyed every conversation with him since the first day I met him. He not only guided me through my PhD but also gave the confidence.

I want to thank my previous co-supervisor Dr. Alan Thursfield for introducing me to this kind of research and training me to perform membrane experiments. Other thanks to my current co-supervisor Dr. Guangru Zhang for designing experiments and interpreting data.

I would like to show my gratitude to Dr. Sureena Abdullah, Dr. Hang Qi, Dr. Evangelos Papaioannou, Dr. Callum Campell and Dr. Ana Dueso-Villalba for their valuable advises during my study. Greetings to all our awesome team of Dr. Brian Ray, Dr. Wei Chen, Dr. Ana Gil, Claire Thomson, Selgin Al, Prasna Ray, Danny Mak, Wan Binti Ramli, Sotiria Tsochataridou, Tarik Gerardin and Jianwei Lu.

It is my pleasure to thank my friends for continuous encouragement. Special thanks go to Dr. Abdulaziz AlOmair, Dr. Hamad AlMotairi, Ahmad AlMotawa, Ahmad AlOnainzi, and Abdulaziz AlSheeredah.

Table of Contents

List of Tables

List of Figures

Nomenclature

Symbol	Description	Unit
A	Effective membrane area	cm^2
D	Diffusion coefficient	$cm^2\ min^{-1}$
F	Volumetric flow rate of gas	$ml\ min^{-1}$
G	Gibbs free energy	$kJ\ mol^{-1}$
H	Enthalpy	$kJ\ mol^{-1}$
J_{O_2}	Oxygen flux	$ml\ cm^{-2}\ min^{-1}$
k_s	Surface reactions coefficient	unitless
m	Mass	g
M_{wt}	Molecular weight	$g\ mol^{-1}$
N_A	Avogadro's number	mol^{-1}
t	Membrane thickness	cm
r	Membrane radius	cm
V	Volume	cm^3
Z	Number of atoms per unit cell	unitless

Greek Letters

ρ	Density
δ	Oxygen vacancy

Abbreviations

BSCF5582	$Ba_{0.5}Sr_{0.5}Co_{0.8}Fe_{0.2}O_{3-\delta}$
EDS	Electron-dispersion x-ray spectroscopy
EDTA	Ethylene-diamine-tetra-acetic acid

GC	Gas chromatograph
LSCF6428	$La_{0.6}Sr_{0.4}Co_{0.2}Fe_{0.8}O_{3-\delta}$
LSF731	$La_{0.7}Sr_{0.3}Fe_{0.1}O_{3-\delta}$
MIEC	Mixed ionic-electronic conductor
pH	Hydrogen number
POM	Partial oxidation of methane
PSA	Pressure swing adsorption
PVC	Polyvinylchloride
SEM	Scanning electron microscopy
SMR	Steam-methane reforming
SSR	Sulphide stress cracking
TGA	Thermogravimetric analyser
WEL	Work exposure limit
XPS	X-ray photoelectron spectroscopy
XRD	X-ray diffraction

Chapter 1: Introduction

Chapter 1: Introduction

1.1 Overview

Hydrogen demand is increasing and it is expected to be five times more by the end of 2030 [1]. The gas is excessively used in ammonia synthesis to make fertilisers and in hydrodesulphurisation to remove sulphur from petroleum streams [2]. Hydrogen is also considered as a coolant in power plants because of its high thermal conductivity [3]. Compared to other fuels, hydrogen has the highest energy when combusted and it produces only water with no carbon. Vehicles operated by hydrogen are available and use of hydrogen as a transportation fuel will greatly reduce air pollution [4, 5].

Industrially, 98% of hydrogen is produced from fossil fuel by either steam-methane reforming (SMR) or partial-oxidation of methane (POM) [6]. SMR involves reaction of methane with water to generate hydrogen and carbon monoxide but the process is energy-intensive due to the endothermic, reversible reaction [7]. On the other hand, POM overcomes these issues by the reaction of methane with oxygen instead of water but the supplement of high purity oxygen by cryogenic distillation greatly influences the process economy [8]. Therefore, SMR is still the dominating process for hydrogen production in industry.

Alternatively, state of art membranes can be integrated in POM process to generate oxygen with 100% purity and use of this technology, compared to cryogenic distillation, will cut down the energy costs by 25 to 35% [9]. Furthermore, the membranes can provide the surface area for the reaction and act as catalysts [10]. Perovskites are the membranes' materials and and they have properties of conducting both ions and electrons which are needed for oxygen transport. In literature, the membranes had been tested for long-term operation of more than 7000 h and methane conversion was 99% [11].

Before commercialisation, the membranes need to be evaluated under industrial conditions rather than pure feeds. Impurities such hydrogen sulphide and carbon dioxide are usually found in natural gas which will be the feedstock for POM in industry [12]. Hydrogen sulphide is a very toxic gas, well-known for its rotten egg smell even in very low concentrations of parts per billion (ppb) [13]. The gas is also corrosive and cause damage to different materials such as metals, ceramics, polymers and composites because of its high reactivity [14].

Performance of the oxygen permeable membranes for hydrogen production under the presence of hydrogen sulphide impurity was not studied before and it is expected to be severe.

1.2 Aims and objectives

The main aim is to investigate the changes in membrane performance for oxygen separation and methane oxidation due to the presence of hydrogen sulphide impurity. Determination of the poisoning mechanism, improving the recovery and modifying the membrane for better stability are the other aims. The following objectives are needed to achieve the aims:

- Select a membrane material.
- Fabricate the membrane.
- Design and build the membrane reactor.
- Gas-tight seal the membrane for long-term operation.
- Perform oxygen separation in presence of hydrogen sulphide and observe the changes.
- Improve the recovery after hydrogen sulphide exposure.
- Perform more studies to determine the poisoning mechanism of hydrogen sulphide.
- Do methane oxidation in presence of hydrogen sulphide to determine the changes.
- Regenerate the membrane after sulphur poisoning in methane oxidation.
- Propose strategies to reduce hydrogen sulphide damage.
- Try to modify the membrane for better stability under hydrogen sulphide.

1.3 Thesis layout

The thesis consists of eight chapters including the introduction. In next chapter, literature review on membranes, hydrogen production and hydrogen sulphide are reported. Chapter 3 demonstrates the methodology of reactor design, membrane material, sealant and characterisation techniques. Chapter 4 discusses the experimental work for oxygen separation using the membrane in presence of hydrogen sulphide. In Chapter 5, further studies on hydrogen sulphide are conducted to understand more about the poisoning mechanism. Methane oxidation along hydrogen sulphide impurity is performed in chapter 6. In chapter 7, possibility of modifying the membrane for better tolerance to sulphur is investigated. Conclusions and future work are given in chapter 8.

Chapter 2: Literature Review

Chapter 2: Literature Review

This chapter gives general view of synthetic membranes; their concept, groups and applications. It focuses on ceramic membranes specifically the mixed conductors. Transport mechanism and materials of the mixed ionic-electronic conductors (MIEC) are described. Conventional processes for hydrogen production and how MIEC membranes can be beneficial are also mentioned. Current challenges for commercialising MIEC membrane are given in this chapter. The last section talks about hydrogen sulphide; its occurrence and impact.

2.1 Membrane definition

Membrane is a barrier which allows certain molecules to pass. The separation mechanism can be based on molecular size, chemical reaction, concentration, electrical gradient or pressure. Compared to other chemical equipment, the membrane: a) contains no mechanical parts therefore it requires less or no maintenance, b) easy to scale-up and occupies small area, c) considered as a green technology (environmentally friendly) because it operates in low energy and has zero emissions [15-17]. These features make the membrane unique and attractive for industry. Today, membranes are heavily used in large scale for: desalination to produce potable water, waste-water treatment of sewage, food processing such as purification of beverages and milk processing, and gas separation mainly for hydrogen production and carbon capture [18-20]. The membranes are used in medical sector as well and they can act as artificial kidneys to remove the waste from blood and maintain an acceptable concentration of metals such as sodium and potassium [21].

The membranes are well implemented in various separation processes such as microfiltration, ultrafiltration, nanofiltration, reverse osmosis and pervaporation. In microfiltration, where the particle size ranges from 1 to 10 μm, suspended particles, blood cells and bacteria are removed while in ultrafiltration (10 to 100 Å), vitamins and enzymes are separated [22]. In nanofiltration and reverse osmosis (< 10 Å), dissolved sugars and salts are taken out from solutions. Liquid-to-liquid separation can be achieved using pervaporation and it is used for water removal from organic solvents [23]. In addition to separation, the membranes can provide the sites for the reaction and therefore they can perform separation and reaction at the same time. One of the advantages of using these membrane reactors is the ability of shifting

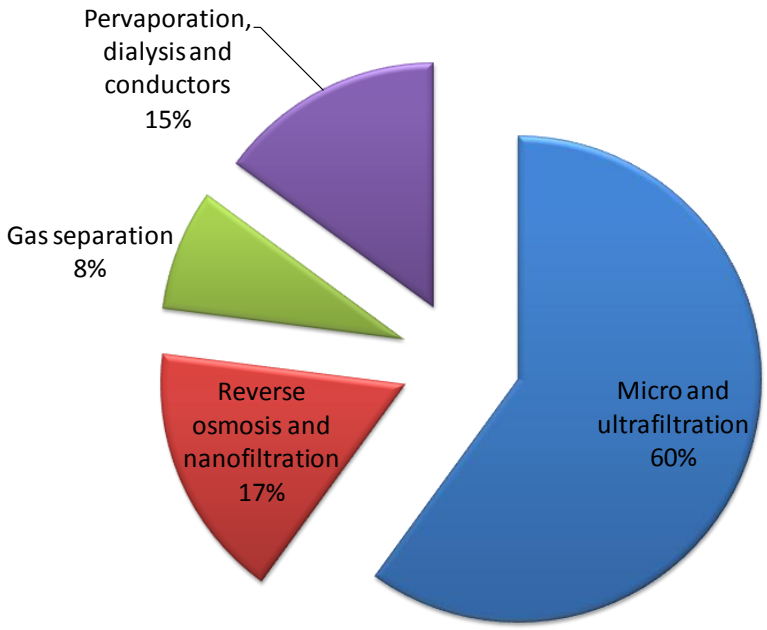

Figure 2.1. Membrane market by its applications [24].

the equilibrium of some reversible reactions and this increases the production rate [24]. Membrane reactors are being employed for dehydrogenation and partial-oxidation of hydrocarbons, catalytic cracking of hydrogen sulphide, methanol production and ammonia oxidation [25, 26]. Current uses of the membranes are given in Figure 2.1.

2.2 Membrane classification

One way to classify synthetic membranes is by the type of material and subsequently it is grouped to metallic, polymeric and ceramic. Metallic membranes are commonly made from palladium which promotes hydrogen transport and this is ideal for hydrogen purification from gas mixtures [27]. Polymeric membranes are generally fabricated from cellulose acetate, polyethylene and polyvinylchloride (PVC). They are implemented for sea-water desalination and gas separation such as oxygen purification, carbon dioxide capture and natural gas enrichment [28-30]. On the other hand, ceramic membranes consist primarily from metal oxides like alumina (Al_2O_3). At home, the tap water can be purified using a filter where unwanted contaminations are removed [31]. Separation of hydrogen, oxygen and carbon dioxide are other applications of ceramic membranes [32]. Today, polymeric membranes dominates industry because of the outstanding performance and economics [33]. However, the low melting point of polymers makes them unsuitable for temperatures over 200°C. Metallic membranes can be applied instead but the rising costs of precious metals greatly

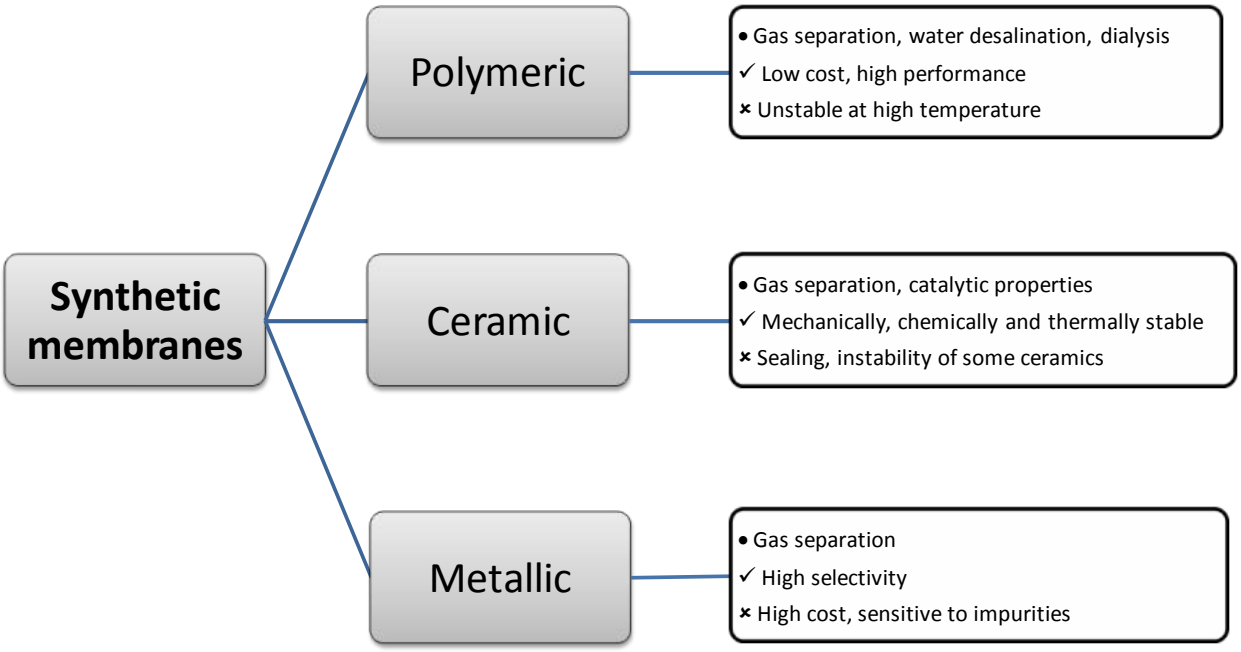

Figure 2.2 Comparison between different types of synthetic membranes.

influence the process economy. Alternatively, ceramic membranes can be operated at high temperature and their prices are 80% lower than the metallic ones [34]. Furthermore, ceramic membranes have excellent mechanical and chemical properties to withstand harsh environments such as corrosive chemicals [35]. Figure 2.2 shows comparison between the polymeric, ceramic and metallic membranes.

2.3 Ceramic membranes

Ceramic membranes are inorganic materials consisting of metal oxides and they can be categorised based on the physical structure to porous and dense. The separation mechanism is based on molecular sieving in case of porous membrane and solution diffusion in case of dense ones. In-expensive porous silica (SiO_2) membranes have a good application in gas separation because of the high permeability and selectivity of hydrogen but it is limited to low temperature (e.g., 200°C) [36, 37]. Another use of silica membranes is for pervaporation for removal of water or alcohol from organic solutions [38]. In pervaporation, the membranes separate the liquids based on molecular size and the permeated liquid is vaporised due the vacuum pressure.

Zeolite (aluminosilicate) is another porous ceramic but unlike silica, it can withstand high temperature over 900°C [39]. The framework of zeolite can be negatively charged to adsorb

metal cations and this is beneficial for water purification [40]. In addition, zeolite has catalytic properties because of the large surface area and the acidic sites. In petroleum refinery, zeolite is used to convert crude oil to lighter, more useful fractions such as gasoline and this process is called fluid catalytic cracking [41, 42]. After production of hydrogen by steam-methane reforming (SMR) and water-gas shift (WGS), hydrogen is separated from carbon dioxide by pressure swing adsorption (PSA) unit where hydrogen passes through the voids of zeolite because of its small molecular size while carbon dioxide is adsorbed on zeolite surface [43].

Porous silicon carbide membranes have unmatched performance for microfiltration and ultrafiltration. Compared to polymeric membranes, silicon carbide membranes have higher flux, longer life, better chemical stability and greater regeneration rate. They are used industrially for water purification, wastewater treatment and gas-oil separation [44].

On the other hand, for dense membranes, the widely accepted theory for transport mechanism is based on the solution-diffusion model where certain molecules dissolve by surface reactions on the membrane surface and then diffuse through the membrane by pressure, concentration or electrical gradient [45]. In ceramic membranes, there are two types of conductors: a) protonic for hydrogen transport and b) ionic for oxygen diffusion. If the membrane contains enough conducting electrons and electrical circuit is not required to promote oxygen or hydrogen transport, the membrane is then called mixed conductor [46]. This study focuses on mixed ionic-electronic conducting (MIEC) membranes because they have promising applications for oxygen separation and they also act as membrane reactors for methane oxidation [32]. Figure 2.3 demonstrates the separation mechanism in porous and dense membranes.

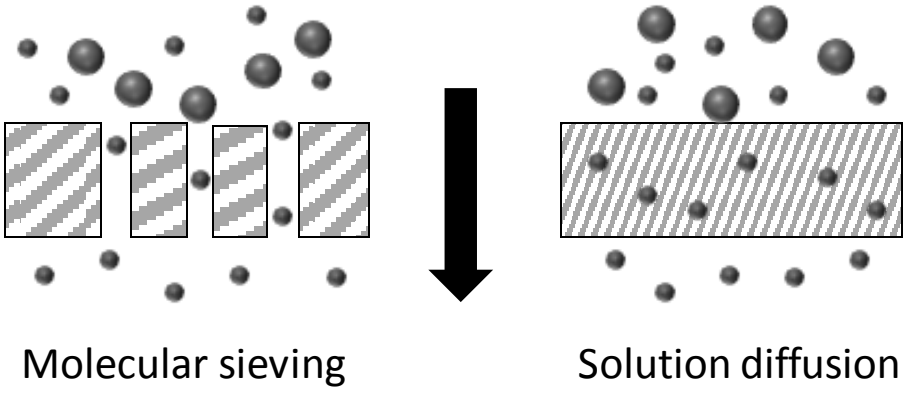

Figure 2.3. Gas separation using ceramic membranes based on molecular sieving (porous membrane) and solution diffusion (dense membrane).

2.4 MIEC membranes

Most of mixed ionic-electronic conducting membranes belong to two groups: fluorites and perovskites. The fluorite-type membranes have chemical formula of AO_2 where A is a four-valent cation such as zirconium (Zr) and cerium (Ce) [46]. When analysed by x-ray diffraction, the crystal structure of these membranes are similar to fluorite compounds (e.g., CaF_2) and hence the name [47]. It is found that fluorites have cubic structure as shown in Figure 2.4. Unfortunately, there is no intensive research on these membranes due to low oxygen flux and poor mechanical properties compared to perovskites [48]. On the other hand, perovskite refers to calcium titanate mineral ($CaTiO_3$) discovered by a Russian scientist called Perovski [49]. The chemical formula for a perovskite is ABO_3 where A stands for an alkali earth metal such as barium or strontium and B is a transition metal like cobalt or iron. The perovskite has an orthorhombic structure at room temperature and a cubic structure at high temperature (above 1250°C) [50]. Other MIEC materials are pyrochlores ($A_2B_2O_7$) and brownmillerties ($A_2B_2O_5$) but they showed lower performance compared to pervoskites and fluorites [51]. In the following sections, transport mechanism, materials and fabrication of perovskite membranes are discussed.

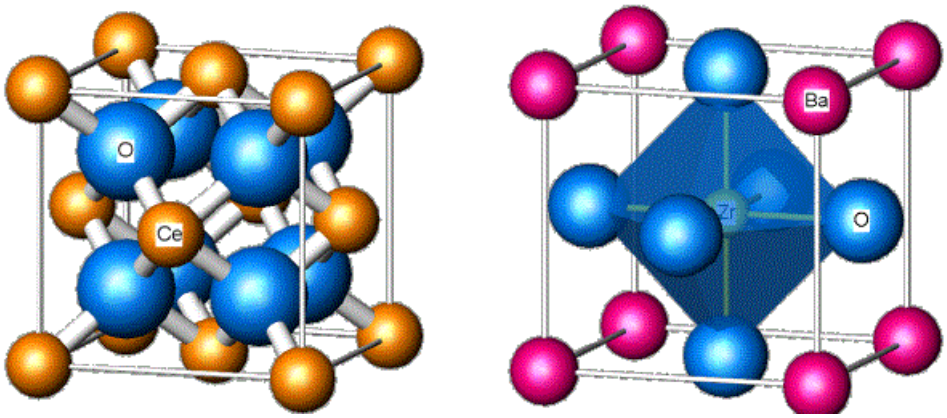

Figure 2.4. Fluorite structure of CeO_2 (left) and perovskite structure of $BaZrO_3$ [52].

2.4.1. *Transport mechanism*

Teraoka et al. were the first to discover the oxygen transport in perovskite membranes since 1985 [53]. These materials are electronically conductive and have oxygen defect where atomic oxygen is missing from the structure creating a vacancy [54, 55]. Naturally, the perovskite has a low amount of oxygen vacancies which is not enough for practical applications. Therefore, to boost oxygen permeation, doping in metal solutions is necessary

[56]. For example, immersing perovskite in a liquid solution containing A′ and B′ cations will give a new material having formula of $A'_{1-x}A_xB'_{1-y}B_yO_{3-\delta}$ where δ expresses the amount of defects or oxygen vacancies [57, 58]. The transport mechanism can be described in three steps: 1) reaction of molecular oxygen on the membrane surface to form ionic oxygen; 2) diffusion of oxygen through the membrane; 3) combination of oxygen anions to form back molecular oxygen [59]. In the first step where oxygen reaches the membrane surface, it reacts with the vacancies to form anions as follows [60]:

$$O_{2_{(g)}} + 2V_O^{\bullet\bullet} + 4e^- \leftrightarrow 2O_o^x \tag{2.1}$$

where $V_O^{\bullet\bullet}$ is the Kroger-Vink notation representing one oxygen vacancy with a double positive charge and O_o^x is an oxygen ion sitting in the oxygen vacancy resulting in a neutral charge [61]. The second step in oxygen transport is the bulk diffusion of oxygen across the membrane. The most accepted theory for the diffusion is the hoping of oxygen ion from a vacancy to adjacent one due to the difference in oxygen potential [62]. The last step in oxygen transport is the formation of molecular oxygen by the combination of ions releasing back the electrons and vacancies as follows:

$$2O_o^x \leftrightarrow O_{2_{(g)}} + 2V_O^{\bullet\bullet} + 4e^- \tag{2.2}$$

As realised, the transport mechanism is controlled by two factors: a) surface exchange reactions and b) bulk diffusion. Bouwmeester et al. defined a parameter called critical thickness (L_c) to determine whether surface exchange reaction or bulk diffusion is the dominant step for oxygen transport [63]:

$$L_c = \frac{D^*}{k_s} \tag{2.3}$$

where D^* is the oxygen diffusion coefficient and k_s is the surface-reaction coefficient determined experimentally using isotope of oxygen ($^{18}O_2$) as a tracer gas [64]. If the membrane thickness is larger than the critical one, this indicates that the bulk diffusion is dominant whereas if the membrane thickness is lower, surface-exchange reactions will dominate and if the membrane thickness equals to the critical one, both surface reactions and bulk diffusion will dominate and this is the optimum value to have the best performance. Figure 2.5 shows the oxygen transport mechanism in MIEC membranes based on the vacancies and the conducting electrons.

Oxygen flux (J_{O_2}) through MIEC membranes can be described using Fick's law of diffusion:

$$J_{O_2} = \frac{D_V}{2L}(C_V'' - C_V') \tag{2.4}$$

Where D_V is the diffusion coefficient of vacancies, L is the membrane thickness, C_V' is the concentration of vacancies in the oxygen-rich side and C_V'' is the concentration of vacancies in the permeating side. This model assumes ideal gas behaviour and one-dimensional diffusion. C_V' and C_V'' are controlled by the surface exchange reactions of Equations 2.1 and 2.2 therefore, the flux can be written as:

$$J_{O_2} = k_f C_V' (P_{O_2}')^{0.5} - k_r \tag{2.5}$$

$$J_{O_2} = k_r - k_f C_V'' (P_{O_2}'')^{0.5} \tag{2.6}$$

Where k_f and k_r are the surface exchange reaction coefficients. Solving for J_{O_2} using Equations 2.4, 2.5 and 2.6 gives:

$$J_{O_2} = \frac{D_V k_r \left[(P_{O_2}')^{0.5} + (P_{O_2}'')^{0.5}\right]}{2L k_f (P_{O_2}' P_{O_2}'')^{0.5} + D_V\left[(P_{O_2}')^{0.5} + (P_{O_2}'')^{0.5}\right]} \tag{2.7}$$

the above equation states that the oxygen permeation is a function of oxygen vacancies, membrane thickness, oxygen partial pressure and temperature. Parameters such as k_f and k_r can be determined experimentally using thermogravimetric analyser (TGA) [65]. Oxygen vacancy (δ) can be calculated based on surface exchange reactions (Equations 2.5 and 2.6)

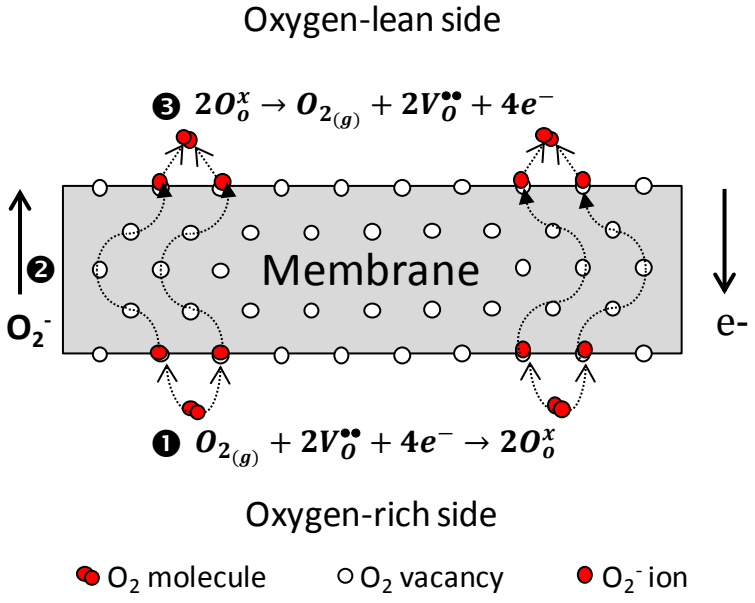

Figure 2.5. Three main steps for oxygen transport in MIEC membranes.

and this property is defined by [66]:

$$\delta = C_V V_M \tag{2.8}$$

Where C_V is the concentration of vacancies and V_M is the molar volume. Substituting C_V in Equations 2.5 and 2.6 for δ gives:

$$\delta' = \frac{V_M(J_{O_2} + k_r)}{k_f(P'_{O_2})^{0.5}} \tag{2.9}$$

$$\delta'' = \frac{V_M(k_r - J_{O_2})}{k_f(P'_{O_2})^{0.5}} \tag{2.10}$$

Where δ' and δ'' is the amount of vacancies (in atomic composition) in the oxygen-rich side and oxygen-lean side, respectively.

2.4.2. *Materials*

In literature, there is a massive number of materials that have mixed conducting properties for oxygen permeation. As mentioned before, the most promising materials are made of perovskites and the oxygen flux of some of these materials is mentioned in Table 2.1. The flux (J_{O_2}) is calculated by:

$$J_{O_2}\ (\text{ml cm}^{-2}\ \text{min}^{-1}) = \frac{F}{A} \tag{2.11}$$

where F is the volumetric flow rate in ml min^{-1} measured at standard temperature and pressure, STP (25°C and 1 atm) and A is the active membrane area in cm^2. For the membrane to be beneficial for industry, it should produce high oxygen flux of more than 1 ml cm^{-2} min^{-1} [67]. The most recent materials that meet this criteria are based on perovskites having formula of $Sr(Co,Fe)O_3$ and $La(Co,Fe)O_3$ [32]. For hydrogen production by methane oxidation, a small number of these materials has been investigated and proved to be promising and they are: $Ba_{1-x}Sr_xCo_{1-y}Fe_yO_{3-\delta}$ (BSCF), $La_{1-x}Sr_xCo_{1-y}Fe_yO_{3-\delta}$ (LSCF) and $La_{1-x}Sr_xFe_yO_{3-\delta}$ (LSF) [11, 68, 69].

BSCF is made by doping strontium-cobalt oxide ($SrCoO_3$) in a solution containing barium and iron ions. Actually, barium occupies strontium sites and this results in creation of more vacancies and addition of iron to the membrane is needed for better chemical stability [70]. On the other hand LSCF is created by doping lanthanum-cobalt oxide ($LaCoO_3$) in strontium

Table 2.1. Oxygen flux of some perovskite materials using air at atmospheric pressure

Material	Temperature (°C)	J_{O_2} (ml cm^{-2} min^{-1})	Reference
$BaBi_{0.5}Co_{0.2}Fe_{0.3}O_{3-\delta}$	800 – 925	0.41 – 0.82	[71]
$BaCe_{0.4}Fe_{0.6}O_{3-\delta}$	800 – 950	0.11 – 0.26	[72]
$Ba_{0.5}Sr_{0.5}Co_{0.8}Fe_{0.2}O_{3-\delta}$	850 – 950	2.07 – 4.78	[73]
$Ba_{0.5}Sr_{0.5}Zn_{0.2}Fe_{0.8}O_{3-\delta}$	800 – 975	1.63 – 3.82	[74]
$BaTi_{0.2}Co_{0.4}Fe_{0.4}O_{3-\delta}$	600 – 950	0 – 9.83	[75]
$CaTi_{0.8}Fe_{0.2}O_{3-\delta}$	800 – 1000	0.01 – 0.03	[76]
$Gd_{0.6}Sr_{0.4}CoO_{3-\delta}$	820	1.73	[77]
$La_{0.4}Ba_{0.6}Co_{0.2}Fe_{0.8}O_{3-\delta}$	900	0.79	[78]
$La_{0.6}Ca_{0.4}Co_{0.8}Fe_{0.2}O_{3-\delta}$	860	2.00	[77]
$La_{0.6}Na_{0.4}Co_{0.8}Fe_{0.2}O_{3-\delta}$	860	0.30	[77]
$La_{0.6}Sr_{0.4}CoO_{3-\delta}$	850	0.60 – 3.40	[65]
$La_{0.6}Sr_{0.4}Co_{0.2}Fe_{0.8}O_{3-\delta}$	900 – 950	1.00 – 3.13	[79]
$La_{0.6}Sr_{0.4}Co_{0.8}Fe_{0.2}O_{3-\delta}$	850 – 1000	0.08 – 0.46	[62]
$La_{0.4}Sr_{0.6}Co_{0.2}Fe_{0.8}O_{3-\delta}$	900	0.60	[80]
$La_{0.2}Sr_{0.8}Co_{0.2}Fe_{0.8}O_{3-\delta}$	900	0.74	[80]
$La_{0.2}Sr_{0.8}Co_{0.4}Fe_{0.6}O_{3-\delta}$	1000 – 1100	0.18 – 0.55	[53]
$La_{0.6}Sr_{0.4}Co_{0.8}Mn_{0.2}O_{3-\delta}$	860	0.55	[77]
$La_{0.6}Sr_{0.4}Co_{0.8}Ni_{0.2}O_{3-\delta}$	860	1.57	[77]
$La_{0.8}Sr_{0.2}FeO_{3-\delta}$	1000	0.15	[81]
$La_{0.7}Sr_{0.3}FeO_{3-\delta}$	1000	0.24	[81]
$La_{0.6}Sr_{0.4}FeO_{3-\delta}$	1000	0.38	[81]
$La_{0.8}Sr_{0.2}Ga_{0.7}Co_{0.3}O_{3-\delta}$	700 – 1000	0.34 – 1.61	[82]
$Nd_{0.6}Sr_{0.4}CoO_{3-\delta}$	820	1.12	[77]
$Pr_{0.6}Sr_{0.4}CoO_{3-\delta}$	820	1.01	[77]
$Sm_{0.6}Sr_{0.4}CoO_{3-\delta}$	820	1.30	[77]
$Sr_{0.5}Bi_{0.5}FeO_{3-\delta}$	825 – 925	0.19 – 0.59	[83]
$SrCoO_{3-\delta}$	850 – 1000	0 – 0.49	[84]
$SrCo_{0.4}Fe_{0.6}O_{3-\delta}$	1000 – 1100	1.06 – 2.18	[53]
$SrCo_{0.8}Fe_{0.2}O_{3-\delta}$	870	3.64	[53]
$SrCo_{0.95}Ti_{0.05}O_{3-\delta}$	880	0.66	[85]
$Sr_{0.7}La_{0.3}CoO_{3-\delta}$	880	0.38	[85]
$Sr_{0.6}La_{0.4}CoO_{3-\delta}$	880	0.29	[85]
$Sr_{0.7}Nd_{0.3}CoO_{3-\delta}$	880	0.23	[85]
$Y_{0.05}Ba_{0.95}CoO_{3-\delta}$	900	0.57	[86]
$Y_{0.1}Ba_{0.9}CoO_{3-\delta}$	900	0.39	[86]

and iron solutions. Strontium occupies some lanthanum atoms and this resulted in better oxygen flux due to the generation of more oxygen vacancies [75]:

$$2SrO + 2La_{La}^{x} + +O_{O}^{x} \xrightarrow{La(Fe,Co)O_3} La_2O_3 + 2Sr'_{La} + V_O^{\bullet\bullet} \quad (2.12)$$

Furthermore, doping strontium-iron oxide ($SrFeO_3$) in lanthanum solution will form LSF membrane. Research proves that $Ba_{0.5}Sr_{0.5}Co_{0.8}Fe_{0.2}O_{3-\delta}$ (BSCF 5582) has the maximum oxygen flux in all groups because it contains barium [48, 87]. On the other hand, $La_{0.6}Sr_{0.4}Co_{0.2}Fe_{0.8}O_{3-\delta}$ (LSCF 6428) shows a better chemical stability than BSCF 5582 but at the expense of oxygen flux [88]. The absence of cobalt in $La_{0.7}Sr_{0.3}FeO_{3-\delta}$ (LSF731) gives the most tolerance under reducing environments but the material has the minimum oxygen flux [89]. Oxygen fluxes of BSCF5582, LSCF6428 and LSF731 as a function of temperature is given in Figure 2.6. It is worth mentioning that the data in Table 2.1 and Figure 2.6 is a strong function of temperature, pressure, membrane area and feed flow rates. Geometry has also a major impact on the oxygen flux and researchers use two types of membrane geometry, either disc or tube. The disc membrane is easy to make and has a constant temperature profile along the membrane however they have low area per unit volume compared to tubular ones.

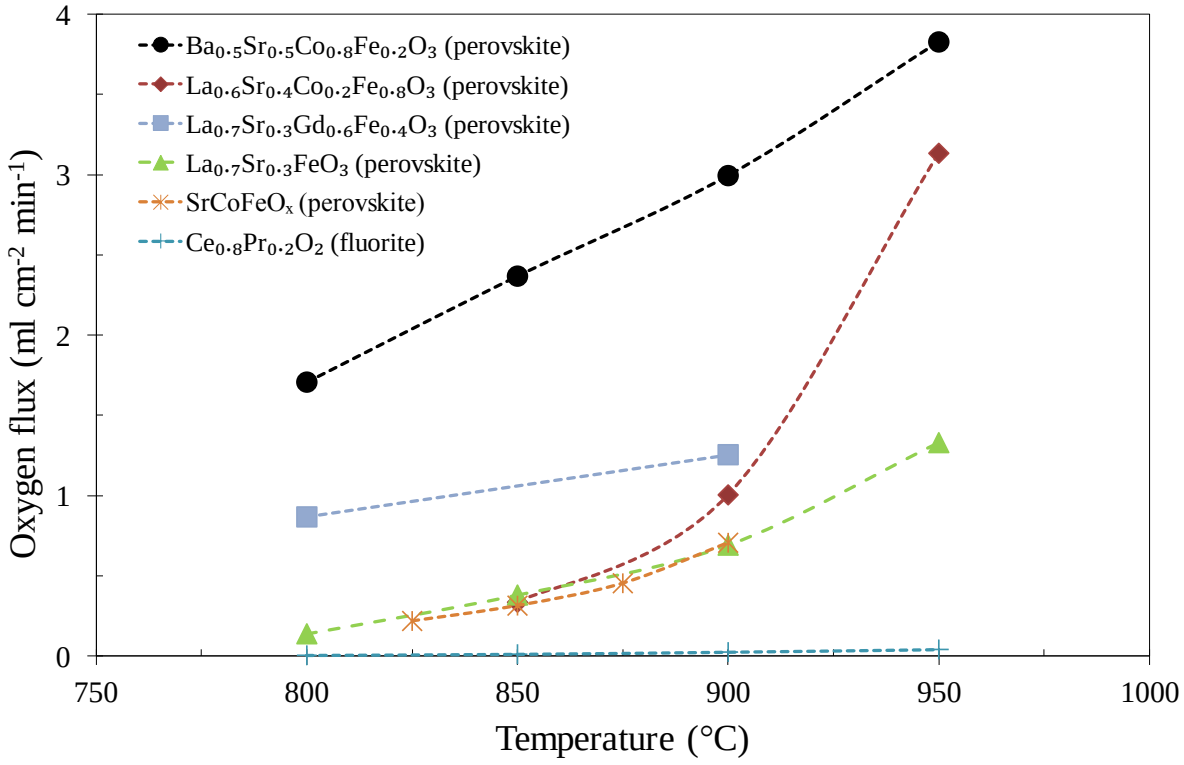

Figure 2.6. Oxygen flux of some fluorite and pervoskite membranes as a function of temeprature under atmospheric pressure [69, 73, 79, 89-93].

Industrially, tubular (also known as hollow fibre) membranes are more favourable because of the large area-to-volume ratio which results in greater oxygen flux.

2.4.3. *Fabrication*

Membrane fabrication plays an important role for determining the performance. High purity powder with particle size in sub-micrometers is preferable for good membrane preparation [94]. The fabrication process has three steps: 1) preparation of ceramic powder; 2) packing the powder into a disc or tubular shape; and 3) heat treatment to transfer the powder into a solid phase. A cost-effective way to prepare the powder is by conventional solid state reactions of raw materials in their stoichiometric basis. For example to prepare $La_{0.6}Sr_{0.4}Co_{0.2}Fe_{0.8}O_{3-\delta}$ powder, metal nitrates are mixed together and heated to a high temperature (e.g., 800°C) to remove nitrates by the following equation [95]:

$$0.6La(NO_3)_3 + 0.4Sr(NO_3)_2 + 0.2Co(NO_3)_2 + 0.8Fe(NO_3)_3 \rightarrow La_{0.6}Sr_{0.4}Co_{0.2}Fe_{0.8}O_{3-\delta} + 2.7N_2 + 0.5(13.2+\delta)O_2 \quad (2.13)$$

After that, the mixture is cooled down to room temperature and a grinder is implemented to decrease the particle size of the mixture to micrometers. Lower particle size gives larger surface area and therefore higher powder density [96]. Another way of preparing fine membrane powder is by sol-gel method where the raw materials are still mixed in their stiochiometric basis but with the addition of agents such as EDTA ($C_{10}H_{16}N_2O_8$), citric acid ($C_6H_8O_7$) and ammonia solution (NH_4NO_3) [95]. EDTA and citric acid acts as chelating agents for proper mixing and binding while ammonia balance the hydrogen number (pH) to 7. The mixture is heated then to a temperature of over 800°C to vaporise solutions and binders used during the participation reaction [25].

The second step is to pack the powder into either disc or tubular shape. For disc membranes, the powder is placed in a steel die where a mechanical press is used to compact the powder into a disc (also known as pellet) as show in Figure 2.7. On the other hand, to have a tubular membrane, usually extrusion technique is employed. This method is very useful for large production and currently used for production of bricks, tiles and furnace tubes [32]. The powder is mixed with additives such as binders or solvents to form a paste and then pressed in an extrusion die. Another common method for making tubular membranes is by the spinning technique. The powder is mixed with binders and plasticisers to form a paste and after that, it is transferred to a spinning apparatus where the precursor passes through a forced nozzle to

form the membrane as shown in Figure 2.7 [32]. The temperature is then heated slowly to vaporise the additives.

The last step for preparing the membrane is sintering which is a heat treatment to convert the compressed powder into a solid. Due to heat, internal diffusion will occur and this causes

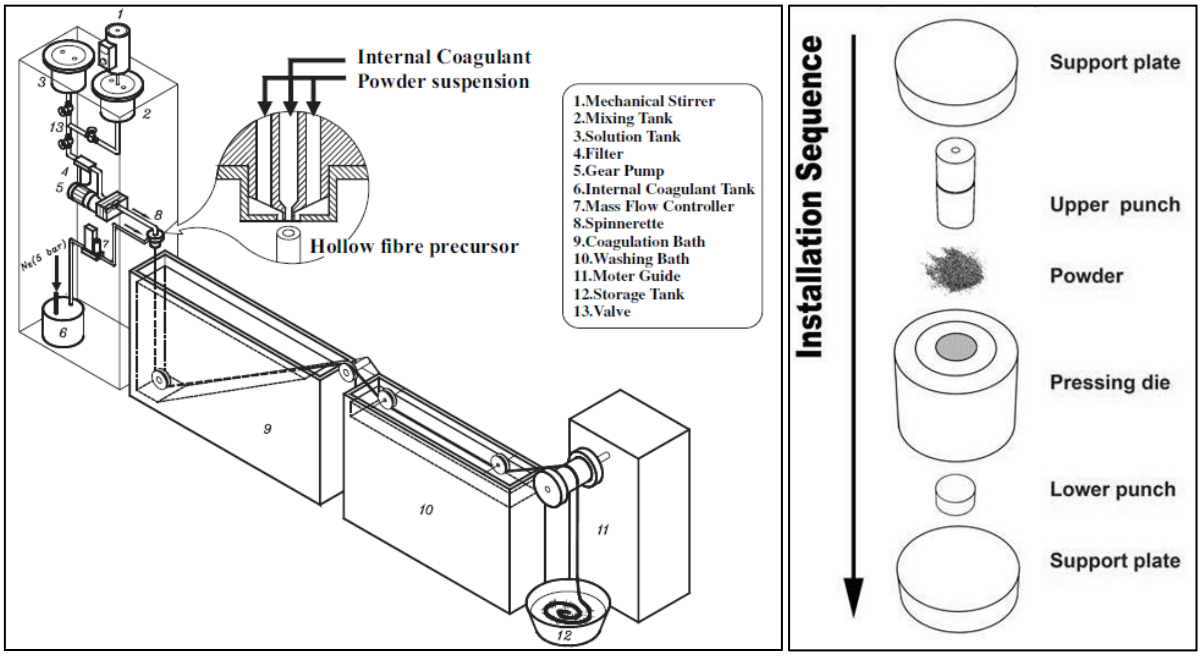

Figure 2.7. Fabrication of tubular (left) and disc (right) membranes from powder [32, 97].

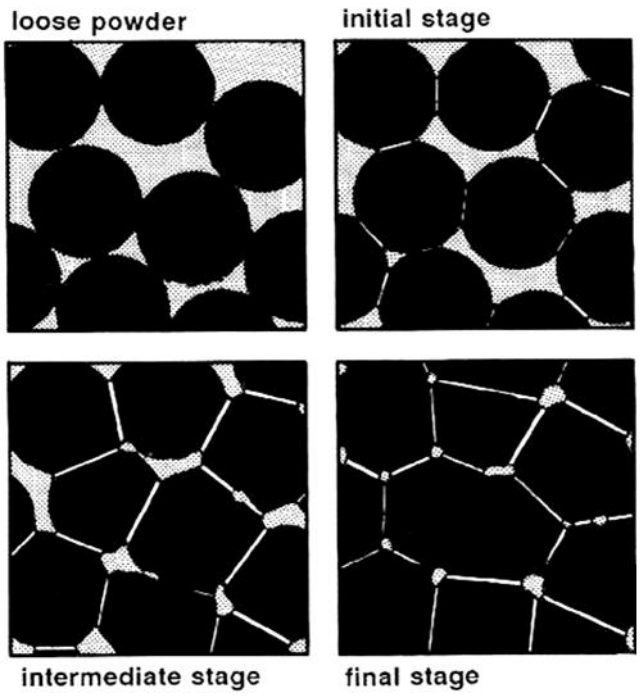

Figure 2.8. Sintering process to solidify the pressed membrane powder and reduce pores [98].

aggregation of particles thus increasing the bulk density as shown in Figure 2.8 [99]. The sintering process starts at two-thirds of the melting point of the membrane material and it is kept at this temperature for a specific time (e.g., 5 to 10 hours).

2.5 Hydrogen production

Hydrogen is the first, lightest element in the periodic table but yet it has the maximum energy. For example, combustion of 1 g of hydrogen gives energy of 141.9 kJ which is three times more compared to 1 g of methane. Hydrogen is considered as an environmentally friendly fuel because it only produces water when combusted. These unique features make hydrogen as the future fuel for transportation [100]. The demand is expected to increase sharply in the following years due to the availability of hydrogen-operated vehicles and trains [101, 102]. Furthermore, hydrogen is extensively used in ammonia synthesis to make fertilisers and in hydrodesulphurisation to remove sulphur impurities from diesel and gasoline [2]. The world trend is to use ultra-low-sulphur diesel containing 10 ppm instead of 500 ppm to reduce pollution and this is estimated to increase hydrogen consumption by 35% [103].

Hydrogen is a sustainable fuel meaning that it can be generated from other sources rather than the non-renewable fossil fuel. However, fossil fuel still remains the main source of hydrogen because other processes like biomass pyrolysis (thermal decomposition of crops, wood, animal waste, ..., etc) and electrolysis (decomposition of water by applying a current) are slow and energy intensive therefore unpractical for large production [104].

As indicated in Figure 2.9, fossil fuel accounts for 96% as the source for hydrogen generation while the remaining is for water electrolysis [105]. The figure also tells that almost half of today's hydrogen is produced from natural gas. Steam methane reforming (SMR) and partial-oxidation of methane (POM) are the two technologies for generating hydrogen [79].

Because of the process economy, steam methane reforming (SMR) is still the dominating method for hydrogen production [106]. The process is carried out at a high temperature of 800 to 1000°C and high pressure of 20 bar with a nickel-based catalyst [107]. Natural gas is fed, as a rich source of methane, to the reformer to react with steam as given below:

$$CH_{4_{(g)}} + H_2O_{(v)} \leftrightarrow CO_{(g)} + 3H_{2_{(g)}} \qquad \Delta H_r^o = 206 \text{ kJ mol}^{-1} \qquad (2.14)$$

positive heat of reaction (ΔH_r^o) indicates that the reaction requires energy to initiate and the reversible sign (↔) in the previous equation means that the formed hydrogen and carbon

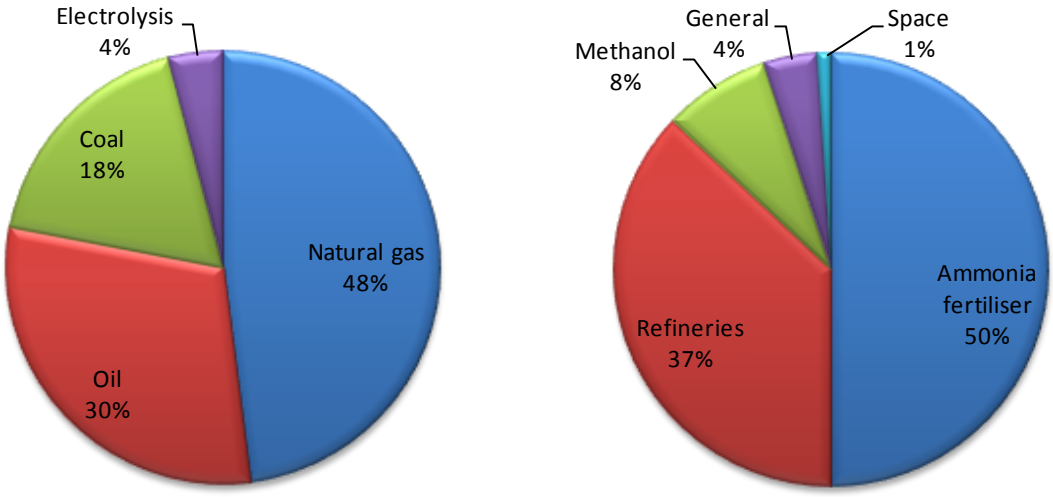

Figure 2.9. Sources to produce today's hydrogen (left) and large-scale uses of hydrogen (right) [108].

monoxide can react back to form methane and water. To increase hydrogen yield, carbon monoxide in Equation 2.14 can be converted to carbon dioxide and hydrogen through water-gas shift (WGS):

$$CO_{(g)} + H_2O_{(v)} \leftrightarrow CO_{2(g)} + H_{2(g)} \qquad \Delta H_r^o = -41 \text{ kJ mol}^{-1} \qquad (2.15)$$

the reaction in Equation 2.15 is exothermic and reversible. The produced hydrogen is then separated from carbon dioxide by pressure swing adsorption (PSA) containing zeolite where carbon dioxide is captured on the zeolite surface. The unit depends on the applied pressure, higher pressure will cause adsorption of carbon dioxide in zeolite and lower pressure will release carbon dioxide from zeolite [109]. The drawbacks of SMR are the high-energy requirement and the reversibility of some reactions [7, 110].

Partial-oxidation of methane provides another route for hydrogen formation by the reaction of methane with oxygen instead of steam:

$$CH_{4(g)} + {}^1/_2\, O_{2(g)} \rightarrow 2H_{2(g)} + CO_{(g)} \qquad \begin{matrix} \Delta H_r^o = -36 \text{ kJ mol}^{-1} \\ \Delta G_r^o = -36 \text{ kJ mol}^{-1} \end{matrix} \qquad (2.16)$$

Unlike Equation 2.14, the reaction in Equation 2.16 is exothermic and does not require heat. Complete oxidation of methane can also occur to form carbon dioxide and water instead of hydrogen:

$$CH_{4(g)} + 2O_{2(g)} \rightarrow CO_{2(g)} + 2H_2O_{(v)} \qquad \begin{matrix} \Delta H_r^o = -803 \text{ kJ mol}^{-1} \\ \Delta G_r^o = -801 \text{ kJ mol}^{-1} \end{matrix} \qquad (2.17)$$

Gibbs energy of reaction (ΔG_r^o) in Equation 2.17 is more negative than Equation 2.16 meanings that complete oxidation is more favourable. However, the reaction can be optimised for partial oxidation by the use of nickel or platinum catalyst [79, 111]. The catalyst also lowers the operating temperature to 350°C [112]. In spite of the advantages in POM such as exothermic reaction and no reversibility, the process is uneconomical compared to SMR because of the expensive cost of cryogenic distillation to supply ultra pure oxygen (99.999%) [8]. In cryogenic distillation, air is fed then cooled to an extreme low temperature of –183°C where nitrogen will liquefy and oxygen is separated [113]. Cryogenic distillation also requires high capital cost because of the necessity of special equipment (e.g, pipes, pumps, valves) that can withstand the extreme temperature [114].

2.6 MIEC membranes for hydrogen production

Mixed ionic-electronic conducting (MIEC) membranes can supply high purity oxygen as a feed for POM process. Compared to cryogenic distillation, it is estimated that MIEC membranes will cut down energy cost by 35% and this is because the membranes operate at high temperature instead of the extreme low temperature which is energy-intensive [9]. The membrane can also provide the surface area for the reaction. As given in Figure 2.10, POM process for hydrogen production consists of four steps: 1) pre-treatment of natural gas to reduce the amounts of sulphur, 2) cryogenic distillation to produce oxygen, 3) reactor where combustion takes place in presence of a catalyst, and 4) removal of carbon monoxide by PSA unit [6]. Employment of MIEC membrane not only eliminates the use of cryogenic distillation but also acts as a catalyst for the oxidation reaction [115-117].

When air is fed to the membrane, only oxygen diffuses and it then reacts with methane on the oxygen-lean surface to form hydrogen as shown in Figure 2.11. It is also possible that methane reacts directly with the ionic oxygen on the membrane surface as given in Equation (2.18 and the reaction is more rapid compared to molecular oxygen:

$$CH_{4(g)} + O_x^o \rightarrow 2H_{2(g)} + CO_{(g)} + 2V_O^{\bullet\bullet} + 4e^- \qquad (2.18)$$

Many researchers successfully used MIEC membranes for long-term POM. Wang et al. prepared tubular BSCF5582 membrane using extrusion method packed with LiLaNiO/Al_2O_3 catalyst then tested it for POM at 875°C. The membrane was stable for 500 h and methane conversion was 94% with carbon monoxide selectivity of 95% using a feed containing 80%

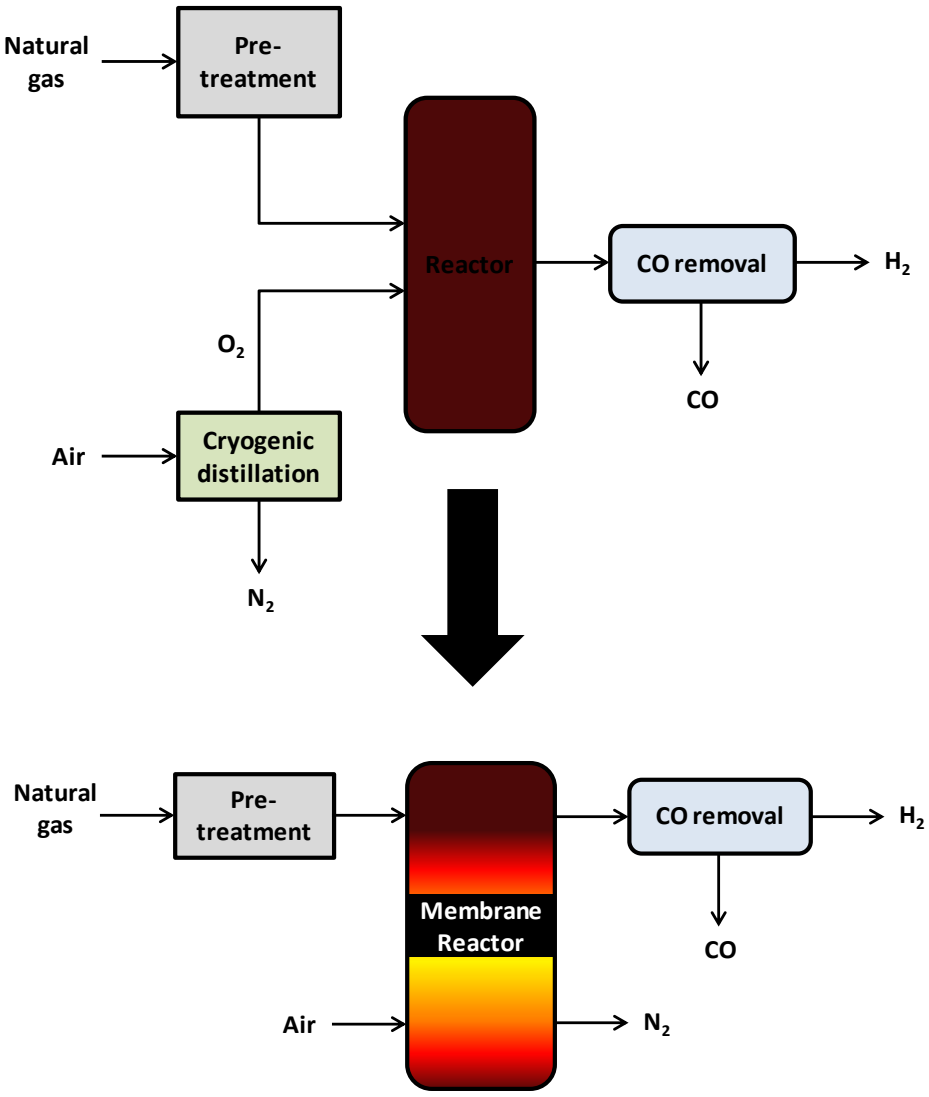

Figure 2.10. Modification of POM process by membrane reactor to supply oxygen and provide the catalytic sites for the oxidation.

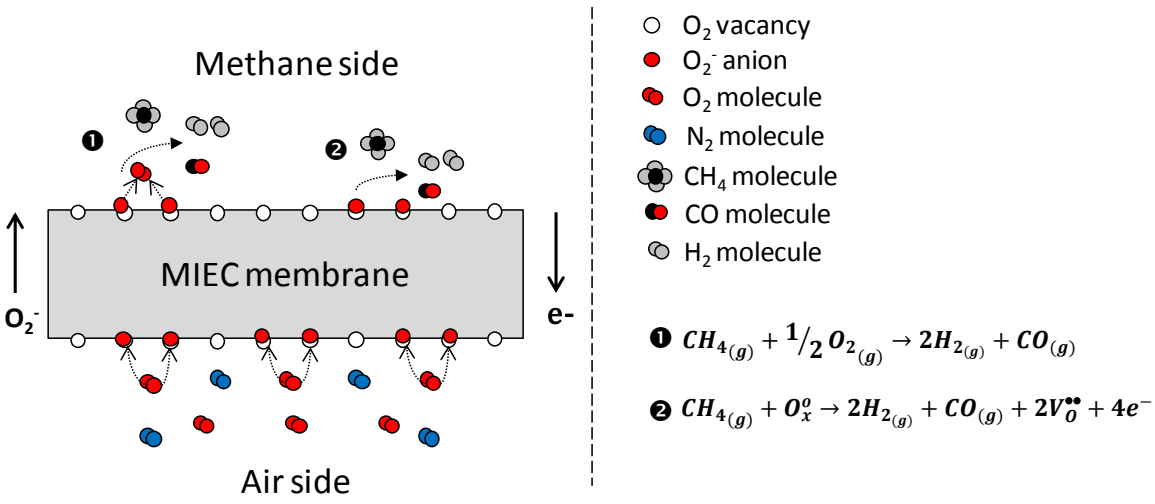

Figure 2.11. Partial-oxidation of methane using MIEC membrane reactor.

(mol) methane [118]. Methane conversion and carbon monoxide is defined by the following equations:

$$\text{CH}_4 \text{ conversion (\%)} = \frac{y_{(CH_4)_{in}} - y_{(CH_4)_{out}}}{y_{(CH_4)_{in}}} \times 100 \quad (2.19)$$

$$\text{CO selectivity (\%)} = \frac{y_{CO}}{y_{CO} + y_{CO_2}} \times 100 \quad (2.20)$$

where $y_{(CH_4)_{in}}$ and $y_{(CH_4)_{out}}$ are the mole fraction of methane in the inlet and outlet gas, respectively. y_{CO} and y_{CO_2} are the mole fraction of carbon monoxide and carbon dioxide in the outlet gas. Jin et al managed to implement LSCF6428 for methane oxidation and they used tubular membrane with nickel over alumina catalyst fed with 8% (mol) methane [119]. The conversion was 97% with carbon monoxide selectivity of 98%. The longest duration for POM was reported by Markov et al. with 7500 h of stable performance using a pure methane feed [11]. The conversion was steady at 99% with 90% carbon monoxide selectivity. Tubular membrane with 10% nickel catalyst was used for that study at 850°C.

2.7 Challenges in MIEC membrane

In spite of the discussed advantages of MIEC membranes, the technology is still not commercialised for industrial scale. The two major issues with these membranes are: sealing and chemical stability [48, 120, 121].

2.7.1. *Sealing*

MIEC membranes are operated at temperature over 800°C and many sealants melt at that temperature. The following properties should be met for sealant selection: a) withstand high temperature of 900°C, b) in the paste form so it can be applied easily, c) viscous to fill in gaps between the membrane and mount, d) inert and does not react, and e) matches thermal expansion of the mount to avoid cracking when heated or cooled [122]. Unfortunately there is no ‘magical’ sealant that works with all MIEC materials due to the difference in thermal expansion between MIEC materials. To seal the membrane, researches use three types of sealant: glass, ceramic and metallic.

Glass sealant is mainly made from pyrex containing silicon oxide (SiO_2) and it softens at temperature over 800°C covering the gap between the membrane and the mount resulting in a gas-tight seal [123]. However, glass continues in expanding with time and this may cover the

membrane and therefore it is not suitable for long-term operation [122]. On the other hand ceramic sealant is made from metal oxide (such as alumina or magnesia) and because of the thermal stability, it can be used even at 1300°C [124, 125]. The sealing material should be carefully selected because most of metal oxides act as catalysts and this will cause unwanted reactions. Another drawback of ceramic sealant is the strong bond and usually the membrane or support needs to be broken before taking the sample [122]. Metallic sealant such as gold or silver is widely used because of its good adhesion and inertness [8, 126, 127]. The sealant sometimes does not give a gas-tight system and therefore caps or springs are used to press the membrane during operation. The pressure should be correctly applied otherwise membrane cracking will occur.

Sealing the membrane using combination of glass and ceramic materials is also possible. The continuous expansion of glass can be slowed down by mixing it with a lower thermal expansion material such as ceramic. For instance, Qi et al. developed a water-based sealant consisting of 50% pyrex, 40% membrane powder and 10% sodium silicate and it showed zero leak for $SrCe_{0.95}Tb_{0.05}O_3$ membrane [122]. The authors also managed to seal other membrane materials such as $SrCe_{0.95}Tm_{0.05}O_3$, $La_{0.8}Sr_{0.2}Co_{0.6}Fe_{0.4}O_{3-\delta}$, $Ce_{1-2x}Zr_xPr_xO_{3-\delta}$ and $Bi_{1.5}Y_{0.3}Sm_{0.2}O_3$ using the composite sealant. Table 2.2 shows different sealing systems for MIEC membranes and the reported leakage rate.

Table 2.2. Sealants for MIEC membranes and the corresponding leaked oxygen to the total permeation flux.

Material	Temperature (°C)	Sealant	Leakage (%)	Ref.
$Ba_{0.5}Sr_{0.5}Co_{0.8}Fe_{0.2}O_{3-\delta}$	800 – 900	gold	2 – 3	[128]
$La_{0.6}Sr_{0.4}Co_{0.2}Fe_{0.8}O_{3-\delta}$	650 – 1000	gold	< 1	[129]
	750 – 950	Pyrex + silver	< 5	[130]
$La_{0.2}Sr_{0.8}Fe_{0.8}Co_{0.1}Cr_{0.2}O_{3-\delta}$	1000	gold	< 2	[131]
$La_{0.2}Ba_{0.8}Fe_{0.8}Co_{0.2}O_{3-\delta}$	850	gold	0 – 2	[8]
$La_{0.4}Sr_{0.6}FeO_{3-\delta}$	800	Glass	< 5	[132]
$SrCe_{0.95}Tb_{0.05}O_3$	600 – 950	Pyrex + ceramic	~ 0	[122]

2.7.2. Chemical stability

Another issue with MIEC membranes is the chemical stability to impurities. Industrial feedstock often contain impurities and purification of these gases is rather costly. For example, after treating natural gas for commercial use, the composition can still have 20% carbon dioxide and 0.02% (200 ppm) of hydrogen sulphide [12]. Unfortunately, few researchers investigated the impact of impurities on MIEC membrane and most of the studies focused on carbon dioxide. For instance, the promising BSCF5582 membrane had been tested for oxygen separation in presence of carbon dioxide and it showed very poor performance when carbon dioxide concentration was 15% [128, 133]. The oxygen flux immediately decreased to almost zero due to formation of strontium and barium carbonates by the following route [128, 134]:

$$Ba_{0.5}Sr_{0.5}Co_{0.8}Fe_{0.2}O_{3-\delta} + CO_2 \rightarrow Ba_{0.5}Sr_{0.5}CO_3 + 0.8CoO + \frac{0.2}{3}Fe_3O_4 + \left(\frac{1.4}{3} - \frac{\delta}{2}\right)O_2 \quad (2.21)$$

LSCF6428 was also tested for carbon dioxide and it showed better results than BSCF5582 because lanthanum was not susceptible to carbon [79]. Feed containing 20% carbon dioxide was introduced to LSCF6428 membrane and only 12% of oxygen flux was lost. However, in pure carbon dioxide environment, oxygen flux decreased to 24 – 34% and it was suggested that the drop in flux was due to adsorption of carbon dioxide on the membrane surface [79, 135, 136]. The absence of cobalt in LSF731 membrane gave better stability under carbon dioxide and the performance was 69 – 73% when pure carbon dioxide was fed [89].

Unlike carbon dioxide, sulphur dioxide showed more damage to MIEC membranes because of the corrosivity of the gas. For example, performance of $Sr_{0.5}Ca_{0.5}Mn_{0.8}Fe_{0.2}O_{3-\delta}$ (SCMF5582) membrane did not change even in pure carbon dioxide but the performance was instantly zero when 360 ppm of sulphur dioxide was presented [128]. Similarly, LSCF6428 suffered from sharp reduction in oxygen flux to 20% when it was exposed to 1773 ppm of sulphur dioxide [137]. The damage was permanent and the membrane could not recover even when sulphur dioxide was removed from the feed. The degradation in performance was related to formation of strontium sulphate reducing the membrane area [128, 137]. Currently, there are no studies on the influence of hydrogen sulphide on MIEC membranes during hydrogen production and this thesis investigates the impact.

2.8 Hydrogen sulphide

Hydrogen sulphide is a flammable gas, well-known for its rotten egg smell even in very low concentration of 25 ppb [138]. Naturally, it is emitted from volcanoes and by bacterial breakdown of organic wastes in sewers [139]. The gas is also found in natural gas as mentioned before. It is a human-made gas too and hydrodesulphurisation accounts as the major source for synthetic hydrogen sulphide [140]. Figure 2.12 shows hydrogen sulphide cycle.

Hydrogen sulphide has an impact on organisms, materials and environment. It is a very toxic gas and exposure to concentrations higher than 1000 ppm causes instant collapse or even death [141]. The workplace exposure limit (WEL) for 8 hours is 5 ppm [142]. The gas is also corrosive and it can cause damage to different materials. For example, steel and titanium alloys are susceptible to hydrogen sulphide attack due to the formation of metal sulphides therefore reducing the material thickness. Furthermore, the generated hydrogen by metal sulphide formation diffuses through the material in the atomic form and combines to form molecular hydrogen inside the material causing a pressure build-up leading to a fracture [143]. This phenomenon is known as sulphide stress cracking (SSC) and it can occur in pipelines made of steel during oil and gas transportation [144].

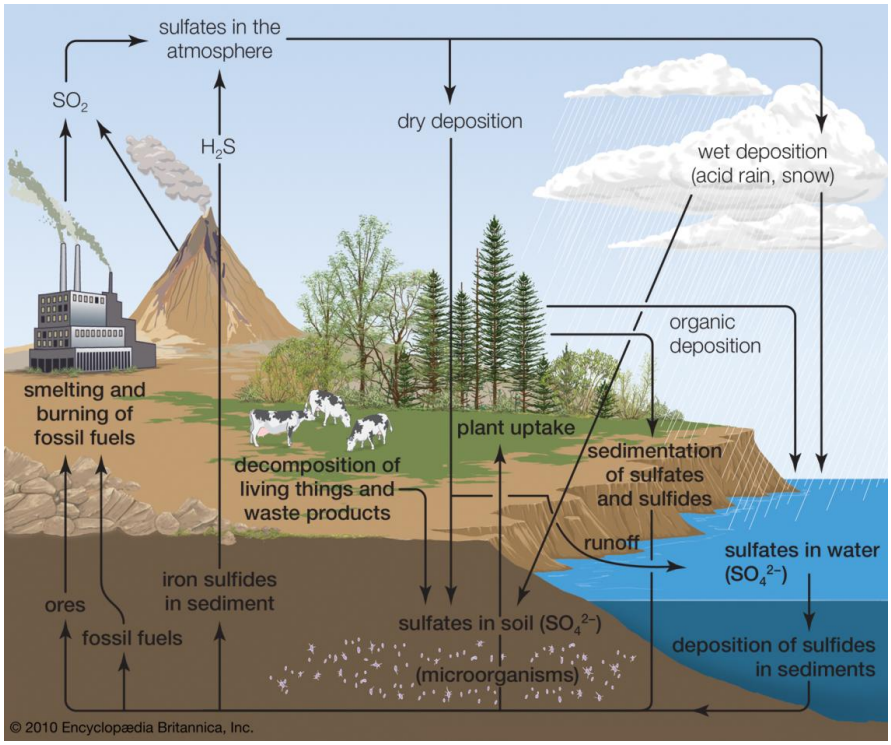

Figure 2.12. Hydrogen sulphide life cycle [145].

Moreover, hydrogen sulphide reacts with silver and copper to form silver and copper sulphates and this will alter the electronic conductivity leading to circuit failure [146, 147]. Environmentally, presence of hydrogen sulphide in the atmosphere contributes in formation of acid rain. Hydrogen sulphide is first combusted to sulphur dioxide and the later will react with water drop to form sulphuric acid. Acid rain attacks concrete, statues and metallic body of cars [148]. In addition, it increases the acidity in soils causing death in some trees [149].

In membrane processes, hydrogen sulphide has a noticeable impact on the membrane performance. For example, metallic membranes made of palladium for hydrogen production failed after exposing it to hydrogen sulphide of 6200 ppm due to adsorption of sulphur on the membrane surface causing internal stress and thus cracks [150]. For polymeric membranes made of polydimethyl siloxane for carbon dioxide separation, the existence of hydrogen sulphide (500 ppm) reduces the permeation by 8 to 15% due to sorption of hydrogen sulphide into the polymeric matrix [151]. On the other hand, ceramic membranes like zirconia and silica are very stable under hydrogen sulphide and they are actually used for hydrogen production by hydrogen sulphide decomposition [152]. Unfortunately, impact of hydrogen sulphide on MIEC membranes for POM is not reported yet.

In spite of the damage hydrogen sulphide can made, the gas is still useful. One of the uses is for identification of metal oxides. For example, reaction of hydrogen sulphide with lead oxide changes the colour of the powder to black while copper oxide changes to dark blue [153]. Other benefits of hydrogen sulphide are for separation of heavy water (^2H_2O) from normal water and a feedstock for making fertilisers, dyes and cosmetics [154]. Furthermore, sulphur bath containing hydrogen sulphide is used for the treatment of arthritis pain [155].

2.9 Summary

MIEC membranes are a promising technology for air separation compared to cryogenic distillation as they operate at lower energy. As an application, the membranes can be used for methane oxidation to produce hydrogen. In addition to oxygen separation, the membranes can act as catalysts for partial-oxidation of methane. In literature, the membranes had been tested for long-term methane oxidation and they showed very stable performance. However, all of the studies were conducted using methane with no sulphur impurities. In industry, natural gas will be used as a source of methane and it usually contains amounts of hydrogen sulphide even after the treatment. Based on the previous section, it is expected for hydrogen sulphide to

cause a significant change on the membrane performance due to the presence of some vulnerable metals in the membrane material. In this study, changes of the membrane performance for air separation and methane oxidation due to hydrogen sulphide impurity were investigated. Other objectives were to propose a mechanism for the poisoning and try to regenerate the membrane after the poisoning.

Chapter 3: Methodology

Chapter 3: Methodology

The purpose of this research is to improve current technologies for hydrogen production by implementing the high efficiency, energy-saving ceramic membranes. Mixed ionic-electronic conducting (MIEC) membranes have been well studied for long-term hydrogen production and the results were promising as mentioned in chapter 2. Before commercialisation, the membranes should be further evaluated using industrial feeds rather than pure ones. The aim of this study is to investigate the impact of hydrogen sulphide impurity on the membrane behaviour during air separation and methane oxidation. To achieve that, the membrane material should be first selected and then the membrane is fabricated. The next steps are to design the reactor and choose a sealant. Other steps are to select the composition of feed gases, pick up gas analysis technique and decide which characterisation technique to use. The last step is to list the required experiments to study hydrogen sulphide poisoning mechanism. The general approach is given in Figure 3.1.

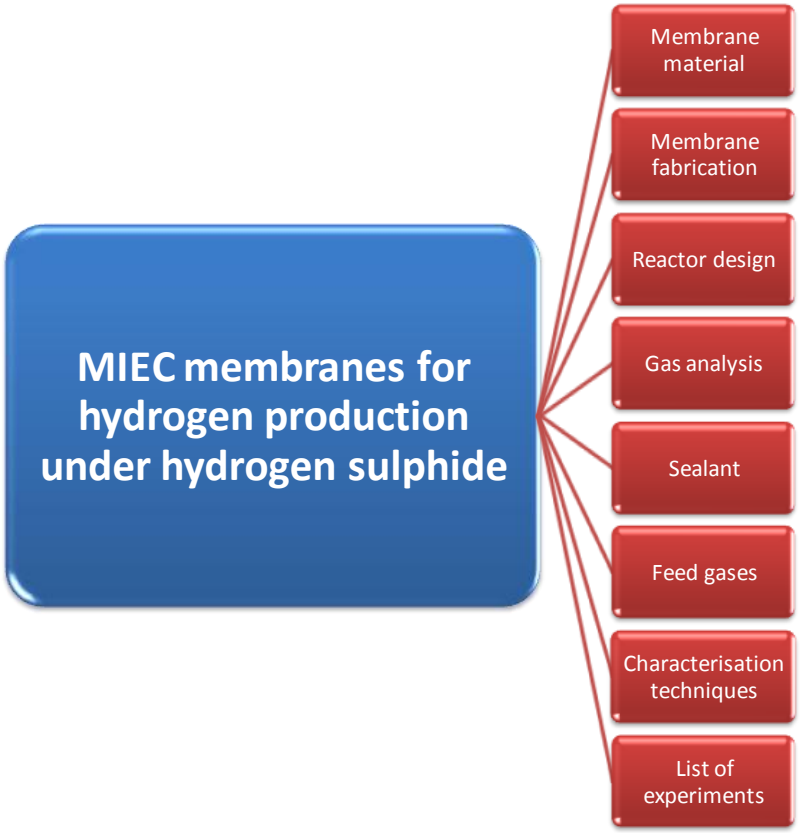

Figure 3.1. Required steps to studysurf hydrogen sulphide poisoning on MIEC membranes for hydrogen production.

3.1 Membrane material

In literature, there are hundreds of MIEC materials and it is challenging to decide which one to use. To narrow the range and make the selection more precise, the material should meet the following conditions: a) has oxygen flux higher than 1 ml cm^{-2} min^{-1}; b) tested for hydrogen production by partial-oxidation of methane; c) has been exposed to some impurities in feedstock. Applying the criteria will result in three groups: $Ba_{1-x}Sr_xCo_{1-y}Fe_yO_{3-\delta}$ (BSCF), $La_{1-x}Sr_xCo_{1-y}Fe_yO_{3-\delta}$ (LSCF) and $La_{1-x}Sr_xFeO_{3-\delta}$ (LSF) [11, 68, 69, 118, 119]. As discussed in chapter 2, BSCF has the highest permeation but lowest stability under carbon dioxide whereas LSF showed best stability but permeation was the lowest. Besides, LSCF gave a balanced performance between stability and permeation, therefore, LSCF had been considered for this study. The next step is to define the composition of $La_{1-x}Sr_xCo_{1-y}Fe_yO_{3-\delta}$ where x and y vary from 0.01 to 0.99. Different compositions such as LSCF6428, LSCF2882, LSCF8264, LSCF8228, LSCF2828, ..., etc have been reported in literature and LSCF6428 showed a balanced performance and accordingly it was picked up [156, 157].

3.2 Membrane fabrication

Disc module was chosen instead of tube because it was easier to fabricate and has isothermal temperature zone. Membrane powder was purchased from Praxair and has 99.9% purity with low particle size ranging from 0.4 to 3.9 µm. The bulk density (density including void volume without compaction) was 1.27 g cm^{-3}. To prepare the membrane, 1.5 g of the powder was weighed then transferred into a steel die of 2 cm in diameter. The die was then inserted in a mechanical press (Atlas Power T25) where compression was applied. The pressure was 3 tonnes-force which equals to 93 MPa. Following, the membrane was carefully taken from the die and then inserted inside an oven (Carbolite RHF1500) to sinter the membrane. Temperature of 1250°C was set with ramping rate of 1°C min^{-1}. The membrane was then kept for 5 hours and then back to room temperature with the same ramping rate. This procedure was proven to produce dense, porous-free membranes [158-160]. One way to confirm that the membrane was dense is by measuring its relative density after the fabrication. The procedure is based on Archimedes method by immersing the membrane inside water in a graduated cylinder then observing the change in volume. The difference in volume before and after immersing the membrane will give its volume. Then, the density is calculated by dividing mass (m) over volume (V):

$$\rho = \frac{m}{V} \tag{3.1}$$

The relative density (ρ_r) is defined by:

$$\rho_r = \frac{\rho}{\rho_{theo}} \times 100 \tag{3.2}$$

where (ρ_{theo}) is the theoretical density which is the maximum density by assuming 100% single-crystal structure [161]. It is calculated by:

$$\rho_{theo} = \frac{M_{wt} \times Z}{V \times N_A} \tag{3.3}$$

where M_{wt}, Z, V, N_A are the molecular weight of the perovskite, number of atoms per unit cell, unit cell volume and Avogadro's number. The value of Z is 1 for cubic structure, 2 for body-centred cubic and 6 for hexagonal close-packed structure [162]. Unit cell volume is determined by a characterisation technique called x-ray diffraction (discussed later) [163]. For LSCF6428, it has rhombohedral structure with hexagonal structure (Z = 6) and unit volume of 3.49 ×1 0^{-22} cm^3. Using these numbers in Equation 3.3 gives theoretical density of 6.36 g cm^{-3} [159, 164, 165]. To have a dense membrane, the relative density should be at least 90% and ours had a value of over 93% [166]. The final membrane has diameter of 1.6 cm and thickness of 1.1 mm.

3.3 Reactor design

The reactor was built in the school workshop and made from aluminium body, alumina tubes and quartz cover. These materials withstand high temperature and resist hydrogen sulphide [14]. As shown in Figure 3.2, the reactor consists of a table and chamber. The overall dimension of the reactor is 43 cm high and 12 cm wide. The chamber itself has a height of 32 cm and diameter of 3.5 cm. The reactor has three inlets located at the bottom: one for air, another for methane and last one for thermocouple. These inlets have diameter of 0.3 cm. The reactor has also two outlets, one for air and the other one for the product gas as shown in Figure 3.2.

The disc membrane was placed on the top of the alumina support tube (air side housing in the figure) and was sealed with a proper material which will be discussed later. Quartz houses the methane side and viton o-ring (EAP Seals) was used to hold quartz tightly and prevent leakage. The o-ring was also used to hold alumina air-side housing tube. The membrane was

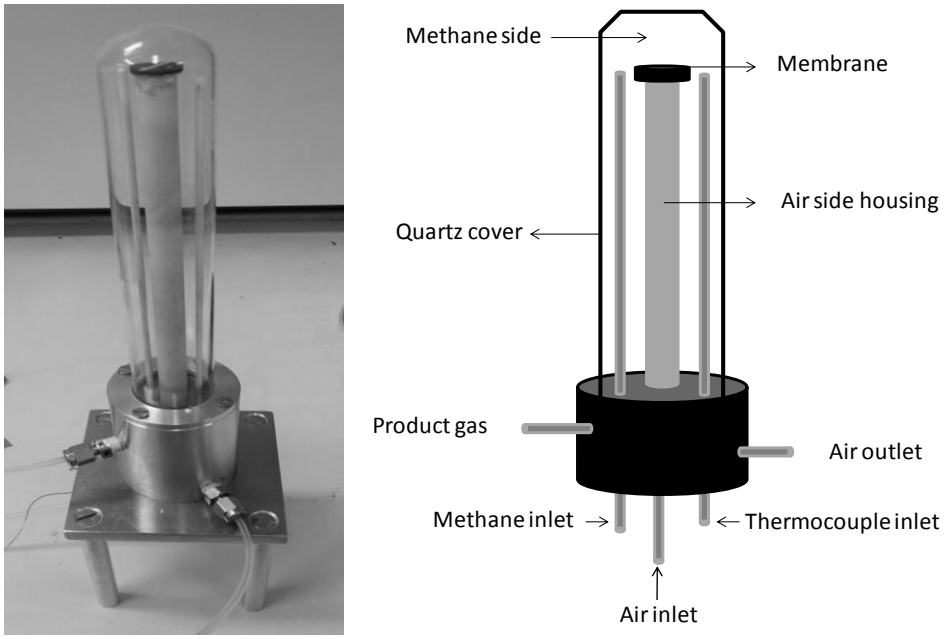

Figure 3.2. Image of the reactor (left) and schematic diagram (right).

heated to 900°C using a furnace (Vecstar VCTF1). This temperature was chosen because LSCF6428 membrane gives high fluxes at 850°C and above [96, 119, 130, 167, 168].

3.4 Gas analysis

Outlet gas from the reactor was analysed by a gas chromatograph, GC (Varian 3800). The concept is based on retention time where a sample is passed through a column and each compound has different retention time depending on the molecular size and the interaction with the column [169]. For example, if the sample gas does not react with the column, small molecules will cross faster than the larger ones and therefore their retention time is shorter. The gas is then identified and quantified by a detector. There are different detectors available based on the analysed gases but the common one is the thermal conductivity detector (TCD) [170]. It uses a filament made from tungsten-rhenium heated by a current. Carrier gas such as helium or argon is always fed to the filament to keep the temperature constant. When the sample is injected, heat conductivity will vary and this changes the filament temperature. The change in temperature can be then related to the gas and its quantity [171]. Figure 3.3 shows GC components.

Before using a GC, the following steps are required: a) installation of a column, b) picking up a carrier gas, and c) performing calibration. Selection of a column depends strongly on the analysed gases. In this study, hydrogen was produced by oxidising methane using air in

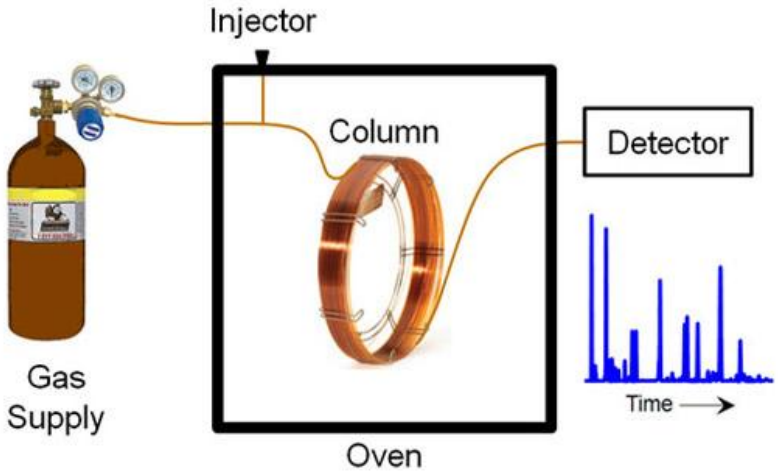

Figure 3.3. Components of gas chromatograph (courtesy of Agilent).

presence of hydrogen sulphide so the outlet gas might contain hydrogen, oxygen, nitrogen, carbon monoxide, carbon dioxide, water, methane, hydrogen sulphide and sulphur dioxide. Unfortunately, there is no single column that can measure all the gases. So, the following columns had been used: a) Molsieve 5A (Restek) made of zeolite bed capable of detecting oxygen and nitrogen with excellent resolution, and b) Shincarbon (Restek) made of special carbon molecular sieve suitable for measuring hydrogen, methane, carbon monoxide and carbon dioxide.

Molsieve 5A column was calibrated using a cylinder having 2% (mol) oxygen and 2% (mol) nitrogen and this is within the expected range of concentrations in the outlet gas. To make sure that the GC was well calibrated, the column was tested for 0.5%, 1% and 20% (mol) oxygen and average relative error was less than 4%. On the other hand, Shincarbon column was calibrated with 2% hydrogen, 2% methane, 2% carbon monoxide and 2% (mol) carbon dioxide. The GC was checked with a cylinder having 1% methane, 1% carbon monoxide and 1% (mol) carbon dioxide and the relative error was less than 3%. In all experiments, argon was the carrier gas.

As discussed, the GC was capable of measuring oxygen, nitrogen, hydrogen, methane, carbon monoxide and carbon dioxide but the remaining sulphur gases (hydrogen sulphide and sulphur dioxide) could not be detected as they require special detector and column. Accordingly, another technique was used to measure sulphur gas called calorimetric tubes. Gas sample was manually collected in a plastic bag and then pumped to a graded tube (Dräger) as shown in Figure 3.4. The tube was packed with metal oxide where reaction of hydrogen sulphide or sulphur dioxide will form metal sulphide and thus changing the colour

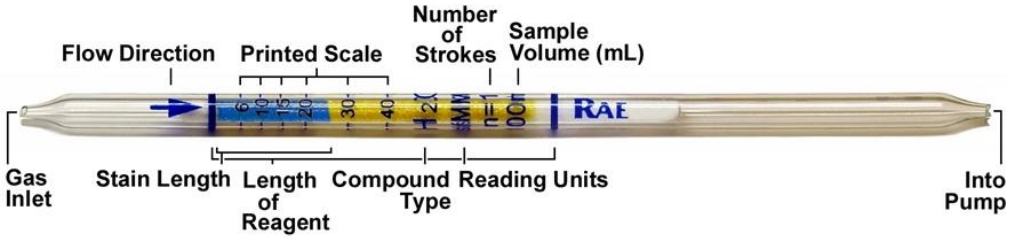

Figure 3.4. Calorimetric tubes for gas analysis (Courtesy of RAE Systems, Honeywell).

of the tube. For example, to measure hydrogen sulphide concentration, a sample is injected to a tube containing copper oxide and reaction of copper with hydrogen sulphide results in formation of copper sulphide and this changes the bed colour from white to brown.

3.5 Sealant

Sealing high temperature membrane for a long term operation is still challenging. As mentioned in chapter 2, the common sealants for MIEC membranes are metal, glass and ceramic. Combination of two sealants like glass and metal is also possible. To determine that the sealant provided a gas-tight system, synthetic air (BOC) was fed to the membrane and both nitrogen and oxygen were monitored in the methane side using GC. Theoretically, to have a gas-tight system, nitrogen should not be detected at all in the methane side. However, there is a chance that nitrogen can pass through the sealant or pores of the membrane. In literature, the acceptable nitrogen leak diverges from 0 to 5% (mol) [8, 122, 128-132]. Because this study involved traces of hydrogen sulphide, the membrane reactor should be gas-tight as much as possible and accordingly, the experiment was considered a failure if nitrogen content in the methane side was higher than 0.5% (mol).

The starting sealant was gold paste (NextTech Materials Au-I) preferred over silver because of the higher melting point and inert properties [172]. The sealant consisted of over than 70% gold and was applied by a brush over the alumina support as demonstrated in Figure 3.5. The thickness of the applied sealant was about 0.5 mm and after that, the membrane was inserted and gently squeezed. It was kept to dry at room temperature for 24 h. After that, alumina support was fit inside the reactor and heated to 900°C by a ramp of 1°C min^{-1} as recommended by the supplier. Nitrogen was monitored however the value was in the range of 0.5 to 1% (mol) indicating a failure. The experiment was repeated but nitrogen leak was still high. In literature, some authors managed to seal the membrane with gold but with applied

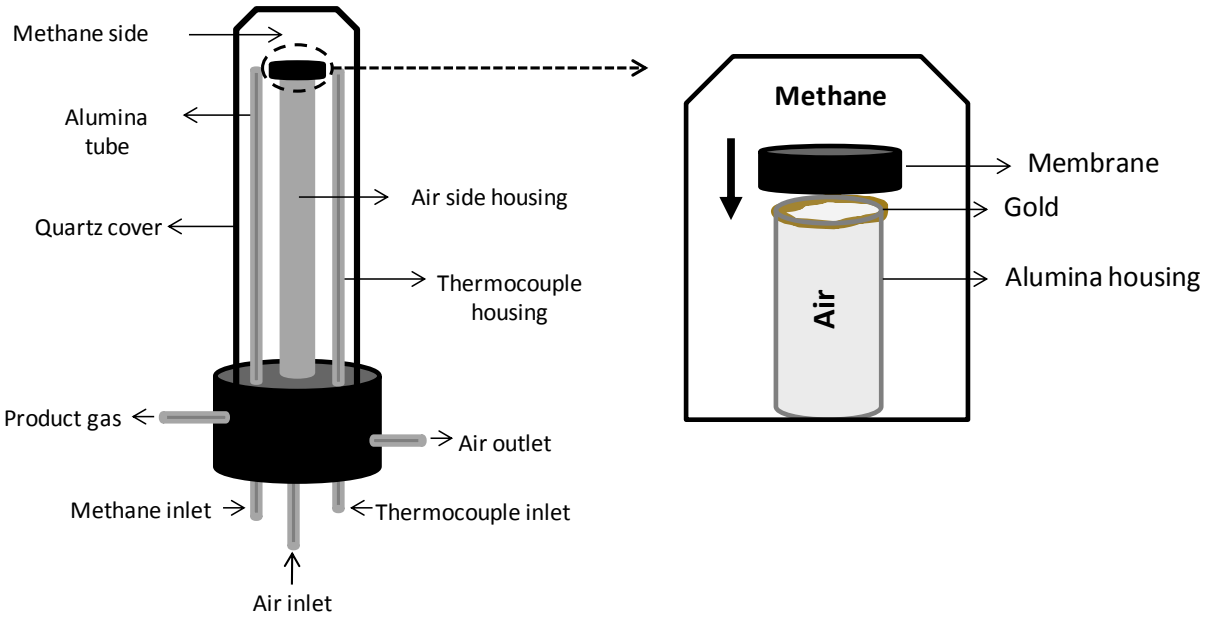

Figure 3.5. Applying gold paste to seal LSCF6428 membrane for high temperature operation.

pressure [8, 128, 129, 131]. This step requires a special reactor design and it is difficult to determine the optimum pressure. Also, the applied pressure with corrosive environment could cause further stress on the membrane and this may alter the results.

The next sealant to try was ceramic magnesium oxide (Aremco 571). It was applied the same way as gold (Figure 3.5). The sealant was then dried at room temperature for few hours then heated to 100°C as suggested by the manufacturer. When the reactor was heated to 900°C, the leak was unacceptable because it was over 1% (mol) nitrogen. The experiment was repeated once but the leak was still over 1% (mol). After terminating the experiment, the membrane was examined and it had cracks. Thermal mismatch between membrane, sealant and support could lead to that. Another drawback of ceramic sealant was the difficulty in removing the membrane from the support due to the strong bond. This gave no choice but to break the membrane and the support.

The third sealant was waterglass (Aremco 571L) containing 30% sodium silicate. The membrane was sealed by applying a thin layer of waterglass over the support same as previously. After that, it was heated to 100°C as suggested by the supplier. The sealant was then tested at 900°C and nitrogen leak was 0.2% (mol) nitrogen which is acceptable. However, oxygen concentration in the product gas was 0.1% (mol) indicating that the membrane is not permeating oxygen. Indeed, after operation, the glass expanded widely and covered the membrane. Also, the adhesion between the membrane and the support was poor.

As indicated, metallic, glass and ceramic sealants did not work and it was the time to try the composite ones. Qi et al developed a glass-ceramic sealant and tested it for LSCF8264 membrane and he stated that the leak was zero [122]. The sealant composed of 50% Pyrex (made by crushing burette), 40% LSCF8264 and 10% sodium aluminate ($Na_2O.Al_2O_3$). The powders were mixed and water was added until thick paste was formed. The paste weighing approximately one gram was applied over alumina support and the membrane was inserted gently. After that, the reactor was heated to 900°C. This procedure was tried once in our study for LSCF6428 membrane and the leak was 0.2% (mol) nitrogen. However, oxygen content in the outlet gas was still low (0.1% mol) suggesting that glass spread and blocked the membrane area.

As discussed, the problem with gold is the requirement of pressure and the issue with glass is the rapid expansion which covers the membrane. In this study, a new gold-glass-ceramic sealant had been developed and tested for long-term operation. Gold sealant was first applied over alumina support and kept for 24 h as demonstrated previously. After that, 0.2 g of LSCF6428 powder was mixed with 0.8 g of waterglass to form a black paste. The paste of 1 g was added by a brush on the sides of the support and membrane as given in Figure 3.6. The membrane was kept to dry at room temperature for a few hours then heated to 100°C for one hour. The membrane is now ready to use. At the operating temperature of 900°C, the waterglass expanded to fill in the gaps in gold sealant and mixing glass with LSCF6428 decelerates the expansion rate. Also, presence of gold acts as a barrier to prevent it from reaching the active area as demonstrated in Figure 3.7. The sealant was evaluated for 963 h and nitrogen leak was 0.01% (mol) and oxygen concentration was higher than 0.2% mole (Figure A.1, Appendix). After the long run, the membrane was examined and it did not suffer from any glass blockage as shown in Figure 3.7. Table 3.1 compares the new sealant with the ones reported in literature for long-term experiments.

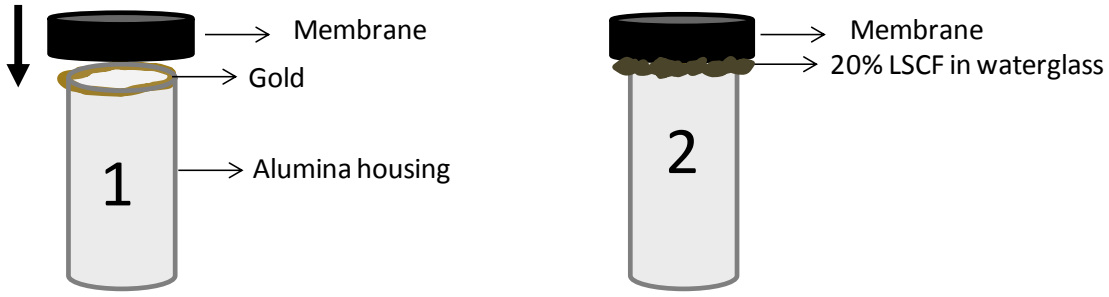

Figure 3.6. Two steps for sealing LSCF6428 membrane with gold-ceramic-glass sealant.

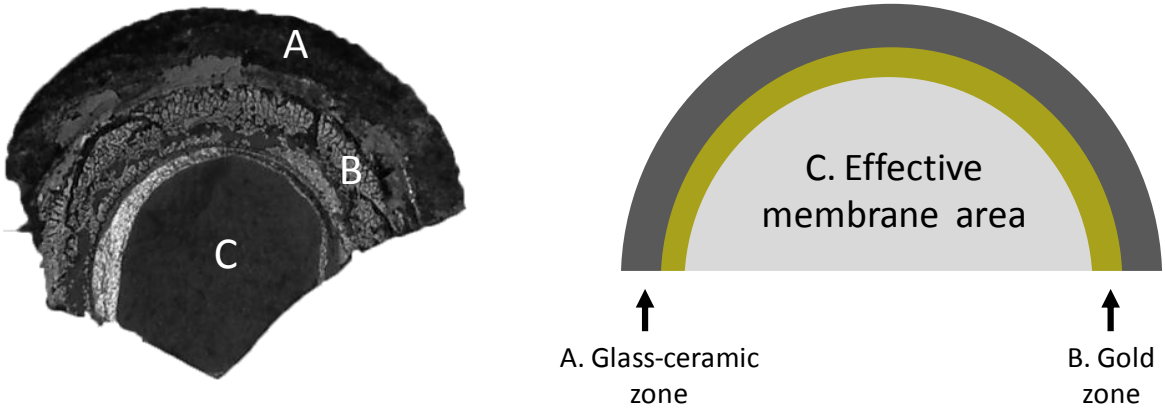

Figure 3.7. Cross section of LSCF6428 membrane after using gold-ceramic-glass sealant for 963 h.

Table 3.1 Methods to seal LSCF6428 membrane at 900°C for long-term operation.

Sealant	N_2 leak (mol %)	Duration (h)	Ref.
Gold paste and 20% LSCF in waterglass	0.01	963	This study
Gold gasket	< 0.04	336	[129]
Pyrex ring	< 5	160	[130]

3.6 Feed gases

Synthetic air (BOC zero-grade) was chosen as a source of oxygen and it contained 21% oxygen and 79% (mol) nitrogen with less than 5 ppm impurities such as water and carbon dioxide. Due to high flammability of methane and working at high temperature of 900°C, the concentration has been diluted to 1% (mol) methane (BOC) and argon was selected as the inert gas. Hydrogen sulphide concentration was 200 ppm and this is the maximum allowable limit in natural gas as discussed in chapter 2. The maximum concentration will accelerate poisoning thus shortening the exposure duration and this kind of experiment is called ageing. All cylinders have a physical size of 50 L and the pressure inside the cylinder was 200 bar. Regulators (BOC) were fitted on the cylinders to reduce the outlet pressure to 5 bar so that mass flow controllers (MFC, Brooks 5580) can operate properly. MFC controls the volume flow rate in ml min^{-1} of the gases at atmospheric pressure based on the thermal conductivity. For example, if no gases were fed, the filament temperature inside MFC would become constant and maximum. But, introduction of the gases would cause a drop in the filament temperature and this can be related to the flow rate [173]. Flow rates of 20 ml min^{-1} were used for feed gases and this number has been used by many authors for long-term experiments

[130, 174]. Gases were transported from the cylinders to the reactor through Swagelok perfluoroalkoxy (PFA) tube. This material has high chemical tolerance and can be operated up to 19 bar and 200°C.

3.7 Characterisation techniques

Before and after operation, the membrane needs to be examined by characterisation techniques to observe the changes. This will help in understanding how the membrane responded during hydrogen sulphide poisoning. In this section, advanced techniques such as scanning electron microscopy (SEM), electron-dispersion x-ray spectroscopy (EDX), x-ray diffraction (XRD) and x-ray photoelectron spectroscopy are discussed. All these techniques had been implemented to characterise the membrane.

3.7.1. *Scanning electron microscopy (SEM)*

Scanning electron microscopy (SEM) gives electronic images of the material with very high resolution in nanometer [175]. It shows the morphology and topography of the surface. Morphology is related to the size, shape and phases distribution along the surface while topography is related to the surface height [176]. SEM is also capable of showing the homogeneity, size and shape of the grains [32]. This characterisation technique is based on concentrating an electron beam on the sample surface and this will cause release of secondary electrons from the sample. These secondary electrons are collected by a detector and analysed to an image as shown in Figure 3.8 [177]. In this work, the technique helped in determining if the fabricated membrane was dense by examining the grains. It also indicated if secondary phases were formed after hydrogen sulphide exposure.

3.7.2. *Electron-dispersion x-ray spectroscopy (EDS)*

The second characterisation technique is the electron-dispersion x-ray spectroscopy (EDS) which uses the same components as SEM and it is usually integrated within the equipment. The technique is for measuring the elemental composition of the sample. The electron beam used in SEM will result in releasing x-rays from the sample due to the collision between the

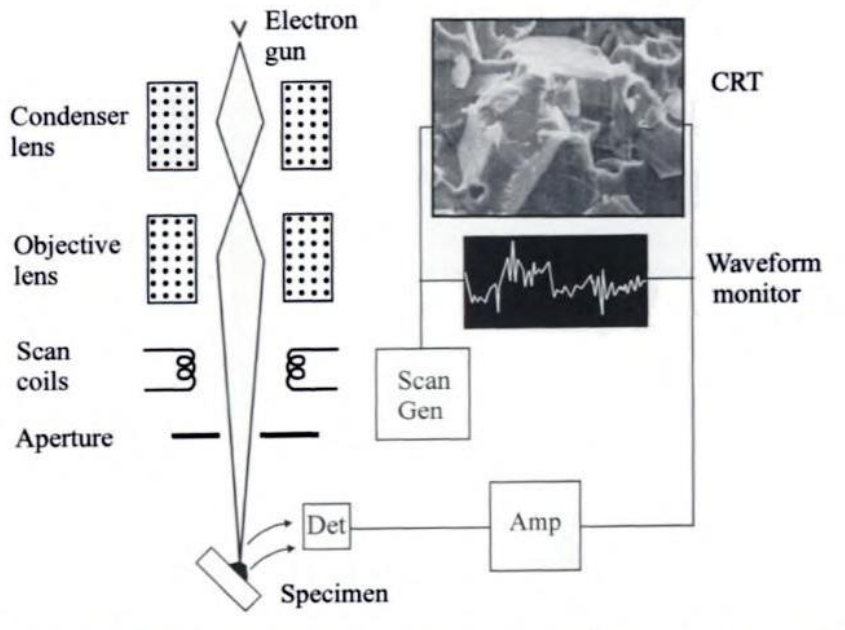

Figure 3.8. Cocept of scanning electron microscope (SEM) [178].

high energy incoming electrons and the atoms [179]. Each element has a unique x-ray spectrum and this helps in identifying the released x-rays from the sample [180]. For this work, EDS was used to determine if sulphur had been adsorbed on the membrane surface and if the elemental composition of the membrane was changed.

3.7.3. *X-ray diffraction (XRD)*

To identify phases and crystalline changes of a sample, x-ray diffraction (XRD) is employed [32]. It is also capable of determining the chemical formula of the phases. XRD is based on sending a beam of x-ray to the sample by heating a metallic filament like tungsten and the scattered x-rays from the sample are then detected and analysed [181]. By knowing the wave length, intensity, and angle, diffraction peaks (intensity VS angle) can be generated and they are unique for every material. By comparing these diffracted peaks with reference ones, the chemical composition of the sample can be identified. The peak height, area and width also represent the crystalline size. The instrument is composed of a generator, sample holder and detector as shown in Figure 3.9. In this study, XRD revealed if the perovskite structure had changed after exposing the membrane to hydrogen sulphide. Also, the chemical composition of the secondary phases can be identified.

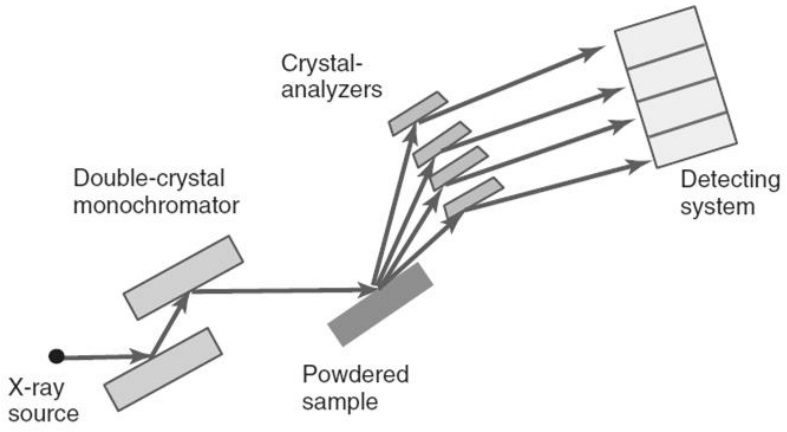

Figure 3.9. Schematic diagram of x-ray diffraction (XRD) [182].

3.7.4. *X-ray photoelectron spectroscopy (XPS)*

Another way to determine the elemental composition is by x-ray photoelectron spectroscopy. The technique has an advantage over EDS as it gives the elemental composition with respect to the membrane depth with better accuracy [179]. Furthermore, EDS measures the bulk surface in micrometers deep while XPS measures nanometers of the surface [183]. The method is based on concentrating a beam of x-ray on the sample and the released electrons and kinetic energy are measured as given in Figure 3.10 [184]. Each element has a specific binding energy and this is useful in identifying the element. The number of measured electrons referred to the amount of element found in the sample. Oxidation state of the element can be also measured using XPS.

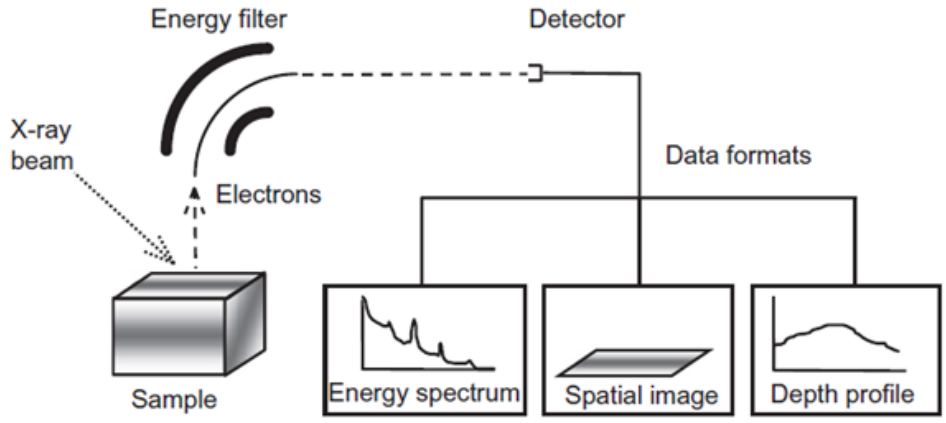

Figure 3.10. XPS for elemental compositon of the membrane surface [185].

In this work, XPS confirmed if sulphur was adsorbed on the membrane surface and it determined the oxidation state of sulphur. For example, if sulphur is in the form of elemental sulphur (S), sulphite (SO_3^{-2}) or sulphate (SO_4^{-2}).

3.8 List of experiments

The main aim of this thesis is to study the influence of hydrogen sulphide on the performance of LSCF6428 membrane for hydrogen production. To understand the impact more closely, the study had been divided into two parts: one for air separation (chapter 4 and 5) and the other one for methane oxidation (chapter 6). In the first part, LSCF6428 membrane was used to produce oxygen only from air in presence of hydrogen sulphide. The first part gave better understanding about the poisoning mechanism because in partial-oxidation of methane there are other gases like methane, hydrogen, carbon monoxide, carbon dioxide and water and they may complicate the mechanism. The objectives of air separation chapters are to determine the poisoning mechanism and investigate the parameters that accelerate it. To achieve that, the following experiments were carried out:

- Oxygen production using LSCF6428 membrane in no sulphur.
- Changes of oxygen flux after introduction of hydrogen sulphide.
- Regeneration of the membrane after sulphur poisoning.
- Role of operating conditions on accelerating the poisoning mechanism.

In chapter 6 where hydrogen was produced by LSCF6428 membrane, the goal is to observe the changes in membrane performance during hydrogen sulphide introduction. The required experiments were:

- Partial-oxidation of methane using LSCF6428 membrane in no sulphur.
- Changes of the membrane performance during hydrogen sulphide exposure.
- Recovery of the membrane after sulphur poisoning.

Another objective of this study is to modify the membrane for better stability under hydrogen sulphide, if possible. The used approaches were:

- Introduction of a new material during membrane fabrication.
- Addition of a protective layer or guard bed over the membrane.

In the following chapter, oxygen flux of LSCF6428 membrane was measured in sulphur free environment. After that, hydrogen sulphide was introduced and changes were determined.

Chapter 4: LSCF6428 membrane for air separation under hydrogen sulphide impurity

Chapter 4: LSCF6428 Membrane for Air Separation under Hydrogen Sulphide Impurity

This chapter investigates the influence of hydrogen sulphide impurity on air separation using LSCF6428 membrane. The chapter proposes a general mechanism for hydrogen sulphide poisoning. It also discusses methods to restore the membrane after the attack.

4.1 Air separation in no sulphur

In this section, long-term operation of LSCF6428 membrane for oxygen production was performed without the presence of hydrogen sulphide impurity. This experiment was considered as a reference one to make sure that the experimental setup was suitable for this kind of operation and to observe the changes to the membrane after oxygen production.

Experimental design: LSCF6428 membrane was fabricated by pressing 1.5 g of powder using a press to form disc membrane as discussed in chapter 3. It was sealed with gold and 20% LSCF6428 in waterglass. The reactor was heated to 900°C using a ramp of 1°C min^{-1}. During the heating process, synthetic air containing 79 % oxygen and 21% nitrogen was fed in the air side to the reactor with volumetric flow rate of 20 ml min^{-1} (STP) while pure argon was introduced to the inert side with the same flow rate as demonstrated in Figure 4.1. When the system reached 900°C, the product gas from the inert side was analysed with a GC. The experiment took 450 h and it was terminated not because it failed, but to perform other experiments.

Results and discussion: oxygen flux (J_{O_2}) was steady at 0.45 ml min cm^{-2} as shown in Figure 4.2 and it was calculated based on the following correlation:

$$J_{O_2}(\text{ml cm}^{-2}\text{ min}^{-1}) = \left[y_{O_2} - \frac{0.21}{0.79} y_{N_2}\right] \times \frac{F}{A} \quad (4.1)$$

where y_{O_2} and y_{N_2} are the molar fractions of oxygen and nitrogen in the product gas, respectively. F is the flow rate of the feed gas (20 ml min^{-1}, STP) and A is the active membrane area. The disc membrane had a diameter of 1.6 cm and because it was mounted over alumina support, the exposed diameter to air was reduced to 0.74 cm and thus the area is calculated by $A = \pi r^2$ which gives 0.44 cm^2. The term 0.21/0.79 in Equation 4.1 represents

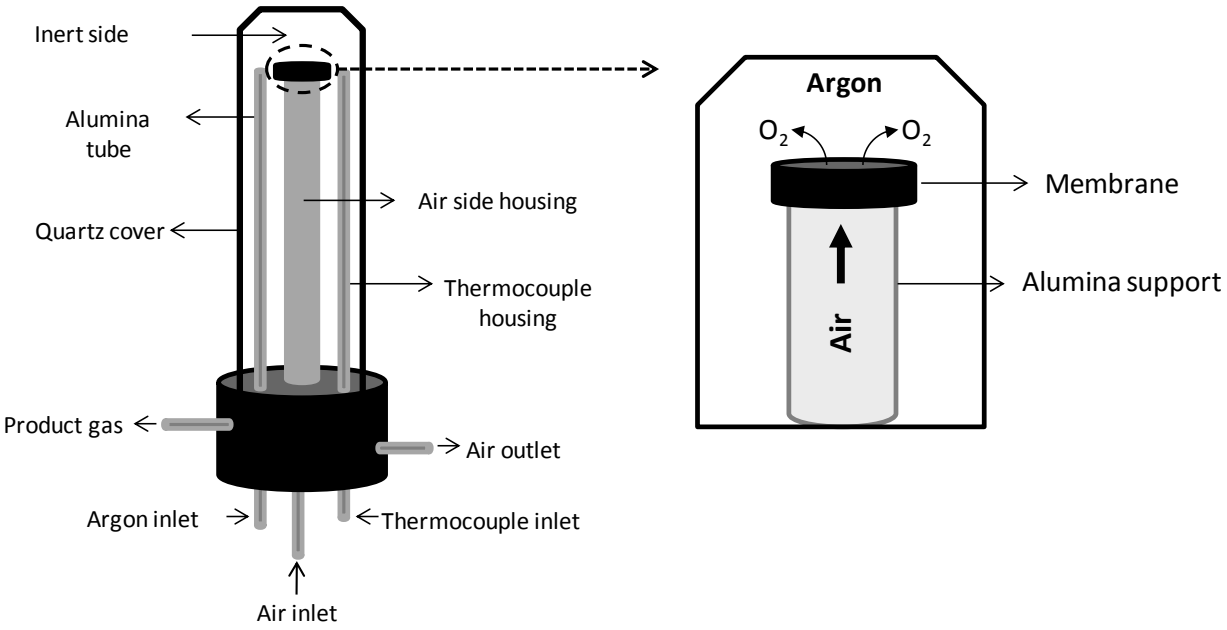

Figure 4.1. Reactor setup for air separation experiment using LSCF6428 membrane.

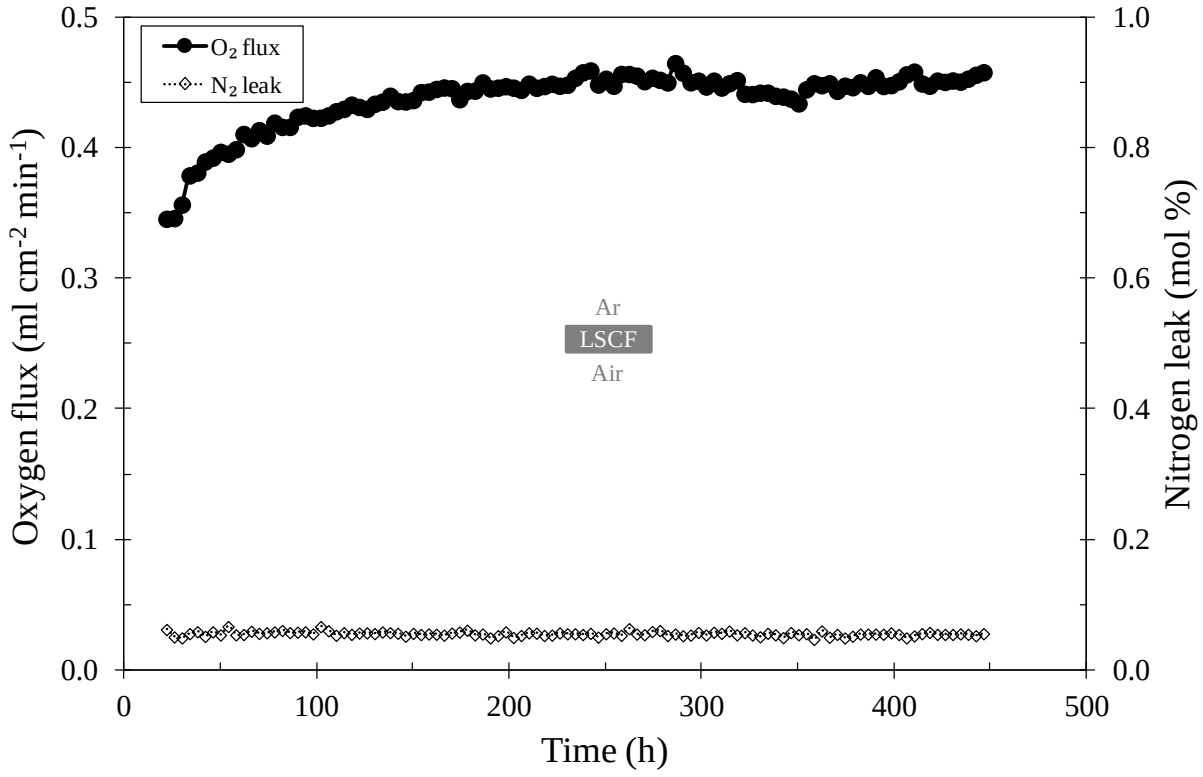

Figure 4.2. Oxygen flux of LSCF6428 membrane for long-term air separation at 900°C using air and argon with flow rates of 20 ml min^{-1}, each.

the amounts of oxygen coming from the leaked nitrogen.

As seen in Figure 4.2, the oxygen flux was increasing in the first 150 h and this behaviour was observed by other researchers due to membrane activation creating more oxygen vacancies [174, 186, 187]. The oxygen flux in this study is the highest compared to those reported literature within the same operating conditions as given in Table 4.1 and this can be related to the gas-tight sealant which improved the driving force for oxygen transport.

Characterisation: before and after operation, the membrane was analysed by characterisation techniques to observe the changes. The membrane was first examined by SEM and both surfaces of inert-side and air-side were checked. Figure 4.3 revealed that the structure did not suffer from any changes indicating that the membrane was stable. This finding was also reported by other researchers [167, 187]. EDS was used to determine the chemical composition of the bulk membrane. Table 4.2 shows no remarkable change in membrane composition however carbon was detected before and after the experiment. It is a phenomenon that carbon dioxide from atmospheric air reacts with the membrane to form strontium carbonate [188]. Other sources of carbon could be dust, handling or storage [189]. It is worthwhile mentioning that strontium content in the air-side surface was higher than the inert-side one. It is known that during air separation some metal like strontium segregates to the air-side surface due to kinetic de-mixing [186]. It is yet unclear why this metal segregates but it is suggested that the changes in chemical, thermal, mechanical or electrical gradients could trigger the accumulation of the metal to one surface [186, 190-196]. Variation of oxygen vacancies along the membrane may also result in metal segregation [197]. The membrane was also characterised by XRD and sharp perovskite peaks were detected when the

Table 4.1. Oxygen flux of disc LSCF6428 membranes for air separation at 900°C and 1 bar.

Study	Sealant	Air flow rate (ml/min)	Diameter × thickness (mm)	J_{O_2} (ml min^{-1} cm^{-2})
This work	Composite	20	16 × 1.1	0.45
Park et al [130]	Glass	20	20 × 1.0	0.30
Xu et al [187]	Gold	2–150	17 × 1.6	0.17
Zeng et al [198]	Silver	100	13 × 0.7	0.37
Asadi et al [96]	Waterglass	200	17 × 1.0	0.32

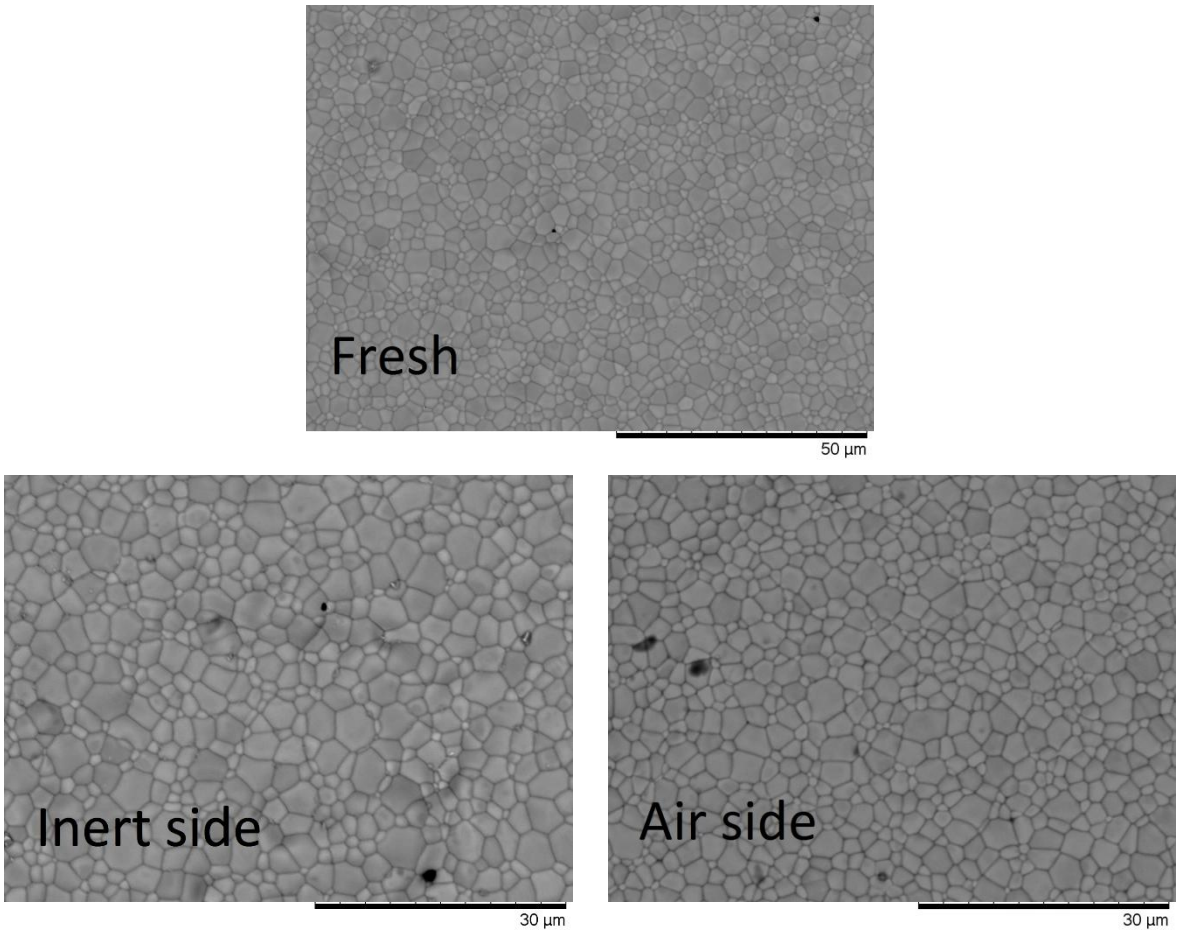

Figure 4.3. SEM images of LSCF6428 membrane before and after oxygen permeation in sulphur-free environment using air and argon for 450 h at 900°C.

Table 4.2. EDS analysis of LSCF6428 membrane before and after long-term air separation for 450 h at 900°C by feeding air and argon.

Membrane	Element (atomic %)						
	La	Sr	Co	Fe	O	C	S
Theoretical	12	8	4	16	60	0	0
Fresh	12	9	4	17	52	6	0
Inert side	12	9	4	17	47	11	0
Air side	11	10	3	16	50	9	0

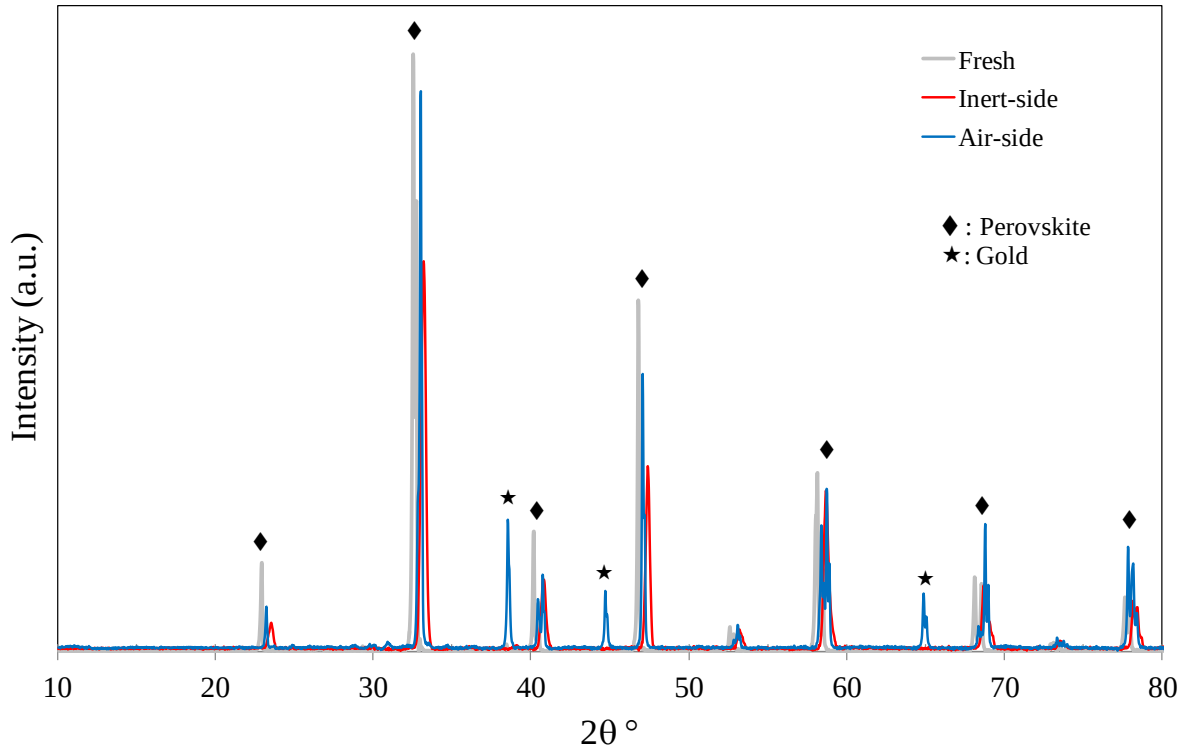

Figure 4.4. XRD analysis of LSCF6428 membrane before and after air separation for 450 h at 900°C using air and argon.

sample was analysed. After operation, the perovskite peaks were still visible on both inert and air sides side surfaces indicating stability as shown in Figure 4.4. Compared to the unused (fresh) membrane, the height of some intensity peaks decreased after operation suggesting that the structure becomes less crystal [199]. This reduction in intensity was also noticed by other researchers [167]. Additional peaks were detected in the air-side surface and they were identified as gold and it is possible that the x-ray beam was wide enough to hit the gold sealant as the membrane sample was small.

The last technique for membrane characterisation was XPS to get elemental composition of the first nanometer layers of the membrane. The results are given in Figure 4.5 in atomic percentage and it is clear that the membrane were enriched with carbon before and after experiment. By looking closely at the data, the binding energy of the detected carbon is 284.6 eV and this matches single bond, adventitious carbon (C-C) [200]. As mentioned previously, this contamination could be from dust, handling or storage. Interestingly, the air-side surface contained some amount of sodium. Waterglass was the only source of sodium and it known that at elevated temperatures, sodium is very mobile and reactive and looks like some sodium, from waterglass, managed to pass through the gold barrier [201]. Whatever the case, sodium

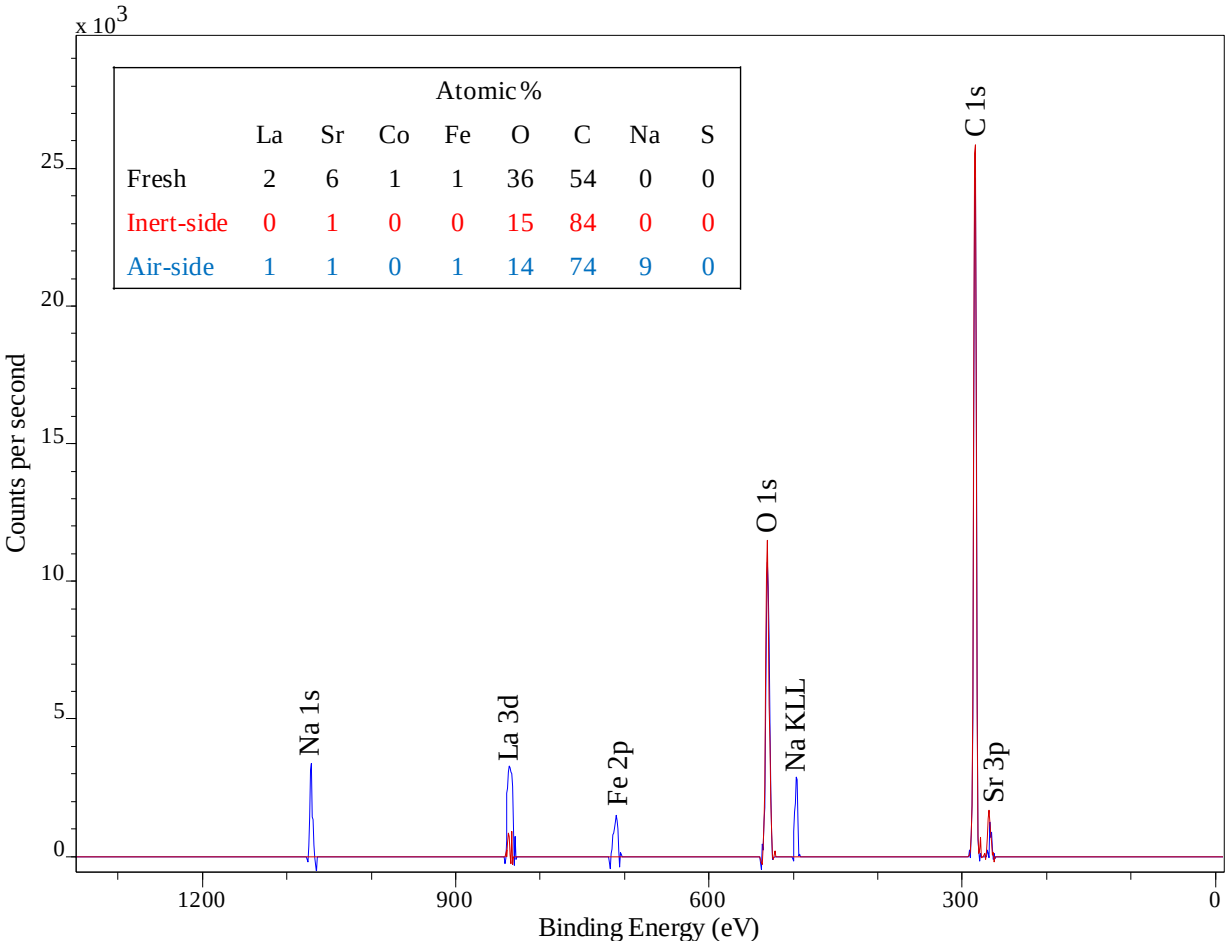

Figure 4.5. XPS analysis of LSCF6428 membrane before and after air separation for 450 h at 900°C by feeding air and argon.

did not cause any interruption during oxygen separation as the flux was steady and did not decrease.

Summary: LSCF6428 membrane showed an excellent performance for oxygen production. The flux was high and steady for long operation of 450 h. Characterisation techniques indicated that the membrane was very stable and it did not suffer from any major changes. Based on this result, it is expected for the membrane to run longer than 450 h without any issues. In the following section, hydrogen sulphide was introduced and changes in flux were monitored.

4.2 Introduction of hydrogen sulphide during air separation

In this experiment, influence of hydrogen sulphide impurity on oxygen flux of LSCF6428 membrane was investigated. The flux was monitored before, during and after hydrogen

sulphide poisoning to look at the changes.

Experimental design: LSCF6428 membrane was heated to 900°C using air and argon with flow rates of 20 ml min^{-1} (STP), each. After that, argon was replaced with a stream containing 200 ppm hydrogen sulphide (balance argon) with same flow rate of 20 ml min^{-1} (STP). The gas was kept for 100 h and after that it was removed and replaced back with pure argon.

Results and discussion: changes of oxygen flux in presence of hydrogen sulphide are given in Figure 4.6. Before the exposure, oxygen flux was 0.30 ml cm^{-2} min^{-1} and it dropped to zero within few hours of hydrogen sulphide introduction. The flux remained at zero for the whole duration of 100 h. After hydrogen sulphide removal from the feedstock, part of the oxygen flux was restored and the value was 0.05 ml cm^{-2} min^{-1} accounting for 16% of the original flux. The flux did not improve with further duration of 100 h indicating a permanent damage. The experiment was repeated and similar results were obtained (Figure B.1, Appendix). To investigate what happened during the poisoning, calorimetric tubes were used to analyse the product gas to see if it contained sulphur. The analysis gave 0 ppm of hydrogen sulphide and 157 ppm of sulphur dioxide. This may suggest that the environment had actually changed

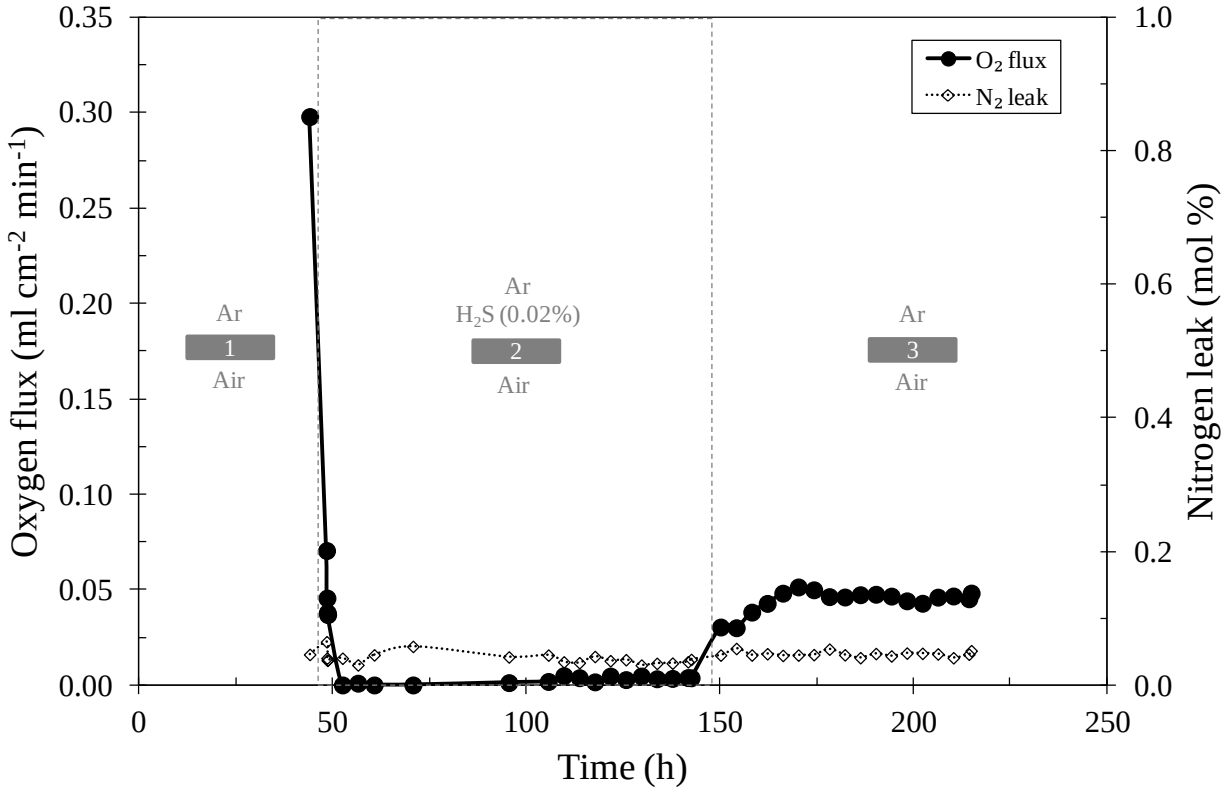

Figure 4.6. Changes of oxygen flux of LSCF6428 membrane for air separation before, during and after hydrogen sulphide exposure of 200 ppm for 100 h at 900°C.

from hydrogen sulphide to sulphur dioxide. To support the statement, the experiment was repeated in sulphur dioxide environment of 200 ppm and same behaviour was observed (Figure C.1, Appendix). Conversion of hydrogen sulphide to sulphur dioxide can have two routes as given in the following equations:

$$H_2S_{(g)} + {}^{3}/_{2}\, O_{2\ (g)} \rightarrow SO_{2\,(g)} + H_2O_{(v)} \tag{4.2}$$

$$H_2S_{(g)} + 3O_o^x \rightarrow SO_{2\,(g)} + H_2O_{(v)} + 3V_O^{\bullet\bullet} + 6e- \tag{4.3}$$

In Equation (4.2, hydrogen sulphide reacts with molecular oxygen (O_2) before reaching the membrane surface while in Equation (4.3, hydrogen sulphide reacts with ionic oxygen (O_o^x) releasing oxygen vacancies ($V_O^{\bullet\bullet}$) and electrons ($e-$). It is difficult to say which reaction was dominant however during the exposure, molecular oxygen was not detected in the product gas. Calorimetric tubes still detected sulphur dioxide in the outlet gas and therefore it is possible that most of hydrogen sulphide reacted with ionic oxygen (Equation 4.3). The reduction in oxygen flux during hydrogen sulphide presence can be related to the adsorption of sulphur on the membrane surface. Oxygen vacancies, which provide the path for oxygen transport, may be targeted by sulphur because both oxygen and sulphur have same oxidation number of –2. Equation 4.4 demonstrates that sulphur atom occupies oxygen vacancy and therefore blocks the transport of oxygen:

$$SO_{2\ (g)} + V_O^{\bullet\bullet} + 2e- \rightarrow S_o^x + O_{2\,(g)} \tag{4.4}$$

where S_o^x refers to sulphur atom with neutral charge sitting on oxygen vacancy. This mechanism was also suggested by many researchers for sulphur dioxide impurity [202-205]. After removing hydrogen sulphide from the feed, the restoration in flux can be related to desorption of some sulphur from the membrane surface in the form of sulphur dioxide as shown in Equation 4.5. The permanent loss in flux could be linked to formation of stable sulphur compounds that cannot be regenerated. Characterisation techniques helped in verifying and identifying these compounds.

$$S_o^x + O_2 \rightarrow SO_{2\ (g)} + V_O^{\bullet\bullet} + 2e- \tag{4.5}$$

Characterisation: SEM images of the membrane surface are given in Figure 4.7. Air-side surface was normal but new phases were observed in the inert-side surface which was exposed to hydrogen sulphide. EDS was performed to analyse the new phases and enrichment of sodium and sulphur were found with general formula of $Na_xS_yO_z$ as given in Table 4.3. As realised, the only source of sodium is waterglass sealant and it likely that hydrogen sulphide

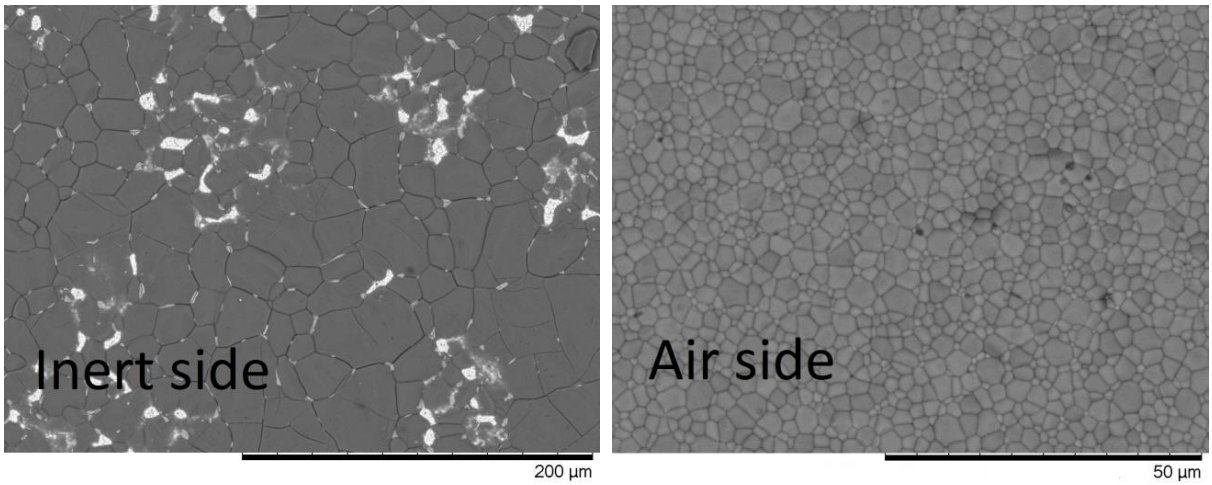

Figure 4.7. SEM images of LSCF6428 membrane after hydrogen sulphide poisoning during air separation for 100 h at 900°C.

Table 4.3. EDS analysis of LSCF6428 membrane after hydrogen sulphide exposure during air separation for 100 h at 900°C.

Membrane	Element (atomic %)							
	La	Sr	Co	Fe	O	C	S	Na
Inert side	1	5	0	1	41	7	20	26
Air side	11	9	3	15	53	9	0	0

reacted with waterglass. XRD (Figure 4.8) was used to identify the sodium-sulphur compound and closest match was sodium sulphate (Na_2SO_4). Metal sulphate peak was detected at 169 eV using XPS (Figure 4.9) and therefore sodium-sulphur compound are now determined as sodium sulphate [206]. It is possible that hydrogen sulphide caused decomposition of waterglass and this released sodium. The later then reacted with the adsorbed sulphur to form sodium sulphate. To make sure that sodium did not alter the results, the experiment was repeated using metallic sealant only and this was studied in the following section.

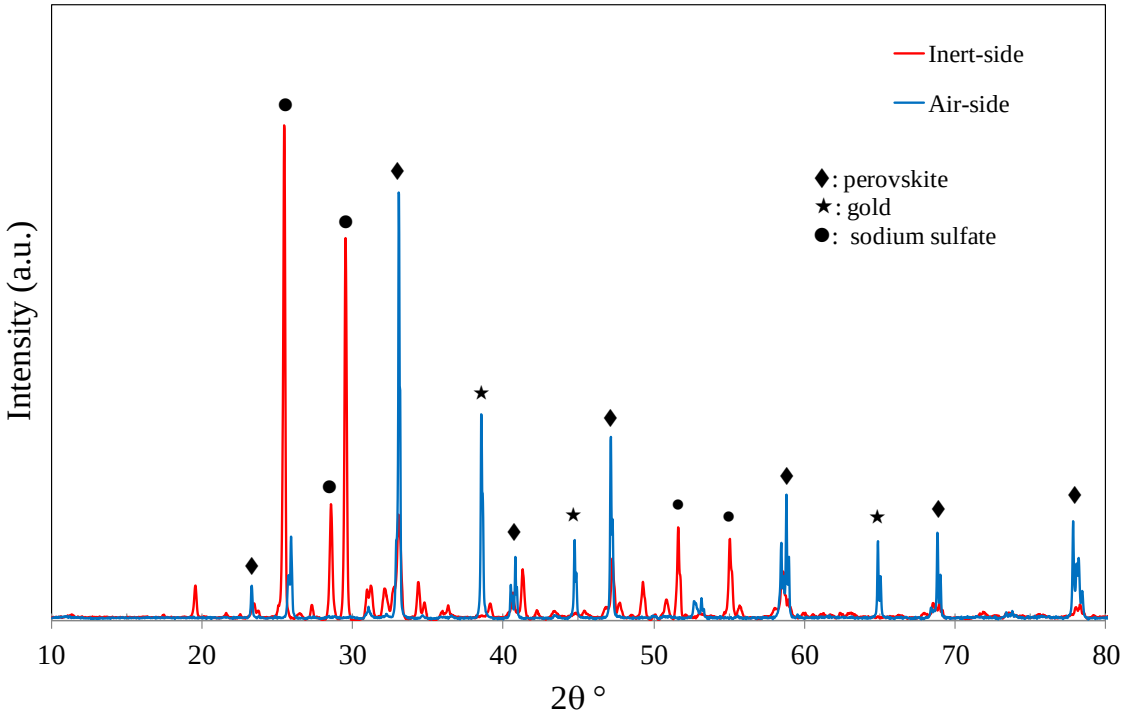

Figure 4.8. XRD analysis of LSCF6428 membrane after hydrogen sulphide exposure during air separation for 100 h at 900°C.

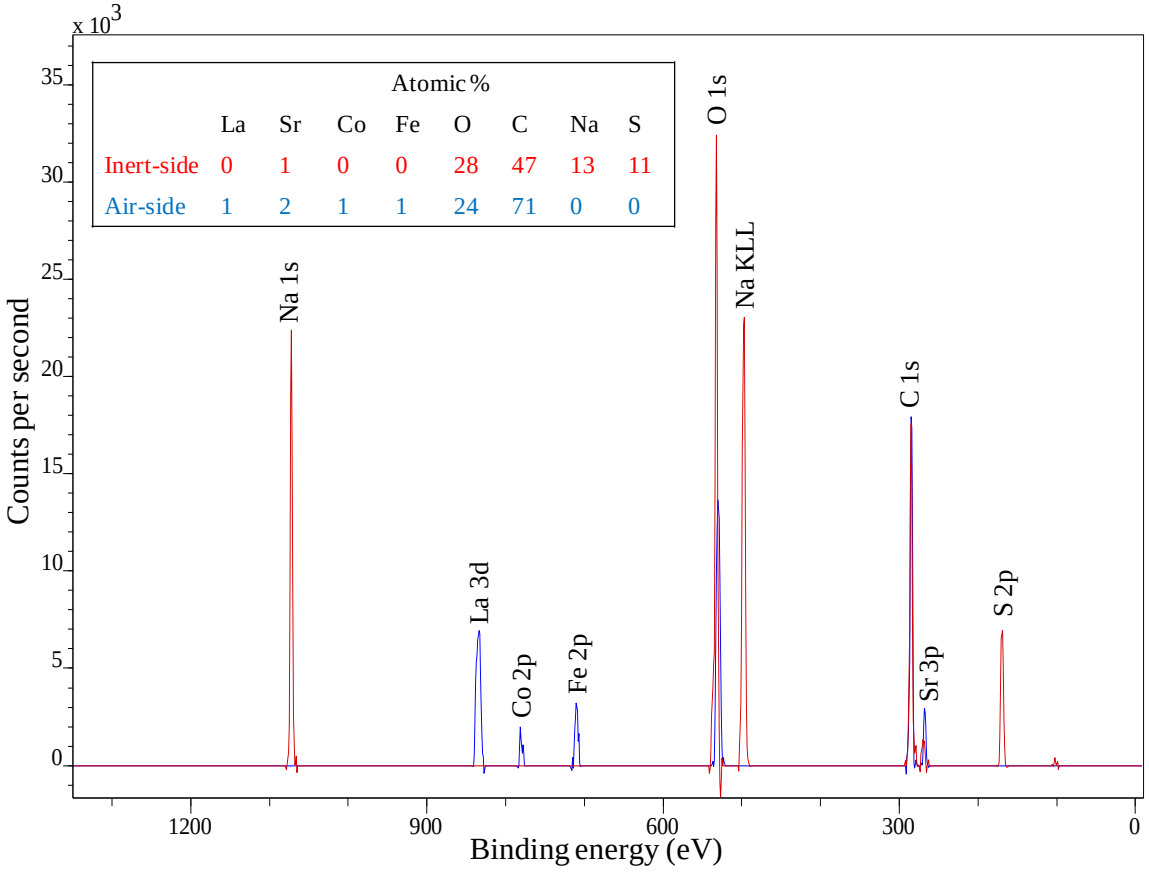

Figure 4.9. XPS analysis of LSCF6428 membrane after hydrogen sulphide exposure during air separation for 100 h at 900°C.

4.2.1. *Effect of sealant*

It was mentioned in chapter 2 that one of the properties of the sealant is the inertness. However, from the previous experiment, waterglass resulted in deposition of sodium sulphate and this compound could be behind the permanent loss of oxygen flux after hydrogen sulphide removal from the feed. In this section, the membrane was sealed using metallic sealant only to see if waterglass changed the results. Silver paste (NextTech Materials Ag-I) was applied over the alumina support and the membrane was inserted as shown previously in Figure 3.6. The membrane was air dried for 24 h and then fitted inside the reactor and heated to 900°C using flows of air and argon (20 ml min^{-1} each, STP). The membrane was then exposed to 200 ppm of hydrogen sulphide for 100 h same as before.

Result is given in Figure 4.10 and the starting flux was 0.04 ml cm^{-2} min^{-1} which is very low compared to 0.30 ml cm^{-2} min^{-1} where gold-glass-ceramic sealant was used. This is because silver did not give a gas-tight system as oxygen content in the product gas was less than nitrogen (0.10% mol oxygen compared to 0.25% mol nitrogen). When hydrogen sulphide was presented, oxygen flux decreased to zero within few hours. After stopping feeding hydrogen

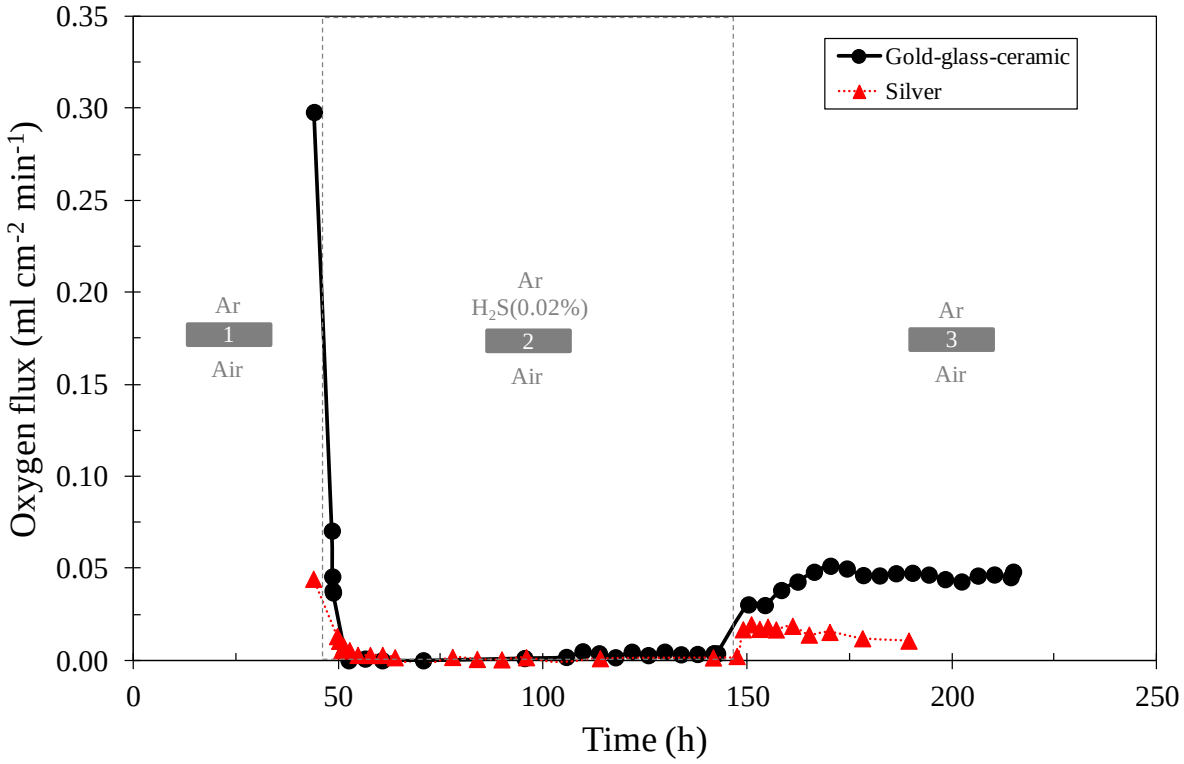

Figure 4.10. Effect of sealant on the changes of oxygen flux during hydrogen sulphide poisoning (200 ppm) at 900°C for 100 h.

sulphide, oxygen flux was regenerating but it was not fully restored. These changes in oxygen flux are similar when the membrane was sealed by the gold-glass-ceramic sealant as shown in Figure 4.10. After operation, the membrane (sealed by silver) was characterised by SEM and a new phase was observed as shown in Figure 4.11. EDS revealed that the new phase is enriched with sulphur and strontium as given in Table 4.4. XRD (Figure 4.12) detected strong perovskite peaks with additional peaks of strontium sulphate ($SrSO_4$). XPS also measured high amounts of sulphur and strontium (Figure 4.13). There are many routes to form strontium sulphate: 1) reaction of hydrogen sulphide with strontium oxide from the bulk membrane, 2) oxidation of hydrogen sulphide to sulphur dioxide then the reaction with strontium oxide, 3) reaction of strontium oxide with the adsorbed sulphur (thermodynamic data from [207]):

$$H_2S_{(g)} + SrO_{(s)} + 2O_{2\ (g)} \rightarrow SrSO_{4\ (s)} + H_2O_{(v)} \qquad \Delta G_{900\,^\circ C} = -664 \text{ kJ mol}^{-1} \qquad (4.6)$$

$$SO_{2\,(g)} + SrO_{(s)} + {}^1/_2\, O_{2\ (g)} \rightarrow SrSO_{4\ (s)} \qquad \Delta G_{900\,^\circ C} = -237 \text{ kJ mol}^{-1} \qquad (4.7)$$

$$S_{(g)} + SrO_{(s)} + {}^3/_2\, O_{2\ (g)} \rightarrow SrSO_{4\ (s)} \qquad \Delta G_{900\,^\circ C} = -659 \text{ kJ mol}^{-1} \qquad (4.8)$$

Gibbs energy of reaction suggested that the first and third reactions (Equations 4.6 and 4.8) are more favourable due to the high negative value. In all cases, oxygen is necessarily for strontium sulphate formation and there is a chance that presence of sulphur (in the form of hydrogen sulphide, sulphur dioxide or molecular sulphur) caused segregation of strontium

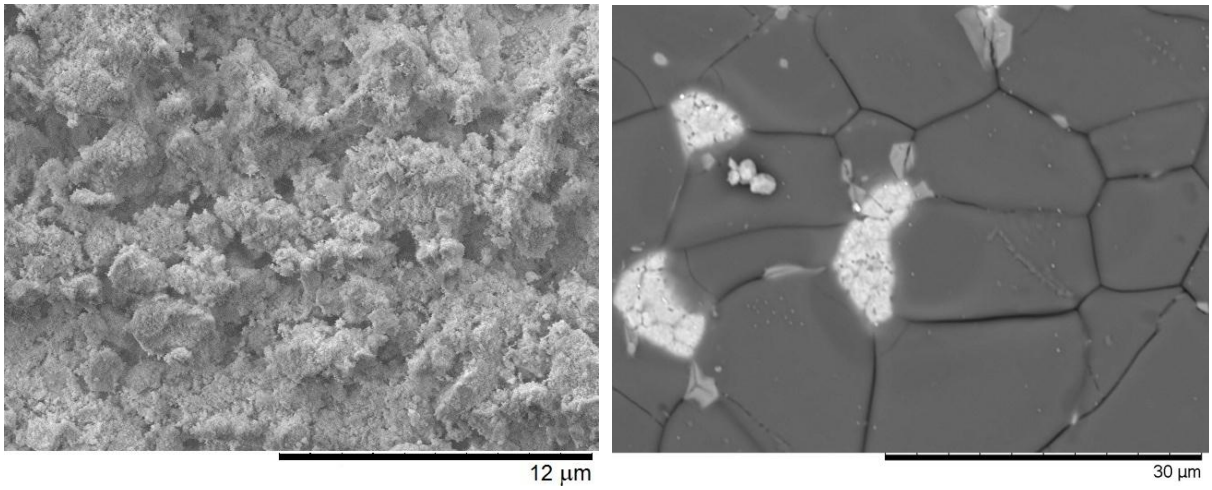

Figure 4.11. SEM images of LSCF6428 membranes after hydrogen sulphide attack (200 ppm) during air separation for 100 h at 900°C using silver sealant (left) and gold-glass-ceramic sealant (right).

Table 4.4. EDS analysis of LSCF6428 membranes sealed by different methods after hydrogen sulphide exposure during air separation for 100 h at 900°C.

Sealant	Element (atomic %)							
	La	Sr	Co	Fe	O	C	S	Na
Silver	5	18	8	4	38	7	20	0
Gold-glass-ceramic	1	5	0	1	41	7	20	26

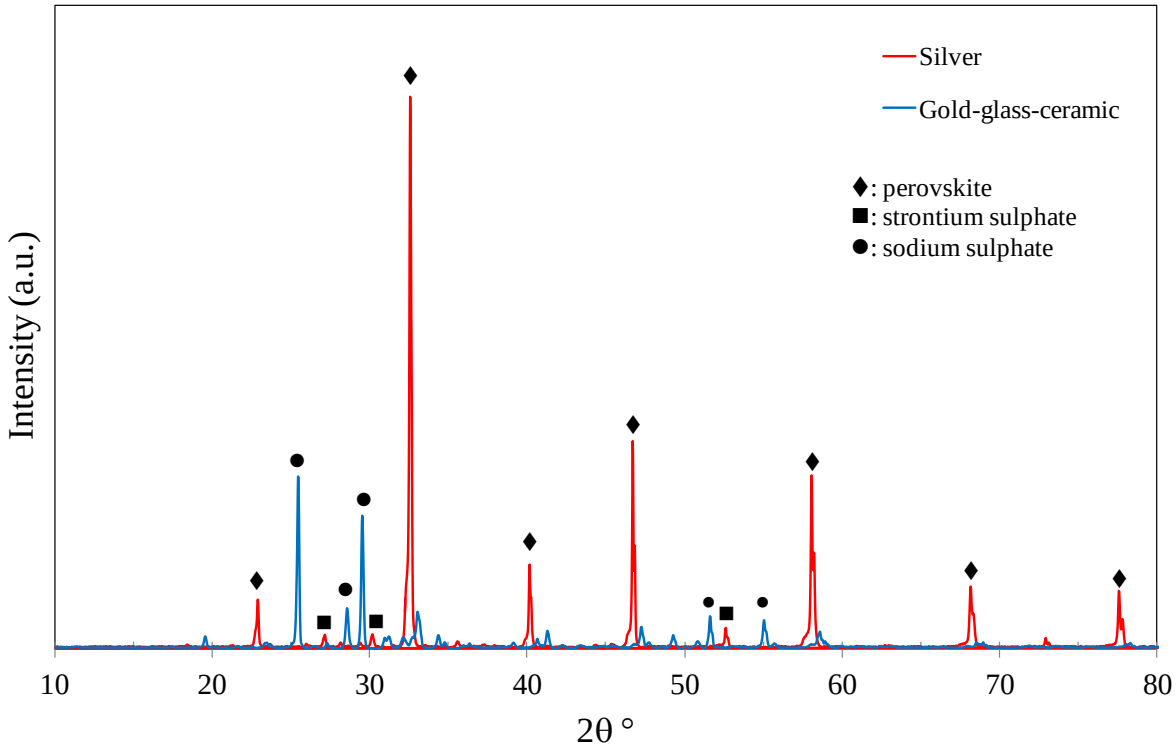

Figure 4.12. XRD analysis of LSCF6428 membranes after hydrogen sulphide poisoning (200 ppm) during air separation for 100 h at with different sealing systems at 900°C.

oxide to the sulphur site. Segregation of metal oxides to sulphur sites was also suggested by many researchers [202-204]. It was mentioned before that strontium segregates to the air-side surface due to kinetic de-mixing but presence of sulphur could diverse the direction of segregation to the inert-side surface.

Based on characterisation techniques, using silver sealant resulted in strontium sulphate deposition while sodium sulphate was seen in case of gold-glass-ceramic sealant.

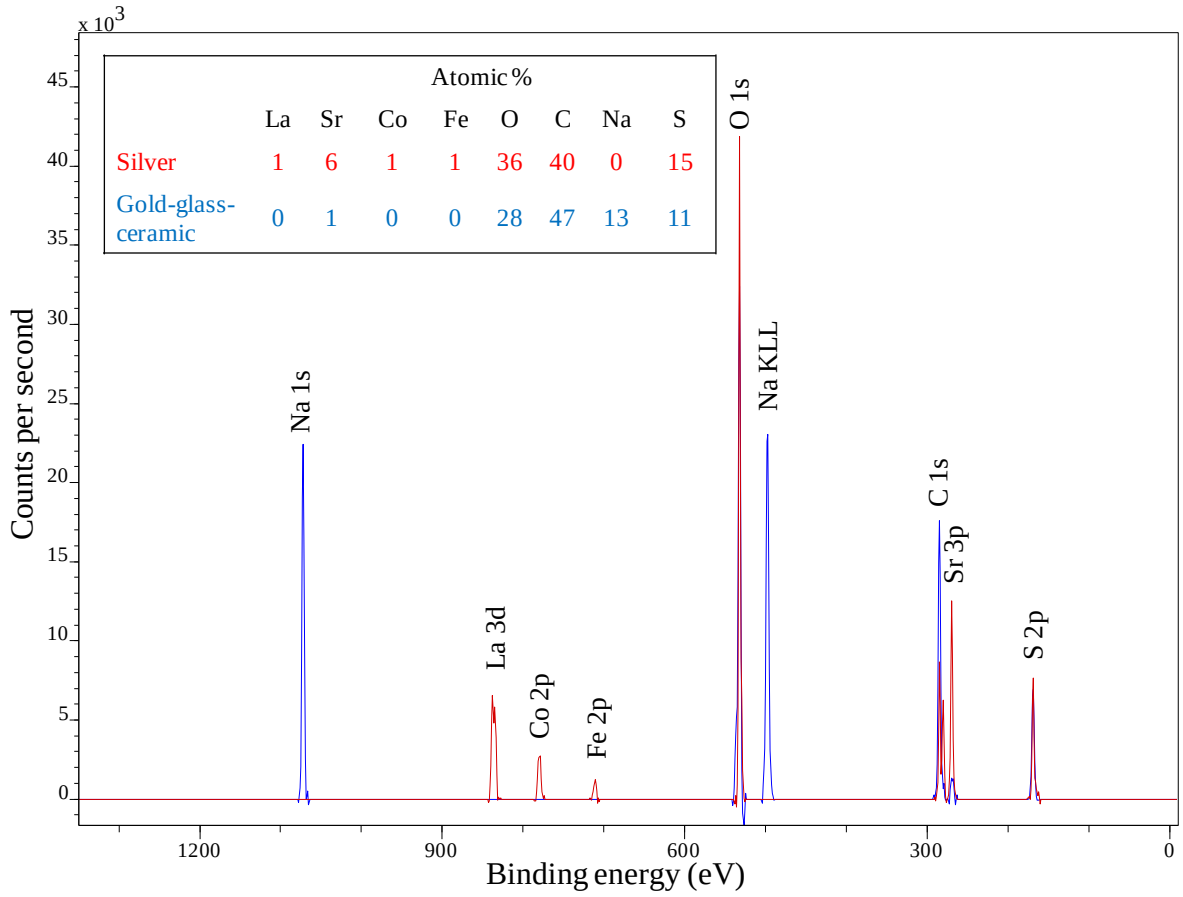

Figure 4.13. XPS analysis of LSCF6428 membranes after hydrogen sulphide exposure during air separation for 100 h at 900°C with varies sealants.

Interestingly, change of oxygen flux was similar for both sealants. There is a chance that during hydrogen sulphide exposure using gold-glass-ceramic sealant, strontium sulphate was formed first and sodium reacted with it later to produce sodium sulphate (thermodynamic data from [207]):

$$SrSO_{4(s)} + 2Na_{(g)} + {}^{1}/_{2}\,O_{2\ (g)} \rightarrow Na_2SO_{4\,(l)} + SrO_{(s)} \qquad \Delta G_{900\,℃} = -396\ \text{kJ mol}^{-1} \qquad (4.9)$$

however, it is known that sodium sulphate decomposes to sodium, sulphur dioxide and oxygen once it reaches the melting point of 880°C [208]:

$$Na_2SO_{4(s)} \rightarrow 2Na_{(g)} + SO_{2(g)} + O_{2(g)} \qquad (4.10)$$

the operating temperature was at 900°C so there is a little chance for sodium sulphate to form. During cooling down (to shutdown the experiment), there is a possibility that sodium reacted with strontium sulphate to produce sodium sulphate and that is why sodium did not cause any interference at 900°C. Despite that the gold-glass-ceramic sealant resulted in deposition of different sulphur compounds compared to silver, it was decided to continue using the

composite sealant because: 1) it gas-tight sealed the membrane and gave high oxygen fluxes, 2) it was stable for long-term operation of 963 h as discussed in previous chapter, and 3) it did not interfere with oxygen flux during sulphur presence. Suggested mechanism for hydrogen sulphide poisoning is given Figure 4.14.

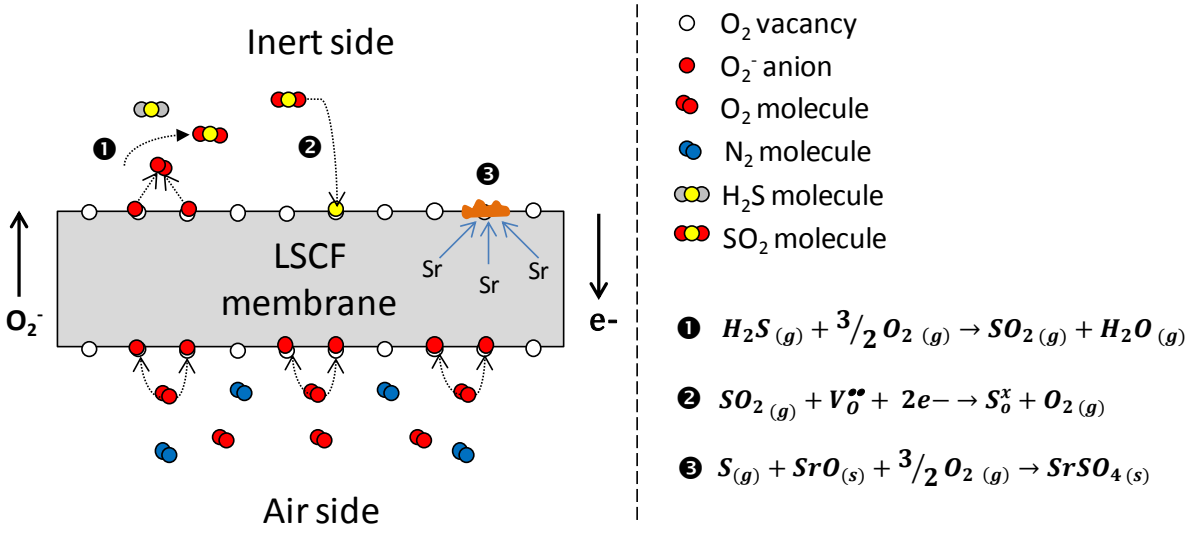

Figure 4.14. Proposed mechanism for hydrogen sulphide poisoning during air separation of LSCF6428 membrane.

4.3 Regeneration of the membrane after hydrogen sulphide poisoning

As discovered, hydrogen sulphide impurity caused permanent damage to the membrane surface and the key to restore the membrane is by removing sulphur compounds from the surface. There are three ways to do so: thermally, mechanically and chemically. It was found that the corrosion products were strontium sulphate and to decompose it thermally, temperature over 1600°C is required [209]. This temperature will not only decompose strontium sulphate but also will melt the membrane, therefore it is not practical [198]. The second way for sulphate removal is by mechanical methods such as sanding. This technique is widely used in industry to remove scales of metal sulphates from pipelines due to the use of seawater [210]. The method was applied by sanding the membrane with extra fine paper (600 Grit) but unfortunately the membrane broke and cracks were formed because the membrane was very fragile after operation. Now, the only technique to try was the chemical one. Liquid chemicals such as acids cannot remove strontium sulphate because of the poor solubility of strontium sulphate in acids [211]. Reducing gases such as hydrogen could decompose strontium sulphate and this was investigated in the following section.

4.3.1 *Hydrogen treatment*

Hydrogen is extensively used in the refinery to remove sulphur from fuels and this process is called hydrodesulphurisation. Actually, a catalyst containing sulphur vacancies (e.g., molybdenum disulphide) adsorbs sulphur from the fuel and then hydrogen remove the sulphur in the form of hydrogen sulphide and generate the vacancy back [212]. The concept is also used to regenerate some metal-based catalysts after sulphur poisoning [202, 213]. In this study, sulphur was in the form of strontium sulphate and Gibbs energy of reaction suggests that hydrogen can decompose strontium sulphate back to strontium oxide at 900°C as follows (thermodynamic data from [207]):

$$SrSO_{4\,(s)} + 4H_{2(g)} \rightarrow SrO_{(s)} + H_2S_{(g)} + 3H_2O_{(v)} \qquad \Delta G_{900\,^{\circ}C} = -341 \text{ kJ mol}^{-1} \qquad (4.11)$$

Experimental design: the previous experiment was repeated by heating the membrane first to 900°C using air and argon with flow rate of 20 ml min^{-1} (STP), each. In the second step, argon was replaced with hydrogen sulphide (200 ppm, balance argon) and fed to the inert side for 100 h. After that, hydrogen sulphide was removed and argon was brought back. The new steps were to introduce hydrogen (1% mol in argon) at 20 ml min^{-1} (STP) to treat the damaged surface for 20 h. The selected hydrogen concentration was 50 times more than hydrogen sulphide and this may accelerate the regeneration process. The final step was to remove hydrogen from the inert side and bring back argon. Oxygen flux was monitored to observe the changes before and after the treatment. Feeds configuration is given in Figure 4.15.

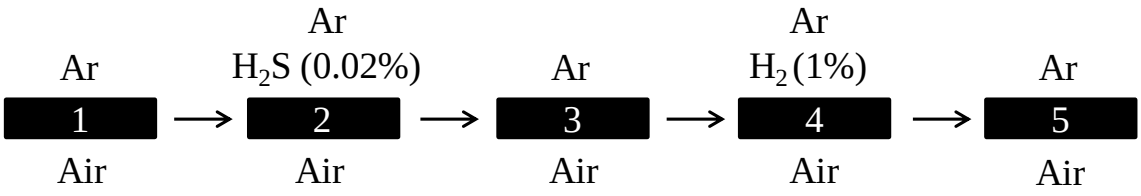

Figure 4.15. Feeds configuration for hydrogen treatment experiment to regenerate LSCF6428 membrane after hydrogen sulphide poisoning (200 ppm) of 100 h.

Results and discussion: the starting oxygen flux was at 0.26 ml cm^{-2} min^{-1} and it was zero once hydrogen sulphide was introduced. After stopping feeding hydrogen sulphide in the inert side, the flux was 0.015 ml cm^{-2} min^{-1} which is 6% of the original one. These fluxes are close to what was found in the previous section and this confirms the repeatability of data. After hydrogen treatment of 20 h, the oxygen flux improved from 0.015 to 0.03 ml cm^{-2} min^{-1}

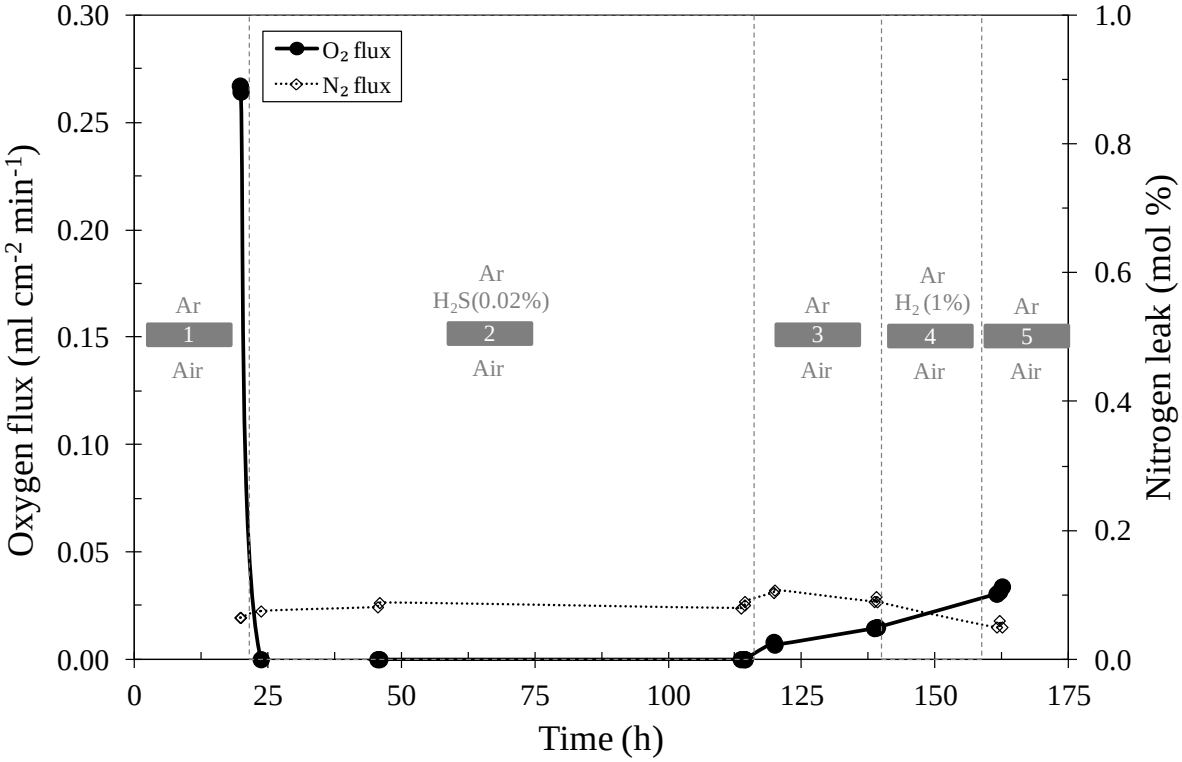

Figure 4.16. Use of hydrogen (1% mol) to recover the poisoned surface of LSCF6428 membrane after hydrogen sulphide attack (200 ppm) for 100 h at 900°C.

which is double the flux before the treatment and this increases the recovery to 12% as shown in Figure 4.16. During hydrogen treatment, calorimetric tubes were used to see if Equation (4.11) took place and indeed 10 to 50 ppm of hydrogen sulphide was detected and this indicates that hydrogen was removing some of the sulphur from the membrane surface. It was expected to see better recovery because hydrogen concentration was 50 times more than hydrogen sulphide but it looks like that the regeneration process was very slow compared to the poisoning. In the following section, the poisoned surface was treated with air by switching the flows.

4.3.2 *Flow switching*

Characterisation techniques revealed that the opened surface to hydrogen sulphide suffered from deposition of sulphur compounds but the non-exposed surface (air side) was absolutely normal as given in Figure 4.7. In this experiment, the feeds were switched (swapped) after hydrogen sulphide exposure meaning that air was fed to the exposed surface while argon was introduced to the air side. Purging the damaged surface with air could regenerate some

sulphur that is not transformed yet to strontium sulphate. Also, change of the inert surface from reducing to oxidising could create further oxygen vacancies and this may help in restoring the membrane.

Experimental setup: LSCF6428 membrane was heated at 900°C using air and argon with flow rates of 20 ml min^{-1} (STP). After that, the membrane was exposed to hydrogen sulphide (200 ppm) for 100 h and then it was removed from the feed. The new step was to switch the flows by feeding air to the inert side and argon to the air side as demonstrated in Figure 4.17. Oxygen flux was monitored to see if the recovery was improved after switching the flows.

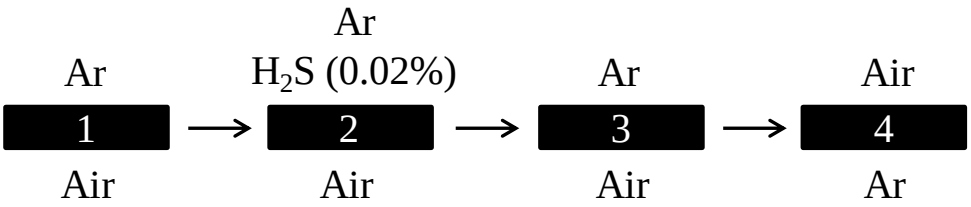

Figure 4.17. Feeds setup for flow-switching experiment after hydrogen sulphide poisoning

Results and discussion: the starting flux was 0.16 ml cm^{-2} min^{-1} and it went to zero after few hours of hydrogen sulphide introduction as shown in Figure 4.18. After stopping feeding hydrogen sulphide, the membrane was restoring and the flux reached 0.05 ml cm^{-2} min^{-1} (35% recovery) after 38 h. This recovery is relatively high compared to previous experiments where the recovery was in the range of 6 to 16%. It should be mentioned that the starting flux of this experiment is almost half to what was measured in the previous experiments. Therefore, it can be deducted that there is a relation between oxygen flux and the poisoning mechanism, the higher the flux, the more damage the membrane will receive due to lower recovery. Higher oxygen flux means that more vacancies are created in the inert-side surface and this may increase the adsorption rate of sulphur on the membrane surface [66].

Unfortunately, when the flows were switched, oxygen flux slightly decreased but nitrogen leak sharply increased from 0.07 to 0.58% (mol) as given in Figure 4.18. To investigate why the leak increased after the switching, the experiment was repeated but in a sulphur-free environment to see if hydrogen sulphide contributed in the increase of leak. Results show that nitrogen leak still increased from 0.01 to 0.22% (mol) after switching the flows despite sulphur was not presented (Figure D.1, Appendix D). This tells that the membrane itself cannot handle the switching and hydrogen sulphide was not behind the leak. Changes of the

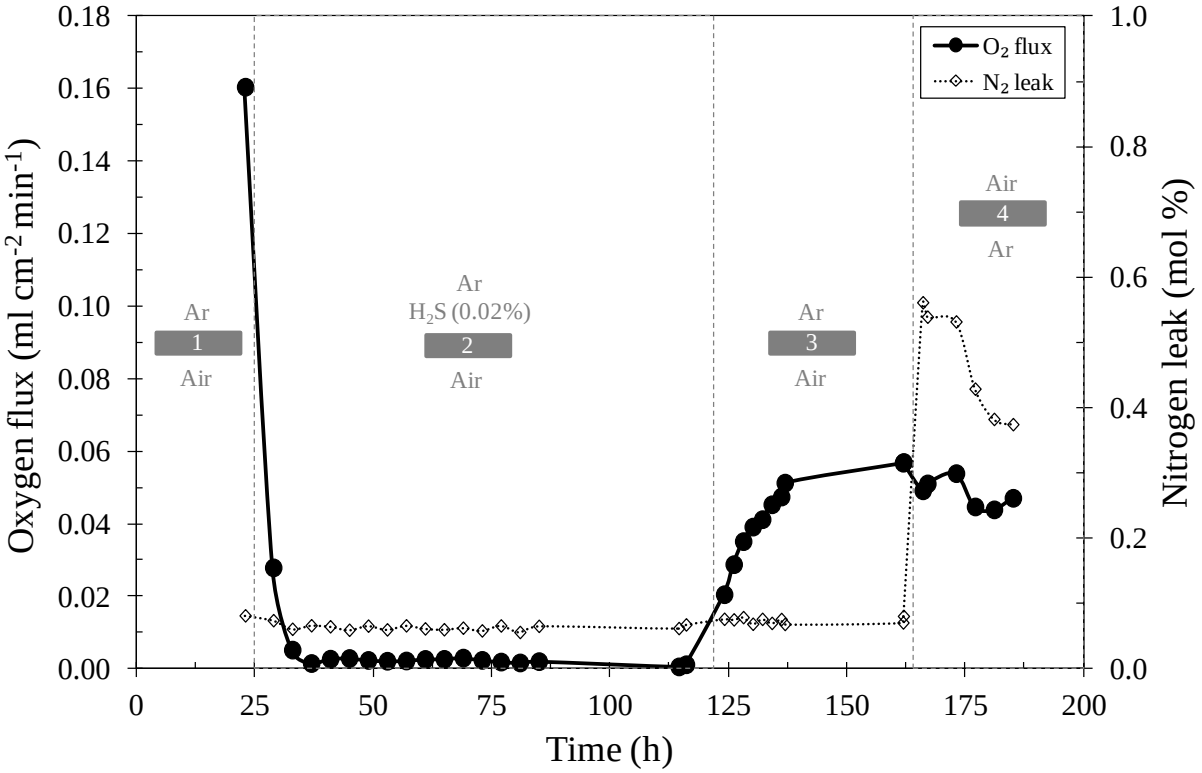

Figure 4.18. Increase in leak after switching the flows of the poisoned membrane by 200 ppm of hydrogen sulphide for 100 h at 900°C.

membrane surface from oxidising to reducing may introduce some internal stress due to re-distribution of oxygen vacancies. It is reported that the concentration of vacancies in the oxygen-lean surface is higher than the oxygen-rich surface and creating too much vacancies can cause membrane failure [66, 70, 187].

4.4 Summary

In this chapter, influence of hydrogen sulphide impurity (200 ppm) during air separation of LSCF6428 membrane was studied. It was found that the impact was severe and the membrane was ‘dead’ during the exposure as the oxygen permeation was zero. This zero flux was related to the adsorption of sulphur on the membrane surface. It was suggested that hydrogen sulphide was first oxidised to sulphur dioxide and the later occupied oxygen vacancy in the form of sulphur. After removal of hydrogen sulphide from the feed, the flux could not be fully restored and only part of it was recovered. Characterisation techniques revealed formation of metal sulphates on the exposed surfaces and these compounds reduced the membrane area and permanently poisoned the vacancy. The key to restore the oxygen flux after sulphur poisoning

is by the removal of strontium sulphates from the surface. Unfortunately thermal and mechanical methods did not work but chemical treatment such as use of hydrogen stream (1% mol) successfully increased the recovery from 6 to 12% after 20 h. It was found that the regeneration process was very slow compared to the poisoning and therefore longer treatment times or higher concentrations of hydrogen may be required. Another way to restore the membrane was tried by switching the flows after hydrogen sulphide exposure. This was done by feeding air to the poisoned surface and argon in the air side however the method caused further damage to the membrane as indicated by the increase in nitrogen leak.

Chapter 5: More studies on hydrogen sulphide mechanism during air separation

Chapter 5: More Studies on Hydrogen Sulphide Mechanism during Air Separation

It was discovered from previous chapter that hydrogen sulphide impurity immobilised oxygen transport in LSCF6428 membrane. The study however was done in certain conditions such as duration of 100 h, temperature of 900°C and hydrogen sulphide concentration of 200 ppm. Change of these parameters could significantly affect the poisoning mechanism of hydrogen sulphide and this is reviewed in this chapter. Role of oxygen partial pressure in the air side on sulphur mechanism is also studied.

5.1 Exposure duration

In chapter 4, the membrane was exposed to long-term poisoning of 100 h and this duration was enough to cause permanent loss to major part of oxygen flux. Theoretically, the longer the exposure time, the more damage the membrane will receive due to adsorption of further mass of sulphur. In this section, the membrane was exposed to short duration of 1 and 24 h to hydrogen sulphide. This may give information about the reversibility of sulphur poisoning.

Experimental setup: two LSCF6428 membranes were sealed by gold-glass-ceramic sealant and heated to 900°C using flows of air and argon at 20 ml min^{-1} (STP), each. After measuring the flux, argon was replaced with hydrogen sulphide (200 ppm, balance argon) with same flow rate of 20 ml min^{-1} for 1 h for the first experiment and 24 h for the second one. After the exposure, hydrogen sulphide was removed by swapping it with argon.

Results and discussion: in the first experiment where the membrane was exposed to one hour, it was interesting to see a full recovery of oxygen flux after 16 h of hydrogen sulphide removal from the feed as shown in Figure 5.1. This experiment revealed that hydrogen sulphide poisoning can be reversible and it strongly depends on the exposure time. It also implied that adsorption of sulphur on oxygen vacancies happens rapidly (as the flux was zero within one hour) but permanent loss of the vacancy by strontium sulphate requires further time as strontium takes a while to segregate toward sulphur.

The second membrane was exposed to 24 h and the recovery was 57% after 26 h of hydrogen sulphide removal as given in Figure 5.2. Similar results were obtained when the experiment

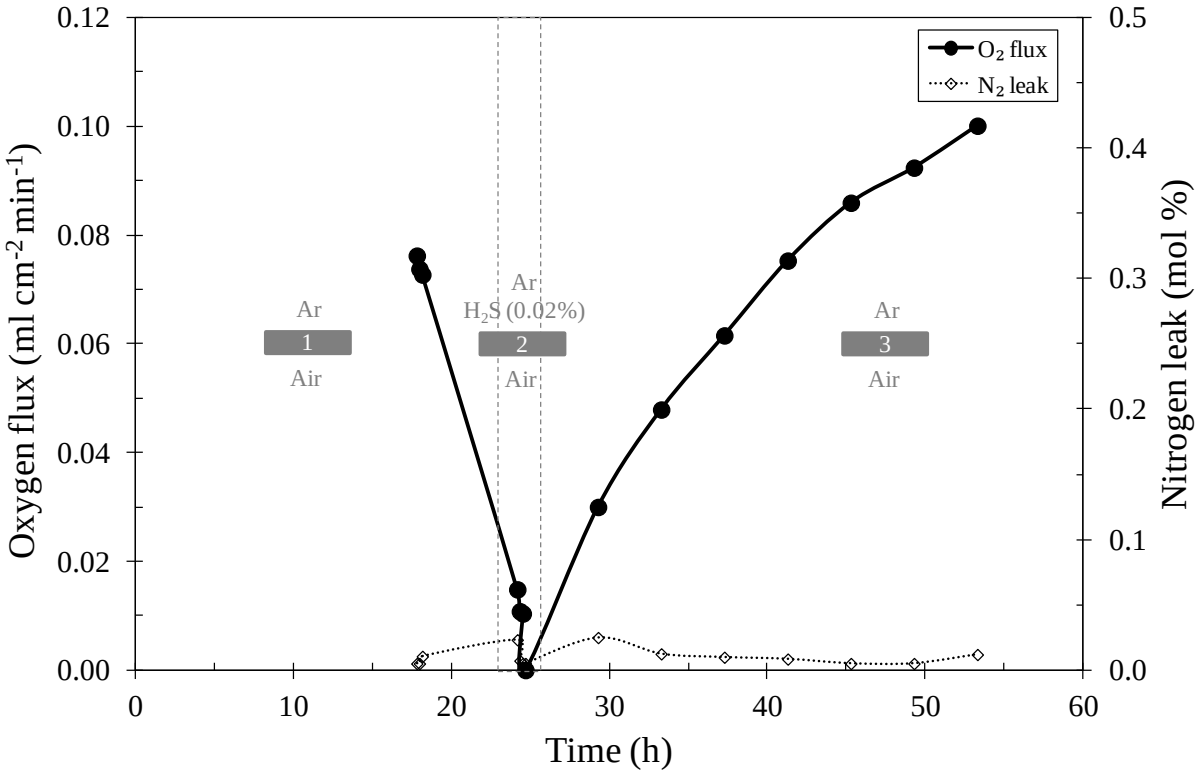

Figure 5.1. Full recovery of oxygen flux of LSCF6428 membrane for air separation after hydrogen sulphide poisoning of 1 h at 900°C.

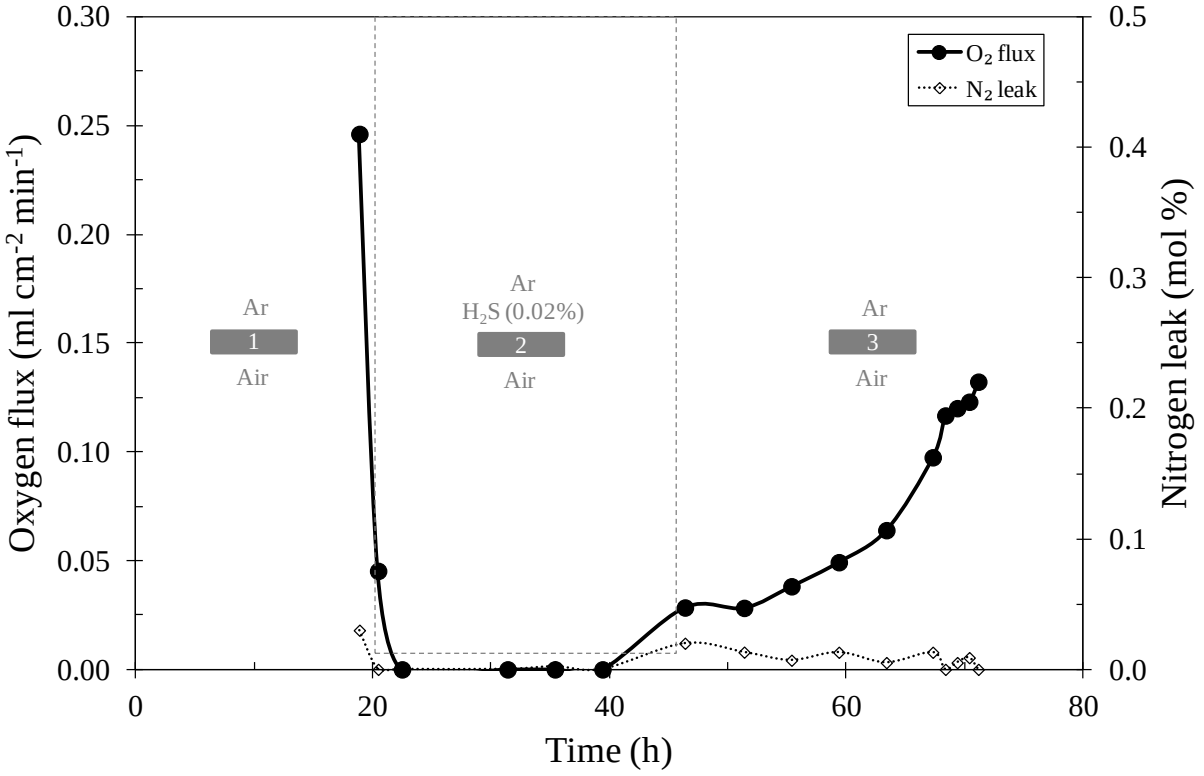

Figure 5.2. Improved recovery of oxygen flux of LSCF6428 membrane for air separation after 24 h of hydrogen sulphide exposure (200 ppm) at 900°C.

was repeated (Figure B.2, Appendix B). Compared to previous chapter where the membrane was opened to 100 h to hydrogen sulphide, exposure of 24 h resulted in higher recovery. So this experiment supports that, the longer the duration of hydrogen sulphide, the more permanent damage the membrane will receive due to formation of further strontium sulphate

Characterisation: the fully recovered membrane, by one hour of hydrogen sulphide exposure, was characterised to see if all of the adsorbed sulphur was removed from the surface. Figure 5.3 shows that new phases were still visible and they are rich in sulphur, sodium and strontium as measured by EDS (Table 5.1). Compared to long term experiments where the membrane was opened to 100 h to hydrogen sulphide, the phases in this experiment were separated and smaller in size. The original membrane surface is also visible and it looks like with time, sulphur deposits combined together to cover larger area as shown in Figure 5.3. These deposits agglomerate with time causing more damage as indicated by the long-term experiment. Despite the new phases were detected along the surface after one hour of exposure, oxygen flux was fully regenerated after hydrogen sulphide removal. Possible explanations are: 1) these deposits were loose and oxygen managed to permeate beneath them, 2) the small poisoned area could be compensated by the creation of more oxygen vacancies with time.

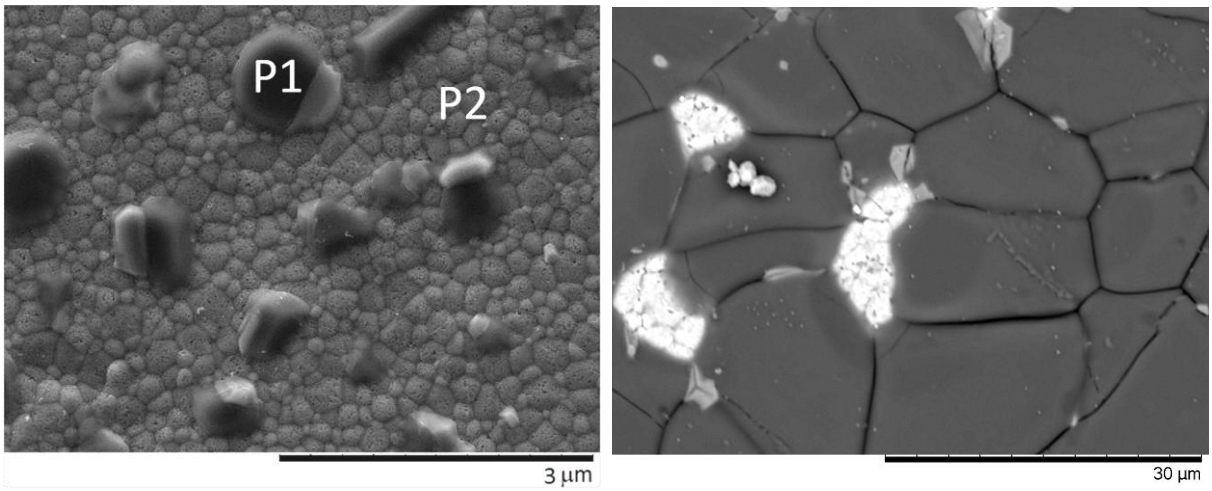

Figure 5.3. SEM images of LSCF6428 membrane after hydrogen sulphide poisoning (200 ppm) of 1 h (left) and 100 h (right) at 900°C using air and argon.

Table 5.1. EDS analysis of LSCF6428 membrane after one hour of hydrogen exposure during air separation at 900°C (points are given in Figure 5.3)

	Element (atomic %)							
	La	Sr	Co	Fe	O	C	S	Na
Point 1	4	11	1	5	54	0	16	9
Point 2	11	5	4	15	65	0	0	0

5.2 Temperature

In previous experiments, the operating temperature was fixed at 900°C but in this section, the membrane was tested for sulphur poisoning under different temperatures of 800 to 950°C to see if the adsorption rate of sulphur or strontium sulphate formation depends on temperature. This may help in optimising the operating temperature for better stability under hydrogen sulphide.

Experimental setup: the experiment was conducted using four membranes sealed by gold-glass-ceramic sealant and operated at different temperatures of 800, 850, 900 and 950°C. For each run, air and argon were fed at 20 ml min^{-1} (STP) to measure the starting flux and monitor nitrogen leak. After that, argon was swapped with hydrogen sulphide (200 ppm, balance argon) fed at 20 ml min^{-1} for 100 h. The final step was to replace hydrogen sulphide with argon.

Results and discussion: data are given in Figure 5.4 and it reveals that oxygen flux was zero during the exposure even if the operating temperature was changed from 800 to 950°C. However, at 950°C it took longer for hydrogen sulphide to totally poison the membrane (33h compared to few hours at 800 to 900°C). In addition, the recovery at 950°C was higher compared to other temperatures and it reached 30% after 50 h of hydrogen sulphide removal. It is possible that the adsorption rate of sulphur on the membrane surface is a function of temperature and the rate reduces at higher temperature. Some catalysts like nickel show better tolerance to sulphur at elevated temperatures due to lower interaction between nickel and sulphur and this could happen here as well to LSCF6428 membrane [214].

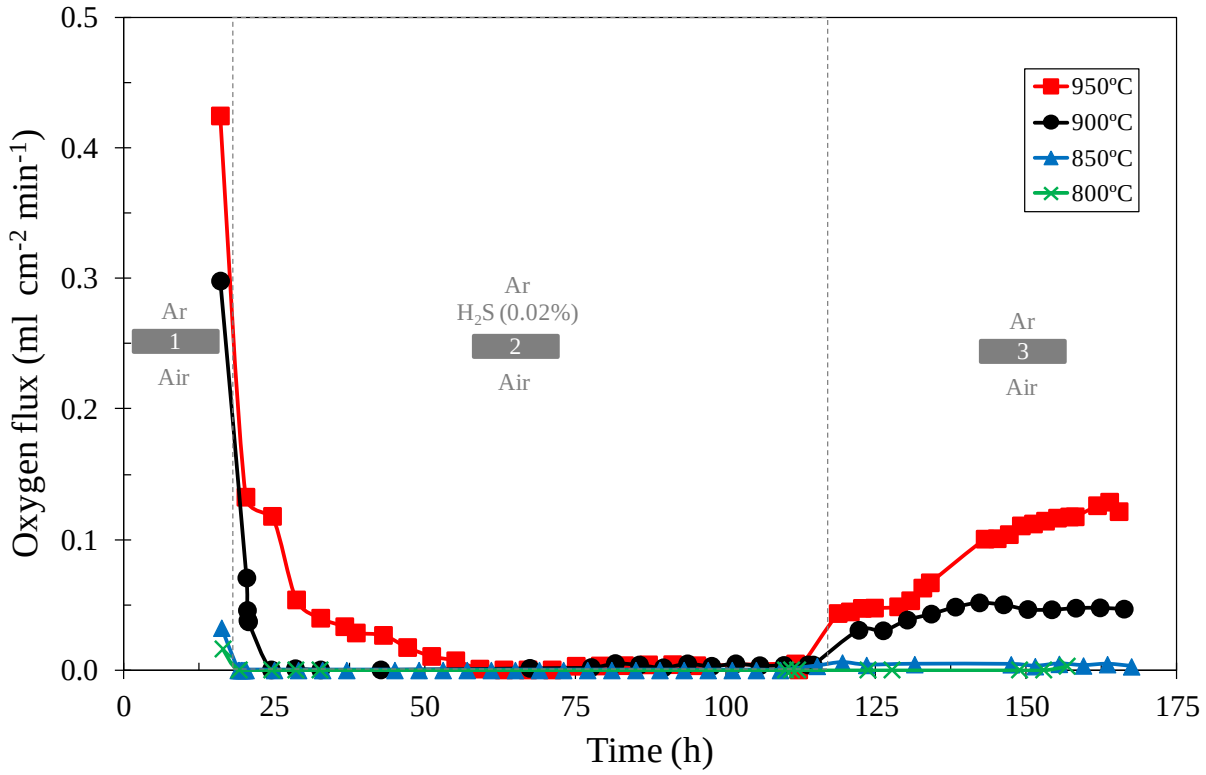

Figure 5.4. Effect of temperature on oxygen separation of LSCF6428 membrane before, during, and after hydrogen sulphide exposure (200 ppm) for 100 h at 900°C

5.3 Concentration of hydrogen sulphide

Until now, LSCF6428 membrane was evaluated for 200 ppm of hydrogen sulphide and this concentration is the maximum allowable limit in natural gas [12]. This concentration was selected to do accelerated ageing tests to study the long-term effect of hydrogen sulphide in a shorter period of time. However, 200 ppm of hydrogen sulphide could be too much for the membrane to handle. Lower concentration may alter the poisoning mechanism and the membrane could show better stability under hydrogen sulphide. In this section, the membrane was evaluated for 100 and 50 ppm of hydrogen sulphide.

Experimental setup: the membrane was heated to 900°C using air and argon at 20 ml min^{-1} (STP), each. After that, to have a stream of 100 ppm of hydrogen sulphide, 10 ml min^{-1} (STP) of argon was mixed with 10 ml min^{-1} (STP) of 200 ppm hydrogen sulphide (balance argon). On the other hand to have 50 ppm of hydrogen sulphide, 15 ml min^{-1} (STP) of argon was added to 5 ml min^{-1} (STP) of 200 ppm of hydrogen sulphide. The membrane was opened to hydrogen sulphide for 100 h and then it was removed and replaced with argon to observe the recovery.

Results and discussion: 200 ppm of hydrogen sulphide caused immediate drop of oxygen flux to zero but at lower concentration, the membrane survived longer as shown in Figure 5.5. At 50 ppm of hydrogen sulphide, the oxygen flux reached zero after 23 h but at 100 ppm, the flux was zero after 6 h of sulphur introduction. From Figure 5.5, it is concluded that hydrogen sulphide with concentration ranging from 50 to 200 ppm was still capable of totally poisoning the membrane resulting in zero flux during the exposure. It was suggested before that the zero flux was related to hydrogen sulphide attacking and occupying oxygen vacancies in the form of sulphur. Based on these results, it is predicted that even at concentrations less than 50 ppm, hydrogen sulphide will cause significant changes in oxygen flux. Figure 5.5 also tells that exposing the membrane to a lower content of hydrogen sulphide will improve the recovery. This can related to the adsorbed mass of sulphur. It is expected that at higher concentrations of hydrogen sulphide, more sulphur will be deposited on the surface. Presence of higher content of sulphur on the membrane surface could also accelerate strontium segregation to form strontium sulphate.

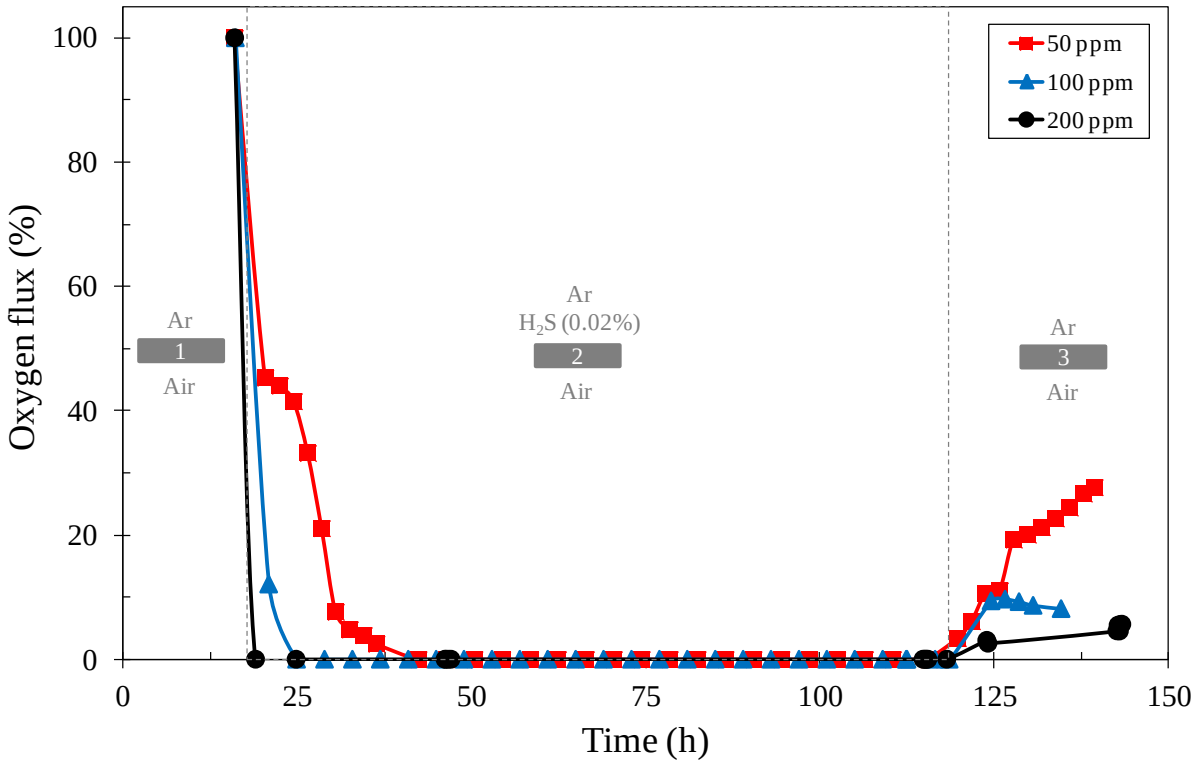

Figure 5.5. Changes of oxygen flux of LSCF membrane during hydrogen sulphide exposure at different concentrations of 50, 100 and 200 ppm for 100 h at 900°C.

5.4 Oxygen partial pressure

It was found that the permanent damage by hydrogen sulphide was related to formation of metal sulphate which altered the conducting properties of the membrane. From Equation (5.1), the corrosion product requires oxygen and it expected that if oxygen content in the air side was reduced, deposition of strontium sulphate would be delayed. Therefore, in this experiment, oxygen partial pressure in the air side was decreased from 0.21 bar to 0.01 bar to see if this cause changes in the poisoning mechanism.

$$SO_{2\,(g)} + SrO + {}^{1}/_{2}\,O_{2\,(g)} \rightarrow SrSO_{4\,(s)} \qquad \Delta G_{900\,℃} = -276 \text{ kJ mol}^{-1} \qquad (5.1)$$

Experimental setup: the experiment consisted of five steps as given in Figure 5.6. The first step was to feed air and argon (20 ml min^{-1}, STP) at 900°C to measure the oxygen flux and check for leak. The second step was to swap air with a stream containing 1% oxygen (balance argon). This step was important to measure the changes in oxygen flux before sulphur introduction. It was estimated to see a drop in oxygen flux because oxygen partial pressure was reduced from 0.21 to 0.01 bar and higher pressure facilitates oxygen transport. The third step was to swap argon with hydrogen sulphide (200 ppm in argon) and keep it for 100 h. The fourth step was to remove hydrogen sulphide and feed back oxygen (1% mol) to measure the recovery. The final step was to go back to the original configuration of air and argon.

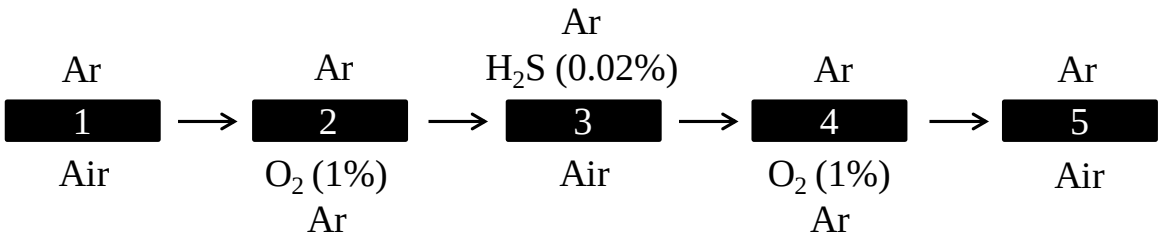

Figure 5.6. Feeds configuration for oxygen partial pressure experiment and sulphur poisoning.

Results and discussion: Figure 5.6 shows interesting results and in brief, 82% of the oxygen flux was recovered when the membrane was exposed to hydrogen sulphide at lower partial pressure of oxygen of 0.01 bar. In details, when air was replaced with 1% (mol) oxygen in the second step, oxygen flux decreased from 0.13 ml cm^{-2} min^{-1} to 0.05 ml cm^{-2} min^{-1} which is 62% reduction in oxygen flux. In the third step where hydrogen sulphide was fed, oxygen permeation was zero as usual but when hydrogen sulphide was removed (fourth step), the flux was recovering and it reached a steady value of 60% of flux before the exposure (second

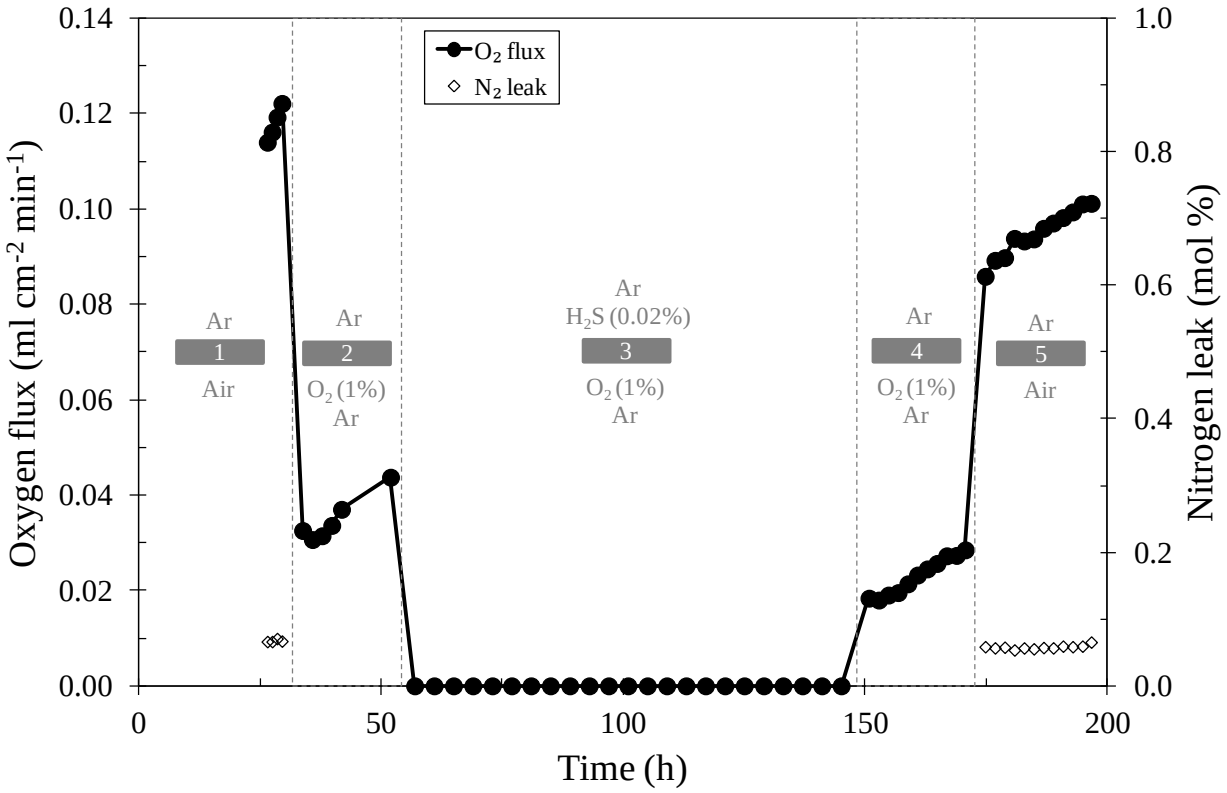

Figure 5.7. Oxygen flux of LSCF6428 membrane after hydrogen sulphide poisoning (200 ppm) using 1% (mol) of oxygen instead of air for 100 h at 900°C.

step). This value is high compared to previous experiments where 6 to 35% was expected. In the fifth step where air was fed back, the flux was 90% of the starting one in step one. The experiment was conducted again, within the same conditions, and the results were repeatable (Figure B.3, Appendix B).

Characterisation: the membrane was characterised by SEM to examine the distribution of metal sulphates at lower oxygen partial pressure. Compared to the primary experiment where the membrane was fed with air and exposed to hydrogen sulphide (section 4.2), metal sulphates of this experiment covered less area and the membrane surface was visible as shown in Figure 5.8. It is possible that these deposits were loose and oxygen managed to diffuse through them.

This experiment revealed that oxygen is critical for strontium sulphate formation and the source of oxygen was from the feed and not from the bulk membrane. To lessen hydrogen sulphide damage after the exposure, oxygen partial pressure in the air side should be reduced. Based on that, it is predicted that minimum damage would be achieved if oxygen partial pressure was set to zero and this was explored in the following section.

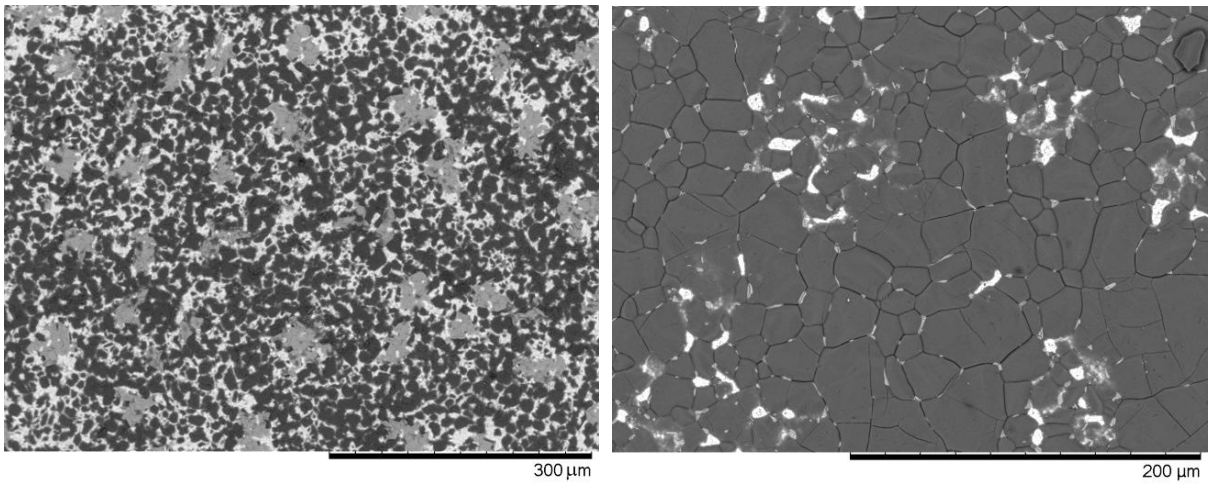

Figure 5.8. SEM images of LSCF6428 membrane after hydrogen sulphide exposure (200 ppm) for 100 h with oxygen partial pressure of 0.01 bar (left) and 0.21 bar (right).

5.5 Absence of oxygen during hydrogen sulphide poisoning

From previous experiment, it was found that oxygen partial pressure played a role in the irreversible poisoning of hydrogen sulphide as it accelerated strontium sulphate formation. The recovery after sulphur exposure was greatly improved if oxygen partial pressure was reduced as this delayed the production of strontium sulphate. In this experiment, oxygen was not fed during the exposure to see if the membrane will receive minimum damage by hydrogen sulphide.

Experimental setup: the membrane was heated to 900°C using flows of air and argon at 20 ml min^{-1} (STP), each. After that, air was replaced with nitrogen to set oxygen partial pressure to zero and argon was replaced with hydrogen sulphide (200 ppm in argon) for 100 h. The final step was to remove hydrogen sulphide and bring back argon and air. Figure 5.9 demonstrates feeds configuration of this experiment.

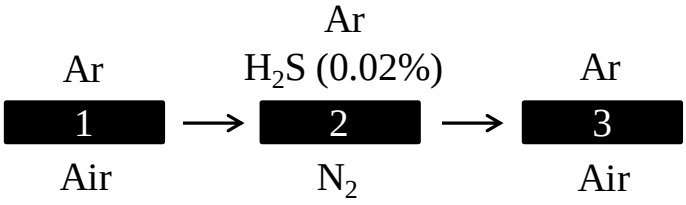

Figure 5.9. Feeds configuration for absence of oxygen experiment during hydrogen sulphide exposure.

Results and discussion: Figure 5.10 gives initial impression that the membrane was fully recovered after hydrogen sulphide exposure in absence of oxygen feed. However, looking closely at the figure, nitrogen leak dramatically increased from 0.02 to 2.15% (mol) which is a hundred times more. The increase in leak was also seen before when the flows were switched after sulphur poisoning. It is known that, at high temperature, if oxygen was not supplied to the membrane, oxygen will be released from the bulk membrane to create vacancies and this will cause membrane expansion [215]. The membrane may expand severely and this resulted in internal stress inside the membrane. The experiment was repeated and the increase in leak was still observed (Figure B.4, Appendix B). The sealant may also contribute in the increase in leak as it may prevent the membrane from expanding freely. Therefore, effect of sealant was investigated by repeating the experiment with silver instead of gold-glass-ceramic sealant. Results show that the leak still increased from 0.3 to 3% (mol) (Figure E.1, Appendix). This may tell that the membrane itself cracked due to loss of oxygen and the sealant did not contribute in the increase of leak.

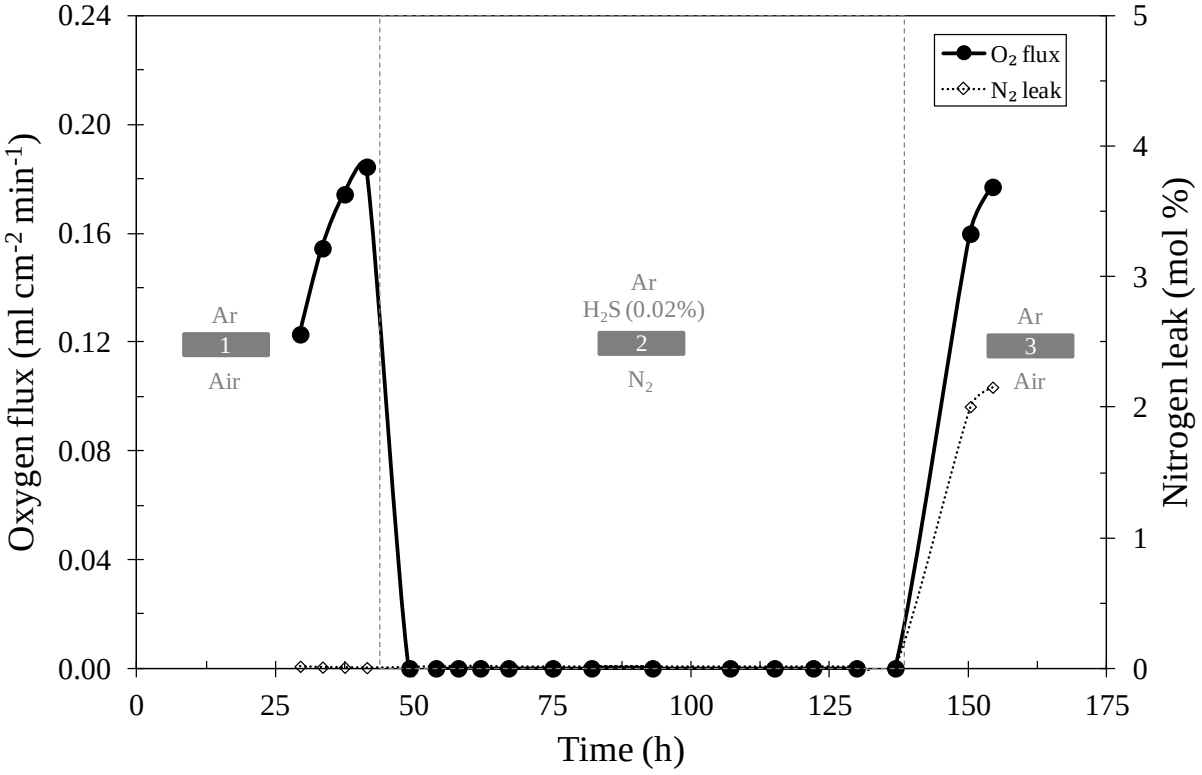

Figure 5.10. Changes of the flux in absence of oxygen feed during hydrogen sulphide poisoning of LSCF6428 membrane at 900°C for 100 h.

5.6 Summary

In this chapter, more experiments of hydrogen sulphide poisoning on LSCF6428 membrane were carried out for better understanding about the mechanism. Effects of exposure duration, temperature, concentration of hydrogen sulphide and oxygen partial pressure were studied. It was found that exposing the membrane to hydrogen sulphide for one hour caused zero flux but it was fully restored after 24 h of hydrogen sulphide removal from the feed. The experiment suggested that the adsorption of sulphur on the membrane surface occurs rapidly but this step was reversible. With time, strontium segregates towards sulphur to form irreversible strontium sulphate. The membrane was also tested for hydrogen sulphide impurity at different temperatures of 800 to 950°C but the oxygen flux was still zero during the exposure. However, operating at 950°C was favourable because it took longer to reach zero flux, also, the recovery was better. Furthermore, LSCF6428 membrane was evaluated for lower concentrations of hydrogen sulphide of 100 and 50 ppm but these values were enough to immobilise the oxygen flux. Based on these results, it is predicted that hydrogen sulphide will cause significant change in the flux even if the concentration was below 50 ppm.

Impact of oxygen partial pressure (in the air side) on sulphur poisoning was investigated and it played a major role in the irreversible damage. This was related to the deposition of strontium sulphate which requires external source of oxygen. It was discovered that higher oxygen partial pressure results in more damage as it accelerates strontium sulphate formation. As a strategy to lessen the damage by hydrogen sulphide, it is advised to reduce the oxygen partial pressure in the air side. The membrane was also tested for hydrogen sulphide poisoning in no oxygen to see if this can give minimum damage but unfortunately, the membrane failed and leak sharply increased. This was explained by the continuous expansion of the membrane due to the loss of lattice oxygen.

Chapter 6: Hydrogen Production by LSCF6428 Membrane in Presence of Hydrogen Sulphide

Chapter 6: Hydrogen Production by LSCF6428 Membrane in Presence of Hydrogen Sulphide

In previous chapters, impact of hydrogen sulphide impurity was studied under air separation and it seriously interrupted the oxygen permeation. In this chapter, LSCF6428 membrane has been used for long-term hydrogen production by partial-oxidation of methane (POM) in existence of hydrogen sulphide. First, blank-run experiments are carried out to make sure that setup does not cause any unwanted reactions. After that, POM is performed in sulphur-free environment as a reference experiment. Next, hydrogen sulphide is introduced during POM and changes in oxygen flux and methane conversion are observed. The chapter also discusses the use hydrogen to restore the membrane after the poisoning. Further study is conducted by pre-poisoning the membrane under air separation and then tests it for POM.

6.1 Blank-run experiments

From methodology chapter, the reactor consisted of quartz, alumina tubes and stainless steel body. There is a possibility that these materials can cause side reactions with methane because of the high operating temperature of 900°C. Thermal decomposition of methane in presence of LSCF6428 membrane may also take place because it is reported that metal oxides cause methane cracking to hydrogen and carbon [216-218]. It is also known that hydrogen sulphide can react with methane to produce hydrogen and carbon disulfide and this process is called hydrogen sulphide-methane reforming [219]. All the above points were investigated in this chapter to help in determining the poisoning mechanism later.

Experimental design: the blank run consisted of five experiments operated at 900°C with different setups. In experiment 1, methane (1% mol, balance argon) was fed at 20 ml min^{-1} (STP) to the reactor without the membrane and the outlet gas was analysed to observe if methane was consumed. This experiment gave information about the possibility of methane reaction with reactor's materials. In experiment 2, the same stream was fed but in presence of LSCF6428 membrane to see if decomposition of methane occurs. In experiment 3, oxygen (1% mol, balance argon) was fed at 20 ml min^{-1} (STP) along methane with no membrane to see if oxidation can take place without the requirement of a catalyst. In experiment 4, a stream containing 1% (mol) of methane and 200 ppm of hydrogen sulphide was fed to the reactor

with no membrane to examine if methane reacts with hydrogen sulphide at 900°C. In the final experiment, oxygen (1% mol, balance argon) was added to the previous stream which contained methane and hydrogen sulphide to notice the effect of hydrogen sulphide on methane oxidation.

Results and discussion: Table 6.1 shows the results of each experiment and methane conversion (x_{CH_4}) was calculated using the following equation:

$$x_{CH_4}(\%) = \frac{y_{CH_{4(in)}} - y_{CH_{4(out)}}}{y_{CH_{4(in)}}} \times 100 \quad (6.1)$$

where $y_{CH_{4(in)}}$ and $y_{CH_{4(out)}}$ are methane mole fraction in the inlet and outlet gases, respectively. The value of $y_{CH_{4(in)}}$ is always 0.01 because methane concentration was 1% (mol) in the inlet gas and $y_{CH_{4(out)}}$ was measured by GC. In experiment 1 where methane was fed with no membrane nor oxygen, conversion was zero meaning that it was not consumed and therefore it did not react with the reactor materials of quartz, alumina or stainless steel. In experiment 2, methane was fed along LSCF6428 membrane (with no oxygen) and the conversion was still zero indicating that methane did not react with the membrane and the later did not promote methane decomposition. When oxygen was introduced to methane in experiment 3 with no membrane, the conversion was 80% meaning that the oxidation process took place at 900°C without a catalyst. In experiment 4 where methane and hydrogen sulphide were fed in absence of the membrane, the zero conversion implied that methane did not react with hydrogen sulphide and it did not cause any cracking or reforming. In experiment 5, presence of hydrogen sulphide along methane and oxygen without the membrane, caused decrease in conversion from 80% to 60%. Sulphur may act as a barrier between oxygen and methane and this reduced the reactivity.

Table 6.1. Blank run experiments for methane oxidation

No.	Feed	$x_{CH_4}(\%)$	Conclusion
1	1% CH_4	0	No reaction with reactor materials
2	1% CH_4 with membrane	0	No CH_4 cracking
3	1% CH_4 + 1% O_2	80	CH_4 oxidation occurs in no catalyst
4	1% CH_4 (200 ppm H_2S)	0	H_2S does not react with CH_4
5	1% CH_4 (200ppm H_2S) + 1% O_2	60	H_2S caused reduction in CH_4 oxidation

6.2 Partial oxidation of methane in sulphur-free experiment

LSCF6428 membrane was tested for methane oxidation and the longest duration was 200 h reported by Iguchi et al. [117]. Many researchers however mentioned membrane failure after few hours of methane introduction [119, 220]. The failure could be related to the reducing environment of methane which increased the release of oxygen from the bulk membrane and as a consequence, the membrane expanded rapidly and this created a mechanical stress [119]. The researchers also suggested that sealant could play a critical role in the failure due to mismatch in expansion rate [119, 220]. In this section, LSCF6428 membrane was tested for long-term methane oxidation using the new gold-glass-ceramic sealant.

Experimental setup: LSCF6428 membrane was heated to 900°C using flows of air and argon at 20 ml min^{-1} (STP), each. After that, argon was replaced with methane (1% mol, balance argon) and fed at flow rate of 20 ml min^{-1} (STP). During operation, the product gas was analysed by GC to measure oxygen flux and methane conversion.

Results and discussion: LSCF6428 membrane was successfully used for long-term methane oxidation and it achieved 340 h as given in Figure 6.1. This period of 340 h outran the maximum reported duration of 200 h by Iguchi et al. [117]. It is worth mentioning that the membrane did not fail after 340 h but it was decided to terminate the experiment. Success of this experiment was strongly related to the gold-glass-ceramic sealant which prevented expansion mismatch between the membrane and the sealant. Methane conversion was 33% and oxygen flux during methane oxidation was calculated by the following equation because some of the oxygen was consumed by methane to form carbon monoxide, carbon dioxide and water:

$$J_{O_2}(\text{ml cm}^{-2}\text{ min}^{-1}) = \left[y_{O_2} + y_{CO_2} + \frac{1}{2}y_{CO} + \frac{1}{2}y_{H_2O} - \frac{0.21}{0.79}y_{N_2}\right] \times \frac{F}{A} \quad (6.2)$$

where y_x is the mole fraction of specie x in the product gas, F is the flow rate (20 ml min^{-1}, STP) and A is the membrane active area (0.44 cm^{-2}). The term $\frac{0.21}{0.79}y_{N_2}$ is the amount of leaked oxygen as mentioned before in chapter 4. Unfortunately, the setup was not capable of detecting water in the product gas (y_{H_2O}), therefore it was calculated based on hydrogen atomic balance:

$$y_{H_2O} = 2y_{CH_{4(in)}} - 2y_{CH_{4(out)}} - y_{H_2} \quad (6.3)$$

As given in Figure 6.1, oxygen was increasing when methane was introduced. It looks like the reducing environment of methane increased the driving force for oxygen transport because

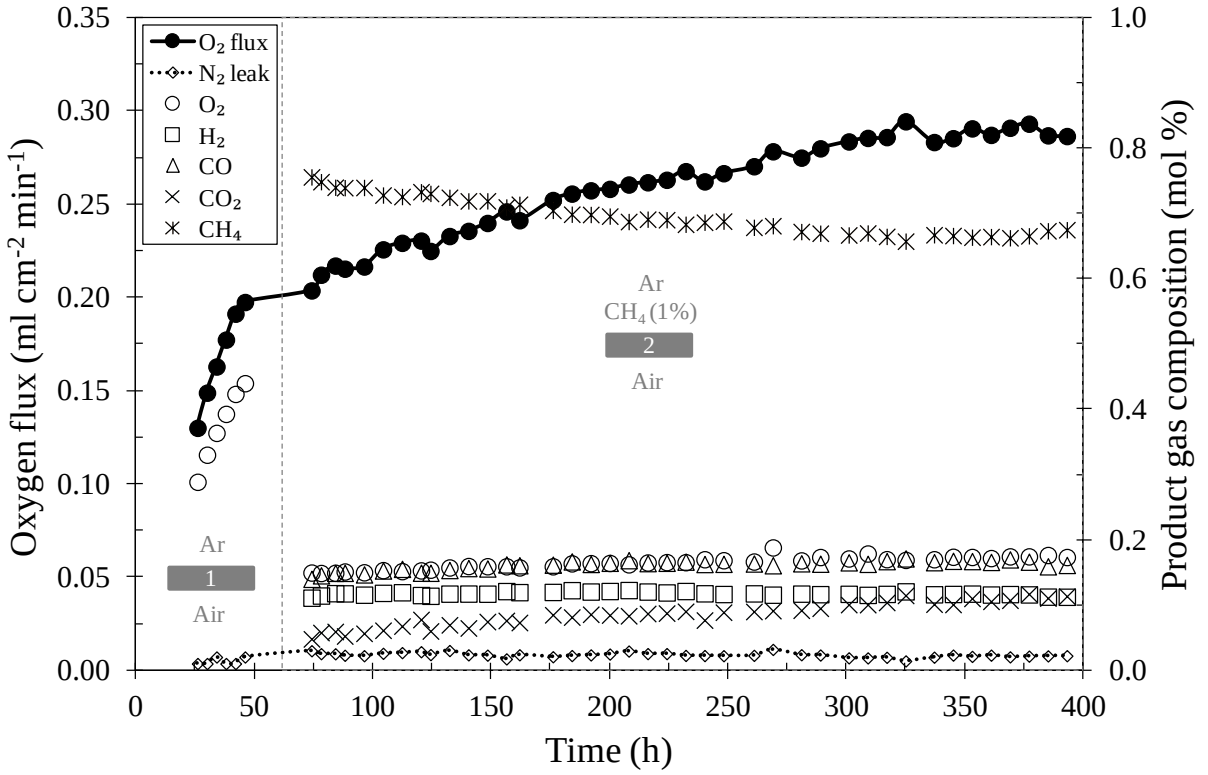

Figure 6.1. Long-term methane oxidation of 340 h using LSCF6428 membrane fed by 1% (mol) methane and air at 900°C.

oxygen was rapidly consumed by methane. When methane reacts with oxygen, there are two routes for the oxidation: a) partial oxidation to form hydrogen and carbon monoxide, and b) complete oxidation to form water and carbon dioxide. Selectivity of carbon monoxide (S_{CO}) refers to the percentage of partial oxidation to the whole reaction and it was calculated by:

$$S_{\mathrm{CO}}(\%) = \frac{y_{CO}}{y_{CO} + y_{CO_2}} \times 100 \tag{6.4}$$

The average value of carbon monoxide selectivity was 65% meaning that 65% of the oxidised methane was partial oxidation and the remaining 35% accounts for total oxidation.

To make sure that the experiment was correctly performed, carbon atomic balance was carried out by:

$$C_{Accumulation}\ (\%) = \left[y_{CH_{4(in)}} - y_{CH_{4(out)}} - y_{CO} - y_{CO_2}\right] \times 100 \tag{6.5}$$

Applying the previous equation gives carbon accumulation of 0.01% meaning that 100 ppm of carbon was deposited on the surface but this within the uncertainty of GC measurements. The average value of hydrogen-to-carbon monoxide ratio (H_2/CO) was 0.7 but it is far from the theoretical value of 2 as shown previously in Equation 2.16. Furthermore, Figure 6.1

shows that the product gas contained some oxygen meaning that it did not react with methane. This behaviour was also seen by other researchers [221]. Therefore, a catalyst is recommended to optimise oxygen consumption and increase the value of hydrogen-to-carbon monoxide ratio. Table 6.2 compares conversion and duration of this experiment to the reported data in literature. In the following section, the membrane was characterised to observe the changes after methane oxidation.

Characterisation: after operation, the membrane was examined by SEM and both methane and air surfaces were normal as given in Figure 6.2. The grain structure did not change and no secondary phases were observed. EDS shows similar elemental composition before and after operation indicating that the membrane was stable under the reducing environment of methane (Table 6.3). Sharp perovskite peaks were detected in methane and air surfaces and

Table 6.2. Reported duration and conversion for methane oxidation using LSCF6428 membrane at 900°C.

Study	Sealant	Air side	Methane side	x_{CH_4} (%)	Duration (h)
Iguchi et al. [117]	Glass	21% O_2 (1–5 ml min^{-1})	25% CH_4 (1–5 ml min^{-1})	7	200
Sureena [221]	Ceramic	2% O_2 (30 ml min^{-1})	5% CH_4 (30 ml min^{-1})	30	45
This work	Gold-glass-ceramic	21% O_2 (20 ml min^{-1})	1% CH_4 (20 ml min^{-1})	33	340

Table 6.3. EDS analysis of LSCF6428 membrane before and after methane oxidation of 340 h at 900°C using 1% (mol) methane and air.

Membrane	Element (atomic %)						
	La	Sr	Co	Fe	O	C	S
Fresh	12	9	4	17	52	6	0
Methane side	12	10	5	18	45	10	0
Air side	12	10	4	17	47	10	0

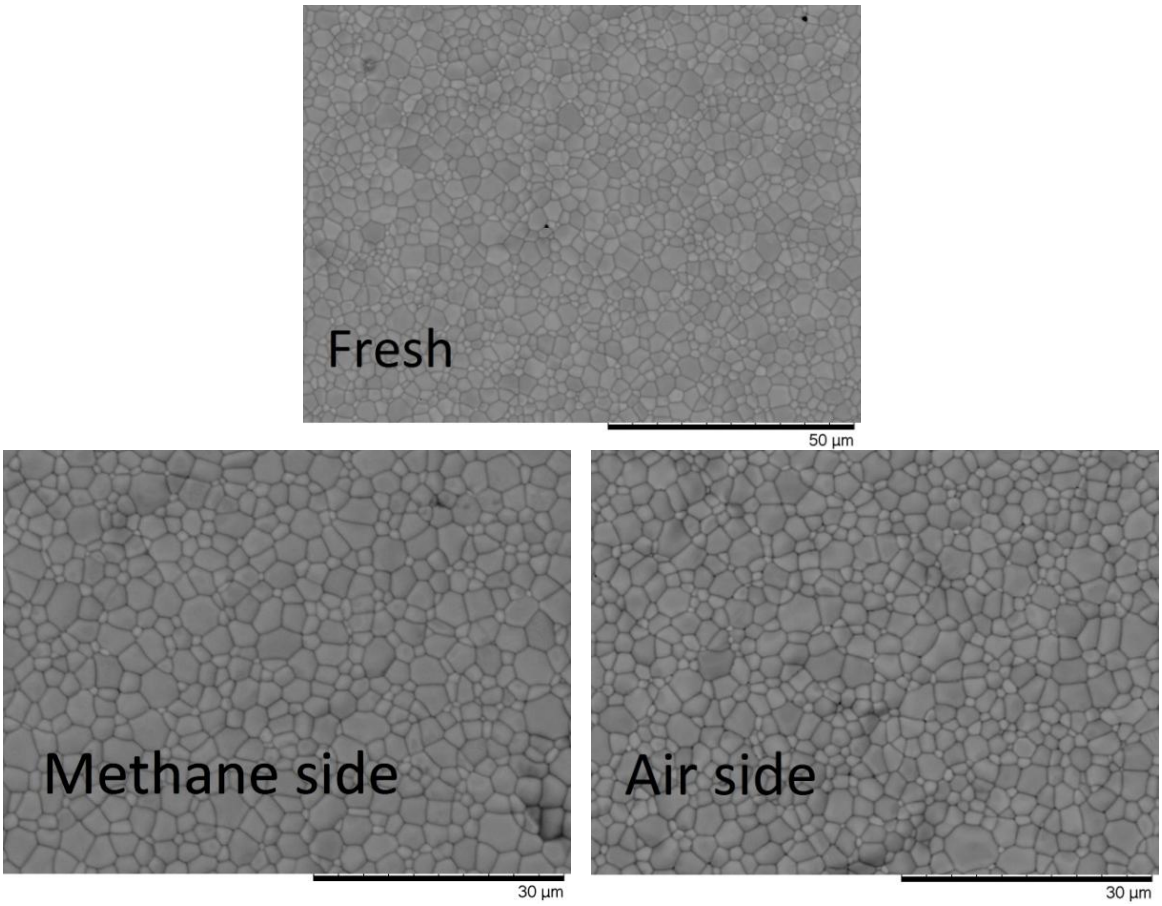

Figure 6.2. SEM images of LSCF6428 membrane before and after methane oxidation of 340 h at 900°C by feeding 1% (mol) methane and air.

this confirms the stability of the membrane (Figure 6.3). XPS however measured large amounts of carbon and as mentioned before, the high content of carbon could be from dust, handling, storage or the reaction of strontium oxide from the bulk membrane to form strontium carbonate due to the high mobility and reactivity of strontium [188].

Interestingly, the characterisation techniques revealed that the membrane did not suffer from any major changes after 340 h of methane oxidation. This result was also found when the membrane was used for air separation for 450 h. In literature, the longest reported duration for air separation using LSCF6428 was 5512 h and therefore it is expected to see the membrane achieve that duration for partial-oxidation of methane [222]. It should be noted that the characterisation techniques did not detect any sodium pinpointing that the sealant was stable under methane environment. In the next section, hydrogen sulphide was fed to see the impact on methane conversion.

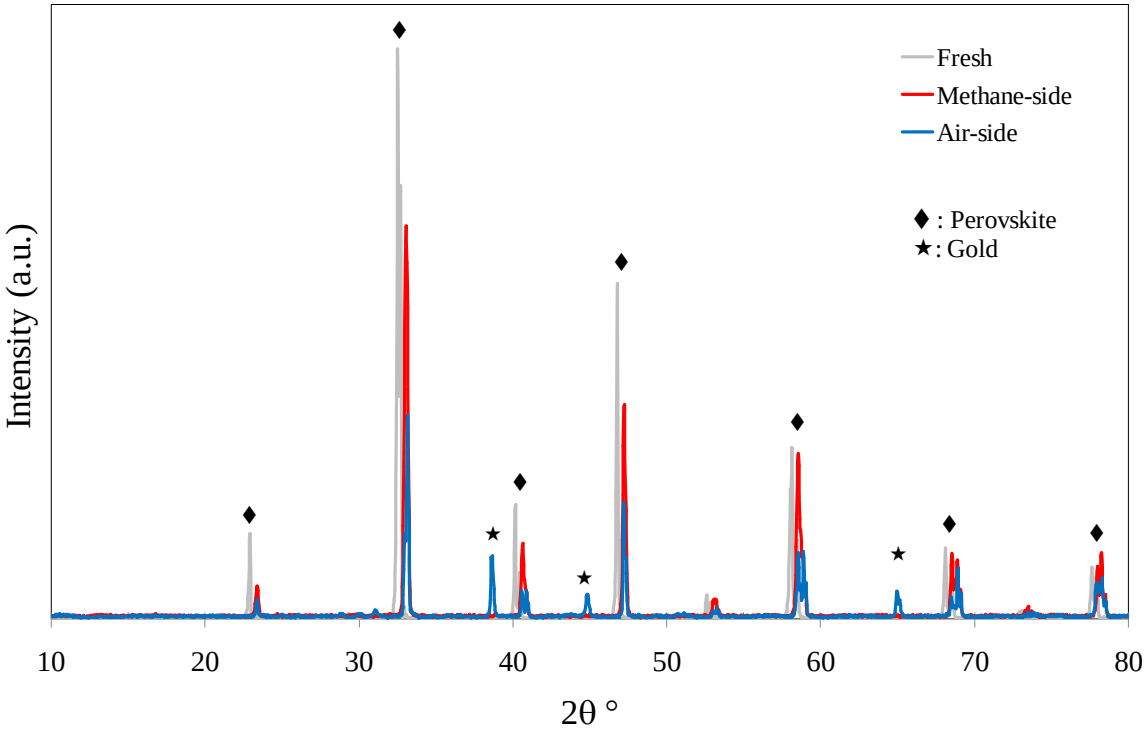

Figure 6.3. XRD analysis of LSCF6428 membrane before and after methane oxidation of 340 h at 900°C using 1% (mol) methane and air.

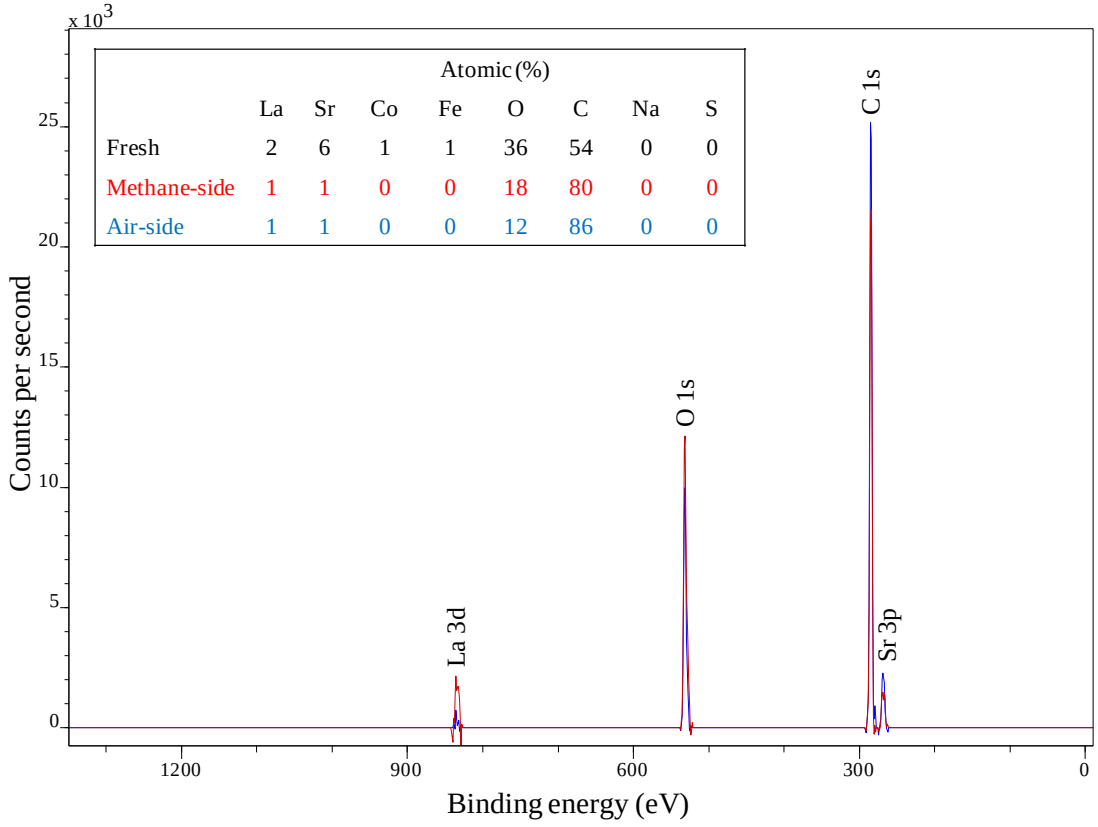

Figure 6.4. XPS analysis of LSCF6428 membrane before and after methane oxidation for 340 h at 900°C by feeding 1% (mol) methane and air.

6.3 Presence of hydrogen sulphide during partial-oxidation of methane

From previous experiment, LSCF6428 membrane was stable for methane oxidation for 340 h without any significant changes. If this technology will be applied in industry, natural gas would be fed rather than pure methane. This gas usually contains impurities of hydrogen sulphide. The maximum allowable limit of hydrogen sulphide in commercial natural gas is 200 ppm and therefore it is important to study the impact of sulphur on the membrane performance during methane oxidation [12]. In chapter 4 for air separation by LSCF6428 membrane, it was discovered that hydrogen sulphide caused total immobilisation of oxygen transport and after the exposure, major of the flux was permanently lost. Based on these findings, it is expected that hydrogen sulphide will greatly interrupt the performance of LSCF6428 for methane oxidation.

Experimental setup: the experiment consisted of four steps as shown in Figure 6.5. In step 1, the membrane was fed with air and argon at 900°C with flow rates of 20 ml min^{-1} (STP), each. In step 2, methane oxidation was carried out by swapping argon with a feed containing 1% (mol) methane (balance argon) at 20 ml min^{-1} (STP). In step 3, methane was replaced with a stream having 1% (mol) methane with 200 ppm hydrogen sulphide (balance argon) for 100 h at 20 ml min^{-1} (STP). In step 4, the stream containing methane only was brought back to measure the recovery after sulphur poisoning.

Results and discussion: the starting oxygen flux (using air and argon) was 0.21 ml min^{-1} and after methane introduction, it increased to 0.35 ml cm^{-2} min^{-1} after 48 h, as given in Figure 6.6. Methane conversion was 47% but after few hours of hydrogen sulphur introduction, it drops to 8% but it was increasing with time and it reached a steady-state value of 15% after 50 h. The same behaviour was noticed for oxygen flux; it decreased to 0.04 ml cm^{-2} min^{-1} after feeding hydrogen sulphide and then it was recovering with time and it reached 0.10 ml min^{-1} which is 29% of the flux in step 2. After hydrogen sulphide removal

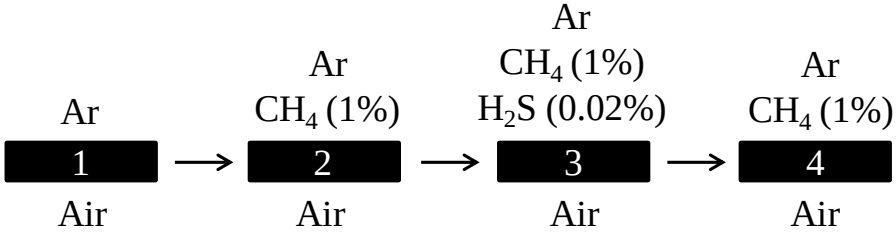

Figure 6.5. Feeds configuration for partial-oxidation of methane in presence of sulphur impurity

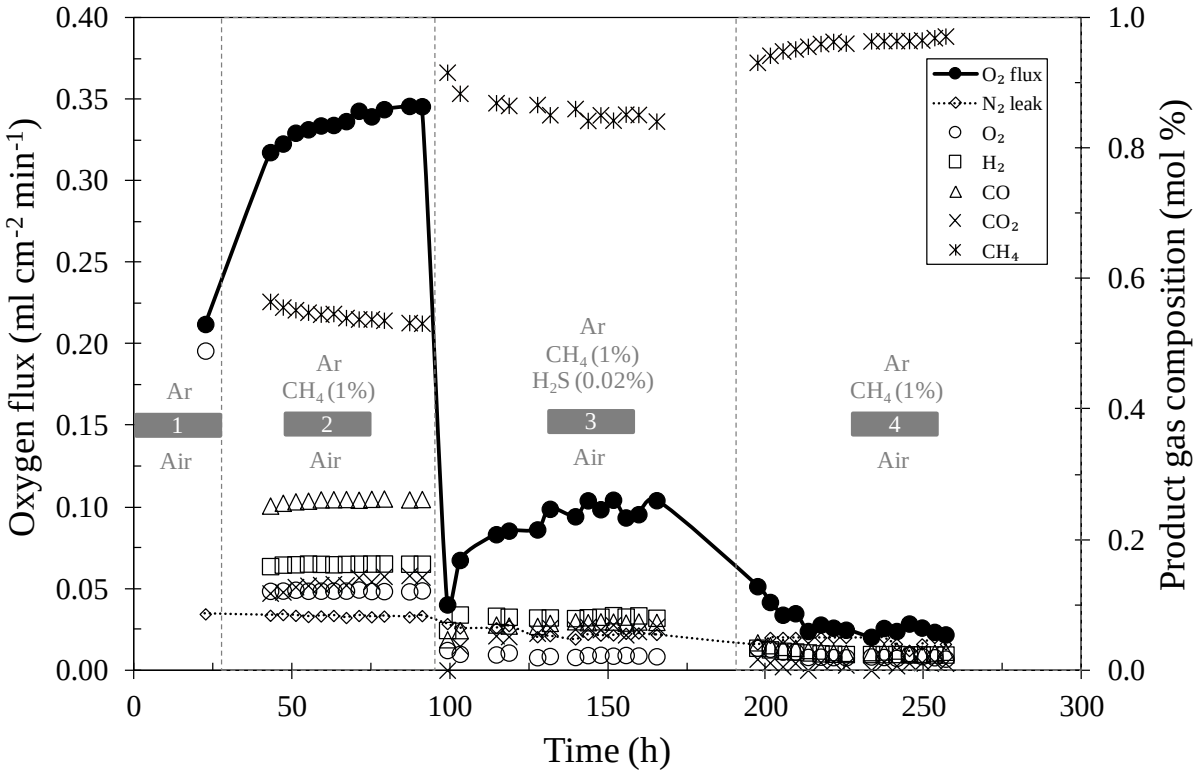

Figure 6.6. Long-term stability of LSCF6428 membrane for methane oxidation in presence of hydrogen sulphide (200 ppm) at 900°C.

from methane (step 4), the conversion kept on decreasing and it hit 3%. This behaviour is unusual and to determine if the data was reliable, the experiment was repeated with same conditions but similar results were obtained (Figure B.5, Appendix B).

Interestingly, the flux was not zero during methane oxidation in presence of hydrogen sulphide (step 3 in Figure 6.6). However, from previous chapters where the membrane was used for air separation, hydrogen sulphide caused drop of oxygen flux to zero within few hours. It was suggested before that hydrogen sulphide was oxidised by the permeated oxygen to produce sulphur dioxide (Equation 6.6) and then sulphur occupied the oxygen vacancy (Equation 6.7):

$$H_2S_{(g)} + {}^3/_2\, O_{2\,(g)} \rightarrow SO_{2\,(g)} + H_2O_{(v)} \tag{6.6}$$

$$SO_{2\,(g)} + V_O^{\bullet\bullet} + 2e- \rightarrow S_O^x + O_{2\,(g)} \tag{6.7}$$

Looking at Figure 6.6, the flux sharply decreased once hydrogen sulphide was introduced and it is possible that Equations 6.6 and 6.7 took place. The non-zero flux during the exposure can be explained by the following mechanisms:

- Mechanism 1: reaction of hydrogen sulphide with methane. From section 6.1, blank run experiment showed that methane does not react with hydrogen sulphide at 900°C but that study was in absence of LSCF6428 membrane. However, in this experiment, there is a possibility that the reaction occurred and the membrane acted as catalyst:

$$CH_{4\,(g)} + 2H_2S_{(g)} \leftrightarrow CS_{2(g)} + 4H_{2(g)} \qquad \Delta G_{900\,℃} = 394 \text{ kJ mol}^{-1} \qquad (6.8)$$

As indicated by positive Gibbs energy (thermodynamic data from [207]), the reaction should not take place at 900°C but it reported that use of a metal-based catalyst can promote the reaction even at 500°C [223, 224]. Presence of metal oxides in the membrane may provide the catalytic sites for the reaction. Although the environment is changed to carbon disulphide (CS_2) as given in Equation 6.8, there is a chance that carbon disulphide was oxidised back to sulphur dioxide:

$$CS_{2\,(g)} + {}^{5}/_{2}\, O_{2\,(g)} \rightarrow CO_{(g)} + 2\, SO_{2(g)} \qquad \Delta G_{900\,℃} = -749 \text{ kJ mol}^{-1} \qquad (6.9)$$

$$CS_{2\,(g)} + 3O_{2\,(g)} \rightarrow CO_{2\,(g)} + 2\, SO_{2\,(g)} \qquad \Delta G_{900\,℃} = -929 \text{ kJ mol}^{-1} \qquad (6.10)$$

Unfortunately, the method of calorimetric tubes was not able to detect carbon disulphide due to the overlap with hydrogen sulphide. But, the method can detect hydrogen sulphide without carbon disulphide interference and 90 ppm of hydrogen sulphide was measured in the product gas. The produced hydrogen by Equation(6.8) may remove some sulphur from the membrane surface and this restored part of the flux. However, the limiting reactant of Equation 6.8 is hydrogen sulphide and thus only 400 ppm of hydrogen will be produced. It was found from chapter 4 that poisoning is quick and the regeneration is very slow even if 1% (mol) of hydrogen was used. So, it is unlikely that 400 ppm of hydrogen is enough to restore 30% of oxygen flux and therefore the suggested mechanism is weak.

- Mechanism 2: methane decomposition. Table 6.1 indicates that methane does not decompose at 900°C even if LSCF6428 membrane was presented. However, presence of hydrogen sulphide and the adsorbed sulphur on the membrane surface may set off methane decomposition:

$$CH_{4\,(g)} \leftrightarrow C_{(s)} + 2H_{2\,(g)} \qquad (6.11)$$

It is reported that a temperature of 1200°C is required to thermally decompose methane but the temperature can be greatly reduced to 500°C if a metal sulphide catalyst was used [216-218, 225, 226]. There is a possibility that metal sulphides were formed during hydrogen sulphide poisoning and they acted as a catalyst for methane decomposition:

$$SrO_{(s)} + H_2S_{(g)} \rightarrow SrS_{(s)} + H_2O_{(g)} \qquad \Delta G_{900\,℃} = -93 \text{ kJ mol}^{-1} \qquad (6.12)$$

$$La_2O_{3\,(s)} + 3H_2S_{(g)} \rightarrow La_2S_{3\,(s)} + 3H_2O_{(g)} \qquad \Delta G_{900\,℃} = -75 \text{ kJ mol}^{-1} \qquad (6.13)$$

$$FeO_{(s)} + H_2S_{(g)} \rightarrow FeS_{(s)} + H_2O_{(g)} \qquad \Delta G_{900\,℃} = -42 \text{ kJ mol}^{-1} \qquad (6.14)$$

$$Fe_2O_{3\,(s)} + H_2S_{(g)} \rightarrow Fe_2S_{3\,(s)} + H_2O_{(g)} \qquad (6.15)$$

$$CoO_{(s)} + H_2S_{(g)} \rightarrow CoS_{(s)} + H_2O_{(g)} \qquad (6.16)$$

negative Gibbs energy of reaction (thermodynamic data from [207]) validates formation of some metal sulphides such as strontium sulphide (SrS), lanthanum sulphide (La_2S_3) and iron sulphide (FeS) at 900°C. Due to lack of data, Gibbs energy of reaction could not be calculated for iron (III) sulphide (Fe_2S_3) and cobalt sulphide (CoS). Carbon balance mass was performed before and during the exposure and the values were 0.06 and 0.02%, respectively. So, the deposition actually decreased during the exposure and it is possible that the deposited carbon was readily converted to carbon dioxide:

$$C_{(s)} + O_{2\,(g)} \rightarrow CO_{2\,(g)} \qquad \Delta G_{900\,℃} = -396 \text{ kJ mol}^{-1} \qquad (6.17)$$

in this mechanism, production of hydrogen is not limited by the concentration of hydrogen sulphide but it is controlled by the presence of metal sulphides on the membrane surface. Thus, this mechanism probably was behind the non-zero conversion during hydrogen sulphide exposure.

When hydrogen sulphide was no longer fed (step 4 in Figure 6.6), methane conversion continued on decreasing at it remained at 3%. It looks like the membrane surface was poisoned by sulphur and this altered the properties of the membrane. Before the poisoning, the membrane could provide the area for the reaction between methane and oxygen but deposition of sulphur on the surface could inhibit the reaction. Based on mechanism 1 which suggests hydrogen sulphide-methane interaction, absence of hydrogen sulphide means that the reforming reaction (Equation 6.8) in no longer valid. In mechanism 2 where methane decomposition was proposed, removal of hydrogen sulphide could result in regeneration of some metal sulphides back to metal oxides (thermodynamic data from [207]):

$$SrS_{(s)} + {}^{3}/_{2}\, O_{2\,(g)} \rightarrow SrO_{(s)} + SO_{2\,(g)} \qquad \Delta G_{900\,℃} = -333 \text{ kJ mol}^{-1} \qquad (6.18)$$

$$La_2S_{3\,(s)} + {}^{9}/_{2}\, O_{2\,(g)} \rightarrow La_2O_{3\,(s)} + 3SO_{2\,(g)} \qquad \Delta G_{900\,℃} = -1204 \text{ kJ mol}^{-1} \qquad (6.19)$$

$$FeS_{(s)} + {}^{3}/_{2}\, O_{2\,(g)} \rightarrow FeO_{(s)} + SO_{2\,(g)} \qquad \Delta G_{900\,℃} = -769 \text{ kJ mol}^{-1} \qquad (6.20)$$

$$Fe_2S_{3\,(s)} + {}^{9}/_{2}\,O_{2\,(g)} \rightarrow Fe_2O_{3\,(s)} + 3SO_{2\,(g)} \quad (6.21)$$

$$CoS_{(s)} + {}^{3}/_{2}\,O_{2\,(g)} \rightarrow CoO_{(s)} + SO_{2\,(g)} \quad (6.22)$$

these sulphides could act as a catalyst for methane decomposition and removal of the sulphides might stop methane decomposition. After operation, the membrane was characterised to look at the changes and this may help in determining the poisoning mechanism of hydrogen sulphide.

Characterisation: new phase was observed on the methane-side surface by SEM as shown in Figure 6.7. This phase is comparable to what was seen before where the membrane was exposed to hydrogen sulphide during air separation. The phase consisted of sodium and sulphur as measured by EDS (Table 6.4). XRD (Figure 6.8) and XPS (Figure 6.9) identified the phase as sodium sulphate. Therefore, all characterisation techniques revealed that the new phase of this experiment is identical in shape and composition to what was found in chapter 4. It was suggested before that hydrogen sulphide exposure resulted in formation of strontium sulphate but sodium from the gold-glass-ceramic sealant reacted with strontium sulphate to form sodium sulphate and this step was during the cooling down process. Based on characterisation techniques, it is possible that after hydrogen sulphide removal, the adsorbed sulphur did not regenerate and instead, it was further poisoned to metal sulphate and this explains the reduction in methane conversion after hydrogen sulphide removal.

Air-side surface was also examined by characterisation techniques but no changes were observed meaning that the adsorbed sulphur did not diffuse to the air side surface. Also, the normal surface indicates the sealant was stable under the reducing environment.

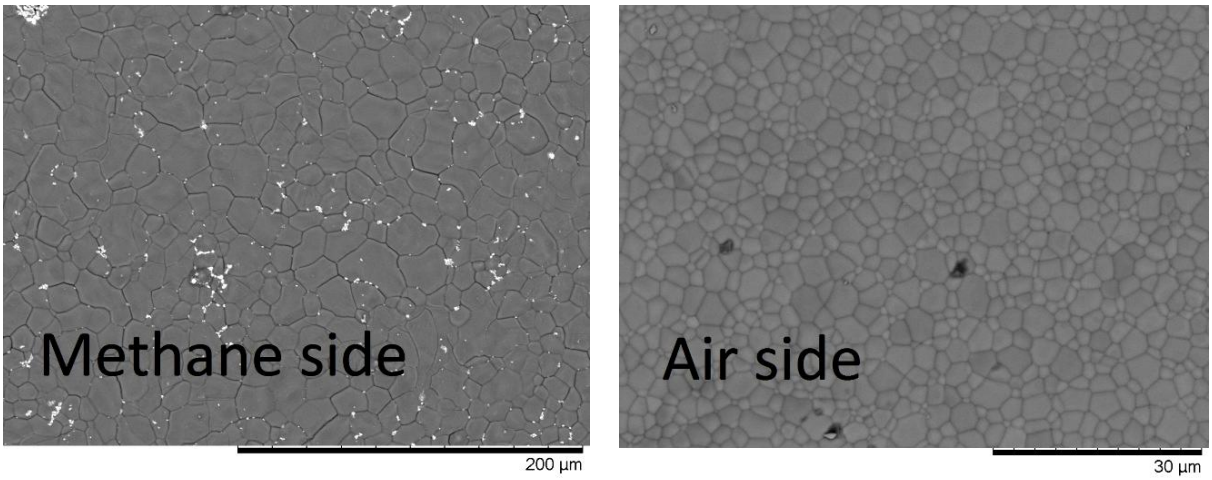

Figure 6.7. SEM images of LSCF6428 membrane after methane oxidation in presence of hydrogen sulphide (200 ppm) for 100 h at 900°C using air and 1% methane.

Table 6.4. EDS analysis of LSCF6428 membrane after methane oxidation in presence of hydrogen sulphide (200 ppm) at 900°C for 100 h by feeding air and 1% methane.

Membrane	Element (atomic %)							
	La	Sr	Co	Fe	O	C	S	Na
Methane side	0	2	0	0	57	0	13	28
Air side	11	8	4	17	52	8	0	0

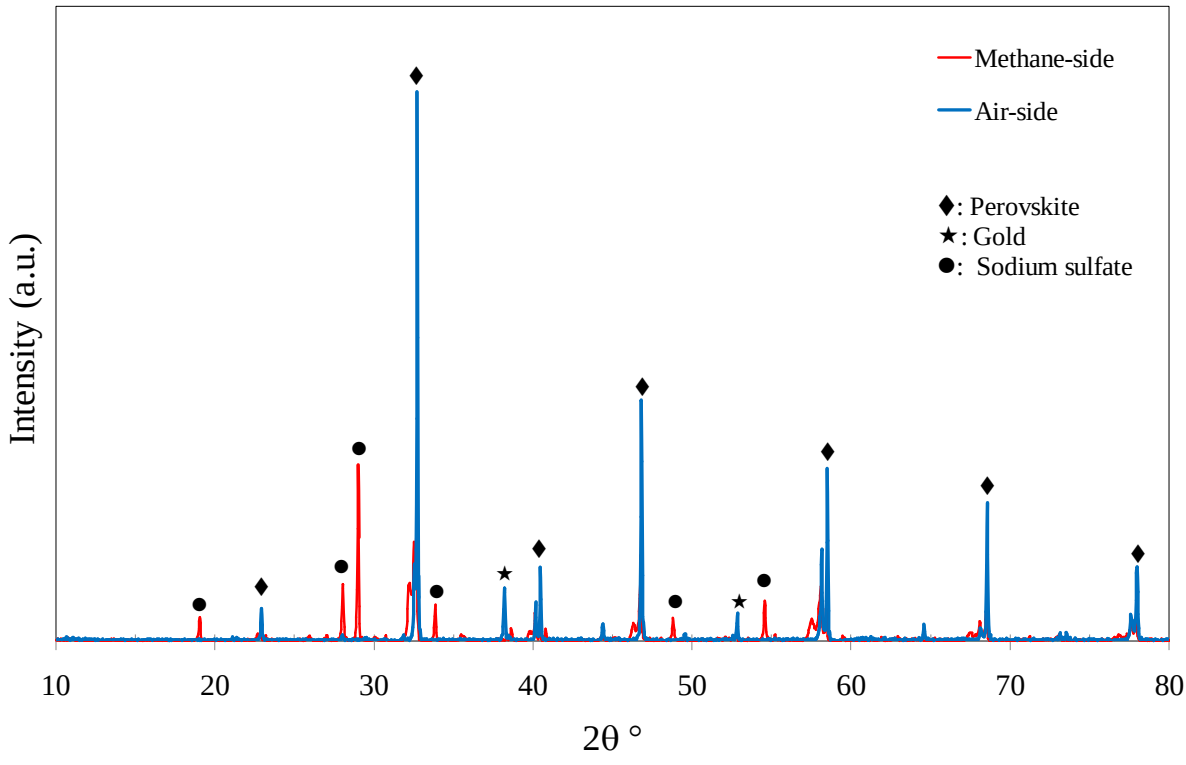

Figure 6.8. XRD analysis of LSCF6428 membrane after hydrogen sulphide exposure for 100 h during methane oxidation at 900°C using air and 1% methane.

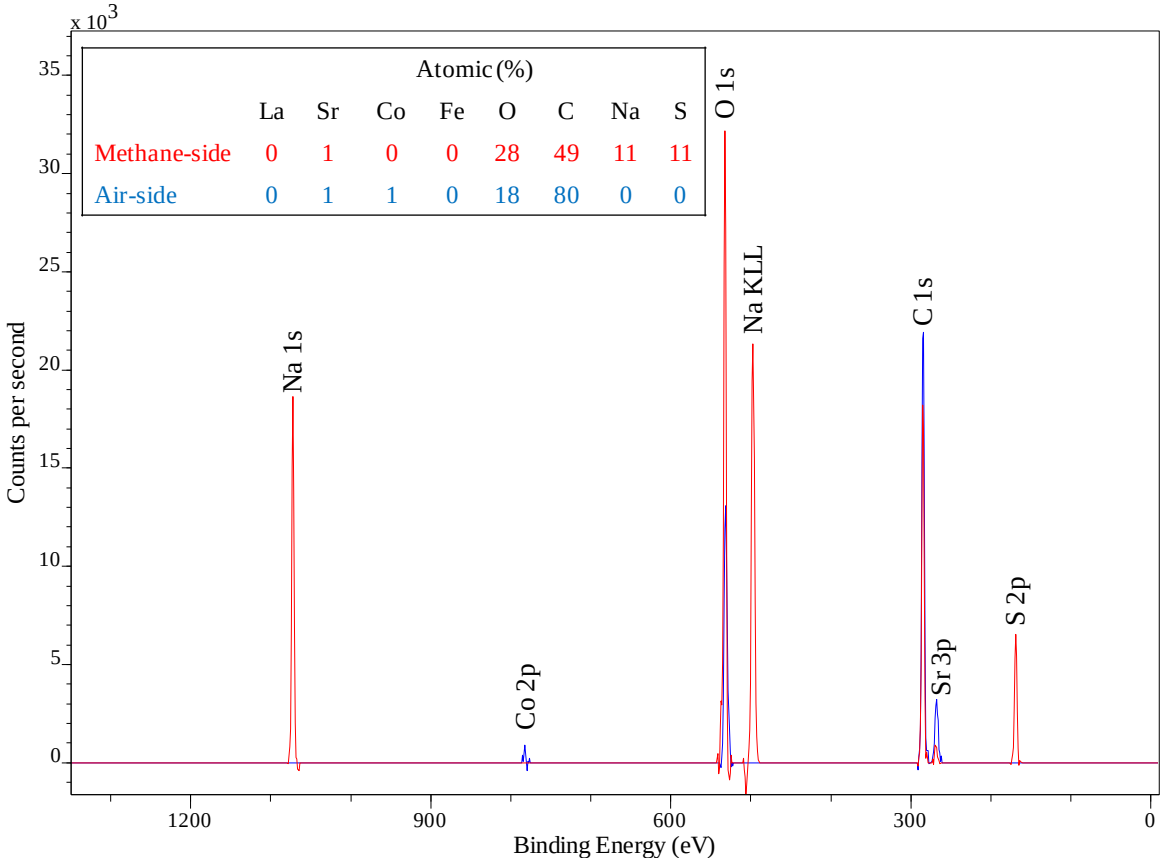

Figure 6.9. XPS analysis of LSCF6428 membrane after sulphur poisoning during methane oxidation for 100 h at 900°C.

Summary: introduction of hydrogen sulphide impurity during methane oxidation resulted in a sharp drop in the conversion. However, during the exposure, the conversion was not zero and it remained at 15%. This steady conversion was interpreted by the reaction of hydrogen sulphide with methane or the decomposition of methane and in either case, the membrane acted as a catalyst for the reactions. When hydrogen sulphide was no longer fed, it was expected to see some recovery but the conversion actually kept on decreasing and it reached 3%. It was proposed that the membrane provided the sites for methane oxidation but after the poisoning, deposition of sulphur caused change in the properties of the membrane and therefore the sites for methane oxidation was lost. Characterisation techniques revealed that the surface was poisoned by metal sulphate and it likely that the adsorbed sulphur did not regenerate after hydrogen sulphide removal but it was further transformed to metal sulphate. The suggested mechanisms for hydrogen sulphide poisoning during methane oxidation is given in Figure 6.10.

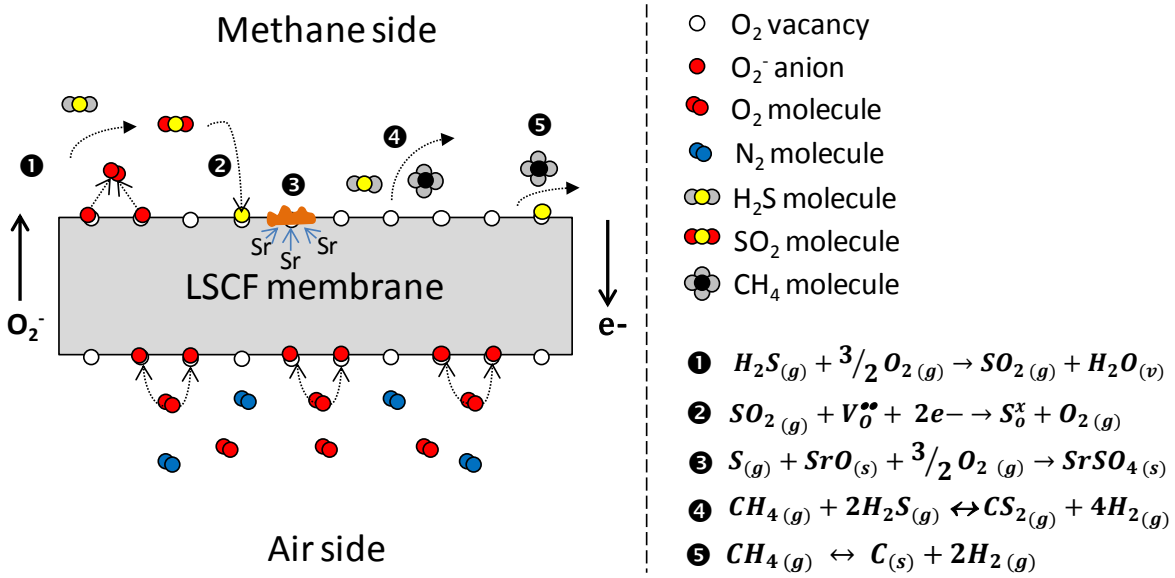

Figure 6.10. Proposed mechanisms for hydrogen sulphide poisoning during methane oxidation using LSCF6428 membrane

6.4 Recovery of the membrane after sulphur poisoning

Thermal, mechanical and chemical methods were discussed before in chapter 4 to restore the membrane after hydrogen sulphide poisoning. The thermal technique was not practical because a temperature of 1600°C is required to decompose strontium sulphate and that temperature is enough to melt down the membrane [209]. The mechanical method of surface sanding did not work neither because the membrane was very fragile. The only method which helped in improving the recovery was hydrogen treatment. After hydrogen sulphide poisoning during air separation, use of 1% (mol) of hydrogen for 20 h doubles the recovery from 6 to 12%. In this section, the membrane which was poisoned by hydrogen sulphide during methane oxidation had been treated with hydrogen and changes of methane conversion were monitored.

Experimental setup: the experiment consisted of 6 steps as shown in Figure 6.11. Step 1 to step 4 was a repeatability of previous experiment where in step 1 air and argon were fed at 900°C with flow rates of 20 ml min^{-1} (STP). In step 2, 1% (mol) of methane was fed and conversion was calculated. Step 3 involved introduction of hydrogen sulphide (200 ppm) along methane for 100 h and changes in the conversion were observed. In step 4, hydrogen sulphide was removed and conversion was measured. In step 5, methane was replaced with a stream containing 1% (mol) of hydrogen (balance argon) and kept for 24 h at 20 ml min^{-1}

(STP). The stream was then replaced with methane (step 6) to see if hydrogen improved the conversion.

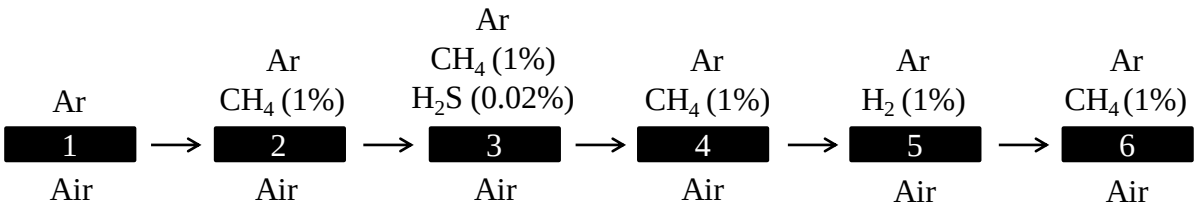

Figure 6.11. Experimental setup to restore the membrane after hydrogen sulphide poisoning during methane oxidation.

Results and discussion: in step 1 where air and argon were fed, oxygen flux was 0.19 ml cm^{-2} min^{-1} as shown in Figure 6.12. After methane introduction (step 2), the flux decreased to 0.14 ml cm^{-2} min^{-1} and conversion was 20% after 16 h. It was expected to see better flux in step 2 but it looks like the membrane was not fully activated and it needed more time. When hydrogen sulphide was fed (step 3), methane conversion decreased to 7% within hours but it was recovering and it reached a steady value of 14% after 15 h of hydrogen sulphide exposure. Oxygen flux was also increasing and a constant value of 0.10 ml cm^{-2} min^{-1} was

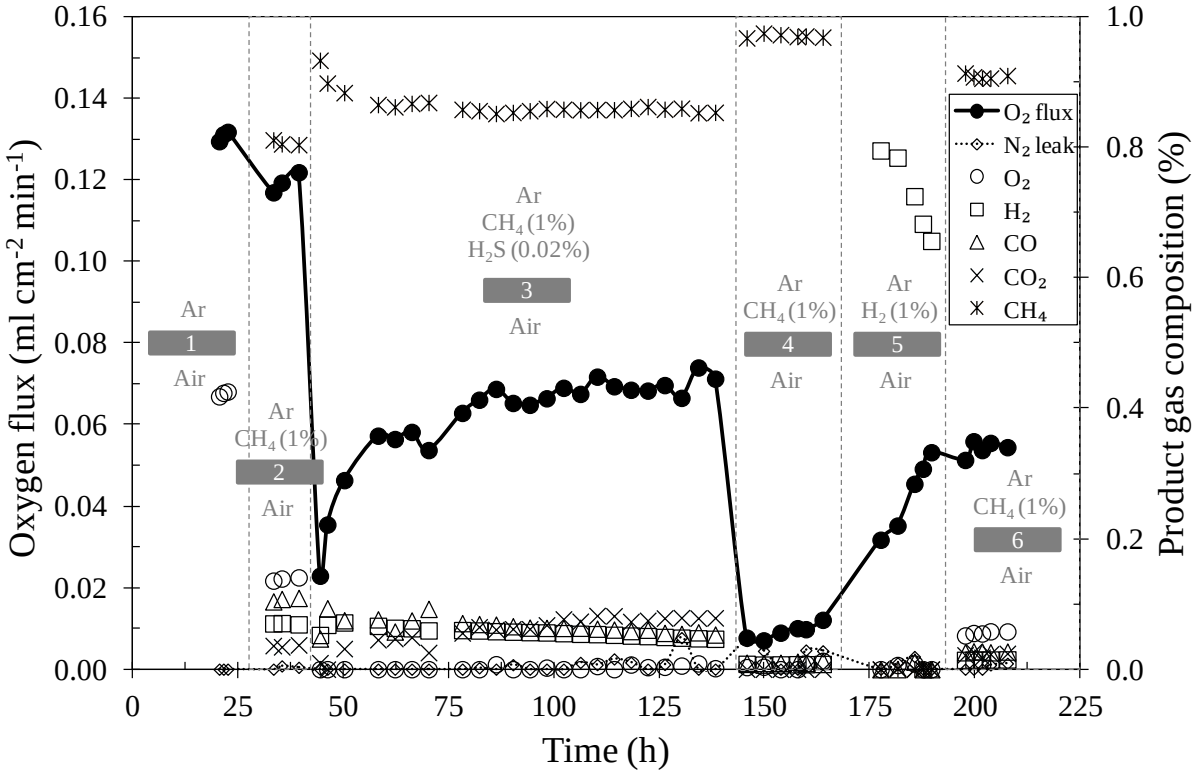

Figure 6.12. Hydrogen treatment to regenerate LSCF6428 membrane after hydrogen sulphide poisoning (200 ppm) during methane oxidation at 900°C.

achieved after 45 h. When hydrogen sulphide was no longer fed (step 4), the conversion decreased to 3% and remained at that value while the flux dropped to 0.02 ml cm^{-2} min^{-1}. In step 5 where the surface was treated with hydrogen, the flux jumped to 0.07 ml cm^{-2} min^{-1} after 22 h. After swapping hydrogen with methane (step 6), the conversion indeed increased and it was steady at 9%. To confirm that the data was repeatable, the experiment was conducted again and similar results were obtained (Figure B.6, Appendix B).

Characterisation: after operation, the membrane was examined by SEM and compared to the non-treated membrane, hydrogen managed to remove some of the deposits and LSCF6428 surface was visible as shown in Figure 6.13. The treated membrane was also analysed by EDS and sulphur amount was reduced from 13 to 9% (atomic) as given in Table 6.5. Metals such as lanthanum, cobalt and iron were also measured after the treatment. XRD detected sharp peaks of the perovskite structure with weak signals of sodium sulphate as shown in Figure 6.14. Furthermore, XPS showed that sulphur content was also decreased from 11 to 7% (atomic) as given in Figure 6.15.

Characterisation techniques revealed that the regeneration process took place and hydrogen was beneficial for restoring some of the surface. In the following section, more studies were conducted on hydrogen sulphide poisoning during methane oxidation to know more about the mechanism.

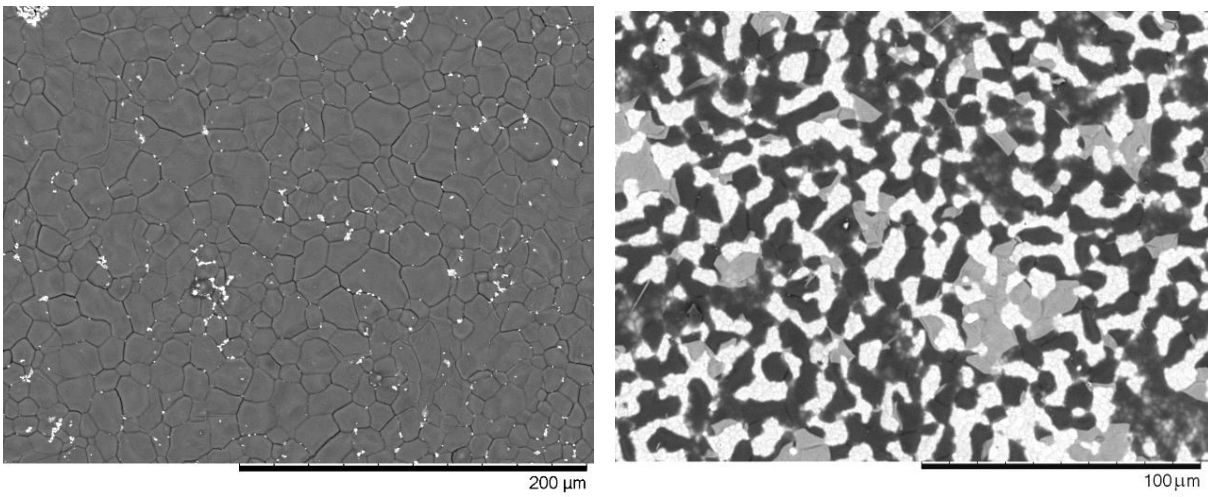

Figure 6.13. Changes of the poisoned surface of LSCF6428 membrane by hydrogen sulphide (200 ppm) during methane oxidation with no treatment (left) and after treatment (right) using 1% (mol) of hydrogen for 24 h.

Table 6.5. EDS analysis of the poisoned membrane by hydrogen sulphide during methane oxidation before and after treatment using 1% (mol) of hydrogen.

Membrane	Element (atomic %)							
	La	Sr	Co	Fe	O	C	S	Na
Before treatment	0	2	0	0	57	0	13	28
After treatment	3	4	1	4	49	7	9	23

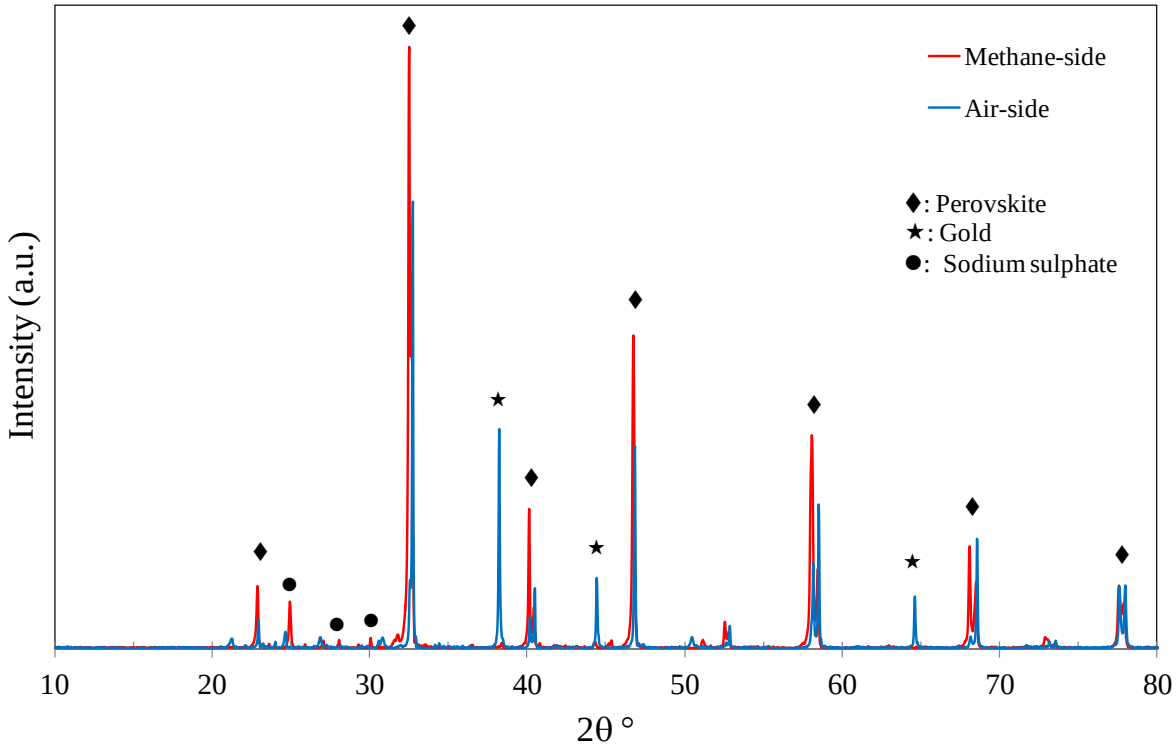

Figure 6.14. XRD analysis of the poisoned membrane by hydrogen sulphide during methane oxidation before and after hydrogen treatment of 1% (mol) for 24h.

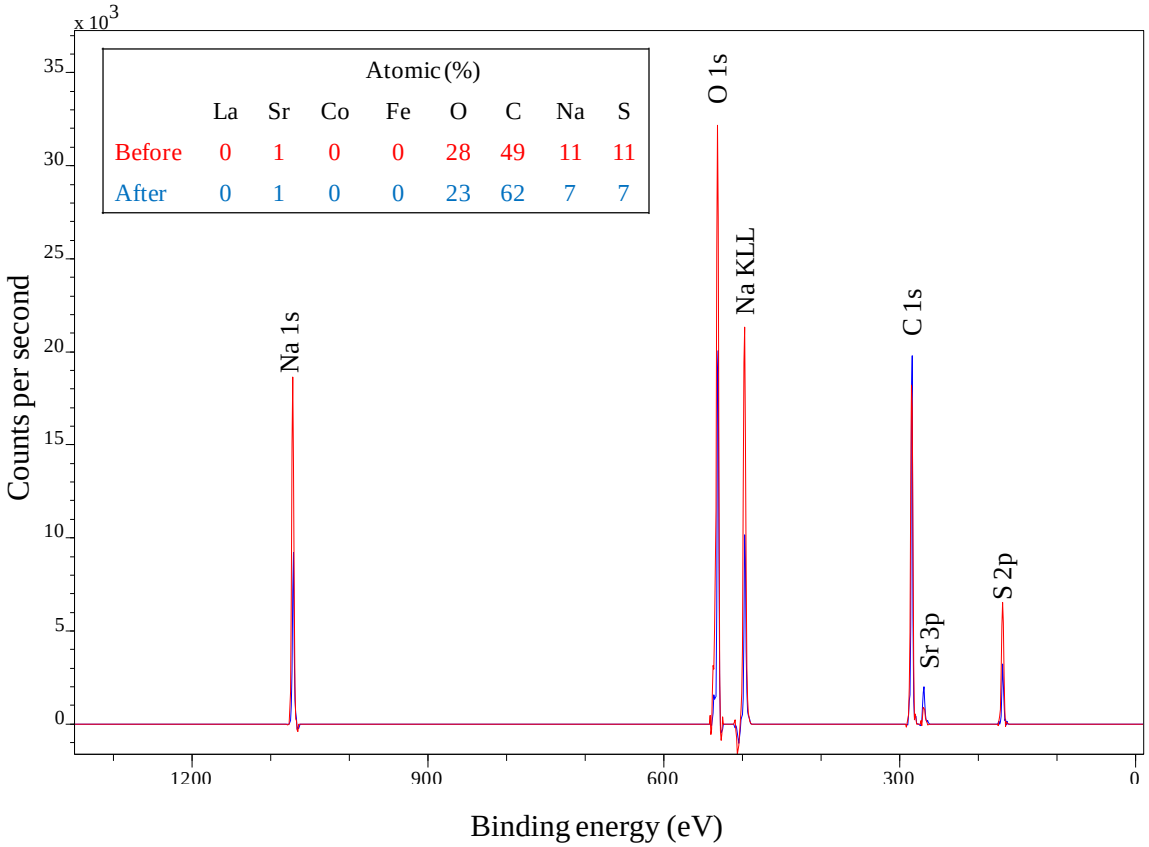

Figure 6.15. XPS analysis of the poisoned membrane by hydrogen sulphide during methane oxidation before and after hydrogen treatment (1% mol) for 24 h.

6.5 More studies on hydrogen sulphide poisoning during methane oxidation

It was proposed that the non-zero conversion during methane oxidation in presence of hydrogen sulphide was related to hydrogen sulphide-methane reforming or decomposition of methane and the membrane provided the catalytic sites for the reaction. To investigate more, the poisoned membrane during air separation (chapter 4) was tested for methane oxidation in existence of hydrogen sulphide. It is predicted that the poisoned membrane will still provide the catalytic sites for methane decomposition and this will produce hydrogen and the later will restore some of the flux.

Experimental setup: this experiment is considered as the longest one with seven steps as demonstrated in Figure 6.16. In step 1, air and argon were fed (20 ml min^{-1} STP, each) at 900°C to measure the starting flux and check for leak. After that (step 2), argon was switched with hydrogen sulphide (200 ppm, balance argon) and kept for 100 h. In step 3, hydrogen sulphide was no longer fed and argon was brought back to measure the recovery. In step 4, argon was replaced with methane (1% mol, balance argon) to see if the poisoned membrane can perform for methane oxidation. In step 5, methane was swapped with a steam containing

1% (mol) methane with 200 ppm of hydrogen sulphide (balance argon) and the membrane was exposed to that stream for another 100 h. In step 6, hydrogen sulphide was removed by replacing the stream with methane only to notice the recovery. In the final step, argon was brought back to compare with the starting flux of step 1. All flow rates were fixed at 20 ml min^{-1} (STP).

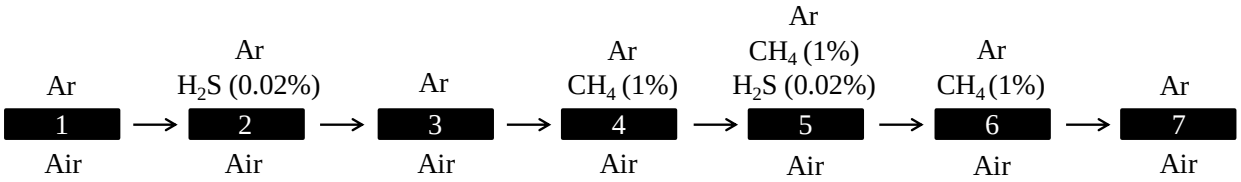

Figure 6.16. Feeds configuration to test the poisoned membrane (by hydrogen sulphide during air separation) for methane oxidation.

Results and discussion: the starting flux was 0.18 ml cm^{-2} min^{-1} and it went to zero once hydrogen sulphide was introduced as shown in Figure 6.17. The membrane showed some sign of recovery after hydrogen sulphide removal (step 3) and 6% of the starting flux was restored. When methane was fed (step 4), the conversion was zero and oxygen flux remained at 8%. It

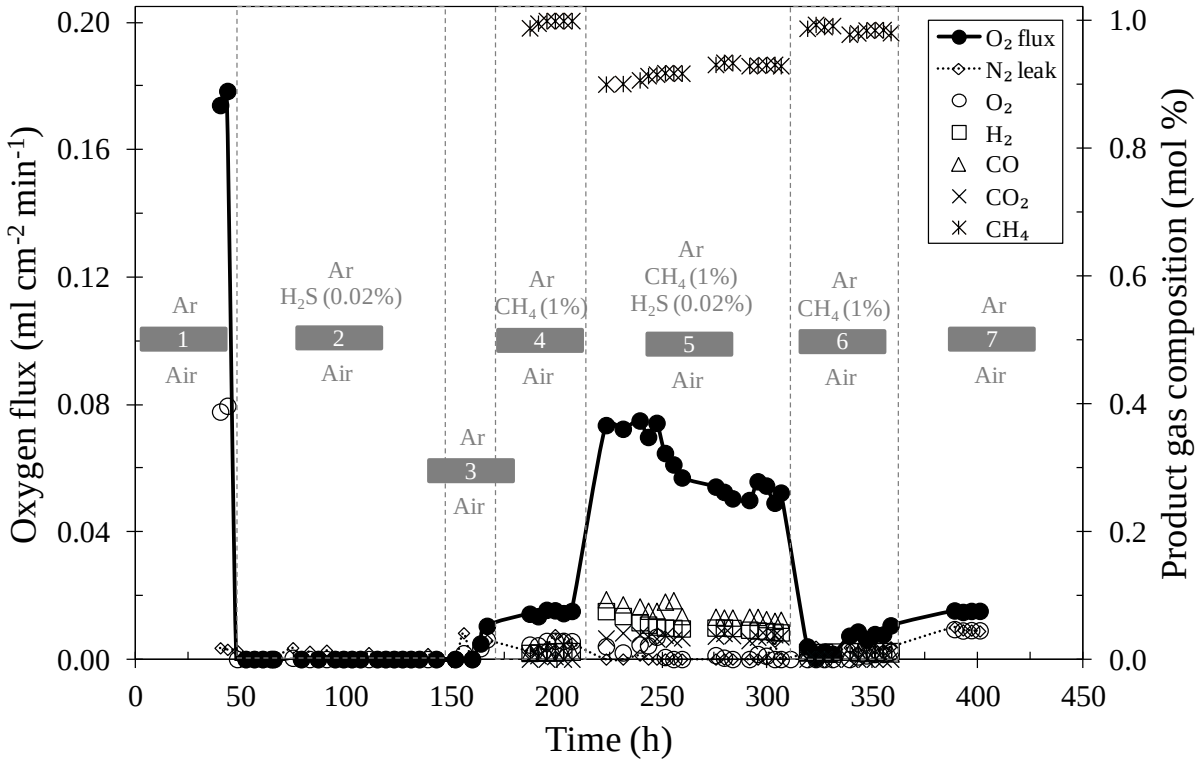

Figure 6.17. Changes of oxygen flux of LSCF6428 membrane after hydrogen sulphide exposure during air separation and methane oxidation for total of 200 h at 900°C.

was predicted not to see any conversion because due to poisoning, the membrane properties were altered and this caused loss of area which provided the reaction sites for methane oxidation. In step 5 where hydrogen sulphide was fed along methane, the conversion jumped to 10% and flux hit 39%. With time, both conversion and flux were slowly decreasing and remained at 7% and 28%, respectively.

This experiment confirmed that the poisoned membrane can still be used for methane oxidation and presence of hydrogen sulphide actually helped in restoring the membrane. The proposed mechanisms in section 6.3 suggested that during hydrogen sulphide exposure along methane, hydrogen sulphide-methane reforming or methane decomposition took place and the membrane provided the catalytic sites for these reactions. The produced hydrogen then regenerated some sulphur and this contributed in restoration of oxygen flux. When hydrogen sulphide was removed and methane was kept (step 6), the conversion and flux moved back to 2% and 6%, respectively. Based on the suggested mechanisms, hydrogen sulphide-methane reforming could not take place because of the absence of hydrogen sulphide and methane decomposition was stopped due to the regeneration of metal sulphides. In step 7 of original configuration (air and argon), the flux was steady at 8%. Interestingly, this value of oxygen flux is higher than the one in step 3 after sulphur poisoning in air separation meaning that presence of hydrogen sulphide along methane did not cause any further damage and instead, it helped in restoring some of the flux. To confirm the reliability of the data, the experiment was repeated and similar results were seen (Figure B.7, Appendix B).

Characterisation: the membrane surface was analysed by SEM and a new phase was observed as given in Figure 6.18. EDS indicated that the phase was enriched with strontium and sulphur suggesting strontium sulphate formation. The membrane was also characterised by XRD and the phase was recognised as strontium sulphate as shown in Figure 6.19. XPS detected amounts of sulphur and strontium as presented in Figure 6.20. Interestingly, the characterisation techniques did not detect any sodium and this is the first time to see strontium sulphate despite the use of gold-glass-ceramic sealant. It looks like the sealant was stable in this experiment and it did not react with hydrogen sulphide.

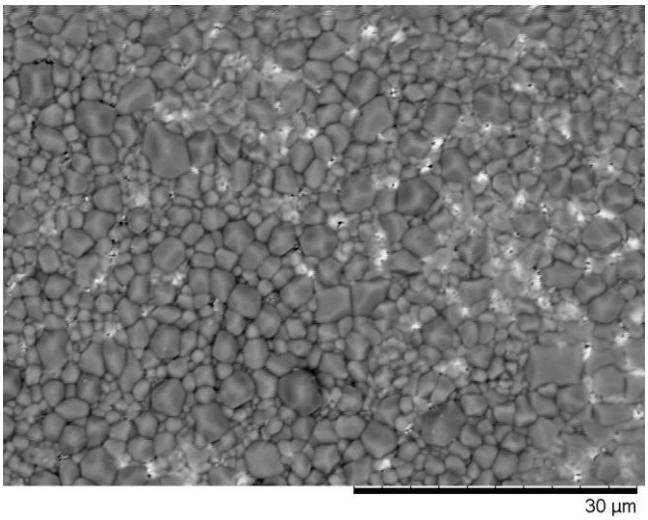

Element	Atomic %
La	2
Sr	17
Co	2
Fe	2
O	62
C	0
S	15
Na	0

Figure 6.18. SEM and EDS analyses of LSCF6428 membrane after air separation and methane oxidation in presence of hydrogen sulphide (200 ppm) for total of 200 h at 900°C.

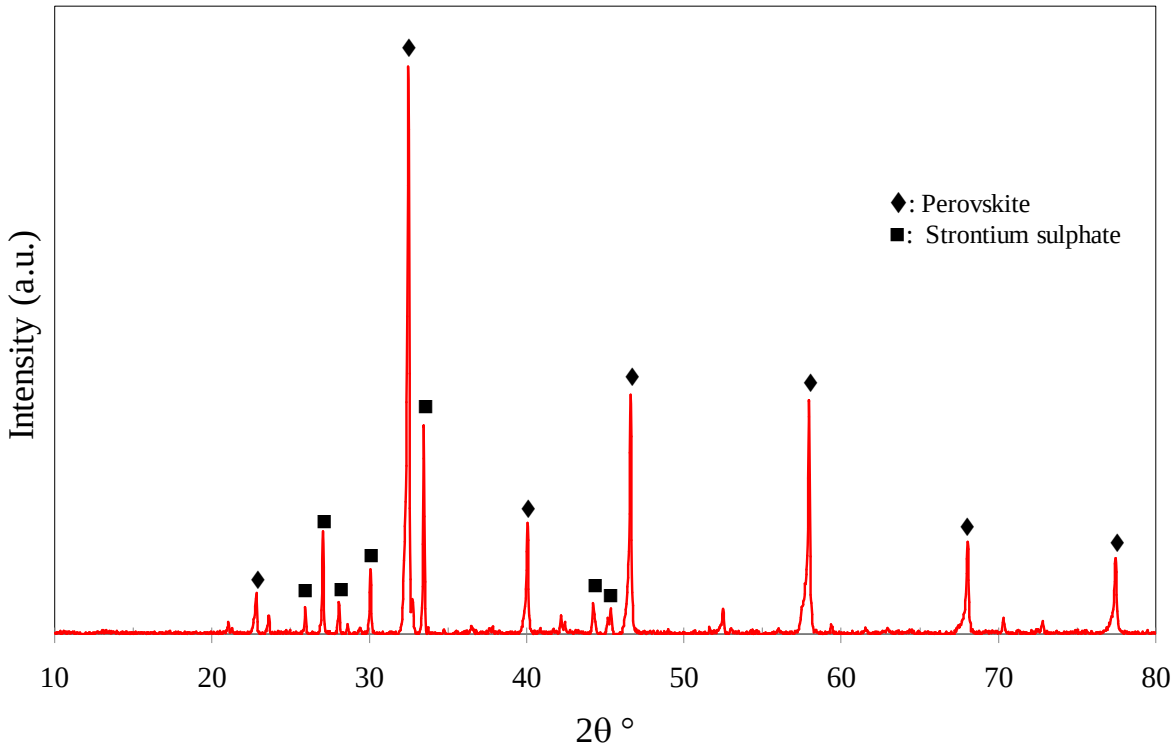

Figure 6.19. XRD analysis of LSCF6428 membrane after hydrogen sulphide exposure in air separation and then methane oxidation for 200 h at 900°C.

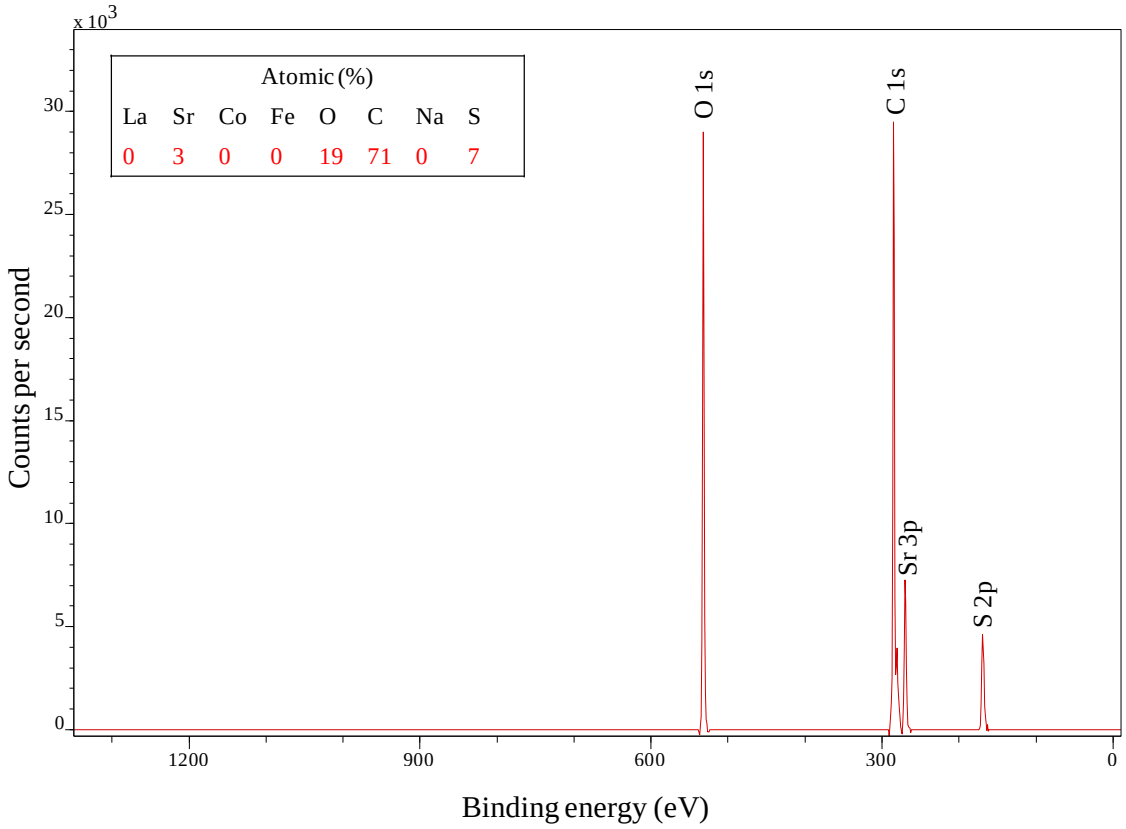

Figure 6.20. XPS analysis of LSCF6428 membrane after hydrogen sulphide exposure during air separation and then methane oxidation for 200 h at 900°C.

6.6 Summary

In this chapter, LSCF6428 membrane was evaluated for long-term methane oxidation. First, it was tested in a sulphur-free environment using a stream containing 1% (mol) methane and the membrane achieved a steady conversion of 33% for 340 h. The gold-glass-ceramic sealant was suitable for the reducing environment of methane and nitrogen leak was 0.02% (mol). Characterisation techniques revealed that the membrane structure and composition did not change and it is predicted that the membrane can be used for longer than 340 h without any issue. When hydrogen sulphide (200 ppm) was introduced along methane, the conversion dropped but remained at 15% for the whole duration of 100 h. It was expected not to see any conversion during the exposure because from previous chapters, oxygen flux was zero once hydrogen sulphide was fed. The non-zero conversion was interpreted by either hydrogen sulphide-methane reforming or methane decomposition and the membrane provided the catalytic sites these reactions. The produced hydrogen from these reactions recovered some area and this restored part of the flux during the exposure. After removing hydrogen sulphide and keeping methane in the feed gas, the conversion continued on decreasing and it reached

3%. It was suggested that removal of hydrogen sulphide interrupted hydrogen production because reforming could not take place and some metal sulphides were regenerated back to oxides and therefore methane decomposition was stopped. Also, after hydrogen sulphide exposure, the membrane properties were altered due to sulphur deposition and this may reduce the sites for methane oxidation. To recover the membrane after hydrogen sulphide poisoning, 1% (mol) of hydrogen was fed to the damaged surface for 24 h and indeed the conversion increased from 3 to 9%. Longer duration or higher hydrogen concentration may be required to improve the recovery process. Further study was done by exposing the membrane to hydrogen sulphide during air separation and then methane oxidation for a total of 200 h. After sulphur poisoning in air separation for 100 h, the membrane could not be used for methane oxidation because the conversion was zero. However, when hydrogen sulphide was fed along methane, the conversion jumped to 7% indicating that hydrogen sulphide actually helped in restoring some of the flux and this was related to hydrogen sulphide-methane reforming or methane decomposition. In the following chapter, LSCF6428 membrane was modified by different methods for better stability under hydrogen sulphide during air separation.

Chapter 7: Modification of LSCF6428 Membrane for better Stability under Hydrogen Sulphide

Chapter 7: Modification of LSCF6428 Membrane for better Stability under Hydrogen Sulphide

It was discovered that hydrogen sulphide impurity caused a major interruption to oxygen transport in LSCF6428 membrane. During air separation, the impurity resulted in drop of oxygen flux to zero and the flux could not be fully restored even when hydrogen sulphide was removed from the feed gas. It was proposed that hydrogen sulphide was first oxidised to sulphur dioxide and the later occupied the oxygen vacancy in the form of sulphur. With time, presence of sulphur on the surface triggered strontium segregation to form strontium sulphate and this permanently poisoned the vacancy.

Based on the suggested mechanism, the key to improve the membrane tolerance to hydrogen sulphide is by preventing or reducing the adsorption rate of sulphur on the surface. This can be achieved by adding a protective layer on the membrane to capture sulphur before it reaches the permeating surface. Another way to increase the stability is by slowing down the formation rate of strontium sulphate and this will greatly improve the recovery.

In this chapter, LSCF6428 membrane is modified and tested for air separation in existence of hydrogen sulphide by three different approaches. In the first method, the membrane is pre-contaminated by adding strontium sulphate during fabrication. The second method involves using a sulphur-reactive material of zinc oxide over the membrane. In the third method, the membrane is protected by a powder layer of LSCF6428 material.

7.1 Pre-contamination by strontium sulphate

Characterisation techniques revealed that exposing LSCF6428 membrane to hydrogen sulphide produced strontium sulphate and this corrosion product was behind the permanent loss of oxygen flux. One strategy to improve the stability is by delaying the formation rate of strontium sulphate for better recovery. In this experiment, strontium sulphate was added to the membrane during fabrication with different concentrations. The experiment gave information about the possibility of the pre-added sulphur to poison the membrane. If the pre-contaminated membrane was able to permeate oxygen, it may give better tolerance under hydrogen sulphide because the presence of the pre-added strontium sulphate may slowdown sulphur adsorption or strontium segregation.

Experimental setup: three membranes were prepared for this experiment and they had different concentrations of strontium sulphate. The first membrane was made by adding 1.5 g of LSCF6428 powder to 1.6 mg of strontium sulphate so that the modified membrane would have 1000 ppm or 0.1% (weight) of strontium sulphate. In the second membrane, 1.5 g of LSCF6428 powder was added to 16 mg of strontium sulphate to have a membrane with 1% (weight) of strontium sulphate. The third membrane contained 10% (weight) strontium sulphate by adding 1.5 g of LSCF6428 powder to 160 mg of strontium sulphate. The mixtures were then ball milled for 5 min for better mixing and pressed at 3 tons then sintered at 1250°C for 5 h using a ramping rate of 1°C min^{-1}. The membranes were sealed with gold-glass-ceramic sealant and heated to 900°C using feeds of air and argon (20 ml min^{-1} STP, each). After that, the pre-contaminated membranes were exposed to 200 ppm of hydrogen sulphide for 100 h. Hydrogen sulphide was thereafter removed and recovery was measured.

Results and discussion: the pre-contaminated membranes were still permeating oxygen and their fluxes were similar to the non-modified membranes as shown in Figure 7.1. For instance, oxygen flux reached 0.33 ml cm^{-2} min^{-1} even if the membrane was contaminated with 10% of strontium sulphate. This indicates that sulphur (from the added strontium sulphate) did not

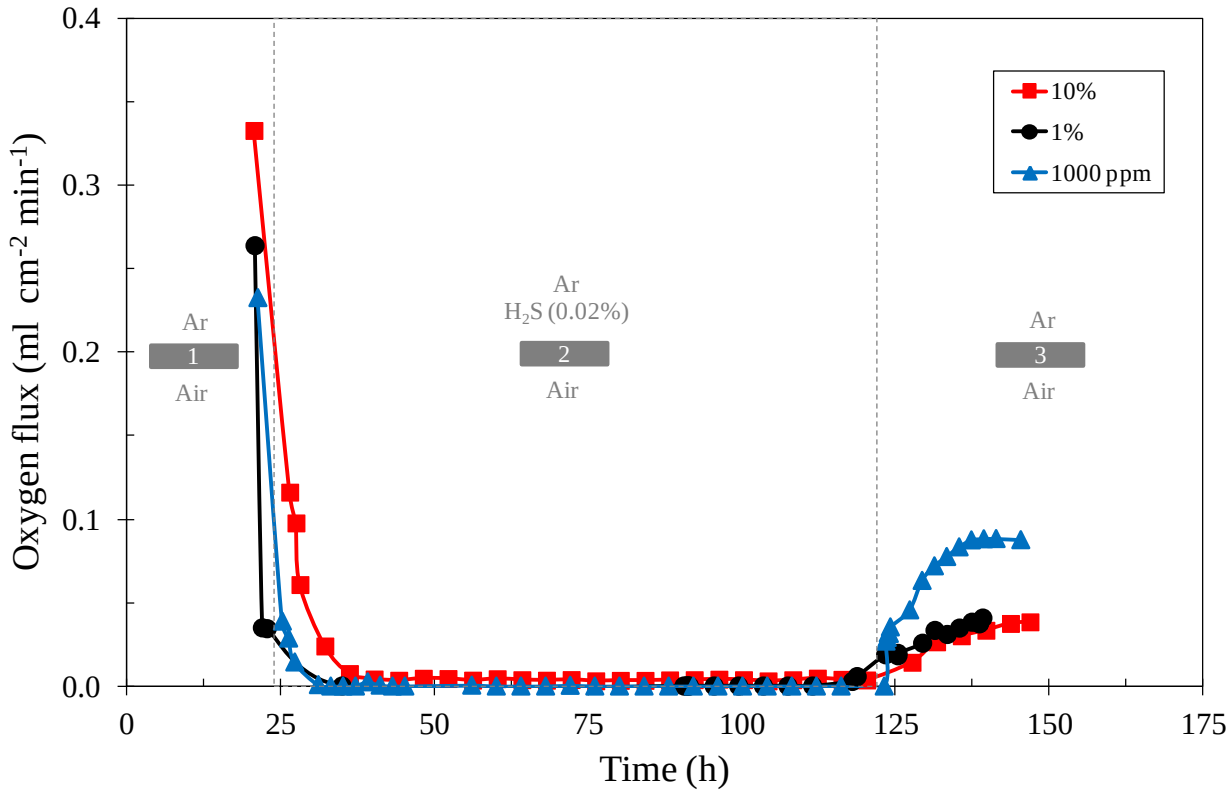

Figure 7.1. Modification of LSCF6428 membrane by adding 0.1, 1 and 10% of strontium sulphate during fabrication and the stability under hydrogen sulphide (200 ppm) at 900°C.

find its way to the surface and blocked the vacancies. High chemical stability of strontium sulphate could prevent sulphur from reaching the vacancies.

Unfortunately, introduction of hydrogen sulphide to the pre-contaminated membranes resulted in drop of oxygen flux to zero as given in Figure 7.1. After hydrogen sulphide removal from the feed, the pre-contaminated membranes showed a recovery of 11 to 33% and this is within the recovery of the non-modified membranes.

Based on this experiment, solid-phase contamination by strontium sulphate prior to hydrogen sulphide exposure did not cause any signification reduction in oxygen flux. However, the contaminated membrane did not show any stability improvement toward hydrogen sulphide.

7.2 Use of zinc oxide bed

Industrially, zinc oxide guard-bed is used to remove hydrogen sulphide from natural gas prior to oxidation [227, 228]. The technology can cut down the concentration of hydrogen sulphide to 0.1 ppm [229]. Actually, zinc oxide captures sulphur by the reaction with hydrogen sulphide to form zinc sulphide and water as demonstrated in Equation 7.1. The poisoned bed can be then regenerated back to zinc oxide at temperature of 450°C as given in Equation 7.2 [230]. Even if zinc sulphate was formed, it can be decomposed to zinc oxide and sulphur dioxide at temperature of 615°C (Equation 7.3) [231]. In our experiments, the operating temperature is 900°C and this temperature should be enough to decompose zinc sulphide and zinc sulphate. Therefore, poisoning and regeneration could occur at simultaneously and this may prevent sulphur from reaching the membrane.

$$H_2S_{(g)} + ZnO_{(s)} \rightarrow H_2O_{(v)} + ZnS_{(s)} \quad (7.1)$$

$$ZnS_{(s)} + {}^{3}/_{2}\, O_{2_{(g)}} \rightarrow ZnO_{(s)} + SO_{2_{(g)}} \quad (7.2)$$

$$ZnSO_{4_{(s)}} \rightarrow ZnO_{(s)} + SO_{2_{(g)}} + {}^{1}/_{2}\, O_{2_{(g)}} \quad (7.3)$$

Experimental setup: LSCF6428 membrane was fabricated by weighing 1.5 g and pressing at 3 tons. The membrane was sintered at 1250°C for 5 h with a ramping rate of 5°C min^{-1}. Next, zinc oxide powder of one gram was diluted in 8 ml of ethanol to have a solution containing 16% mass concentration of zinc oxide. Portion of the solution was applied over the membrane surface using a brush. The solution was kept to dry for few hours. Following, the composite membrane was weighed and zinc oxide accounted for 0.15 g. The composite membrane was

sealed using gold-glass-ceramic sealant and then heated to 900°C using flows of air and argon at 20 ml min^{-1} (STP), each. Argon was swapped with hydrogen sulphide (200 ppm, balance argon) for 100 h and after that argon was brought back to measure the recovery.

Results and discussion: the starting flux was relatively low at 0.08 ml cm^{-2} min^{-1} as shown in Figure 7.2. This could be related to zinc oxide covering some membrane area. After few hours of hydrogen sulphide presence, oxygen flux dropped to nearly zero and it remained at that value for the whole duration. This reduction in oxygen flux is almost similar to the non-modified membrane. It looks like the poisoning rate was too rapid compared to the regeneration and therefore hydrogen sulphide reached the membrane surface quickly. When hydrogen sulphide was no longer fed, recovery reached 16% and this value is within the non-modified membrane.

Characterisation: After operation, the guard bed was analysed by XRD and it consisted of zinc oxide with no sign of zinc sulphide or sulphate as shown in Figure 7.3. It is feasible that the bed adsorbed sulphur during the exposure and the bed was regenerated back to zinc oxide once hydrogen sulphide was removed from the feed. The operating temperature of 900°C

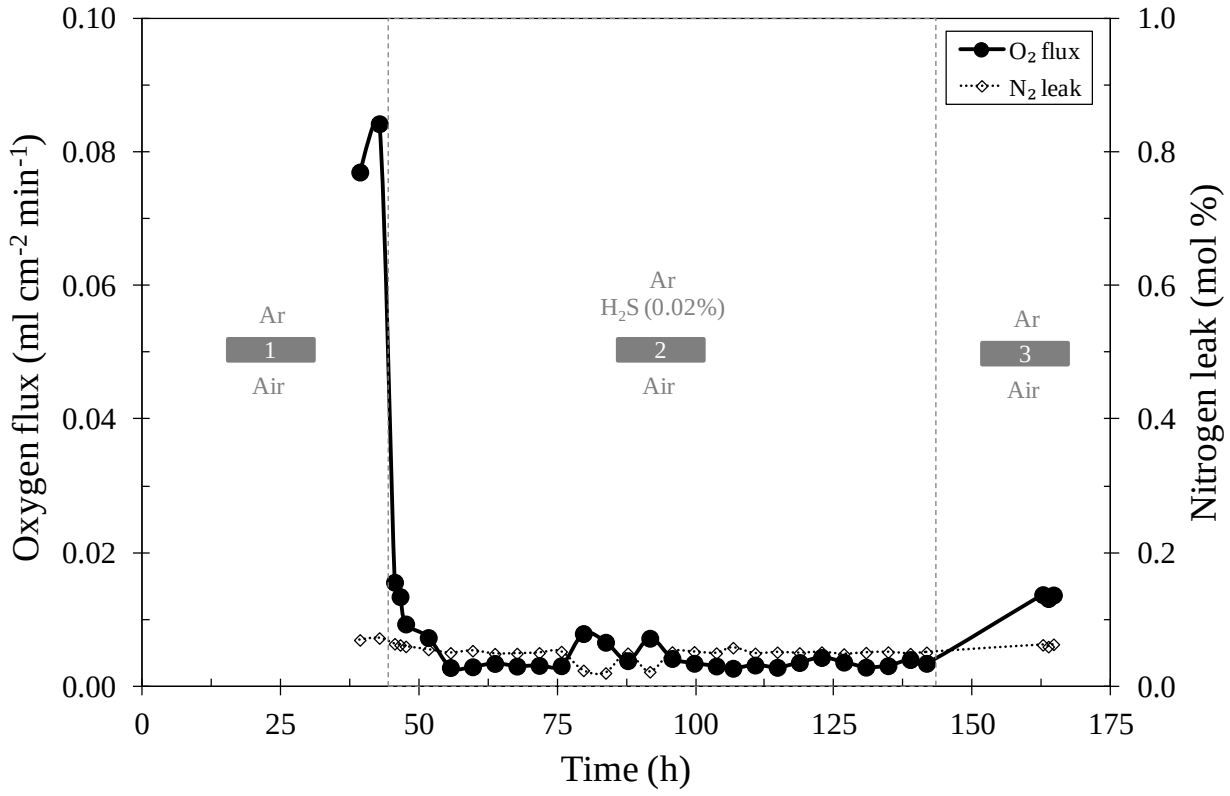

Figure 7.2. Composite LSCF-ZnO membrane for air separation under hydrogen sulphide (200 ppm) for 100 h at 900°C.

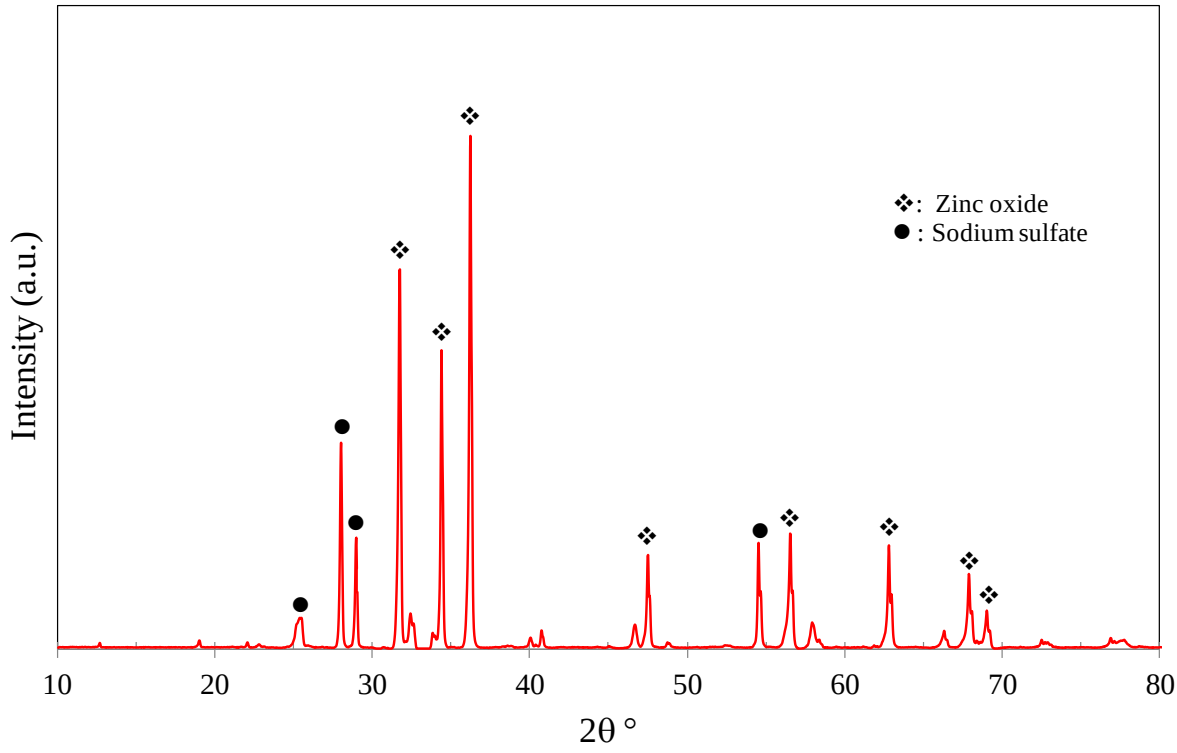

Figure 7.3. XRD analysis of LSCF-ZnO membrane after hydrogen sulphide poisoning (200 ppm) for 100 h at 900°C.

should be enough to decompose sulphides and sulphates of zinc as mentioned before. Interestingly, XRD detected peaks of sodium sulphate and it is possible that the x-ray beam was deep and it hit the membrane surface.

As discussed, the concept of using zinc oxide did not work experimentally but theoretically it should work because the guard-bed is used in industry for hydrogen sulphide capture. It is reported that zinc oxide has a pickup capacity of hydrogen sulphide near 20% (weight) at temperatures of 350 to 400°C [232]. In this experiment 0.15 g of zinc oxide was used and this amount should adsorb 0.03 g of hydrogen sulphide based on the previous statement. Argon containing 200 ppm of hydrogen sulphide was fed in this experiment at 20 ml min^{-1} and this gave 0.005 mg min^{-1} of hydrogen sulphide (assuming gas density of 1.4 g L^{-1} [233]). By dividing the capacity of zinc oxide (0.03 g) over the mass flow rate of hydrogen sulphide (0.005 mg min^{-1}), the guard-bed should adsorb hydrogen sulphide for 100 h. However, this was not the case and introduction of hydrogen sulphide caused drop of oxygen flux to nearly zero within few hours as shown in Figure 7.2. It is possible that the reaction of zinc oxide with hydrogen sulphide did not take place at all due to the high temperature of 900°C. It was

later found that the bed was not suitable for sulphur capture above 750°C due to decomposition of zinc oxide to vapour zinc [234].

7.3 Dual-layer LSCF6428 membrane

Until now, pre-addition of strontium sulphate or use of zinc oxide bed was not helpful in improving the tolerance toward hydrogen sulphide. In this section, powder of LSCF6428 material was added over the dense membrane not only to protect it from hydrogen sulphide, but also to study the effect of physical phase on the poisoning mechanism. The added powder can provide a larger surface area and it may act as a sieve or scavenger to trap sulphur before reaching the permeating surface.

Experimental setup: dense LSCF6428 membrane was prepared by weighing 1.5 g of powder and then pressed at 3 tons. Before sintering, 0.5 g of membrane powder was placed over the dense membrane. The dual-layer membrane was then sintered at 1250°C with a ramping rate of 5°C min^{-1}. After sintering, the powder was adhered to the dense surface as shown in Figure 7.4.

Results and discussion: the starting flux of the dual-layer membrane was 0.26 ml cm^{-2} min^{-1} and this value is within the flux of the non-modified membrane. After exposing the dual-layer membrane for few hours to hydrogen sulphide, the flux slightly decreased to 95% of its original value which is great. The flux was steady for 33 h but after that, it dropped to 2% and remained at that value as shown in Figure 7.5. It seems that hydrogen sulphide was busy poisoning the powder for the first 33 h and after that it managed to reach the permeating surface.

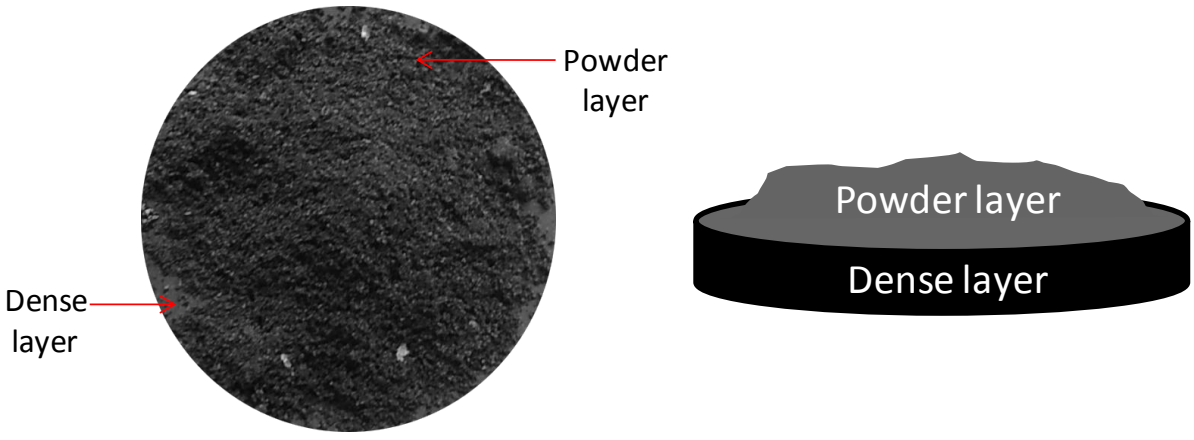

Figure 7.4. Dual-layer LSCF6428 membrane consisting of powder and dense layers.

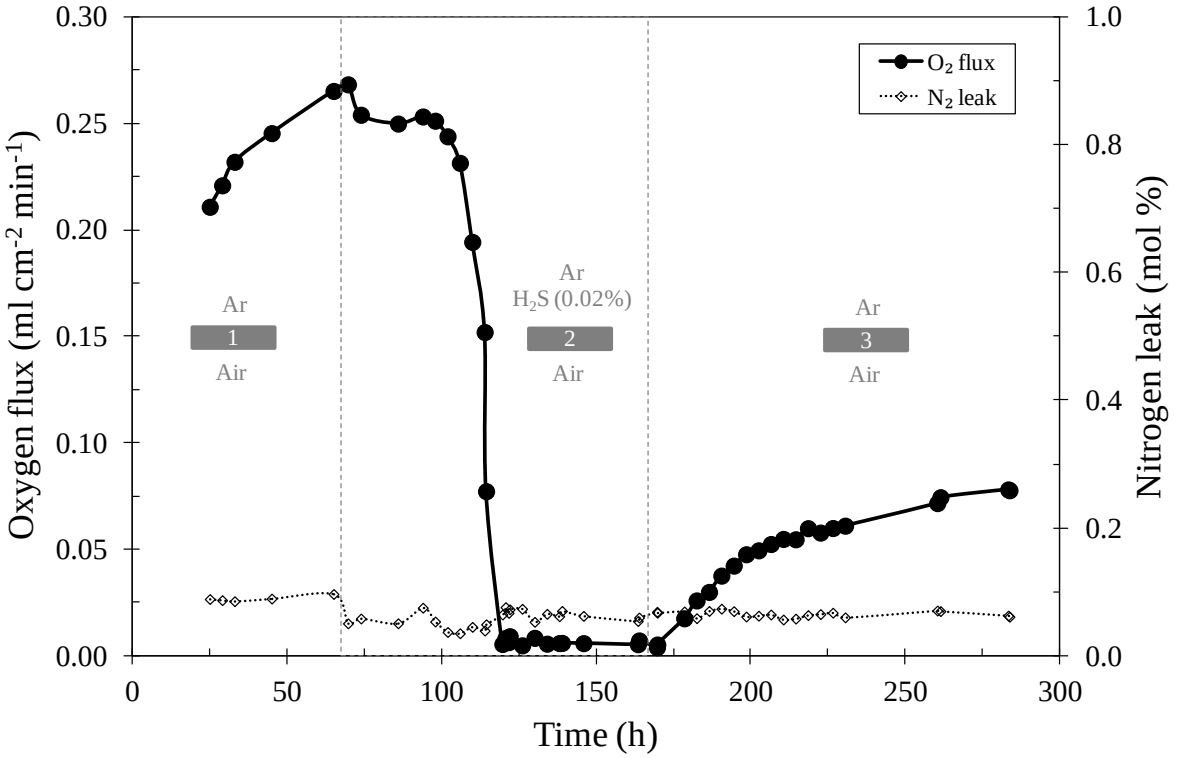

Figure 7.5. Oxygen flux of the dual-layer membrane for air separation under hydrogen sulphide impurity (200 ppm) for 100 h at 900°C.

After hydrogen sulphide removal from the feed, the membrane was recovering and 29% of the flux was restored.

Characterisation: after operation, the powder of the dual-layer membrane was analysed by XRD to observe any changes. Surprisingly, strong perovskite peaks were detected with weak signals of strontium sulphate as shown in Figure 7.6. Based on that, the good stability of the dual-layer membrane for the first 33 h and the reduction of flux after that can be explained by:

- Mechanism 1: reaction of hydrogen sulphide with the powder was very slow due to the low concentration of oxygen vacancies. In this experiment, the powder was not in direct contact with air (high oxygen partial pressure) and this may reduce the tendency to create more vacancies. Also, the powder was sintered before operation and this may result in lower porosity. Therefore, the powder may act as a molecular sieve rather than a sacrificial surface and this slowed down hydrogen sulphide movement.
- Mechanism 2: hydrogen sulphide was rapidly adsorbed on the powder in the form of sulphur. With time, the powder reached the maximum capacity and it cannot take any further sulphur. Most of the adsorbed sulphur did not transform to strontium sulphate because from chapter 5, it was discovered that high oxygen partial pressure is needed

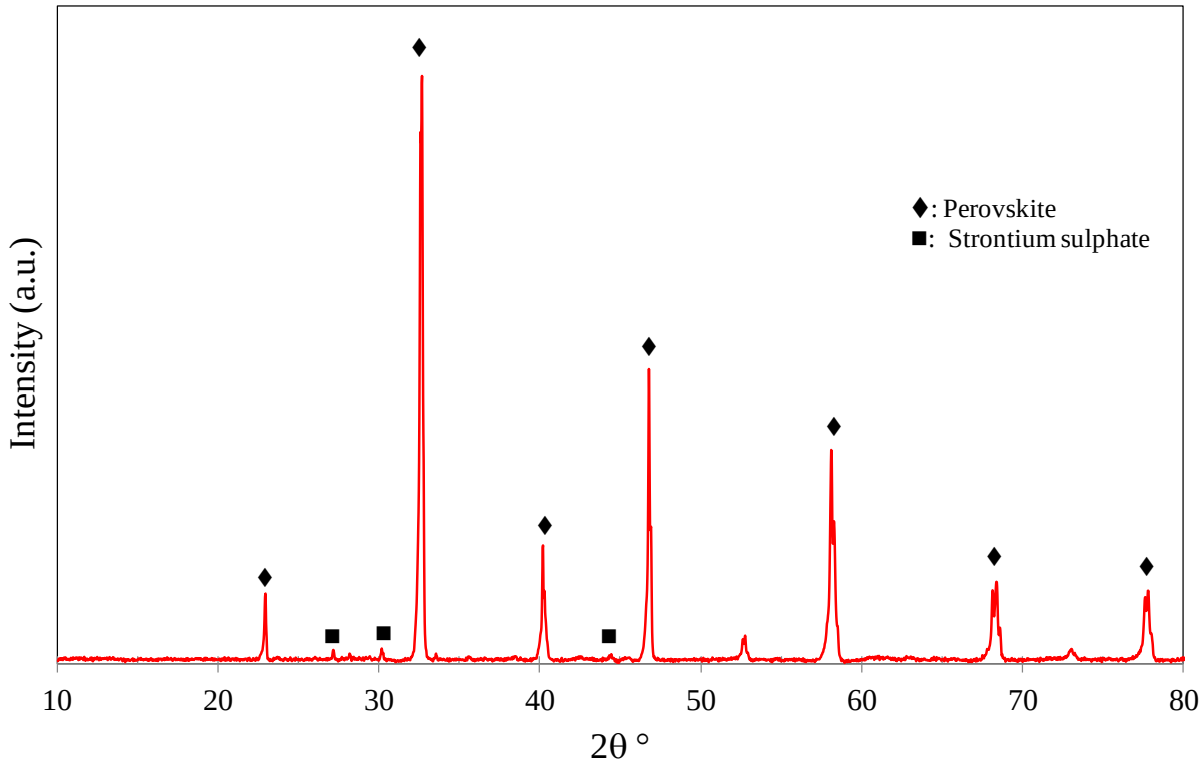

Figure 7.6. XRD analysis of the powder of dual-layer LSCF6428 membrane after hydrogen sulphide poisoning of 100 h at 900°C.

for strontium sulphate formation. When the impurity was no longer fed, the adsorbed sulphur was regenerating and the surface was restored.

Both mechanisms suggest that hydrogen sulphide poisoning depends also on the phase of the membrane and this was evidenced by XRD. The powder membrane received minor damage after the exposure and this was could be related to the low oxygen partial pressure.

7.4 Summary

In this chapter, LSCF6428 membrane was modified by three methods for better tolerance under hydrogen sulphide. Unfortunately, none of these methods showed a better stability for long-term operation of 100 h because the flux reached zero during the exposure. The first technique involved addition of strontium sulphate at different concentrations of 0.1, 1% and 10% (weight) during membrane fabrication. It was found that the pre-contaminated membranes were still permeating oxygen and their fluxes were within the non modified ones. This implied that that sulphur from the pre-added strontium sulphate did not find its way to the surface to poison the vacancy due to the chemical stability of strontium sulphate. The

second method to improve the membrane stability was associated with the addition of zinc oxide as a guard bed over the membrane surface. The technique is used in industry to treat natural gas by the reaction of zinc oxide with hydrogen sulphide to form zinc sulphide. The bed should be regenerated at the operating temperature of 900°C however results showed that the bed was unstable and hydrogen sulphide managed to reach the permeating surface within few hours. In the third method, powder of LSCF6428 material was added and sintered over the dense membrane to see if the powder can trap sulphur before reaching the permeating surface. Results indicated that the modified membrane was stable under hydrogen sulphide for 33 h and oxygen flux was 95%. But after that, the flux was zero. The powder was characterised by XRD afterwards and it contained a few amounts of strontium sulphate and the remaining was LSCF6428. Two mechanisms were proposed and the first one suggested that the reaction of hydrogen sulphide with the powder was slow due to the low concentration of oxygen vacancies and the powder acted as a molecular sieve. The second mechanism suggested that hydrogen sulphide was rapidly adsorbed on the membrane surface until maximum capacity was reached. After hydrogen sulphide removal, sulphur was regenerated and LSCF powder was restored.

At this stage, LSCF6428 membrane could not be modified to withstand hydrogen sulphide impurity for long-term operation. This because the oxygen vacancies, which provide the path for oxygen transport, are easily susceptible to sulphur poisoning and this step is difficult to control. One solution is to purify the streams from hydrogen sulphide before feeding them to the membrane. However, based on this study, it is predicted that even low concentration of hydrogen sulphide (e.g., 1 ppm) will cause significant changes in oxygen flux. Further purification of the streams could be costly and this may affect the choice of using the membrane in industry.

Chapter 8: Conclusions and Future Work

Chapter 8: Conclusions and Future Work

In this study, ceramic membrane made of the mixed ionic-electronic conductor $La_{0.6}Sr_{0.4}Co_{0.2}Fe_{0.8}O_{3-\delta}$ had been investigated for oxygen separation under the presence of industrial impurities such as hydrogen sulphide. The membrane was fabricated in the form of disc and fitted inside the reactor by gold-glass-ceramic sealant which provided a gas-tight system for 963 h. During air separation, oxygen flux was stable at 0.45 ml cm^{-2} min^{-1} for 450 h and this value is higher compared to those reported in literature within the same setup. This is due to the new sealant which gave a leak-free system and therefore increased the driving force for oxygen transport. When hydrogen sulphide (200 ppm) was fed in the inert side, oxygen flux dropped to zero within hours and remained at that value for the whole period of 100 h. After stopping feeding hydrogen sulphide, the membrane showed a sign of recovery but only 6 to 35% of the starting flux was restored. It was proposed that, during the exposure, sulphur was adsorbed on the membrane surface and oxygen vacancies could be attractive for sulphur due to the similarity in oxidation state. Occupying these vacancies resulted in immediate decrease in oxygen flux. It was found that with time, strontium segregates to sulphur to form irreversible layer of strontium sulphate and this compound was behind the permanent loss of the vacancy.

Thermal, mechanical and chemical methods were reviewed to restore the oxygen flux after sulphur poisoning. Strontium sulphate required a temperature of 1600°C but this temperature is enough to melt the membrane. The mechanical method was not suitable because the membrane was very fragile and it broke immediately after sanding. Chemical treatment such as purging the exposed surface with 1% (mol) of hydrogen for 20 h improved the recovery from 6 to 12%. However, the regeneration process was very slow and therefore longer duration or higher concentration of hydrogen may be required for better recovery.

More studies on hydrogen sulphide were carried out to determine the parameters that critically affect the mechanism. It was discovered that exposure time is a strong function of the mechanism and if the membrane was exposed to short term of one hour, the oxygen flux will be fully restored. This implied that sulphur poisoning consists of two steps; rapid adsorption of sulphur on the membrane surface causing zero flux (reversible step) and segregation of strontium towards sulphur to form strontium sulphate (non-reversible step). Hydrogen

sulphide poisoning was also performed at different temperatures of 800 to 950°C and it was found that operating at high temperature was favourable because the recovery was higher. However, in all temperatures, the oxygen flux was still zero during the exposure. Furthermore, LSCF6428 membrane was tested at various concentrations of hydrogen sulphide (50 to 200 ppm) but in all cases the oxygen flux was again zero during the presence of hydrogen sulphide. Based on these results, it is expected that hydrogen sulphide will cause a significant change in oxygen flux even in very low concentration of 1 ppm.

Impact of oxygen partial pressure on sulphur mechanism was also studied and it played a major role in the reversibility of the poisoning. Oxygen partial pressure in the air side was reduced from 0.21 to 0.01 bar and this greatly improved the recovery to 90%. The importance of oxygen was related to strontium sulphate formation which requires an external source of oxygen. Lowering the oxygen partial pressure during sulphur poisoning can be used as a strategy to reduce the damage but if oxygen partial pressure was zero, the membrane would fail due to the increase in leakage rate. This was related to the loss of lattice oxygen causing membrane expansion.

In the second part of the thesis, LSCF6428 membrane was used for hydrogen production by methane oxidation and it showed an outstanding stability for 350 h and average methane conversion of 33%. Compared to literature, the membrane showed the highest conversion and the longest duration. This superior performance was strongly related to the new gold-glass-ceramic sealant which was suitable for the reducing environment of methane. When hydrogen sulphide was fed along methane, the conversion dropped to 11% within hours and it remained at that value. Adsorption of sulphur on the membrane surface was behind the reduction in flux. After stopping feeding the impurity, the conversion kept on decreasing and it reached 3%.

Two mechanisms were proposed to explain the non-zero conversion during hydrogen sulphide presence and the first one suggested that hydrogen sulphide-methane reforming took place and the membrane provided the catalytic sites. The produced hydrogen then regenerated some oxygen flux during the exposure. On the other hand, the second mechanism advised that methane decomposition to carbon and hydrogen occurred and the adsorbed sulphur (in the form of metal sulphide) acted as a catalyst. After hydrogen sulphide removal from the feed, the conversion kept on decreasing because the adsorbed sulphur could be further poisoned to metal sulphate instead of regenerating. After sulphur poisoning during methane oxidation, the membrane was treated for 24 h of 1% (mol) hydrogen and the conversion increased from 3 to

9%. Longer treatment period may be required for better recovery because the regeneration process was very slow compared to the poisoning.

The poisoned membrane by hydrogen sulphide during air separation was tested for methane oxidation to see if the poisoned membrane can still be used. Results showed that the pre-poisoned membrane cannot be used for methane oxidation because the conversion was zero but surprisingly, when hydrogen sulphide was fed, the conversion jumped to 8% and this can support the previous statement that the non-zero conversion during hydrogen sulphide was not related to oxygen flux but to the membrane which promoted hydrogen sulphide-methane reforming or methane decomposition.

The key to improve the membrane tolerance to hydrogen sulphide is by reducing the adsorption rate of sulphur on the membrane surface or slowing down strontium sulphate formation. To achieve that, the membrane was modified by three different methods for better oxygen flux during air separation in presence of hydrogen sulphide. The first method involved addition of strontium sulphate with different concentrations of 0.1, 1 and 10% (weight) to the membrane during fabrication. These pre-contaminated membranes were able to permeate oxygen and the fluxes were close to the non-modified ones. This indicated that sulphur from the pre-added strontium sulphate did not poison the vacancies because of the chemical stability of strontium sulphate. When hydrogen sulphide was fed, oxygen fluxes of the pre-contaminated membranes were zero implying that the technique did not improve the stability.

In the second method, the membrane was guarded by zinc oxide and the powder was placed over the dense membrane. Zinc oxide is widely used in industry for hydrogen sulphide capture and the bed can be regenerated at temperature of 450°C. The modified membrane was tested for hydrogen sulphide but unfortunately, the flux decreased to zero after few hours. It was suggested that the guard bed was not stable at 900°C due to the decomposition of zinc oxide to vapour zinc.

In the third method, the membrane was protected by a powder layer of the same material which can capture sulphur before reaching the permeating surface. Results show that indeed the stability was improved and oxygen flux was 95% during the exposure for 33 h but after that, the flux decreased to zero. The powder was characterised after operation and low amounts of strontium sulphate were detected. This was explained by the slow adsorption rate of sulphur on the powder due to the low concentration of oxygen vacancies because the powder was not in direct contact with air and accordingly, the powder acted as a molecular sieve. Other explanation suggested that adsorption of sulphur actually occurred but strontium

sulphate formation was slow due to the absence of high oxygen partial pressure. Therefore, most of the powder was regenerated after hydrogen sulphide removal.

As a conclusion, hydrogen sulphide impurity caused total immobilisation of oxygen transport and it permanently damaged most of the membrane surface. Based on this study, it is predicted that hydrogen sulphide will cause signification change in oxygen flux even in low concentration of 1 ppm. Therefore, for LSCF6428 membrane to work properly, the environment should be free from sulphur otherwise the membrane is useless. It was difficult to modify the membrane for better stability because oxygen vacancies were easy susceptible to hydrogen sulphide and it is difficult to control that step. Industrially, the membrane can be used for air separation because it is rarely to have hydrogen sulphide in inert or air streams. However, for hydrogen production by methane oxidation, natural gas is usually contaminated by hydrogen sulphide and therefore it is not advised to use the membrane. Further purification of natural gas to totally remove hydrogen sulphide could be costly and this may affect the economics of using the membrane for hydrogen production.

8.1 Future Work

The following points may alter the poisoning mechanism of hydrogen sulphide:

- Catalyst: methane oxidation was performed in no catalyst and using a catalyst can boost the conversion to over 90% and sulphur poisoning may differ because the first target could be the catalyst instead of oxygen vacancies.

- Membrane geometry: disc membrane was only used in this study but in industry, tubular (hollow-fibre) shape is more desired because of the high surface area. Also, it has a temperature profile along the tube and therefore sulphur poisoning could be different.

- Methane concentration: in this study, methane concentration was diluted to 1% due to safety issues. Operating at 100% methane with 200 ppm hydrogen sulphide could give different results.

- Other impurities: methane oxidation was performed in presence of hydrogen sulphide only but natural gas usually contains other impurities such as carbon dioxide and water. Combination of all impurities may alter the poisoning mechanism.

References

References

[1] Ball, M. and M. Wietschel, *The hydrogen economy: opportunities and challenges*. 2009: Cambridge University Press.
[2] Gupta, R., *Hydrogen fuel: production, transport, and storage*. 2008: CRC Press.
[3] Krishnaswamy, K. and P. Bala, *Power plant instrumentation*. 2013: PHI Learning.
[4] Cebolla, R., et al., *Effect of precooled inlet gas temperature and mass flow rate on final state of charge during hydrogen vehicle refueling.* International Journal of Hydrogen Energy, 2015. 40(13): p. 4698-4706.
[5] Colella, W., M. Jacobson, and D. Golden, *Switching to a U.S. hydrogen fuel cell vehicle fleet: The resultant change in emissions, energy use, and greenhouse gases.* Journal of Power Sources, 2005. 150(0): p. 150-181.
[6] Bharadwaj, S. and L. Schmidt, *Catalytic partial oxidation of natural gas to syngas.* Fuel Processing Technology, 1995. 42(2-3): p. 109-127.
[7] Lee, S. and S. Hong, *Effect of palladium addition on catalytic activity in steam methane reforming over Ni-YSZ porous membrane.* International Journal of Hydrogen Energy, 2014. 39(36): p. 21037-21043.
[8] Tsai, C.-Y., et al., *Dense perovskite membrane reactors for partial oxidation of methane to syngas.* AIChE Journal, 1997. 43(S11): p. 2741-2750.
[9] Dong, X. and W. Jin, *Mixed conducting ceramic membranes for high efficiency power generation with CO_2 capture.* Current Opinion in Chemical Engineering, 2012. 1(2): p. 163-170.
[10] Richardson, R., R. Ormerod, and J. Cotton, *Preparation and performance of a perovskite-type tubular membrane for the partial oxidation of methane.* Ionics, 2003. 9(5-6): p. 411-416.
[11] Markov, A., et al., *Reaction control and long-term stability of partial methane oxidation over an oxygen membrane.* Journal of Solid State Electrochemistry, 2011. 15(2): p. 253-257.
[12] Maxwell, T. and J. Jones, *Alternative fuels emissions and technology*. 1995, Warrendale, PA: Society of Automotive Engineers.
[13] Williams, P., R. James, and S. Roberts, *Principles of toxicology: environmental and industrial applications*. 2003: Wiley.
[14] Craig, B. and D. Anderson, *Handbook of Corrosion Data*. 1999: ASM International.
[15] Ebadi, A., et al., *Mathematical modeling of mass transfer in multicomponent gas mixture across the synthesized composite polymeric membrane.* Journal of Industrial and Engineering Chemistry, 2013. 19(3): p. 870-885.

[16] He, X. and M.-B. Hägg, *Membranes for environmentally friendly energy processes.* Membranes, 2012. 2(4): p. 706-726.
[17] Manjumol, K., et al., *An 'Eco-friendly' all aqueous sol gel process for multi functional ultrafiltration membrane on porous tubular alumina substrate.* Journal of Membrane Science, 2011. 375(1–2): p. 134-140.
[18] Basile, A. and A. Rastogi, *Advances in membrane technologies for water treatment*. 2015, Oxford: Woodhead Publishing.
[19] Pinelo, M., G. Jonsson, and A. Meyer, *Separation, extraction and concentration processes in the food, beverage and nutraceutical industries*. 2013: Woodhead Publishing.
[20] Tarleton, S., *Progress in Filtration and Separation*. 2015, Oxford: Academic Press. 557-584.
[21] Cui, Z. and H. Muralidhara, *Membrane technology: a practical guide to membrane technology and applications in food and bioprocessing*. 2010: Elsevier Science.
[22] Cheryan, M., *Ultrafiltration and microfiltration handbook*. 1998: Taylor & Francis.
[23] Baker, R., *Membrane technology and applications*. 2012: Wiley.
[24] G. Park and A. Crull, *Membrane technology: a new era*. 2000.
[25] Basile, A. and F. Gallucci, *Membranes for membrane reactors: preparation, optimization and selection*. 2011: John Wiley & Sons, Ltd. i-xxiv.
[26] Tan, X. and K. Li, *Inorganic membrane reactors: fundamentals and applications*. 2015: Wiley.
[27] Decaux, C., et al., *Dynamics of hydrogen permeation across metallic membranes.* International Journal of Hydrogen Energy, 2013. 38(20): p. 8584-8589.
[28] Lee, K., T. Arnot, and D. Mattia, *A review of reverse osmosis membrane materials for desalination—development to date and future potential.* Journal of Membrane Science, 2011. 370(1–2): p. 1-22.
[29] Meriläinen, A., A. Seppälä, and P. Kauranen, *Minimizing specific energy consumption of oxygen enrichment in polymeric hollow fiber membrane modules.* Applied Energy, 2012. 94(0): p. 285-294.
[30] Powell, C. and G. Qiao, *Polymeric CO_2/N_2 gas separation membranes for the capture of carbon dioxide from power plant flue gases.* Journal of Membrane Science, 2006. 279(1–2): p. 1-49.
[31] Imanaka, Y., *Advanced ceramic technologies & products*. 2012: The Ceramic Society of Japan, Springer.
[32] Li, K., *Ceramic Membranes for Separation and Reaction*. 2007: Wiley.
[33] Green, D. and R. Perry, *Perry's chemical Engineers' handbook*. 8th ed. 2007: McGraw-Hill Education.
[34] Nandi, B., R. Uppaluri, and M. Purkait, *Preparation and characterization of low cost ceramic membranes for micro-filtration applications.* Applied Clay Science, 2008. 42(1–2): p. 102-110.

[35] Tan, X., S. Liu, and K. Li, *Preparation and characterization of inorganic hollow fiber membranes.* Journal of Membrane Science, 2001. 188(1): p. 87-95.
[36] Lin, Y., *Microporous and dense inorganic membranes: current status and prospective.* Separation and Purification Technology, 2001. 25(1-3): p. 39-55.
[37] de Vos, R. and H. Verweij, *High-selectivity, high-flux silica membranes for gas separation.* Science, 1998. 279(5357): p. 1710-1711.
[38] Mallada, R. and M. Menéndez, *Inorganic membranes: synthesis, characterization and applications*. 2008: Elsevier Science.
[39] Wong, W., et al., *Effects of synthesis parameters on the zeolite membrane morphology.* Journal of Membrane Science, 2001. 193(2): p. 141-161.
[40] Alvarez-Ayuso, E., A. Garcia-Sanchez, and X. Querol, *Purification of metal electroplating waste waters using zeolites.* Water Res, 2003. 37(20): p. 4855-62.
[41] Sadeghbeigi, R., *Fluid catalytic cracking handbook*. 3rd ed. 2011, Oxford: Butterworth-Heinemann.
[42] Ribeiro, F., *Deactivation and regeneration of zeolite catalysts*. 2011: Imperial College Press.
[43] Kesraoui-Ouki, S., C. Cheeseman, and R. Perry, *Natural zeolite utilisation in pollution control: A review of applications to metals' effluents.* Journal of Chemical Technology & Biotechnology, 1994. 59(2): p. 121-126.
[44] Pabby, A., S. Rizvi, and A. Requena, *Handbook of membrane separations: chemical, pharmaceutical, food, and biotechnological applications*. 2nd ed. 2015: CRC Press.
[45] Wijmans, J. and R. Baker, *The solution-diffusion model: a review.* Journal of Membrane Science, 1995. 107(1-2): p. 1-21.
[46] Oyama, S. and M. Susan, *Membrane science and technology*. Vol. Volume 14. 2011: Elsevier.
[47] Fagg, D., et al., *High oxygen permeability in fluorite-type $Ce_{0.8}Pr_{0.2}O_{2-\delta}$ via the use of sintering aids.* Journal of Membrane Science, 2007. 299(1–2): p. 1-7.
[48] Leo, A., S. Liu, and J. Costa, *Development of mixed conducting membranes for clean coal energy delivery.* International Journal of Greenhouse Gas Control, 2009. 3(4): p. 357-367.
[49] Bhalla, A., R. Guo, and R. Roy, *The perovskite structure – a review of its role in ceramic science and technology.* Material Research Innovations, 2000. 4(1): p. 3-26.
[50] Simon, R., *High-temperature structural phase transitions in perovskite ($CaTiO_3$).* Journal of Physics: Condensed Matter, 1996. 8(43): p. 8267-8275.
[51] Sunarso, J., et al., *Mixed ionic-electronic conducting (MIEC) ceramic-based membranes for oxygen separation.* Journal of Membrane Science, 2008. 320(1-2): p. 13-41.
[52] Haile, S., *Fuel cell materials and components.* Acta Materialia, 2003. 51: p. 5981-6000.

[53] Teraoka, Y., et al., *Oxygen permeation through perovskite-type oxides.* Chemistry Letters, 1985(11): p. 1743-1746.
[54] W. Kingery, et al., *Oxygen ion mobility in cubic $Zr_{0.85}Ca_{0.15}O_{1.85}$,*. Journal of the American Ceramic Society, 1959. 42(10): p. 393.
[55] Kofstad., P., *Nonstoichiometry, diffusion, and electrical conductivity in binary metal oxides.* Materials and Corrosion, 1972. 25(10): p. 801-802.
[56] Knauth, P. and H. Tuller, *Solid-state ionics: roots, status, and future prospects.* Journal of the American Ceramic Society, 2002. 85(7): p. 1654-1680.
[57] Liu, Y., X. Tan, and K. Li, *Mixed conducting ceramics for catalytic membrane processing.* Catalysis Reviews - Science and Engineering, 2006. 48(2): p. 145-198.
[58] Kharton, V., et al., *Mixed electronic and ionic conductivity of $LaCo(M)O_3$ (M = Ga, Cr, Fe or Ni): II. Oxygen permeation through Cr- and Ni-substituted $LaCoO_3$.* Solid State Ionics, 1998. 110(1-2): p. 53-60.
[59] Zeng, Y. and Y. Lin, *Catalytic properties of yttria-doped bismuth oxide ceramics for oxidative coupling of methane.* Applied Catalysis A: General, 1997. 159(1-2): p. 101-117.
[60] Steele, B., *Oxygen ion conductors and their technological applications.* Materials Science and Engineering B, 1992. 13(2): p. 79-87.
[61] Kröger, F. and H. Vink, *Relations between the concentrations of imperfections in crystalline solids.* Journal of Physics and Chemistry of Solids, 1956. 3: p. 307-435.
[62] Elshof, J., H. Bouwmeester, and H. Verweij, *Oxidative coupling of methane in a mixed-conducting perovskite membrane reactor.* Applied Catalysis A: General, 1995. 130(2): p. 195-212.
[63] Bouwmeester, H., H. Kruidhof, and A. Burggraaf, *Importance of the surface exchange kinetics as rate limiting step in oxygen permeation through mixed-conducting oxides.* Solid State Ionics, 1994. 72, Part 2: p. 185-194.
[64] De Souza, R., *A universal empirical expression for the isotope surface exchange coefficients (k*) of acceptor-doped perovskite and fluorite oxides.* Physical Chemistry Chemical Physics, 2006. 8(7): p. 890-897.
[65] Miura, N., et al., *Oxygen semipermeability of mixed-conductive oxide thick-film prepared by slip casting.* Solid State Ionics, 1995. 79: p. 195-200.
[66] Hunt, A., G. Dimitrakopoulos, and A. Ghoniem, *Surface oxygen vacancy and oxygen permeation flux limits of perovskite ion transport membranes.* Journal of Membrane Science, 2015. 489: p. 248-257.
[67] Steele, B., *Ceramic ion conducting membranes and their technological applications.* Comptes Rendus de l'Académie des Sciences - Series IIC - Chemistry, 1998. 1(9): p. 533-543.
[68] Faraji, S., K. Nordheden, and S. Stagg-Williams, *A comparative study of $Ba_{0.5}Sr_{0.5}Co_{0.8}Fe_{0.2}O_x$ (BSCF) and $SrFeCo_{0.5}O_x$ (SFC) ceramic membranes used for syngas production.* Applied Catalysis B: Environmental, 2010. 99(1-2): p. 118-126.

[69] Kniep, J. and Y. Lin, *Partial oxidation of methane and oxygen permeation in SrCoFeOx membrane reactor with different catalysts.* Industrial & Engineering Chemistry Research, 2011. 50(13): p. 7941-7948.
[70] Ellett, A., *Oxygen permeation and thermo-chemical stability of oxygen separation membrane materials for the oxyfuel process*. 2010: Forschungszentrum.
[71] Shao, Z., et al., *Synthesis and oxygen permeation study of novel perovskite-type $BaBi_xCo_{0.2}Fe_{0.8-x}O_{3-\delta}$ ceramic membranes.* Journal of Membrane Science, 2000. 164(1-2): p. 167-176.
[72] Zhu, X., H. Wang, and W. Yang, *Novel cobalt-free oxygen permeable membrane.* Chemical Communications, 2004(9): p. 1130-1131.
[73] Liu, S. and G. Gavalas, *Oxygen selective ceramic hollow fiber membranes.* Journal of Membrane Science, 2005. 246(1): p. 103-108.
[74] Wang, H., et al., *A cobalt-free oxygen-permeable membrane based on the perovskite-type oxide $Ba_{0.5}Sr_{0.5}Zn_{0.2}Fe_{0.8}O_{3-\delta}$.* Advanced Materials, 2005. 17(14): p. 1785-1788.
[75] Tong, J., et al., *Investigation on the structure stability and oxygen permeability of titanium-doped perovskite-type oxides of $BaTi_{0.2}Co_xFe_{0.8-x}O_{3-\delta}$ (x=0.2-0.6).* Separation and Purification Technology, 2003. 32(1-3): p. 289-299.
[76] Iwahara, H., T. Esaka, and T. Mangahara, *Mixed conduction and oxygen permeation in the substituted oxides for $CaTiO_3$.* Journal of Applied Electrochemistry, 1988. 18(2): p. 173-177.
[77] Y. Teraoka, T. Nobunaga, and N. Yamazoe, *Effect of cation substitution on the oxygen semipermeability of perovskite-type oxides.* Chemistry Letters, 1988. 3(3): p. 503-506.
[78] Tsai, C.-Y., et al., *Dense Perovskite, $La_{1-x}A'_xFe_{1-y}Co_yO_{3-\delta}$ (A′= Ba, Sr, Ca), Membrane Synthesis, Applications, and Characterization.* Journal of the American Ceramic Society, 1998. 81(6): p. 1437-1444.
[79] Tan, X., et al., *Oxygen permeation behavior of $La_{0.6}Sr_{0.4}Co_{0.8}Fe_{0.2}O_{3-d}$ hollow fibre membranes with highly concentrated CO_2 exposure.* Journal of Membrane Science, 2012. 389: p. 216-222.
[80] Stevenson, J., et al., *Electrochemical properties of mixed conducting perovskites $La_{1-x}M_xCo_{1-y}Fe_yO_{3-\delta}$(M = Sr, Ba, Ca).* Journal of The Electrochemical Society, 1996. 143(9): p. 2722-2729.
[81] Elshof, J., H. Bouwmeester, and H. Verweij, *Oxygen transport through $La_{1-x}Sr_xFeO_{3-\delta}$ membranes. I. Permeation in air/He gradients.* Solid State Ionics, 1995. 81(1-2): p. 97-109.
[82] Ishihara, T., et al., *Mixed electronic–oxide ionic conductivity and oxygen permeating property of Fe-, Co- or Ni-doped $LaGaO_3$ perovskite oxide.* Solid State Ionics, 2000. 135(1–4): p. 631-636.
[83] Siwen, L., et al., *Oxygen permeating properties of the mixed conducting membranes without cobalt.* Materials Research Bulletin, 1998. 33(2): p. 183-188.

[84] Kruidhof, H., et al., *Influence of order-disorder transitions on oxygen permeability through selected nonstoichiometric perovskite-type oxides.* Solid State Ionics, 1993. 63–65: p. 816-822.
[85] Kharton, V., et al., *Perovskite-type oxides for high-temperature oxygen separation membranes.* Journal of Membrane Science, 1999. 163(2): p. 307-317.
[86] Brinkman, H., H. Kruidhof, and A. Burggraaf, *Mixed conducting yttrium-barium-cobalt-oxide for high oxygen permeation.* Solid State Ionics, 1994. 68(3–4): p. 173-176.
[87] Dong, H., et al., *Investigation on POM reaction in a new perovskite membrane reactor.* Catalysis Today, 2001. 67(1–3): p. 3-13.
[88] Dong, X., et al., *Dense ceramic catalytic membranes and membrane reactors for energy and environmental applications.* Chemical Communications, 2011. 47(39): p. 10886-10902.
[89] Tan, X., et al., *$La_{0.7}Sr_{0.3}FeO_{3-\delta}$ perovskite hollow fiber membranes for oxygen permeation and methane conversion.* Separation and Purification Technology, 2012. 96(0): p. 89-97.
[90] Han, J., Y. Zeng, and Y. Lin, *Oxygen permeation through fluorite-type bismuth-yttrium-copper oxide membranes.* Journal of Membrane Science, 1997. 132(2): p. 235-243.
[91] Zeng, Y. and Y. Lin, *Oxidative coupling of methane on improved bismuth oxide membrane reactors.* AIChE Journal, 2001. 47(2): p. 436-444.
[92] Fagg, D., et al., *Oxygen permeability, thermal expansion and mixed conductivity of $Gd_xCe_{0.8-x}Pr_{0.2}O_{2-\delta}$, x=0, 0.15, 0.2.* Journal of Solid State Chemistry, 2006. 179(11): p. 3347-3356.
[93] Ishihara, T., et al., *Fe doped $LaGaO_3$ perovskite oxide as an oxygen separating membrane for CH_4 partial oxidation.* Solid State Ionics, 2002. 152–153: p. 709-714.
[94] Drioli, E. and L. Giorno, in *Comprehensive membrane science and engineering*. 2010, Elsevier: Oxford. p. 311-335.
[95] Hashim, S., A. Mohamed, and S. Bhatia, *Preparation and characterization of $La_{0.6}Sr_{0.4}Co_{0.2}Fe_{0.8}O_{3-\delta}$ thin-film membrane on porous support by dip-coating method.* Journal of Sol-Gel Science and Technology, 2011. 59(3): p. 505-512.
[96] Asadi, A., et al., *Preparation and oxygen permeation of $La_{0.6}Sr_{0.4}Co_{0.2}Fe_{0.8}O_{3-\delta}$ (LSCF) perovskite-type membranes: experimental study and mathematical modeling.* Industrial & Engineering Chemistry Research, 2012. 51(7): p. 3069-3080.
[97] *MTI Corporation.* http://www.mtixtl.com. Cited 26/05/2015.
[98] Sikalidis, C., *Advances in ceramics: synthesis and characterization, processing and specific applications*. 2011: InTech.
[99] Martynczuk, J., M. Arnold, and A. Feldhoff, *Influence of grain size on the oxygen permeation performance of perovskite-type $(Ba_{0.5}Sr_{0.5})(Fe_{0.8}Zn_{0.2})O_{3-\delta}$ membranes.* Journal of Membrane Science, 2008. 322(2): p. 375-382.

[100] Sharma, S. and S. Ghoshal, *Hydrogen the future transportation fuel: from production to applications.* Renewable and Sustainable Energy Reviews, 2015. 43(0): p. 1151-1158.
[101] Corbo, P., et al., *Experimental study of a fuel cell power train for road transport application.* Journal of Power Sources, 2005. 145(2): p. 610-619.
[102] Patterson, T., et al., *Life cycle assessment of the electrolytic production and utilization of low carbon hydrogen vehicle fuel.* International Journal of Hydrogen Energy, 2014. 39(14): p. 7190-7201.
[103] Gatan, R., et al., *Oxidative desulfurization: a new technology for ULSD.* ACS Division of Fuel Chemistry, Preprints, 2004. 49: p. 577-579.
[104] Saetre, T., *Hydrogen power: theoretical and engineering solutions*. 2014: Springer Netherlands.
[105] Balat, M. and M. Balat, *Political, economic and environmental impacts of biomass-based hydrogen.* International Journal of Hydrogen Energy, 2009. 34(9): p. 3589-3603.
[106] Malaika, A., B. Krzyzynska, and M. Kozlowski, *Catalytic decomposition of methane in the presence of in situ obtained ethylene as a method of hydrogen production.* International Journal of Hydrogen Energy, 2010. 35(14): p. 7470-7475.
[107] Barelli, L., et al., *Hydrogen production through sorption-enhanced steam methane reforming and membrane technology: A review.* Energy, 2008. 33(4): p. 554-570.
[108] Kruse, B., S. Grinna, and C. Buch, *Hydrogen status og muligneter.* Bellona rapport nr. 6 2002.
[109] Kolb, G., *Fuel processing: for fuel cells*. 2008: Wiley.
[110] Zhang, T. and M. Amiridis, *Hydrogen production via the direct cracking of methane over silica-supported nickel catalysts.* Applied Catalysis A: General, 1998. 167(2): p. 161-172.
[111] Larminie, J., et al., *Fuel cell systems explained*. 2013: John Wiley & Sons. 1-24.
[112] Chang, Y. and H. Heinemann, *Partial oxidation of methane to syngas over Co/MgO catalysts. Is it low temperature?* Catalysis Letters, 1993. 21(3-4): p. 215-224.
[113] Koros, W. and R. Mahajan, *Pushing the limits on possibilities for large scale gas separation: which strategies?* Journal of Membrane Science, 2000. 175(2): p. 181-196.
[114] Cook, P., *Geologically storing carbon: learning from the Otway project experience*. 2014: Csiro Publishing.
[115] Zhang, C., et al., *The oxidative stream reforming of methane to syngas in a thin tubular mixed-conducting membrane reactor.* Journal of Membrane Science, 2008. 320(1–2): p. 401-406.

[116] Zhang, Y., et al., *Performance of an oxygen-permeable membrane reactor for partial oxidation of methane in coke oven gas to syngas.* Fuel, 2011. 90(1): p. 324-330.
[117] Iguchi, F., et al., *Oxygen permeation properties and the stability of $La_{0.6}Sr_{0.4}Fe_{0.8}Co_{0.2}O_3$ studied by Raman spectroscopy.* Solid State Ionics, 2006. 177(26-32): p. 2281-2284.
[118] Wang, H., Y. Cong, and W. Yang, *Investigation on the partial oxidation of methane to syngas in a tubular $Ba_{0.5}Sr_{0.5}Co_{0.8}Fe_{0.2}O_{3-\delta}$ membrane reactor.* Catalysis Today, 2003. 82(1–4): p. 157-166.
[119] Jin, W., et al., *Tubular lanthanum cobaltite perovskite-type membrane reactors for partial oxidation of methane to syngas.* Journal of Membrane Science, 2000. 166(1): p. 13-22.
[120] Yang, W., et al., *Development and application of oxygen permeable membrane in selective oxidation of light alkanes.* Topics in Catalysis, 2005. 35(1-2): p. 155-167.
[121] Wang, H., et al., *Production of high-purity oxygen by perovskite hollow fiber membranes swept with steam.* Journal of Membrane Science, 2006. 284(1-2): p. 5-8.
[122] Qi, X., F. Akin, and Y. Lin, *Ceramic–glass composite high temperature seals for dense ionic-conducting ceramic membranes.* Journal of Membrane Science, 2001. 193(2): p. 185-193.
[123] Vivet, A., et al., *Influence of glass and gold sealants materials on oxygen permeation performances in $La_{0.8}Sr_{0.2}Fe_{0.7}Ga_{0.3}O_{3-\delta}$ perovskite membranes.* Journal of Membrane Science, 2011. 366(1–2): p. 132-138.
[124] Bae, H. and G. Choi, *Novel modification of anode microstructure for proton-conducting solid oxide fuel cells with $BaZr_{0.8}Y_{0.2}O_{3-\delta}$ electrolytes.* Journal of Power Sources, 2015. 285(0): p. 431-438.
[125] Laguna-Bercero, M., et al., *Microtubular solid oxide fuel cells with lanthanum strontium manganite infiltrated cathodes.* International Journal of Hydrogen Energy, 2015. 40(15): p. 5469-5474.
[126] Xu, S. and W. Thomson, *Perovskite-type oxide membranes for the oxidative coupling of methane.* American Institute of Chemical Engineers, 1997. 43(S11): p. 2731-2740.
[127] Qiu, L., et al., *Oxygen permeation studies of $SrCo_{0.8}Fe_{0.2}O_{3-\delta}$.* Solid State Ionics, 1995. 76(3-4): p. 321-329.
[128] Engels, S., et al., *Oxygen permeation and stability investigations on MIEC membrane materials under operating conditions for power plant processes.* Journal of Membrane Science, 2011. 370(1-2): p. 58-69.
[129] García-Torregrosa, I., et al., *Development of CO_2 protective layers by spray pyrolysis for ceramic oxygen transport membranes.* Advanced Energy Materials, 2011. 1(4): p. 618-625.

[130] Park, J. and S. Park, *Oxygen permeability and structural stability of $La_{0.6}Sr_{0.4}Co_{0.2}Fe_{0.8}O_{3-\delta}$ membrane.* Korean Journal of Chemical Engineering, 2007. 24(5): p. 897-905.
[131] Stephens, W., T. Mazanec, and H. Anderson, *Influence of gas flow rate on oxygen flux measurements for dense oxygen conducting ceramic membranes.* Solid State Ionics, 2000. 129(1–4): p. 271-284.
[132] Samson, A., M. Søgaard, and P. Hendriksen, *$(Ce,Gd)O_{2-\delta}$–based dual phase membranes for oxygen separation.* Journal of Membrane Science. 470(0): p. 178-188.
[133] Arnold, M., H. Wang, and A. Feldhoff, *Influence of CO_2 on the oxygen permeation performance and the microstructure of perovskite-type $(Ba_{0.5}Sr_{0.5})(Co_{0.8}Fe_{0.2})O_{3-\delta}$ membranes.* Journal of Membrane Science, 2007. 293(1-2): p. 44-52.
[134] Yi, J. and M. Schroeder, *High temperature degradation of $Ba_{0.5}Sr_{0.5}Co_{0.8}Fe_{0.2}O_{3-\delta}$ membranes in atmospheres containing concentrated carbon dioxide.* Journal of Membrane Science, 2011. 378(1–2): p. 163-170.
[135] Homonnay, Z., et al., *Simultaneous probing of the Fe and Co sites in the CO_2-absorber perovskite $Sr_{0.95}Ca_{0.05}Co_{0.5}Fe_{0.5}O_{3-\delta}$: a Mössbauer Study.* Chemistry of Materials, 2002. 14(3): p. 1127-1135.
[136] Nomura, K., et al., *CO_2 absorption properties and characterization of perovskite oxides, (Ba,Ca) (Co,Fe) $O_{3-\delta}$.* Applied Catalysis A: General, 1996. 137(1): p. 25-36.
[137] Gao, J., et al., *Poisoning effect of SO_2 on the oxygen permeation behavior of $La_{0.6}Sr_{0.4}Co_{0.2}Fe_{0.8}O_{3-\delta}$ perovskite hollow fiber membranes.* Journal of Membrane Science, 2014. 455(0): p. 341-348.
[138] Kent, C., *Basics of toxicology*. 1998: Wiley.
[139] Mara, D. and N. Horan, *Handbook of water and wastewater microbiology*. 2003, London: Academic Press.
[140] Lens, P. and L. Pol, *Environmental technologies to treat sulfur pollution: principles and engineering*. 2000: IWA Publishing.
[141] McManus, N., *Safety and health in confined spaces*. 1998: Taylor & Francis.
[142] *EH40/2005 workplace exposure limits*. 2005: Health and Safety Executive.
[143] Raymond, L., *Hydrogen embrittlement: prevention and control*. 1988: American Society for Testing and Materials.
[144] Radkevych, O. and H. Chumalo, *Damage to the metal of industrial pipelines in a hydrogen sulfide environment.* Materials Science, 2003. 39(4): p. 596-600.
[145] *Encyclopaedia Britannica.* http://www.britannica.com/science/sulfur-cycle/images-videos/The-sulfur-cycle/111671. Cited 07/09/2015.
[146] Graedel, T., et al., *On the mechanism of silver and copper sulfidation by atmospheric H_2S and OCS.* Corrosion Science, 1985. 25(12): p. 1163-1180.

[147] Viswanadham, P. and P. Singh, *Failure modes and mechanisms in electronic packages*. 1998: Springer.
[148] Petheram, L., *Acid Rain*. 2002: Bridgestone Books.
[149] Lane, C., *Acid rain: overview and abstracts*. 2003: Nova Science Publishers.
[150] Kajiwara, M., S. Uemiya, and T. Kojima, *Stability and hydrogen permeation behavior of supported platinum membranes in presence of hydrogen sulfide.* International Journal of Hydrogen Energy, 1999. 24(9): p. 839-844.
[151] Scholes, C., G. Stevens, and S. Kentish, *The effect of hydrogen sulfide, carbon monoxide and water on the performance of a PDMS membrane in carbon dioxide/nitrogen separation.* Journal of Membrane Science, 2010. 350(1-2): p. 189-199.
[152] Ohashi, H., et al., *Hydrogen production from hydrogen sulfide using membrane reactor integrated with porous membrane having thermal and corrosion resistance.* Journal of Membrane Science, 1998. 146(1): p. 39-52.
[153] Walker, P. and W. Tarn, *Handbook of metal etchants*. 1990: CRC Press.
[154] World Health Organization, *Hydrogen sulphide*. Vol. 19. 1981: Environmental Health Criteria.
[155] Quick Access, *Patient information on conditions, herbs & supplements*. 2000: Integrative Medicine Communications.
[156] Tai, L., et al., *Structure and electrical properties of* $La_{1-x}Sr_xCo_{1-y}Fe_yO_3$. *Part 2. The system* $La_{1-x}Sr_xCo_{0.2}Fe_{0.8}O3$. Solid State Ionics, 1995. 76(3-4): p. 273-283.
[157] Petric, A., P. Huang, and F. Tietz, *Evaluation of La-Sr-Co-F-O perovskites for solid oxide fuel cells and gas separation membranes.* Solid State Ionics, 2000. 135(1-4): p. 719-725.
[158] Hatcher, J., et al., *Development and testing of an intermediate temperature glass sealant for use in mixed ionic and electronic conducting membrane reactors.* Solid State Ionics, 2010. 181(15–16): p. 767-774.
[159] Möbius, A., D. Henriques, and T. Markus, *Sintering behaviour of* $La_{1-x}Sr_xCo_{0.2}Fe_{0.8}O_{3-\delta}$ *mixed conducting materials.* Journal of the European Ceramic Society, 2009. 29(13): p. 2831-2839.
[160] Alqaheem, Y., et al., *The impact of sulfur contamination on the performance of* $La_{0.6}Sr_{0.4}Co_{0.2}Fe_{0.8}O_{3-\delta}$ *oxygen transport membranes.* Solid State Ionics, 2014. 262: p. 262-265.
[161] Chawla, K., *Composite materials: science and engineering*. 1998: Springer.
[162] Murray, G., C. White, and W. Weise, *Introduction to engineering materials: behavior: properties, and selection*. 1993: Taylor & Francis.
[163] Ebbing, D. and S. Gammon, *General Chemistry*. 10th ed. 2012: Cengage Learning.

[164] Waller, D., et al., *The effect of thermal treatment on the resistance of LSCF electrodes on gadolinia doped ceria electrolytes.* Solid State Ionics, 1996. 86-88(0): p. 767-772.
[165] Itoh, T., et al., *Oxygen partial pressure dependence of in situ X-ray absorption spectroscopy at the Co and Fe K edges for* $(La_{0.6}Sr_{0.4})(Co_{0.2}Fe_{0.8})O_{3-\delta}$. Solid State Communications, 2012. 152(4): p. 278-283.
[166] Mosadeghkhah, A., M. Alaee, and T. Mohammadi, *Effect of sintering temperature and dwell time and pressing pressure on* $Ba_{0.5}Sr_{0.5}Co_{0.8}Fe_{0.2}O_{3-\delta}$ *perovskite-type membranes.* Materials & Design, 2007. 28(5): p. 1699-1706.
[167] Tan, X., Z. Pang, and K. Li, *Oxygen production using* $La_{0.6}Sr_{0.4}Co_{0.2}Fe_{0.8}O3-\delta$ *(LSCF) perovskite hollow fibre membrane modules.* Journal of Membrane Science, 2008. 310(1-2): p. 550-556.
[168] Tan, X., Y. Liu, and K. Li, *Preparation of LSCF ceramic hollow-fiber membranes for oxygen production by a phase-inversion/sintering technique.* Industrial & Engineering Chemistry Research, 2004. 44(1): p. 61-66.
[169] Rotzsche, H., *Stationary phases in gas chromatography*. 1991: Elsevier Science.
[170] Karasek, F. and R. Clement, *Basic gas chromatography-mass spectrometry: principles and techniques*. 2012: Elsevier Science.
[171] Cazes, J. and R. Scott, *Chromatography theory*. 2002: CRC Press.
[172] Kim, J. and Y. Lin, *Synthesis and oxygen permeation properties of ceramic-metal dual-phase membranes.* Journal of Membrane Science, 2000. 167(1): p. 123-133.
[173] Liptak, B., *Instrument engineers' handbook: process control and optimization*. 4th ed. 2005: Taylor & Francis.
[174] Franca, R., A. Thursfield, and I. Metcalfe, $La_{0.6}Sr_{0.4}Co_{0.2}Fe_{0.8}O_{3-\delta}$ *microtubular membranes for hydrogen production from water splitting.* Journal of Membrane Science, 2012. 389: p. 173-181.
[175] Yao, N. and Z. Wang, *Handbook of microscopy for nanotechnology*. 2006: Springer.
[176] Lyman, C., et al., *Scanning electron microscopy, x-ray microanalysis, and analytical electron microscopy: a laboratory workbook*. 2012: Springer.
[177] Kokare, C., *Pharmaceutical microbiology: principles and applications*. 2008: Nirali Prakashan.
[178] Goodhew, P., J. Humphreys, and R. Beanland, *Electron microscopy and analysis*. 3rd ed. 2000: Taylor & Francis.
[179] Ross, R., *Microelectronics failure analysis desk reference* 6th ed. 2011: ASM International.
[180] Goldstein, J., *Scanning electron microscopy and x-ray microanalysis*. 2003: Kluwer Academic/Plenum Publishers.
[181] Weller, M., *Inorganic materials chemistry*. 1995: Oxford University Press.

[182] Zolotoyabko, E., *Basic concepts of x-ray diffraction*. 2014: Wiley.
[183] Weidner, J., *Separators and membranes for batteries, capacitors, fuel cells, and other electrochemical systems*. 2009: Electrochemical Society.
[184] Hüfner, S., *Photoelectron spectroscopy: principles and applications*. 2003: Springer.
[185] van der Heide, P., *X-ray photoelectron spectroscopy : an introduction to principles and practices*. 2011, Wiley.
[186] Wang, B., et al., *Stabilities of $La_{0.6}Sr_{0.4}Co_{0.2}Fe_{0.8}O_{3-\delta}$ oxygen separation membranes-effects of kinetic demixing/decomposition and impurity segregation.* Journal of Membrane Science, 2009. 344(1-2): p. 101-106.
[187] Xu, S. and W. Thomson, *Stability of $La_{0.6}Sr_{0.4}Co_{0.2}Fe_{0.8}O_{3-\delta}$ perovskite membranes in reducing and nonreducing environments.* Industrial and Engineering Chemistry Research, 1998. 37(4): p. 1290-1299.
[188] Zawadzki, M., H. Grabowska, and J. Trawczyński, *Effect of synthesis method of LSCF perovskite on its catalytic properties for phenol methylation.* Solid State Ionics, 2010. 181(23–24): p. 1131-1139.
[189] Kanegsberg, B. and E. Kanegsberg, *Handbook for critical cleaning*. 2000: CRC Press.
[190] Ding, H., et al., *Suppression of Sr surface segregation in $La_{1-x}Sr_xCo_{1-y}Fe_yO_{3-\delta}$: A first principles study.* Physical Chemistry Chemical Physics, 2013. 15(2): p. 489-496.
[191] Reinke, C. and W. Johnson, *Influence of coherency stress on kinetic demixing.* Journal of the American Ceramic Society, 1995. 78(10): p. 2593-2602.
[192] Monceau, D., C. Petot, and G. Petot-Ervas, *Kinetic demixing profile calculation in oxide solid solutions under a chemical potential gradient.* Solid State Ionics, 1991. 45(3–4): p. 231-237.
[193] Shao, Z. and S. Haile, *A high-performance cathode for the next generation of solid-oxide fuel cells.* Nature, 2004. 431(7005): p. 170-173.
[194] Jung, W. and H. Tuller, *Investigation of surface Sr segregation in model thin film solid oxide fuel cell perovskite electrodes.* Energy & Environmental Science, 2012. 5(1): p. 5370-5378.
[195] Crumlin, E., et al., *Surface strontium enrichment on highly active perovskites for oxygen electrocatalysis in solid oxide fuel cells.* Energy & Environmental Science, 2012. 5(3): p. 6081-6088.
[196] Zhang, W., *Investigation of degradation mechanisms of LSCF based SOFC cathodes by CALPHAD modeling and experiments*. 2012, Technical University of Denmark: PhD Thesis.
[197] Fister, T., et al., *In situ characterization of strontium surface segregation in epitaxial $La_{0.7}Sr_{0.3}MnO_3$ thin films as a function of oxygen partial pressure.* Applied Physics Letters, 2008. 93(15).

[198] Zeng, P., et al., *Significant effects of sintering temperature on the performance of $La_{0.6}Sr_{0.4}Co_{0.2}Fe_{0.8}O_{3-\delta}$ oxygen selective membranes.* Journal of Membrane Science, 2007. 302(1-2): p. 171-179.
[199] Smith, F., *Industrial applications of x-Ray diffraction*. 1999: Taylor & Francis.
[200] Yasuda, E., et al., *Carbon alloys: novel concepts to develop carbon acience and technology*. 2003: Elsevier Science.
[201] Hume, S., *Influence of raw material properties on the reactivity of carbon anodes used in the electrolytic production of aluminium*. 1993: Aluminium-Verlag.
[202] Rossetti, I., et al., *Effect of sulphur poisoning on perovskite catalysts prepared by flame-pyrolysis.* Applied Catalysis B: Environmental, 2009. 89(3-4): p. 383-390.
[203] Alifanti, M., et al., *Activity in methane combustion and sensitivity to sulfur poisoning of $La_{1-x}Ce_xMn_{1-y}Co_yO_3$ perovskite oxides.* Applied Catalysis B: Environmental, 2003. 41(1-2): p. 71-81.
[204] Tejuca, L. and J. Fierro, *Properties and applications of perovskite-type oxides*. 2000: Taylor & Francis.
[205] Wang, F., et al., *Effect of strontium concentration on sulfur poisoning of LSCF cathodes.* Solid State Ionics, 2012. 225(0): p. 157-160.
[206] Karr, C., *Analytical methods for coal and coal products*. 2012: Elsevier.
[207] Barin, I., *Thermochemical data of pure substances*. 2008: Wiley-VCH Verlag GmbH.
[208] Halle, J. and K. Stern, *Vaporization and decomposition of sodium sulfate: thermodynamics and kinetics.* The Journal of Physical Chemistry, 1980. 84(13): p. 1699-1704.
[209] Perry, D. and S. Phillips, *Handbook of inorganic compounds*. 1995: Taylor & Francis.
[210] Stewart, M. and K. Arnold, *Emulsions and oil treating equipment: selection, sizing and troubleshooting*. 2008: Elsevier Science.
[211] Cholet, H., *Well production practical handbook*. 2000: Technip.
[212] Paul, J.-F. and E. Payen, *Vacancy formation on MoS_2 hydrodesulfurization catalyst: DFT study of the mechanism.* The Journal of Physical Chemistry B, 2003. 107(17): p. 4057-4064.
[213] Figoli, N., et al., *Regeneration of Ni/SiO_2 poisoned with carbon disulfide.* Catalysis Letters, 1996. 38(3-4): p. 171-174.
[214] da Silva, A. and N. Heck, *Thermodynamics of sulfur poisoning in solid oxide fuel cells revisited: The effect of H_2S concentration, temperature, current density and fuel utilization.* Journal of Power Sources, 2015. 296: p. 92-101.
[215] Oyama, S. and S. Stagg-Williams, *Inorganic, polymeric and composite membranes: structure, function and other correlations*. 2011: Elsevier.

[216] Catón, N., et al., *Hydrogen production by catalytic cracking of methane using Ni-Al_2O_3 catalysts. Influence of the operating conditions*, in *Studies in Surface Science and Catalysis*. 2001, Elsevier. p. 391-398.
[217] Amin, A., E. Croiset, and W. Epling, *Review of methane catalytic cracking for hydrogen production.* International Journal of Hydrogen Energy, 2011. 36(4): p. 2904-2935.
[218] Han, K.-S., et al., *Direct methane cracking using a mixed conducting ceramic membrane for production of hydrogen and carbon.* International Journal of Hydrogen Energy, 2013. 38(36): p. 16133-16139.
[219] Huang, C. and A. T-Raissi, *Liquid hydrogen production via hydrogen sulfide methane reformation.* Journal of Power Sources, 2008. 175(1): p. 464-472.
[220] Balachandran, U., et al., *Dense ceramic membranes for partial oxidation of methane to syngas.* Applied Catalysis A: General, 1995. 133(1): p. 19-29.
[221] Abdullah, S., *Hydrogen production via simultaneous methane reforming and water splitting processes using membrane reactor*. 2014, Newcastle University: PhD Thesis.
[222] Wang, B., et al., *A further investigation of the kinetic demixing/decomposition of $La_{0.6}Sr_{0.4}Co_{0.2}Fe_{0.8}O_{3-\delta}$ oxygen separation membranes.* Journal of Membrane Science. 369(1-2): p. 526-535.
[223] Martínez-Salazar, A., et al., *Hydrogen production by methane and hydrogen sulphide reaction: kinetics and modeling study over Mo/La_2O_3-ZrO_2 catalyst.* International Journal of Hydrogen Energy, 2015. In Press.
[224] Megalofonos, S. and N. Papayannakos, *Kinetics of catalytic reaction of methane and hydrogen sulphide over MoS_2.* Applied Catalysis A: General, 1997. 165(1-2): p. 249-258.
[225] Konieczny, A., et al., *Catalyst development for thermocatalytic decomposition of methane to hydrogen.* International Journal of Hydrogen Energy, 2008. 33(1): p. 264-272.
[226] Zhu, Q., et al., *Sulfur as a selective 'soft' oxidant for catalytic methane conversion probed by experiment and theory.* Nature Chemistry. 5(2): p. 104-109.
[227] Rao, T. and R. Kumar, *An experimental study of oxidation of zinc sulphide pellets.* Chemical Engineering Science, 1982. 37(7): p. 987-996.
[228] Shangguan, J., et al., *Desulfurization behavior of zinc oxide based sorbent modified by the combination of Al_2O_3 and K_2CO_3.* Fuel, 2013. 108(0): p. 80-84.
[229] Bartholomew, C. and J. Butt, *Catalyst deactivation: studies in surface science and catalysis*. 1991: Elsevier Science.
[230] Rosso, I., et al., *Zinc oxide sorbents for the removal of hydrogen sulfide from syngas.* Industrial & Engineering Chemistry Research, 2003. 42(8): p. 1688-1697.
[231] Tagawa, H., *Thermal decomposition temperatures of metal sulfates.* Thermochimica Acta, 1984. 80(1): p. 23-33.

[232] Higman, C. and M. van der Burgt, *Gasification*. 2011: Elsevier Science.
[233] *Emergency response planning guideline for hydrogen sulfide*. 1991: American Industrial Hygiene Association.
[234] Atimtay, A. and S. Littlefield, *Use of zinc oxide sorbents to remove hydrogen sulfide from coal gases.* ACS Division of Fuel Chemistry, Preprints, 1987. 32: p. 526-533.

Appendix

Appendix A: Long-term stability of gold-glass-sealant

In this study, a new sealant was developed consisting of gold paste and 20% LSCF6428 powder in waterglass. The sealant was tested for long term operation of *ca.* 1000 h and nitrogen leak was almost zero as shown in the figure below. Air and argon were fed at flow rate of 20 ml min^{-1} (STP) and temperature was at 900°C. The increase in oxygen flux indicates that the membrane was activating and the glass from the sealant did not cover the membrane.

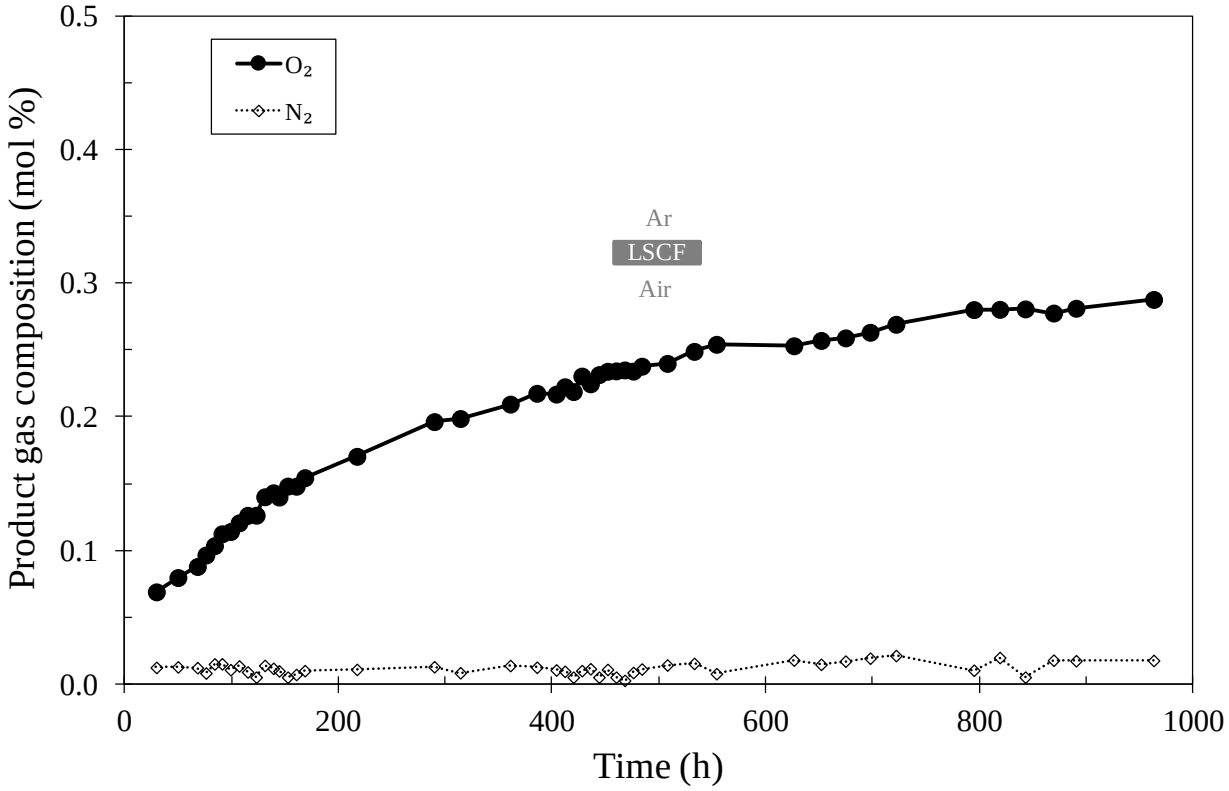

Figure A.1. Analysis of the product gas during air separation using LSCF6428 membrane sealed with gold-glass-ceramic sealant at 900°C.

Appendix B: Repeatability of experiments

To make sure that the data is reliable, most of the experiments were repeated and similar results were obtained. In this appendix, the following experiments were re-conducted:

- Oxygen flux of LSCF6428 membrane for air separation during hydrogen sulphide impurity (200 ppm) in inert side for 100 h at 900°C.
- Oxygen flux of LSCF6428 membrane after 24 h of hydrogen sulphide exposure (200 ppm) during air separation at 900°C.
- Changes of oxygen flux of LSCF6428 membrane during hydrogen sulphide poisoning (200 ppm) using 1% (mol) oxygen instead of air at 900°C.
- Increase in leak of LSCF6428 membrane after hydrogen sulphide poisoning (200 ppm) in absence of oxygen source for 100 h at 900°C.
- Methane oxidation by LSCF6428 membrane in presence of hydrogen sulphide (200 ppm) for 100 h at 900°C.
- Use of 1% (mol) hydrogen to restore LSCF6428 membrane after hydrogen sulphide poisoning (200 ppm) during methane oxidation at 900°C.
- Use of the pre-poisoned membrane by 100 h of hydrogen sulphide (200 ppm) during air separation for methane oxidation.

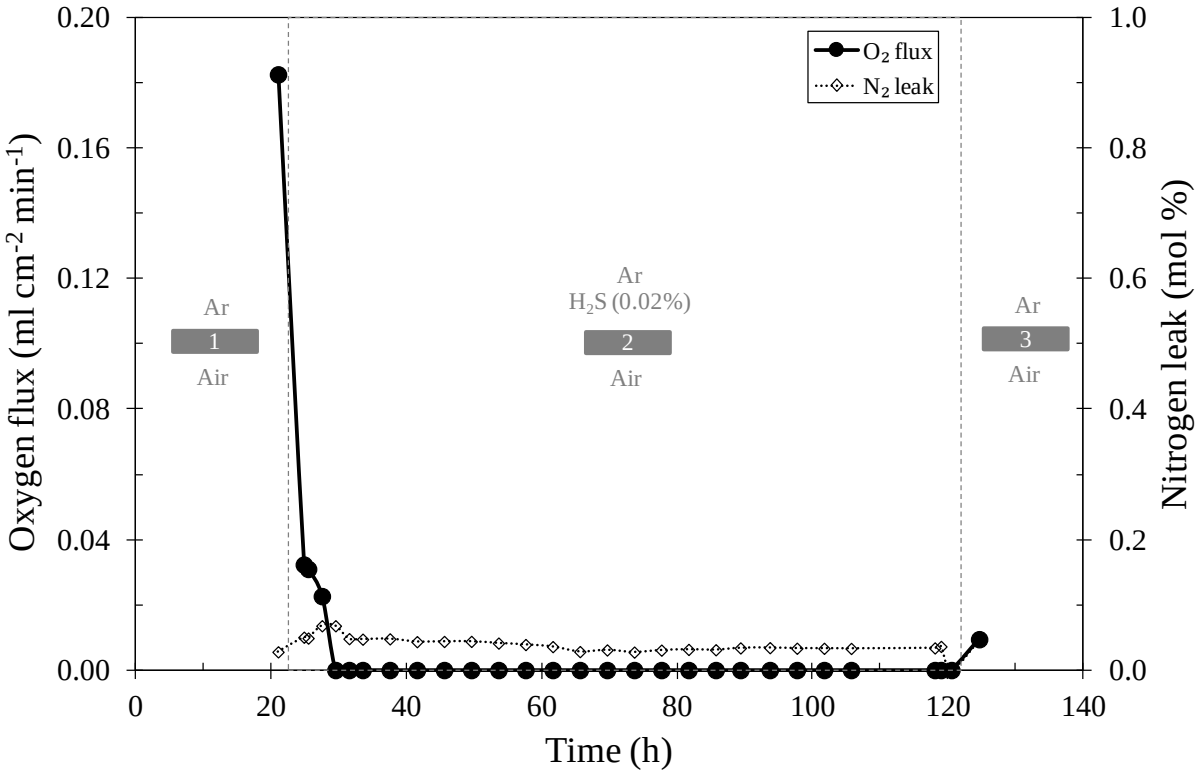

Figure B.1. Oxygen flux of LSCF6428 membrane for air separation during hydrogen sulphide impurity (200 ppm) in inert side for 100 h at 900°C (repeatability of Figure 4.6).

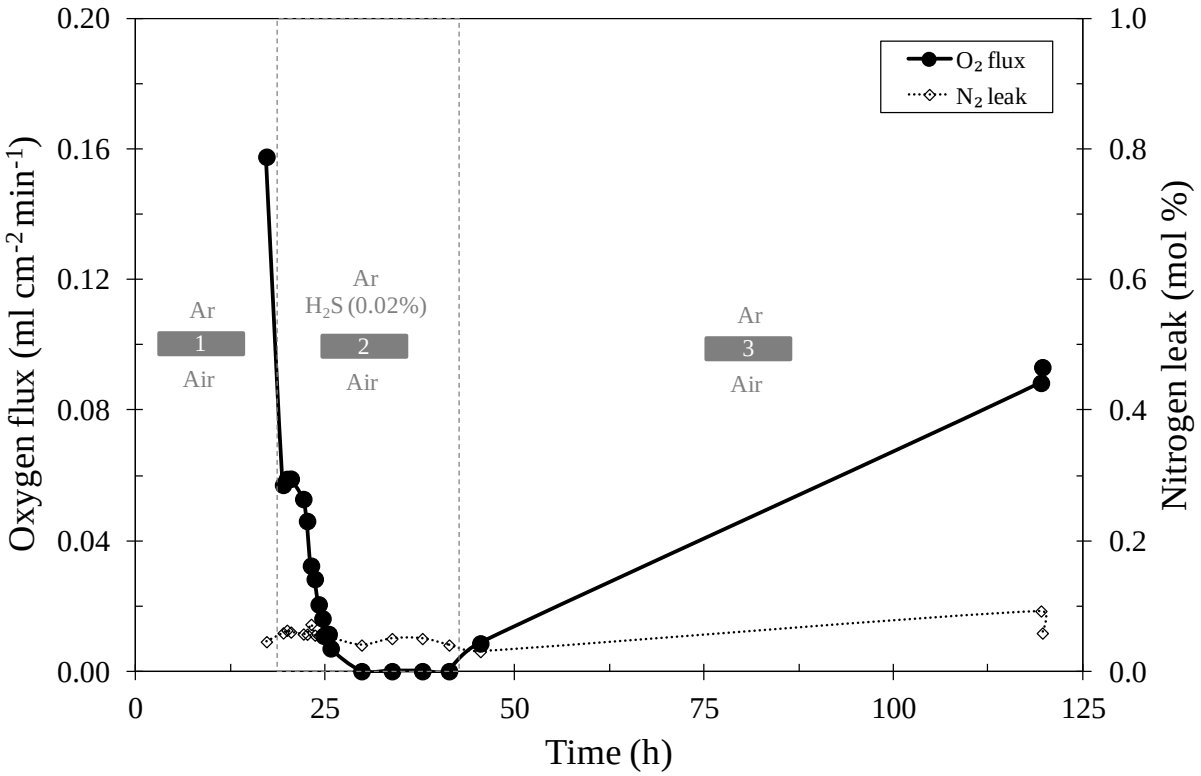

Figure B.2. Oxygen flux of LSCF6428 membrane after 24 h of hydrogen sulphide exposure (200 ppm) during air separation at 900°C (repeatability of Figure 5.2).

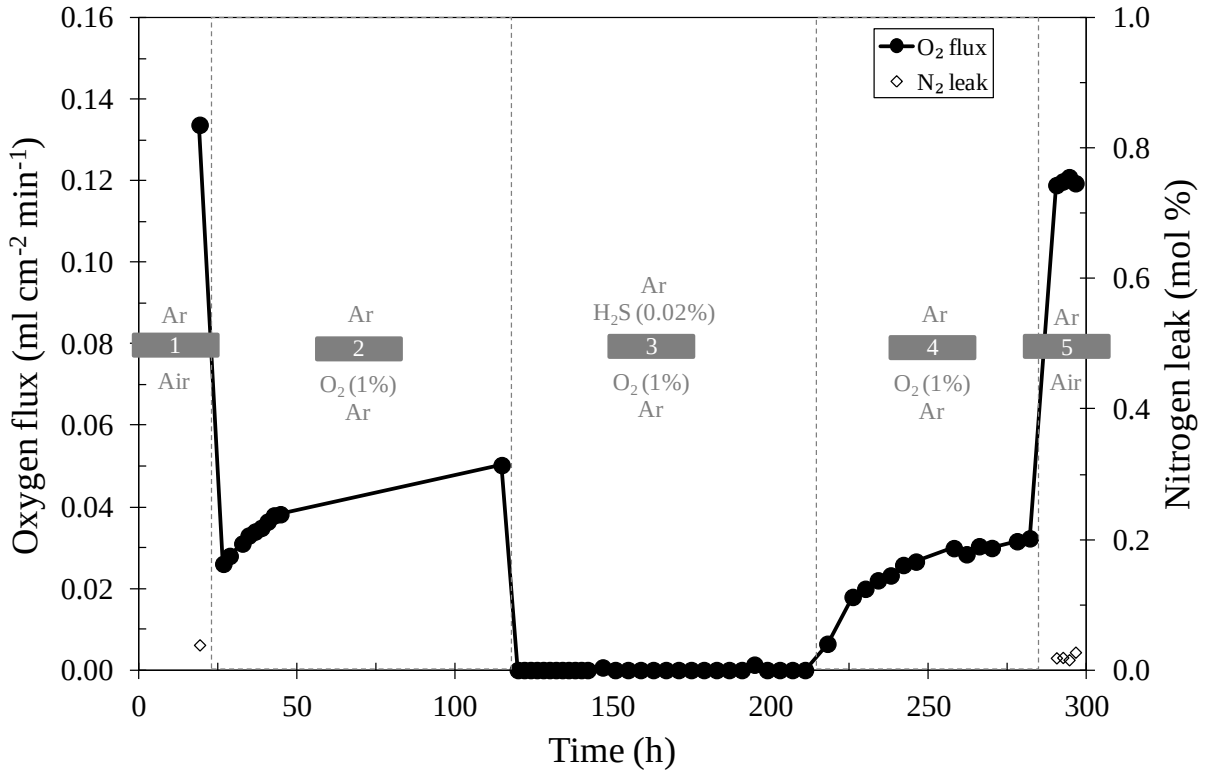

Figure B.3. Changes of oxygen flux of LSCF6428 membrane during hydrogen sulphide poisoning (200 ppm) using 1% (mol) oxygen instead of air at 900°C (repeatability of Figure 5.7).

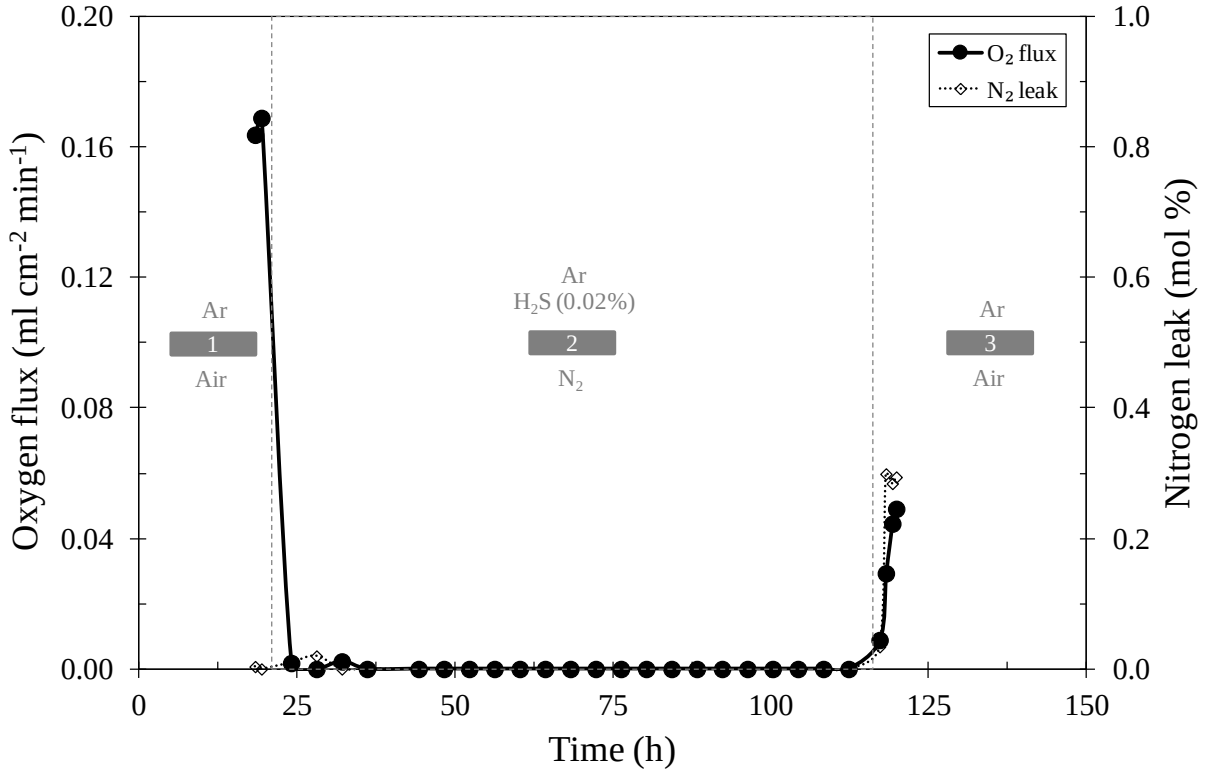

Figure B.4. Increase in leak of LSCF6428 membrane after hydrogen sulphide poisoning (200 ppm) in absence of oxygen source for 100 h at 900°C (repeatability of Figure 5.10).

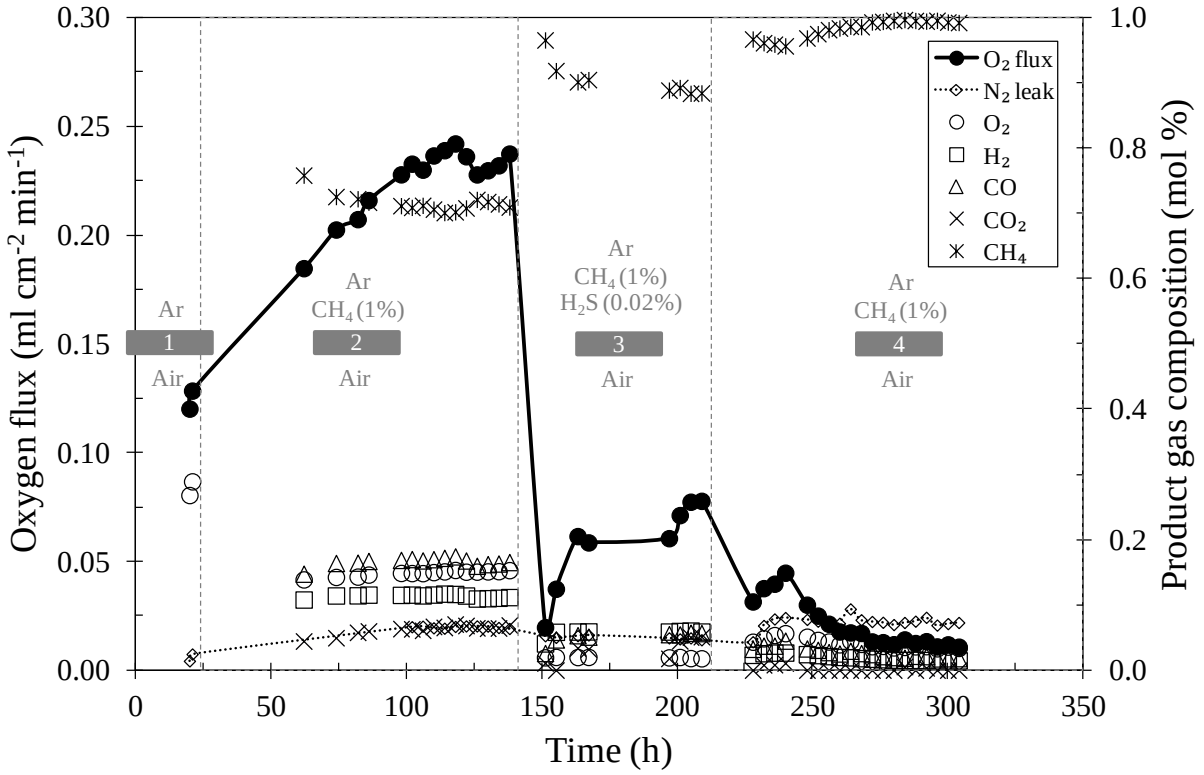

Figure B.5. Methane oxidation using LSCF6428 membrane in presence of hydrogen sulphide (200 ppm) at 900°C (repeatability of Figure 6.6).

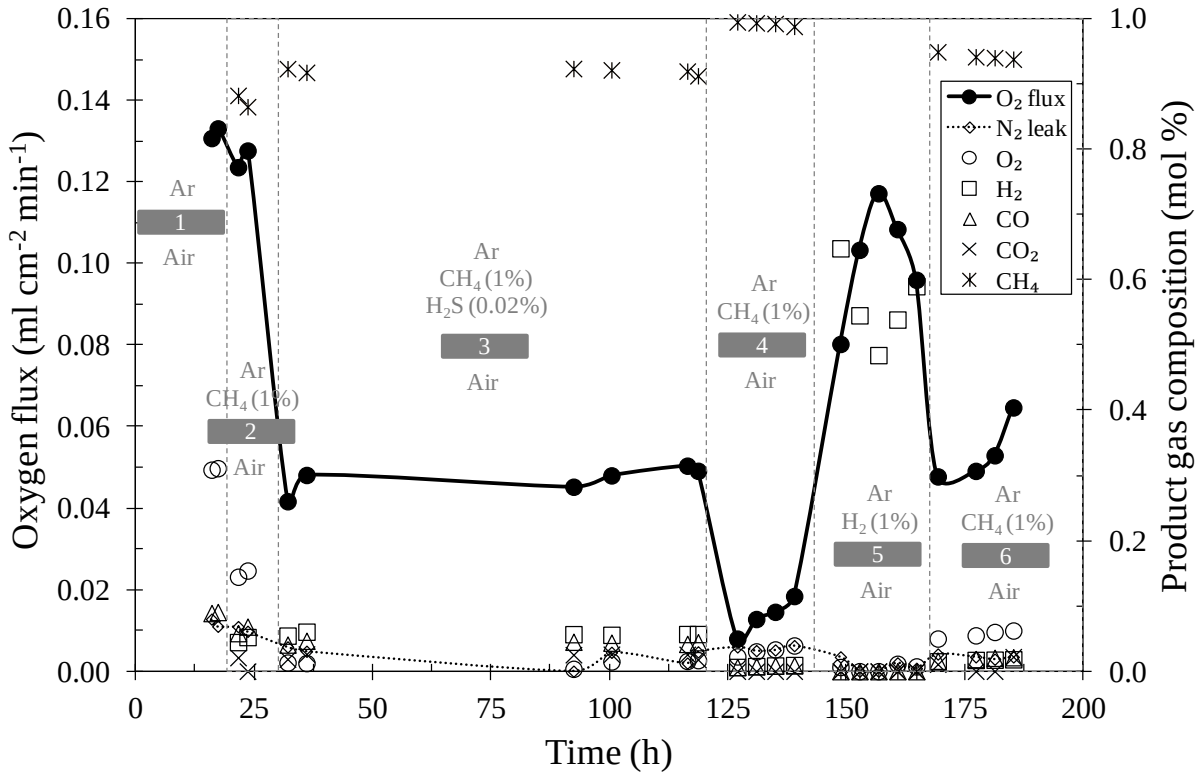

Figure B.6. Use of 1% (mol) hydrogen to restore LSCF6428 membrane after hydrogen sulphide poisoning (200 ppm) during methane oxidation at 900°C (repeatability of Figure 6.12).

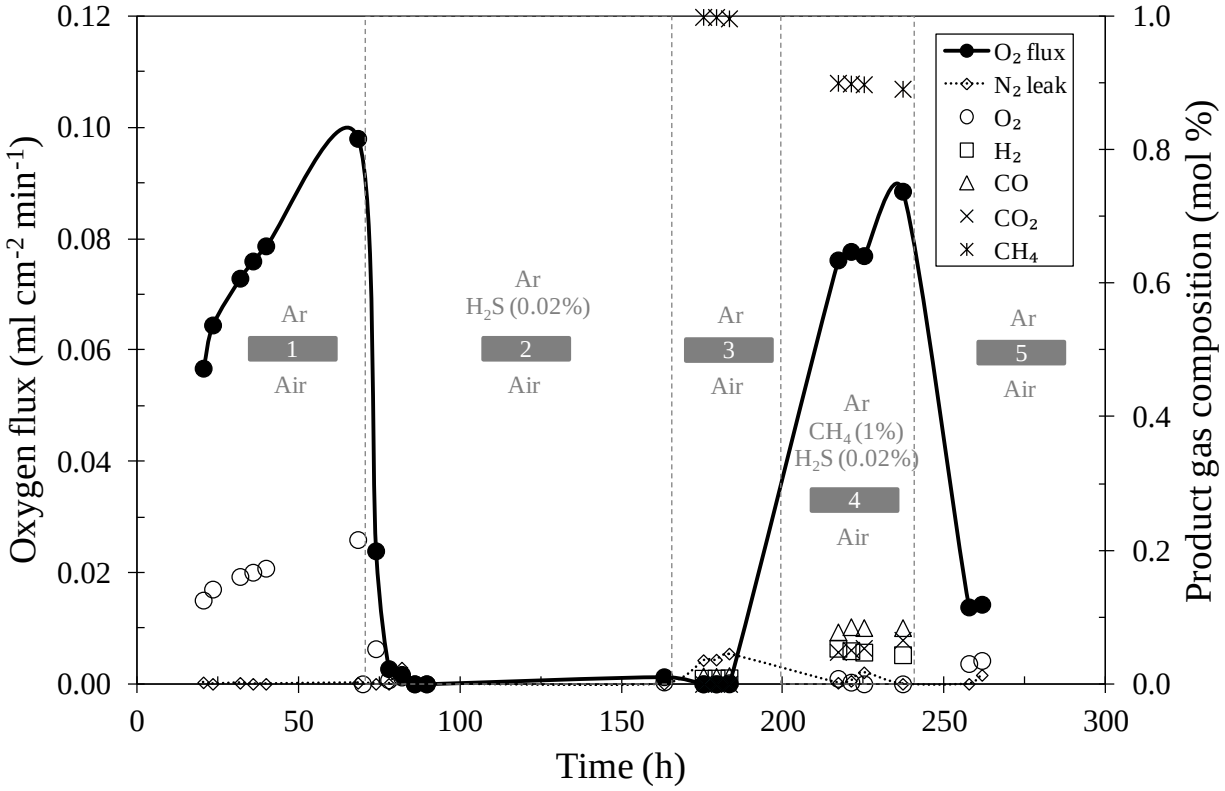

Figure B.7. Use of the pre-poisoned membrane by 100 h of hydrogen sulphide (200 ppm) during air separation for methane oxidation (repeatability of Figure 6.17)

Appendix C: Impact of sulphur dioxide impurity on oxygen permeation of LSCF6428

In chapter 4 section 2, it was suggested that hydrogen sulphide environment was changed to sulphur dioxide when it was fed to LSCF6428 membrane during air separation. Hydrogen sulphide can react with the permeated oxygen to form sulphur dioxide. To confirm that hydrogen sulphide was actually changed to sulphur dioxide, LSCF6428 was tested for sulphur dioxide impurity of 200 ppm in inert side at 900°C with flow rates of 20 ml min^{-1} (STP). Figure C.1 shows that oxygen flux was zero during the exposure and part of the flux was restored after sulphur dioxide removal. This change in oxygen flux is similar to what was seen in case of hydrogen sulphide.

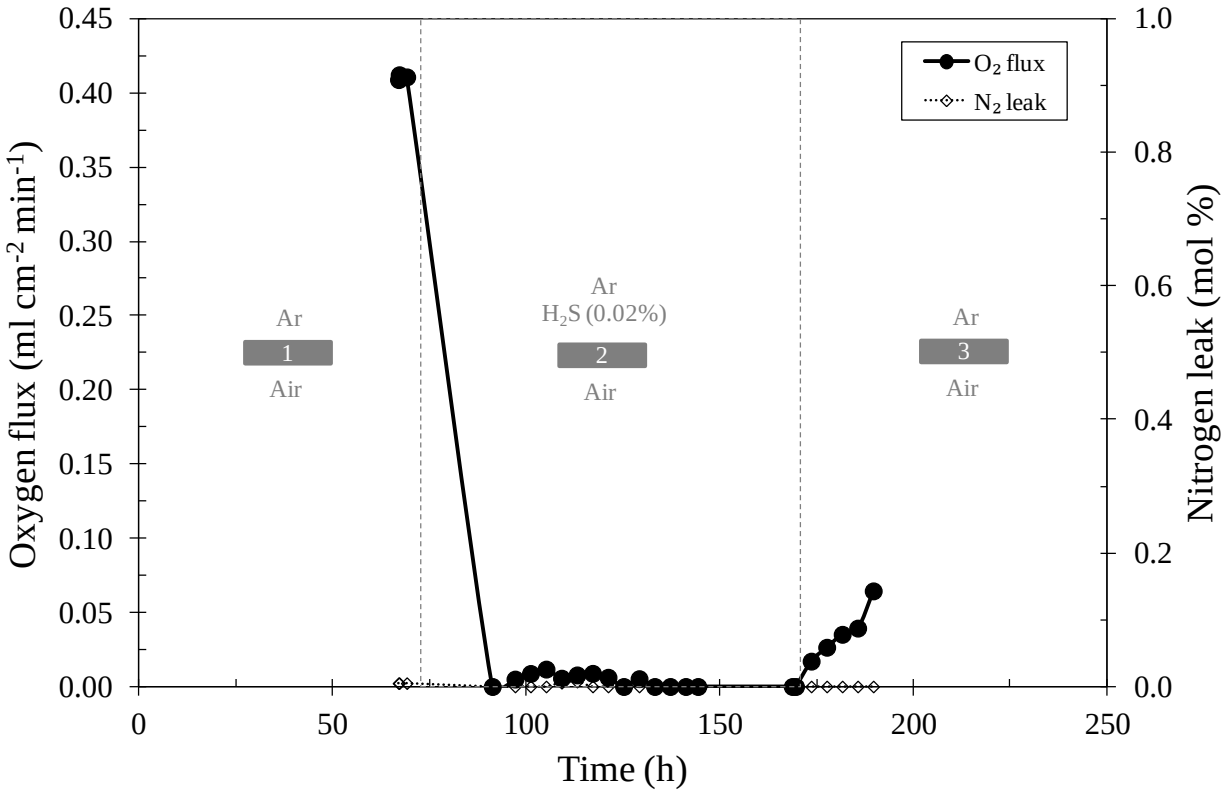

Figure C.1. Changes of oxygen flux of LSCF6428 membrane during air separation in presence of sulphur dioxide (200 ppm) for 100 h at 900°C.

Appendix D: Increase in nitrogen leak after flow switching in LSCF6428 membrane

In chapter 4 section 3, flows were switched after hydrogen sulphide attack to see if feeding air to the poisoned surface can regenerate some sulphur from the membrane surface. However, results showed that the membrane actually failed due to the increase in nitrogen leak from 0.07 to 0.58% (mol). To see whether hydrogen sulphide caused the leak, the experiment was repeated in a sulphur-free environment. LSCF6428 membrane was first heated to 900°C using air and argon at 20 ml cm^{-2} min^{-1} (STP), each. After that, flows were switched by feeding air in the inert side and argon in the air side. Result is given in Figure D.1 but the leak still increased after switching indicating that the issue was from the membrane itself not from hydrogen sulphide.

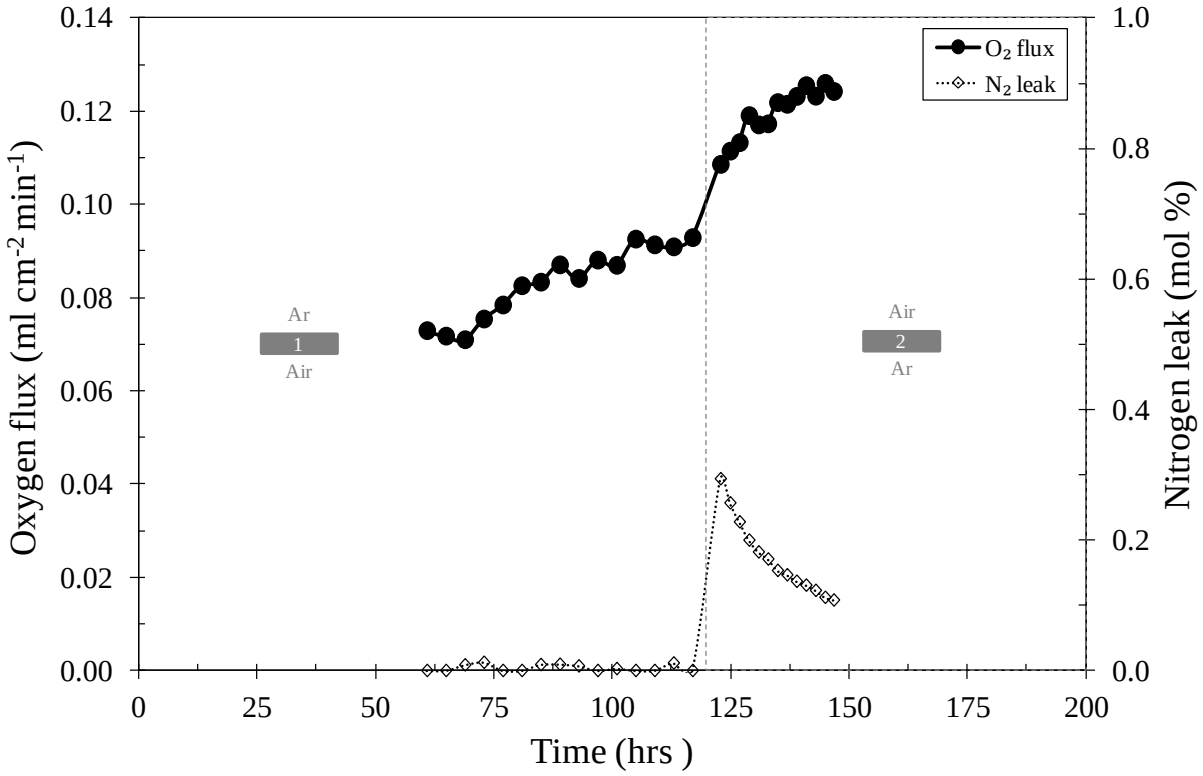

Figure D.1. Increase in nitrogen leak in LSCF6428 membrane after flow switching by introducing air in "inert side" and argon in "air side" at 900°C.

Appendix E: Increase in nitrogen leak after hydrogen sulphide poisoning in absence of oxygen

In chapter 5 section 5, exposing the membrane to hydrogen sulphide without the supplement of oxygen caused sharp increase in nitrogen leak from 0.02 to 2.1% (mol). It was suggested the membrane continued in expansion due to the loss of oxygen from the bulk membrane and this resulted in membrane expansion. Because the membrane was gas-tight sealed, it may not expand freely and therefore the membrane cracked. In this experiment, effect of sealant on the increase in leak was investigated by using silver sealant instead of gold-glass-ceramic sealant. LSCF6428 membrane was heated to 900°C using air and argon at 20 ml cm^{-2} min^{-1} (STP), each. After that, air was no longer fed and argon was replaced with hydrogen sulphide (200 ppm in argon) for 100 h. After that, air and argon were brought back. Result is shown in Figure E.1 and the leak still increased after sulphur poisoning. This experiment may suggest that the membrane itself cracked due to the loss of oxygen.

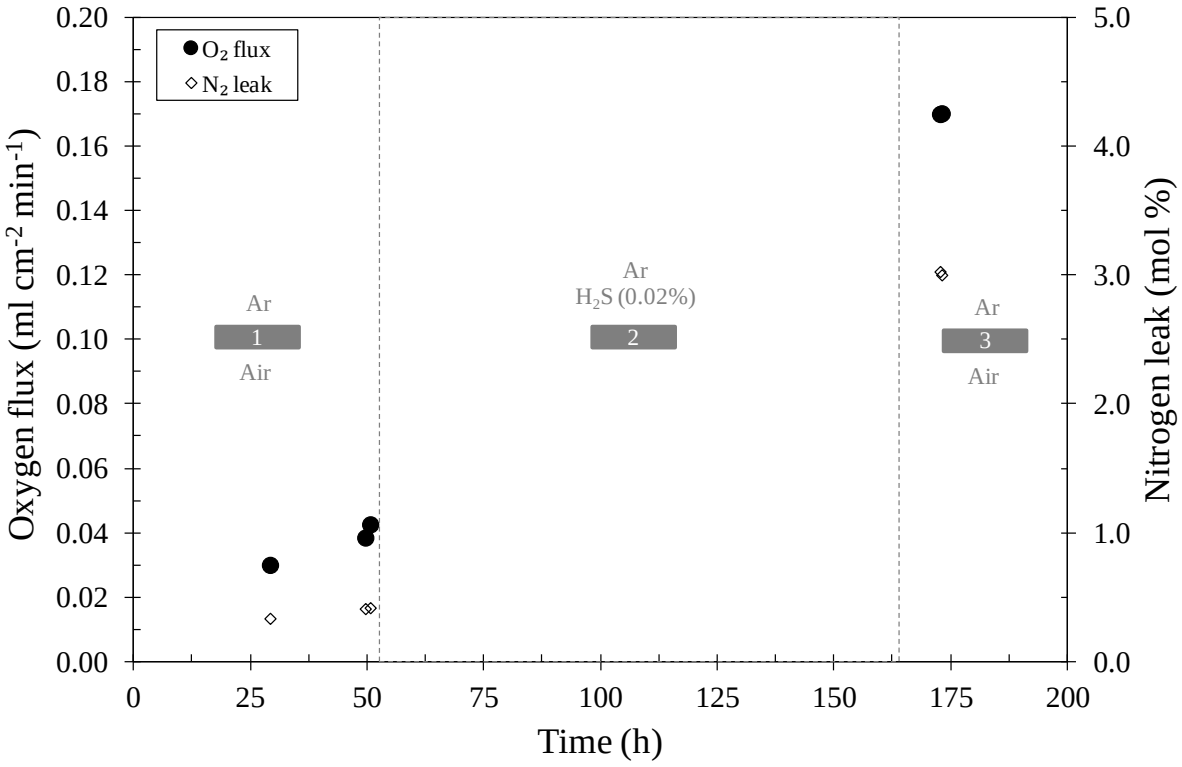

Figure E.1. Increase in nitrogen leak in LSCF6428 membrane after hydrogen sulphide exposure in absence of oxygen at 900°C using silver sealant.

Appendix F: Publications

Solid State Ionics 262 (2014) 262–265

Contents lists available at ScienceDirect

Solid State Ionics

journal homepage: www.elsevier.com/locate/ssi

The impact of sulfur contamination on the performance of $La_{0.6}Sr_{0.4}Co_{0.2}Fe_{0.8}O_{3-\delta}$ oxygen transport membranes

Yousef Alqaheem, Alan Thursfield, Guangru Zhang, Ian S. Metcalfe *

School of Chemical Engineering and Advanced Materials, Newcastle University, Merz Court, NE1 7RU Newcastle-upon-Tyne, United Kingdom

ARTICLE INFO

Article history:
Received 17 May 2013
Received in revised form 17 December 2013
Accepted 4 January 2014
Available online 18 January 2014

Keywords:
Perovskite
Oxygen transport membrane
Sulfur contamination
Segregation
Oxygen flux

ABSTRACT

An oxygen transport membrane made from $La_{0.6}Sr_{0.4}Co_{0.2}Fe_{0.8}O_{3-\delta}$ (LSCF6428) has been tested for air separation by oxygen permeation at 900 °C with the introduction of sulfur in the form of hydrogen sulfide. 200 ppm of hydrogen sulfide was fed either in the sweep-side (argon-side) or the air-side. The membrane was exposed to hydrogen sulfide for 100 h. Results show that the presence of hydrogen sulfide negatively influenced the oxygen permeation due to the formation of strontium sulfate blocking the oxygen permeation pathway. When the hydrogen sulfide was removed from the system, the oxygen permeation was partially restored in the case of argon-side contamination, while being fully restored in the case of air-side contamination.

1. Introduction

Attention has recently turned to the investigation of new processes to produce large scale, high purity hydrogen. Currently, the main process is the energy intensive steam reforming of methane (SRM) to produce synthesis gas, a carbon monoxide and hydrogen mixture,

$$CH_{4(g)} + H_2O_{(g)} \rightarrow CO_{(g)} + 3H_{2(g)}. \quad (1)$$

Careful control of the rate of supply of oxygen can facilitate the exothermic partial oxidation of methane (POM) to also produce syngas with the hydrogen to carbon monoxide ratio of two-to-one,

$$CH_{4(g)} + {}^1/_2O_{2(g)} \rightarrow CO_{(g)} + 2H_{2(g)}. \quad (2)$$

The POM process has advantages over SRM as it does not require heat to initiate the reaction and it overcomes chemical equilibrium limitation. However, the high cost of cryogenic units, to produce high purity oxygen, greatly influences the economics of this process. As an alternative, the emerging oxygen transport membrane (OTM) technology can be integrated in the POM process to offer the following features as they: (i) produce oxygen with 100% purity, (ii) provide a catalytic, active surface area for the reaction and (iii) reduce the oxygen production costs by 35% compared to cryogenic distillation [1–5]. Investigation of OTM materials is currently based on mixed oxygen ion and electron conducting (MIEC) perovskite-type metal oxides of general formula (ABO_3). These materials can be formed into gas-tight membrane structures and possess, theoretically, 100% selectivity to oxygen transport. The oxygen is transported via mobile point-defect oxygen vacancies ($V_O^{\cdot\cdot}$) under an oxygen chemical potential difference across the membrane.

In order for this technology to be transferred from the research environment to the industry, the long term durability of OTMs must be tested under simulated, severe operating conditions for prolonged periods of time. The main issues are: (i) segregation of constituent oxides (kinetic demixing) often leading to the formation of new phases at the surfaces, (ii) reaction of constituent oxides with traces of acid gasses e.g., CO_2, SO_2 and H_2S present in the hydrocarbon feed (e.g., natural gas) to form carbonates, sulfates and sulfides, and (iii) reaction of products with the OTM [6–11]. These mechanisms can act to reduce the performance of the OTM in the long term and may give rise to failure.

In this contribution we focus on the impact of hydrogen sulfide on the oxygen transport properties of $La_{0.6}Sr_{0.4}Co_{0.2}Fe_{0.8}O_{3-\delta}$ (LSCF6428) planar membranes introduced on one side of the membrane. Post-operation analyses using SEM–EDS, XRD and XPS on the OTM exposed surface are reported.

2. Experimental

2.1. Membrane reactor and oxygen permeation studies

The gas-tight, LSCF6428 disk membrane (nominally of diameter 1.6 cm and 0.18 cm thickness, geometric area of 2.1 cm^2) was fabricated from commercial powder (Praxair). Approximately two grams of the powder were weighed and transferred to a steel die with a diameter of 2 cm. The die was then inserted into a mechanical press (Specac, Atlas Power T25) and pressed (3 tonnes) to form the green membrane. The

* Corresponding author. Tel.: +44 191 222 5279; fax: +44 191 222 5292.
E-mail address: I.Metcalfe@newcastle.ac.uk (I.S. Metcalfe).

0167-2738/$ – see front matter © 2014 Elsevier B.V. All rights reserved.
http://dx.doi.org/10.1016/j.ssi.2014.01.011

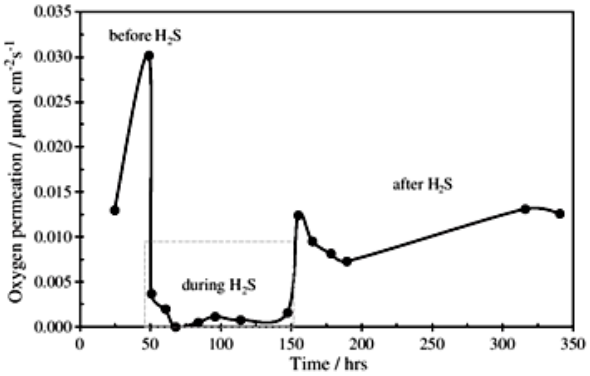

Fig. 1. Oxygen permeation of LSCF6428 membrane after introduction of hydrogen sulfide (200 ppm in argon) in the argon-side at 900 °C. The permeation was partially restored after removal of hydrogen sulfide feed.

membrane was then sintered at 1250 °C using a box furnace (Carbolite, RHF1500) for five hours. The membrane reactor or membrane module was fabricated from quartz with alumina tubing employed internally. The LSCF6428 active membrane was sealed to the alumina tube using silver paste (Fuel Cell Materials, Ag-I) chosen for the long-term experiments because of its high stability compared to glass and ceramic sealants [12]. Synthetic air (20.5% O_2, 79.5% N_2) was used as the source of oxygen for the air-side while argon (99.999%) was used for the sweep-side (argon-side). Hydrogen sulfide with a concentration of 200 ppm in argon was used as the sulfur-containing gas and it was introduced either in the argon-side or the air-side. The gas supply to the membrane was controlled using a bank of mass flow controllers (Brooks, SLA5850). The gas from the argon-side was fed to a gas chromatograph (Varian, CP-3800) equipped with a thermal conductivity detector (TCD) and a molecular sieve 5 Å column. The gas chromatograph was calibrated using a cylinder containing 2% O_2 and 2% N_2 in argon. The membrane was positioned close to the center and in the isothermal zone of a vertical tube furnace (Vecstar, VCTF1). The temperature near the membrane was measured using an internal thermocouple.

Assuming ideal gas behavior, the oxygen flux (J_{O_2}), μmol (NTP) cm^{-2} s^{-1}, is calculated by,

$$J_{O_2} = \frac{\left[y_{O_2} - \frac{0.21}{0.79} y_{N_2}\right]}{24,465 \times 60} \times \frac{F}{A} \times 10^6. \quad (3)$$

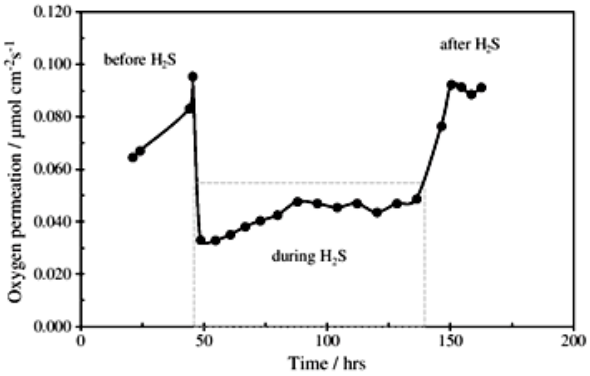

Fig. 2. Oxygen permeation of LSCF6428 membrane after exposure to hydrogen sulfide (200 ppm in argon) fed to the air-side at 900 °C.

Where y_{O_2} and y_{N_2} are the mole fractions of oxygen and nitrogen in the argon-side gas measured by the gas chromatograph. F is the flow rate of the inlet gas in ml (NTP) min^{-1} and A is the active membrane cross-sectional area (cm^2). The term $\frac{0.21}{0.79} y_{N_2}$ refers to the amount of leaked oxygen from the air-side to the argon-side through the sealant. Leak monitoring was performed by determining the nitrogen in the argon-side. The experiment was considered a failure if more than 5 mol% (1.5 μmol cm^{-2} s^{-1}) of nitrogen was detected in the argon-side [12]. In the reported experiments the nitrogen mole fraction was less than 2 mol% (0.6 μmol cm^{-2} s^{-1}). The experiments were performed at atmospheric pressure and the temperature was set to 900 °C by ramping at 1 °C min^{-1}. For experiments with argon-side contamination by hydrogen sulfide, flow rates of 20 ml (NTP) min^{-1}, each, were used for the air and the argon. Hydrogen sulfide was introduced in the argon-side by replacing the pure argon with argon containing 200 ppm of hydrogen sulfide. For experiments with air-side contamination by hydrogen sulfide, air and pure argon, 20 ml (NTP) min^{-1} each, were mixed and fed to the air-side while pure argon was fed to the argon-side using a flow rate of 20 ml (NTP) min^{-1}. The mixing in the air-side results in a lowering of the oxygen partial pressure from 0.21 atm (the reactor was operated at atmospheric pressure) to 0.105 atm and hydrogen sulfide concentration to 100 ppm. In both experiments of argon-side and air-side contamination, the oxygen permeation was measured before, during and after the hydrogen sulfide exposure. The membrane was exposed to hydrogen sulfide for 100 h.

2.2. Characterization techniques

A Rontec Quantax 1.2 FEI XL30 ESEM-FEG system was used to carry out microstructural characterization by scanning electron microscopy (SEM) and non-quantitative elemental analysis by energy dispersive X-ray spectroscopy (EDS). Crystallinity and phase purity were determined by powder X-ray diffraction (XRD) using a PANalytical X'Pert Pro multipurpose diffractometer (PW3040/60) fitted with an X'Celerator and a secondary monochromator. For data acquisition, the Cu anode was supplied with 40 kV and a current of 40 mA to generate Cu K-α radiation (λ = 1.54180 Å) or Cu K-α1 (λ = 1.54060 Å). X-ray photoelectron spectroscopy (XPS) was employed to determine the elemental composition and the data was collected on a Theta Probe (Thermo Scientific) using a microfocused monochromatic AlKa X-ray source operated at 100 W.

3. Results and discussion

3.1. Oxygen permeation studies with argon-side contamination by hydrogen sulfide

Oxygen permeation was measured at 900 °C using feeds of air and argon for 49 h. Fig. 1 shows that the permeation was 0.030 μmol cm^{-2} s^{-1} immediately before hydrogen sulfide introduction. The figure also shows that the permeation increases with time. Such behavior has been reported by many researchers; the time to reach the steady state can be between 25 and 300 h [13,14]. The increase in the permeation rate may be related to the changing degree of reduction of the membrane leading to a change in oxygen vacancy concentration and a decrease in the bulk resistance or a modification of the surface kinetics. After replacing the pure argon with argon containing 200 ppm of hydrogen sulfide, the oxygen permeation instantly dropped (on the timescale of gas sampling of 30 min for the GC) to zero (within the measurement uncertainty of the system – a flux of 0.0001 μmol cm^2 s^{-1} could be measured). The flux showed some sign of recovery when the hydrogen sulfide was replaced with argon and 42% (0.012 μmol cm^2 s^{-1}) of the permeation was restored and remained approximately constant for a further 193 h.

SEM was used to characterize the membrane surface after the exposure to hydrogen sulfide and secondary phases were apparent. EDS

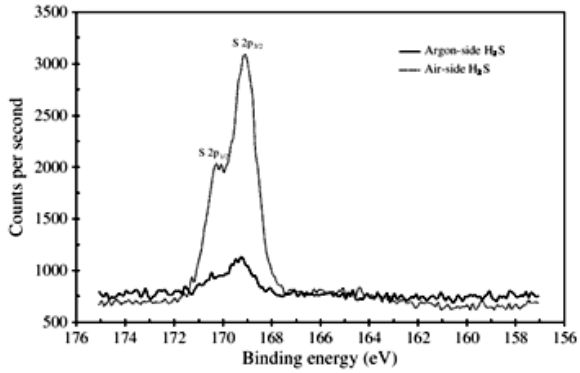

Fig. 3. XPS analysis of the surface exposed to hydrogen sulfide (200 ppm in argon) for the two experiments of argon-side and air-side contamination.

indicated that these phases have high amounts of sulfur and strontium. XPS was employed to determine the form of sulfur and it was assigned to metal sulfate with a binding energy of 169.1 and 170.2 eV for S $2p_{3/2}$ and S $2p_{1/2}$, respectively (Fig. 3). No metal sulfide or elemental sulfur was detected at 161 eV. XRD also identified this metal sulfate as strontium sulfate (Fig. 4). Strontium sulfate can be formed by the following reaction, thermodynamic data as taken from [15].

$$SrO_{(s)} + H_2S_{(g)} + 2O_{2(g)} \rightarrow SrSO_{4(s)} + H_2O_{(g)} \quad \Delta G_{900^\circ C} = -664\ \text{kJ mol}^{-1}. \tag{4}$$

The rate of oxygen release into the argon side should not be confused with the rate of oxygen permeation through the membrane. Oxygen permeation coupled with complete conversion of this oxygen through reaction (4) may result in no oxygen release into the argon side. To investigate this statement, an oxygen mass balance was performed and there should be 0.019 μmol cm^{-2} s^{-1} of oxygen in excess after the consumption in reaction (4). However, the rate of oxygen permeation was undetectable in the argon-side and this could be due to the formation of strontium sulfate on the surface blocking the surface and preventing sufficient release of oxygen. After the removal of hydrogen sulfide from the argon-side, a fraction of the initial oxygen permeation (42% or 0.012 μmol cm^{-2} s^{-1}) was recovered. This value of oxygen permeation is the same as that required to fully oxidize the hydrogen sulfide in reaction (4). Therefore, restoration of the oxygen permeation may have been due to the absence of hydrogen sulfide rather than any reverse of the poisoning mechanism.

3.2. Oxygen permeation studies with air-side contamination by hydrogen sulfide

Oxygen permeation was measured at 900 °C over 98 h before hydrogen sulfide introduction to the air side. Immediately before hydrogen sulfide introduction the permeation rate was 0.095 μmol cm^{-2} s^{-1} (Fig. 2). The permeation rate decreased to 44% of its initial value (0.042 μmol cm^{-2} s^{-1}) during the exposure but was fully restored after the removal of hydrogen sulfide from the air-side. SEM and EDS showed a secondary phase enriched with strontium and sulfur on the surface exposed to hydrogen sulfide. XRD confirmed that the phase is strontium sulfate (Fig. 3). Interestingly, XPS analysis (Fig. 4) indicated that the amount of strontium sulfate on the surface in the air-side experiment is higher than the argon-side experiment. This could be as a result of strontium segregation to the air-side surface increasing the formation of strontium sulfate [16]. It is difficult to draw definite conclusions about the different deactivation mechanisms that may be occurring in the presence of the argon-side and air-side contamination. However we must recall that the environments of the two surfaces are quite different. First, the membrane surface under air-side contamination will have a higher oxygen chemical potential than the argon-side contamination. Second, the oxygen in the air-side could react with hydrogen sulfide to form sulfur dioxide before interacting with the membrane surface thus; the environment is also different from that of the case of argon-side contamination.

4. Conclusions

In this study, membranes made of LSCF6428 were investigated for oxygen permeation using air under the presence of hydrogen sulfide introduced with the sweep argon or the air feeds. Results show that the presence of hydrogen sulfide instantly decreases oxygen permeation. Characterization of the membrane surface indicated formation of strontium sulfate and this blocking layer could be the reason for the reduction in oxygen permeation. After removing the hydrogen sulfide from the feed, the membrane performance was partially restored in the case of argon-side contamination, while being fully restored in the case of air-side contamination. This partial restoration of permeation in the case of argon-side contamination could be due to the fact that oxygen is no longer being consumed by strontium sulfate formation as

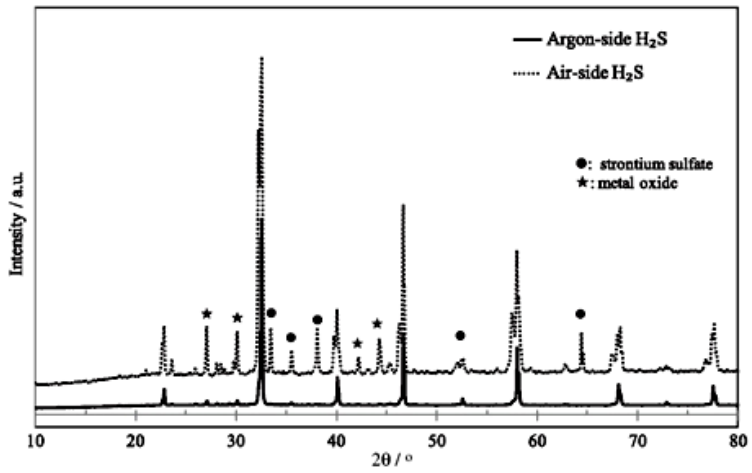

Fig. 4. XRD data of the surface exposed to hydrogen sulfide (200 ppm in argon) in the argon-side and air-side experiments.

well as reversal of the poisoning of the membrane surface. The fact that oxygen permeation could be fully restored in the air-side contamination experiment could be related to the higher oxygen chemical potential of that surface (resulting in a resistance to poisoning) or the different gaseous environments as hydrogen sulfide could be converted to sulfur dioxide before interacting with the membrane in this case.

Acknowledgments

The authors are grateful to Dr. Anders Barlow, Mrs. Pauline Carrick and Mrs. Maggie White at the Advanced Chemical and Material Analysis Centre at Newcastle University for their assistance with XPS, SEM and EDS, and XRD. YA acknowledges the Kuwait Institute for Scientific Research (KISR) for their financial support and AT and GZ acknowledge support through EPSRC (EP/G012865/1).

References

[1] A. Thursfield, I.S. Metcalfe, J. Mater. Chem. 14 (2004) 2475–2485.
[2] Y. Liu, X. Tan, K. Li, Catal. Rev. Sci. Eng. 48 (2006) 145–198.
[3] J. Sunarso, S. Baumann, J.M. Serra, W.A. Meulenberg, S. Liu, Y.S. Lin, J.C. Diniz da Costa, J. Membr. Sci. 320 (2008) 13–41.
[4] X. Dong, W. Jin, N. Xu, K. Li, Chem. Commun. 47 (2011) 10886–10902.
[5] X. Dong, W. Jin, Curr. Opin. Chem. Eng. 1 (2012) 163–170.
[6] B. Wang, B. Zydorczak, Z.T. Wu, K. Li, J. Membr. Sci. 344 (2009) 101–106.
[7] M. Arnold, H. Wang, A. Feldhoff, J. Membr. Sci. 293 (2007) 44–52.
[8] X. Tan, N. Liu, B. Meng, J. Sunarso, K. Zhang, S. Liu, J. Membr. Sci. 389 (2012) 216–222.
[9] G.M. Medine, K.J. Klabunde, V. Zaikovskii, J. Nanoparticle Res. 4 (2002) 357–366.
[10] S. Engels, T. Markus, M. Modigell, L. Singheiser, J. Membr. Sci. 370 (2011) 58–69.
[11] H. Ding, A.V. Virkar, M. Liu, F. Liu, Phys. Chem. Chem. Phys. 15 (2013) 489–496.
[12] J. Park, S. Park, Korean J. Chem. Eng. 24 (2007) 897–905.
[13] S.J. Xu, W.J. Thomson, Ind. Eng. Chem. Res. 37 (1998) 1290–1299.
[14] R.V. Franca, A. Thursfield, I.S. Metcalfe, J. Membr. Sci. 389 (2012) 173–181.
[15] I. Barin, Thermochemical Data of Pure Substances, Wiley-VCH Verlag GmbH, 2008.
[16] H. Ding, A.V. Virkar, M. Liu, F. Liu, Phys. Chem. Chem. Phys. 15 (2013) 489–496.